SYNTHESIS AND CHARACTERIZATION OF SILOXANE-TERMINATED LIQUID CRYSTALS AND PHOTOCHROMIC FULGIDE DOPANTS FOR LIQUID CRYSTAL PHOTONICS APPLICATIONS

By

LI LI

A thesis submitted to the Department of Chemistry

in conformity with the requirements for

the degree of Doctor of Philosophy

Queen's University

Kingston, Ontario, Canada

May 2009

For my grandma, Shufang Sha

Abstract

The goal of this thesis is to design both liquid crystal hosts and photochromic dopants terminated with short siloxane oligomers in order to produce homogeneous liquid crystal mixtures containing a photochromic component for liquid crystal photoswitches. Some of the liquid crystals terminated with short siloxane oligomers were also found to form 'de Vries'-type SmA phases, which minimize the formation of chevrons and zigzag defects that severely degrade the quality of electro-optic devices.

In the first part of the thesis, siloxane-terminated phenylpyrimidine liquid crystals were synthesized and characterized. They form SmC phases and, in some cases, SmA phases. Addition of a terminal halogen substituent on the alkoxy side-chain broadens the SmA temperature range. It was shown that combining a structural element that promotes the formation of a SmC phase with one that promotes the formation of a SmA phase in a mesogen with a 2-phenylpyrimidine core results in a maximum layer contraction of 1.6% for 2-(4-(11-(1,1,1,3,3,5,5-heptamethyltrisiloxanyl)undecyloxy)phenyl)-5-(1-chlorooctyloxy)pyrimidine (**33a**), which may be considered a ‘de Vries’ material.

As an extension of the result obtained in the first project, siloxane-terminated biphenyl benzoate and phenyl benzoate liquid crystals were synthesized and their phase behavior studied. They form SmC phases and, in some cases, SmA and SmI phases. Addition of a terminal chloro substituent on alkoxy side-chain results in a broader SmA temperature range and, in some cases, also affects the nature of the mesophase formed. The compound 4-[6-(1,1,1,3,3,5,5-heptamethyltrisiloxanyl)hexanoyloxy]phenyl 4-(8-

chlorooctyloxy)benzoate (**40b**) is characterized by a maximum layer shrinkage of only 1.7%, which may be considered to possess some 'de Vries' character.

Finally, siloxane-terminated fulgide derivatives were designed as photochromic dopants for liquid crystal photoswitches. Compound **41** was designed and synthesized and proved to be an oil at room temperature. Solid fulgide precusors **42**, **43a** and **44b** were then assessed as photochromic dopants in terms of fast switching and high quantum yield requirements of a photoswitch, and their photophysical properties were studied in solution. The isomer composition at the photostationary state suggests that the competition from E-Z isomerization is likely too high for compounds **42**, **43a** and **44b** to be suitable as photochromic dopants for photoswitches.

Acknowledgement

First, I would like to express my deepest gratitude to my supervisor, Dr. Robert P. Lemieux who has been a fantastic supervisor and mentor. Thank him for giving me this excellent opportunity of Ph.D. studies. His guidance, patience, enthusiasm, encouragement, care, and financial support throughout the duration of my studies have been very much appreciated. My thanks also to the members of my graduate supervisory committee, Dr. Suning Wang and Dr. Ralph Whitney for their encouragement, advice and support over the years.

Thank you to the Lemieux group members past and present, especially Scott Hartley, Christa Huntley, Jeremy Finden, Matthew Thompson, Eagranie Yuh, Adam McCubbin, Naohiko Ikuma, Jeffrey Roberts, Peng Zhang, Mark Moran, Rebecca Cui, Wei Gan, Linli Fang, Markus Ohlin, Eric Ekengard, Qingxiang Song and Sunny Lai for helpful advice and for making this lab a fun and rewarding place to work. Big thanks to Dr. Francoise Sauriol, Sui Jie, Dr. Bernd Keller and Dr. Yimin She who did a fantastic job on keeping things running with the NMRs and Mass Spectrometry and were always there for advice. Thanks to Robin Roberts and Ed Maracle for keeping our instruments running and helping to set up new equipment and computers. I am also grateful for the support of friends near and far, who have always been there when I needed them.

Last, and far from least, thank you to my parents, my aunt Dr. Lijuan Li and my husband Runkai Li for their love and support.

Statement of Co-Authorship and Originality

All of the experimental research presented in this thesis was performed by the author under the supervision of Dr. R. P. Lemieux in the Department of Chemistry, Queen's University, unless otherwise noted. Original work presented includes: the synthesis and physical characterization of novel siloxane-terminated phenylpyrimidine liquid crystals, siloxane-terminated biphenyl liquid crystals, and siloxane-terminated benzoate and phenyl benzoate liquid crystals, fulgide and fulgimide, physical characterization of various liquid crystal phases using polarized microscopy and differential scanning calorimetry, measurement of optical tilt angle performed on mixtures of a chiral dopant in siloxane-terminated liquid crystal hosts, study of photoisomerization of fulgide and fulgimide compounds synthesized in isotropic solution were studied using HPLC and UV-vis spectroscopy.

Table of Contents

List of Tables

List of Figures

Abbreviations

XRD	X-ray diffraction
P_S	Spontaneous polarization
p	helical pitch
2θ	Bragg angle
NMR	nuclear magnetic resonance
δ	chemical shift
5CB	4-pentyl-4'-biphenylcarbonitrile
λmax	wavelength of absorbance maxima
θ	tilt angle
ΔH	change of enthalpy
A	absorbance
$CDCl_3$	deuterated chloroform
EI	electron impact ionization
d	lamellar or smectic spacing
Cr	crystalline state

DIAD	diisopropylazodicarboxylate
DSC	differential scanning calorimetry
ES	electrospray ionization
I	isotropic liquid crystal
FLC	ferroelectric liquid crystal
L	molecular length
K	degrees Kelvin
LC	liquid crystal
LCD	liquid crystal display
M	molar
Mmol	millimole
mol%	dopant mole percent
mp	melting point
MS	mass spectroscopy
HPLC	high performance liquid chromatography
N	nematic phase
POM	polarized optical microscopy

SLM	spatial light modulator
SmA	smectic A phase
SmC	smectic C phase
SSFLC	surface-stabilized ferroelectric liquid crystal
t	time
T	temperature
T_C	Curie temperature
THF	tetrahydrofuran
CH_2Cl_2	dichloromethane
UV-vis	ultraviolet-visible
UV	ultraviolet
z	layer normal
n	director
SmC*	chiral smectic C phase
SmI	smectic I phase
C_{dV}	de Vries coefficients
LDA	lithium diisopropylamide

NBS	N-bromosuccinimide
HMDS	hexamethyldisilazane
MOM	methoxymethyl ether
PhP1	2-(4-butyloxyphenyl)-5-octyloxypyrimidine
MALDI	matrix-assisted laser desorption/ionization
EtOAc	ethyl acetate
ITO	indium/tin oxide
AC	alternating current
DC	direct current
DMF	dimethylformamide
THF	Tetrahydrofuran
HRMS	high-resolution mass spectroscopy
PTFE	Polytetrafluoroethylene
DCC	N,N'-Dicyclohexylcarbodiimide
DMAP	4-dimethylaminopyridine
DMSO-d6	deuterated Dimethyl sulfoxide
IPA	isopropanol

APT	automated polarization testbed
Φ	quantum yield
Ph	phenyl
S	order parameter (equation 1-1)

Chapter 1. Introduction

1.1 Liquid Crystals

1.1.1 General Description

In 1888, while trying to melt a sample of cholesteryl benzoate, the Austrian botanist Reinitzer observed that the compound exhibited two melting points. At 145.5 ^{o}C, the compound melted to form a cloudy liquid which then became completely clear at 178.5 ^{o}C.[1] This work was taken up by Lehmann who coined the term "liquid crystal" to describe this new state of matter. In the intervening century since their discovery, considerable advances have been made in the study into the nature and properties of liquid crystals. [2]

A liquid crystal (LC) is a state that exists between the solid and isotropic liquid phase (mesophase). While exhibiting the fluid character of an isotropic liquid, liquid crystal phases possess one- or two- dimensional ordering that imparts crystalline properties such as birefringence. Compounds forming liquid crystal phases are described as mesomorphic, or said to possess mesogenic properties. Liquid crystal phases may be divided into two broad categories: a lyotropic liquid crystal phase is formed by a mixture of amphiphilic molecules and a solvent, and a thermotropic liquid crystal phase is intrinsic to a given compound and appears as a function of temperature. Only thermotropic liquid crystal materials will be considered here. Thermodynamically stable

mesophases, which appear on heating and cooling, are referred to as enantiotropic. Mesophases that appear only on cooling are referred to as monotropic.

Low molecular weight thermotropic liquid crystals (as opposed to liquid crystalline polymers) are classified according to their structure and shape: calamatic, discotic, polycatenar, and amphiphilic (Figure 1-1). Calamitic mesogens, which have an overall rod-like shape, are the most commonly known; discotic mesogens have a disc-like shape; polycatenar mesogens which have more than two alkyl side-chains, are neither rod- nor disc-shaped but may form liquid crystal phases typical of both categories.

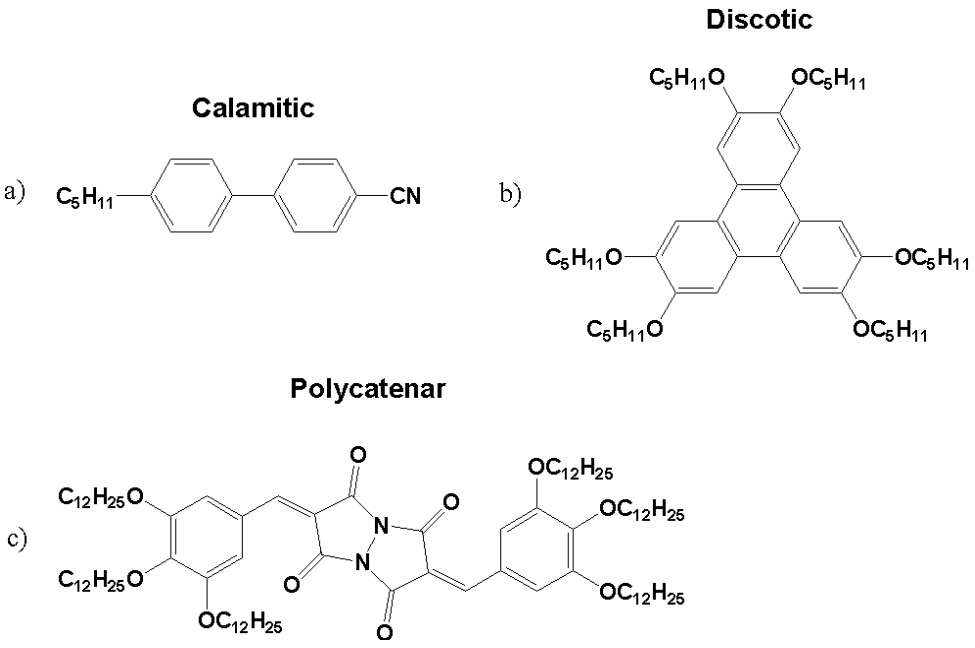

Figure 1-1. Examples of a) calamatic, b) discotic, and c) polycatenar mesogens.

The formation of thermotropic liquid crystal phases can also be promoted by the nanosegregation of incompatible moieties in neat amphiphilic molecules, such as polyols, organosiloxanes, and organic molecules with perfluorinated side-chains (see Figure 1-2).[3]

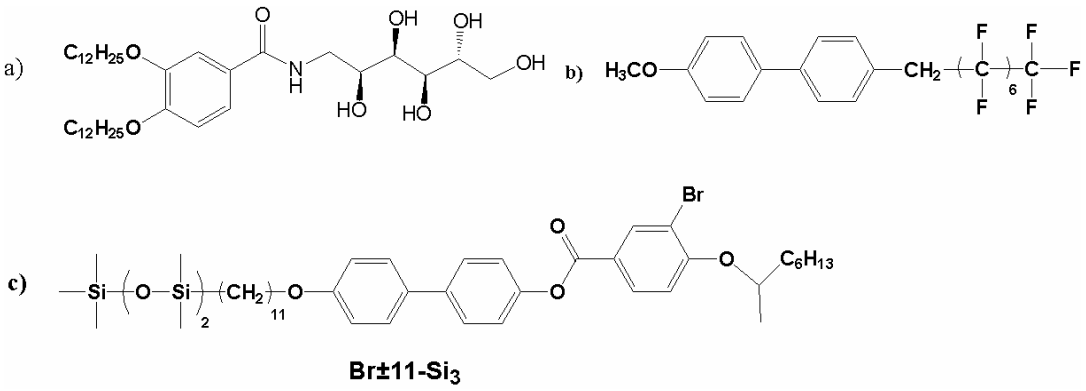

Figure 1-2. Examples of amphiphilic mesogens a) polyol, b) perfluorinated, c) organosiloxane.

In general, calamitic mesogens may form a nematic (N) phase and one or more smectic phases. The two most commonly observed smectic phases are the smectic A (SmA) and smectic C (SmC) phases. A typical thermotropic phase sequence is shown in Figure 1-3. Hence, cooling from the isotropic liquid state can result in the formation of a N phase which, upon further cooling, can form more highly ordered SmA and SmC phases, and finally a crystalline phase.

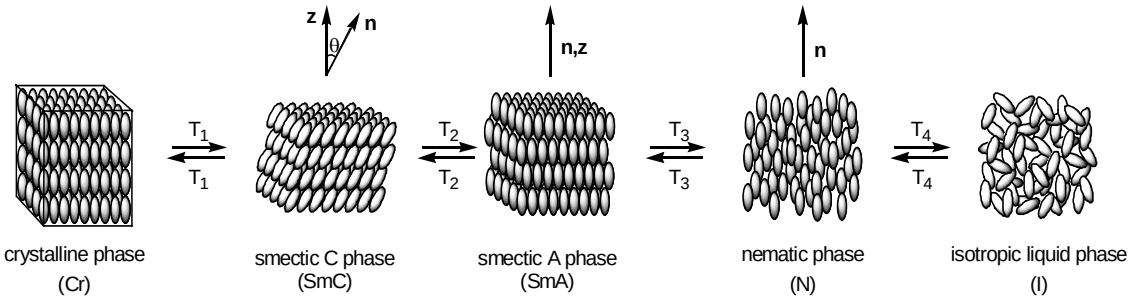

Figure 1-3. Schematic representation of isotropic (I), nematic (N), smectic A (SmA), smectic C (SmC) and crystalline (Cr) phases of calamitic liquid crystals.

Although there are no firm rules with respect to the structural requirements for LC properties, most calamitic materials conform to the basic structure shown in Figure 1-4. Units A and B are linear rigid core units (e.g., 1,4-phenylene), Y is an optional linear linking group (e.g., ester or azo), R^1 is an alkyl or alkoxy chain, and R^2 is either a polar group or another alkyl/alkoxy chain. This gives an overall rod-shape structure, although the molecules are bent at the core/side-chain interfaces. The units that are used in this general structure and their combinations determine the types of liquid crystal phases formed by the compound. Extensive structure-property relationship studies have been carried out within the basic calamitic mesogen template to determine the effects of structure variations on the types and stabilities of liquid crystal phases formed. Because one molecule may form several different liquid crystal phases, it is difficult to establish conclusive trends. In general, liquid crystal phases are favored by molecules having large polarizability anisotropy and low lateral bulk. Certain generalizations can be made for specific phases as well.[4]

Figure 1-4. General structure of a calamatic mesogen.

1.1.2 Nematic Liquid Crystals

The simplest and least ordered thermotropic mesophase is the N phase in which the long molecular axes are aligned parallel along a director (**n**), as shown in Figure 1-5. The molecular centers of mass are distributed randomly as they would be in an ordinary liquid and the molecules can rotate freely about their long axes, corresponding to a long range one-dimensional orientational ordering without any positional ordering. The parallel alignment of the molecules within a nematic phase is only an approximate, time-averaged view of the molecular orientation. In reality, the molecular orientation is better described by a distribution of angles (θ) that the molecules assume with respect to the director, **n**. To describe this distribution, Tsvetkov defined the order parameter, **S**, according to equation 1-1:

$$S = \langle \frac{3\cos^2\theta - 1}{2} \rangle \qquad (1\text{-}1)$$

The brackets in this case denote that S is a statistical average of the angles assumed by the molecules. In an "ideal" nematic, the order parameter S=1, while for an isotropic liquid, S=0. The order parameter can be determined experimentally by a number of methods, including measurement of linear dichroism in UV and IR absorptions and by deuterium NMR.[5]

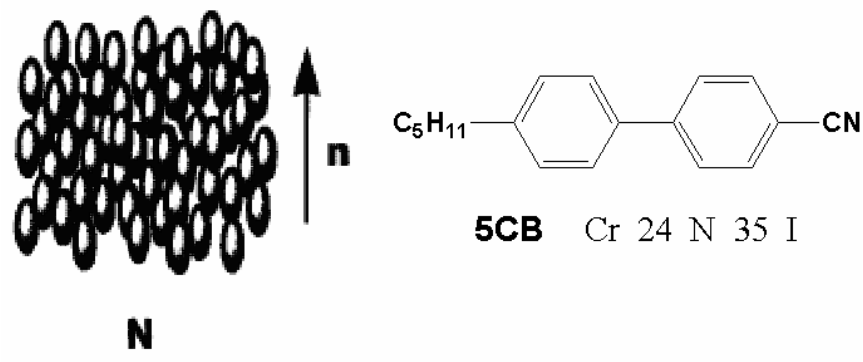

Figure 1-5. The nematic phase and a typical nematic mesogen **5CB**.

Nematic materials appear as cloudy liquids and their viscosity is comparable to that of liquids. The formation of nematic phases is favored by unsymmetrical calamitic molecules such as **5CB** which has a polar terminal group and one short alkyl side-chain. In the absence of any special surface treatment, polarized optical micrographs of nematic phases show a so-called Schlieren texture characterized by point defects and extinction brushes (Figure1-6 (a)).

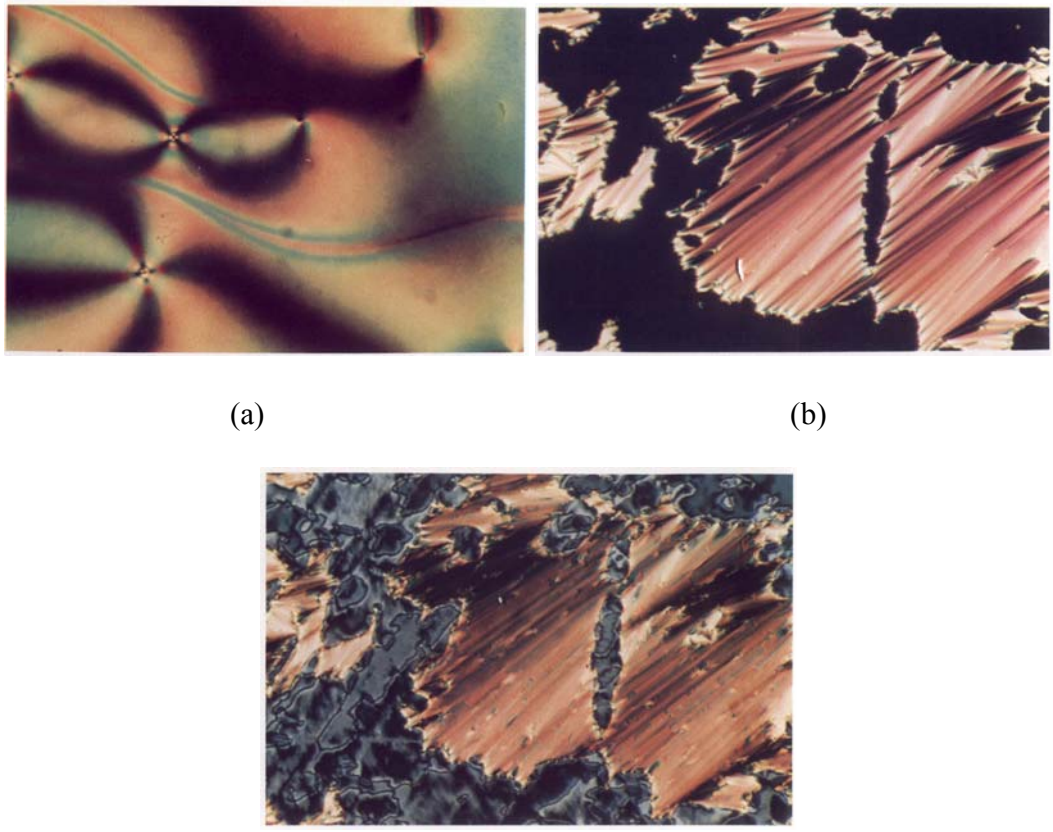

(a) (b)

(c)

Figure 1-6. Polarized optical micrographs showing (a) a N phase with a Schlieren texture featuring point defects with 4-brush disclinations, (b) a SmA phase with fan and homeotropic textures, and (c) a SmC phase with broken fan and Schlieren textures. Reproduced from Reference 6.

1.1.3 Smectic A Liquid Crystals

The simplest smectic phase is the SmA phase in which the director (**n**) is aligned parallel to the layer normal (**z**) on the time average, as shown in Figure 1-7.[5,7] Molecules in the SmA phase are free to rotate about their long axes, and have orientational and one dimensional long-range positional order. The SmA phase is normally formed by molecules with non-polar aromatic cores and two alkyl side chains. The powder X-ray

diffraction profile of an unorientated SmA phase shows a diffuse outer ring and a sharp inner ring at a Bragg angle of 2θ corresponding to the smectic layer spacing, which is normally on the order of the molecular length. According to differential scanning calorimetry (DSC), the first order phase transition from the I or the N phase to the SmA phase generally has a ΔH on the order of 4-6 kJ/mol.

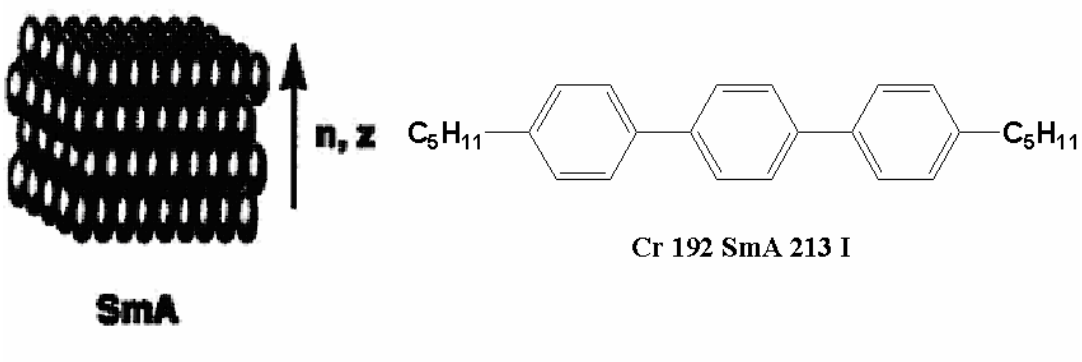

Figure 1-7. The smectic A phase and a typical smectic A mesogen.

The concept of nanosegregation is important to understanding the formation of smectic lamellar structure; it refers to the assembly of chemically incompatible blocks within the mesogens into distinct domains or sublayers.[3] According to the general structure of calamitic mesogen depicted in Figure 1-4, the formation of smectic phases is driven, in part, by nanosegregation of the rigid, aromatic molecular cores from the flexible aliphatic side-chains, as shown in Figure 1-8. Generally, nanosegregation, and thus the smectic lamellar structure, is favored by molecules with a well-defined amphiphilic character, i.e. in compounds with distinct polar/rigid and less polar/flexible segments. For example, the formation of smectic phases can be strongly promoted by

designing calamitic mesogens that combine hydrophilic and lipophilic segments, fluorocarbon and hydrocarbon segments, or siloxane and hydrocarbon segments. If the different regions are mixed up, the stability of the liquid crystal phases decreases.

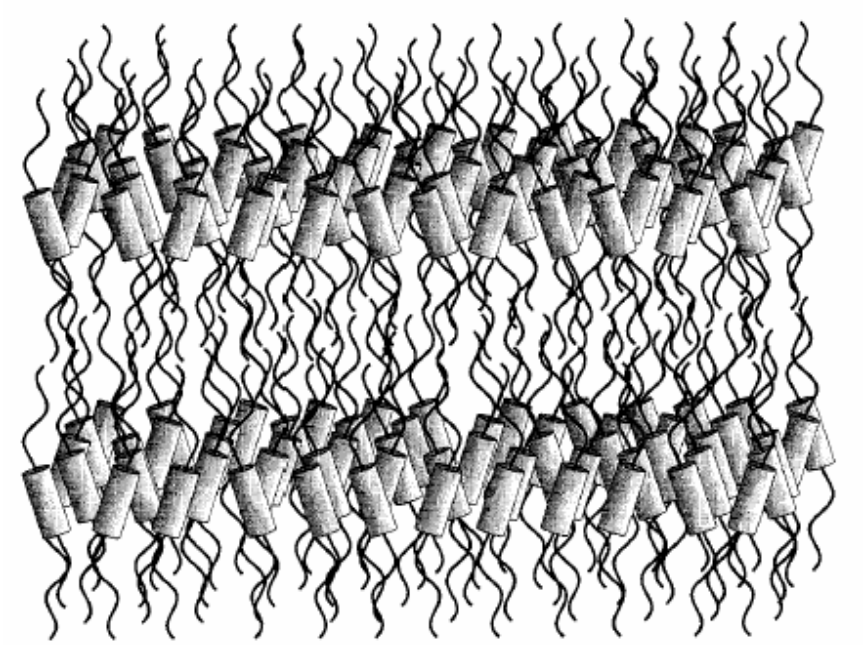

Figure 1-8. Nanosegregation in the SmA phase of a calamitic mesogen.

Many SmA phases undergo second-order transitions to the tilted SmC phase. As the temperature is lowered below the SmA-SmC transition, the director (**n**) tilts away from the smectic layer normal (**z**). In the majority of SmA-SmC transitions, molecular tilt results in a substantial shrinkage (~7-10%) of the smectic layer spacing (***d***), which is consistent with a conventional picture of the SmA phase as a lamellar assembly of rigid rods with uniform orientation, as shown in Figure 1-9. According to this classic "rigid rod model", the layer spacing of the SmC phase ($\boldsymbol{d}_{\mathbf{C}}$) decreases as:

$$d_C = d_A \cos\theta \tag{1-2}$$

where d_A denotes the layer spacing of the SmA phase, and θ is the angle formed by director (**n**) and the layer normal (**z**).

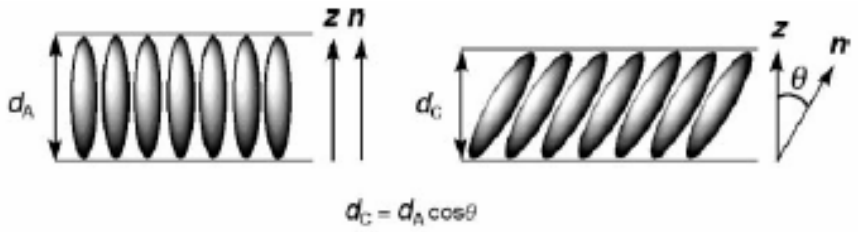

Figure 1-9. The rigid rod model of the SmA phase predicts a substantial layer shrinkage upon transition to the SmC phase.

The significant smectic layer shrinkage at the SmA-SmC transition is the source of problems in ferro- and antiferroelectric liquid crystals display applications (*vide infra*)[9]. As the layers are normally anchored at glass surfaces in a display device, they buckle in a chevron geometry (Figure 1-10) at the SmA-SmC transition to accommodate the layer shrinkage. Chevrons of opposite fold directions are separated from each other by striking defects called zigzag lines, as shown in Figure 1-11.[9] The formation of chevrons and zigzags severely degrades the quality of any electro-optic device based on liquid crystal materials forming SmA and SmC phases.

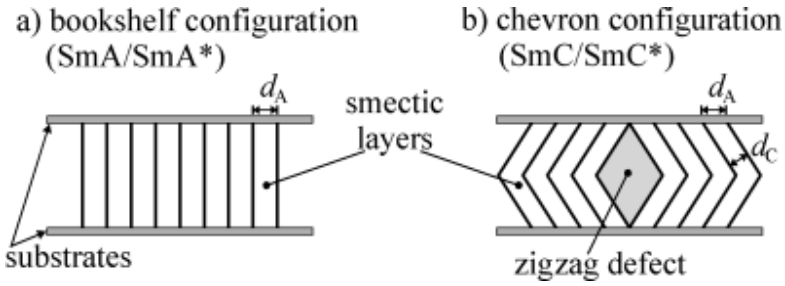

Figure 1-10. As a result of smectic layer shrinkage, a SmA sample confined between two glass substrates in the bookshelf configuration (a) transforms into the chevron configuration (b) when entering the SmC phase. Reproduced from reference 9.

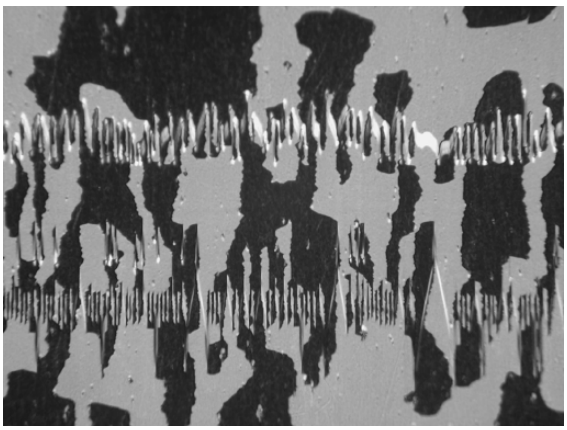

Figure 1-11. Example of zigzag defects in the SmC phase of the nonchiral 4-octyloxy- 4-octylphenylpyrimidine seen by polarized microscopy. Reproduced from reference 9.

1.1.3.1 'de Vries'-type Smectic A phase

Some liquid crystal material forming SmA and SmC phases show negligible layer shrinkage at the SmA-SmC transition. This type of SmA phase is called 'de Vries'-type SmA phase and has significant potential for useful applications in displays and devices.

The best known 'de Vries'-type material are listed in Figure 1-12, and the corresponding profiles of smectic layer spacings *d* as a function of temperature *d*(T) are

shown in Figure 1-13 and compared with the profiles of two conventional SmA-SmC materials CS-1013 and DOBAMBC.[10-12] The typical extent of layer shrinkage in conventional materials is in the range of 5–10% (DOBAMBC: 7.2%, CS-1013: 5.5%). In general, the maximum layer shrinkage for 'de Vries'-type material is about one order of magnitude less than for conventional materials. In the case of 3M 8422[2F3], for example, *d* decreases marginally at the transition to the SmC* phase. The minimum *d* value, observed at 15 K below the transition, is only 0.3 Å less than the layer spacing measured at the SmA-SmC transition. On further cooling, *d* actually increases again and finally regains the value of 38.7 Å observed at the transition point because of an increase in conformational order of the aliphatic side-chain. The maximum layer shrinkage in the SmC* phase of 3M 8422[2F3] is thus ca. 0.8 %.

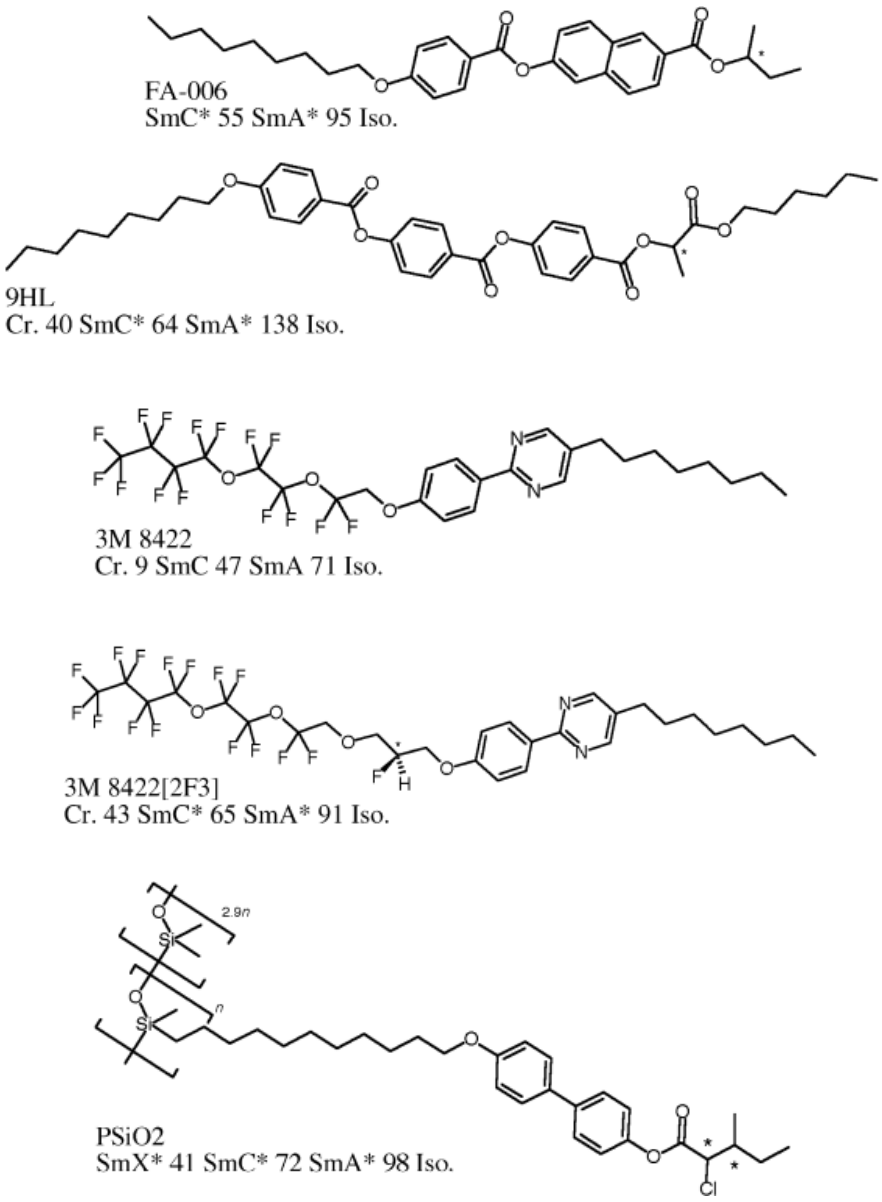

Figure 1-12. Compounds with 'de Vries'-type SmA–SmC transitions. Transition temperatures are in ^{o}C. Reproduced from reference 9.

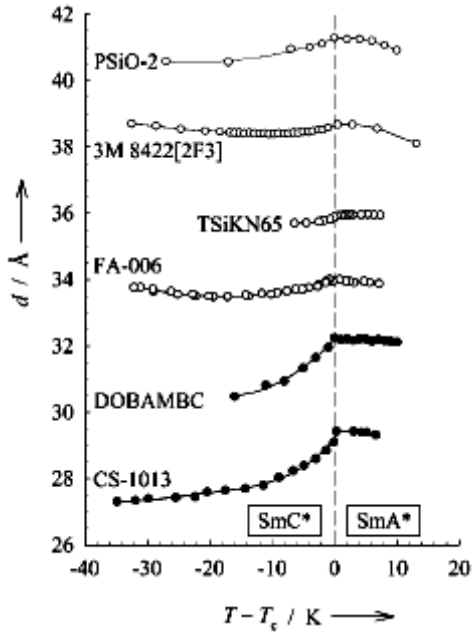

Figure 1-13. Smectic layer spacing *d vs.* temperature T for 'de Vries'-type materials (see Figure 1-12) and the conventional materials DOBAMBC and CS-1013 in the vicinity of the tilting transition (T=Tc). Reproduced from reference 9.

The unsually small layer shrinkage of 'de Vries'-type material can't be explained by the conventional rigid-rod model. In 1979, de Vries *et al.* proposed a Diffuse Cone Model, [13,14] in which the molecules are already tilted with respect to the smectic layer normal (**k**) in the SmA phase, but the tilt direction (**n**) is randomly oriented within the layer, i.e., there is no long-range correlation in the azimuthal angle. As shown in Figure 1-14, all possible directions of orientational fluctions are represented by a (diffuse) cone. Due to the averaging in any smectic layer, the uniaxial symmetry of the SmA phase is observed. The overall symmetry of this arrangement as well as the local symmetry is $D_{\infty h}$, the same as a conventional SmA phase in the rigid-rod model. At the transition from SmA to SmC phase, a long-range correlation in the azimuthal angle of the layers is developed, i.e., the

molecules in smectic layers start to orient in the same direction. As long as the magnitude of molecular tilt (θ) remains unchanged, this process in itself does not produce any change in d and the diffuse cone model could thus explain the rare cases of tilting transitions without layer shrinkage.

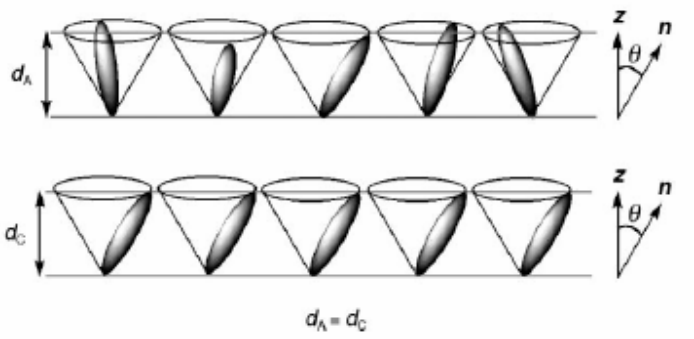

Figure 1-14. de Vries's diffuse cone mode predicts no layer shrinkage at SmA-SmC transition.

If the rigid rod model and de Vries diffuse cone model are considered to be two extremes in a continuum, most materials are likely to exhibit layer shrinkage behavior that lie between the two extremes, and possess some de Vries character.

Besides the minimal change in layer spacing, a 'de Vries'-type transition may be distinguished from a normal SmA-SmC transition by a large increase in birefringence (Δn).[11,13,15] In a normal SmA-C transition that is consistent with the rigid-rod model, molecules have relatively high orientational order in SmA phase, corresponding to a high birefringence. At the SmA-SmC transition, the molecules maintain the orientational order but uniformly tilt in one direction and the birefringence should therefore not change

significantly. By contrast, in the 'de Vries' case, the molecules have a random distribution of tilt orientations in SmA phase, and the birefringence should be much smaller compared to the rigid-rod model because of the orientational averaging. At the SmA-SmC transition, the ordering of molecular tilt directions results in a higher orientational order, and therefore should result in a large increase in birefringence. Such large increase in birefringence for 'de Vries'-type materials has been observed by polarized microscopy experiments (see Figure 1-15, for example).

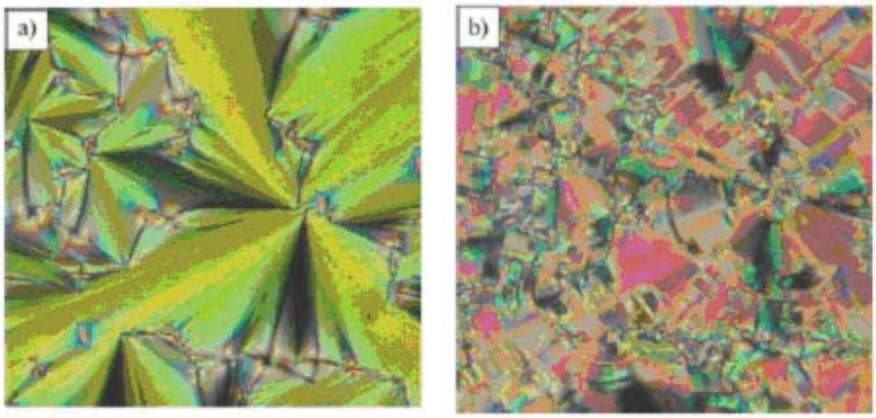

Figure 1-15. Polarized micrographs of a 10μm planar sample of 3M 8422 (see Figure 1-12) in (a) the SmA phase at 71°C, and (b) in the SmC phase at 47°C. The distinct change in interference color from yellowish green to red corresponds to an increase in birefringence from $\Delta n \approx 0.07$ to $\Delta n \approx 0.09$. Reproduced from reference 9.

The structure of 'de Vries'-type SmA materials has not been fully elucidated, although recent theoretical studies suggest that calamitic materials combining low orientational order and high lamellar order are likely to exhibit this behavior.[16,17] This is consistent with the fact that most 'de Vries'-type materials feature nanosegregating

structural elements such as siloxane end-groups or partially fluorinated side-chains that strongly promote lamellar order.[9]

1.1.4 Smectic C Liquid Crystals

The SmC phase is similar to the SmA phase except that molecules are uniformly tilted at some angle (θ) with respect to the layer normal (**z**) as shown in Figure 1-16. Like the SmA phase, the SmC phase possesses short range orientational and positional order. The synclinic layer interface of the SmC phase is entropically favored and allows for interlayer fluctuations. The formation of the SmC phase is favored by molecules with unsymmetrical polar aromatic cores. The antiparallel coupling of out-board terminal dipoles is thought to create a torque which induces a tilt according to the McMillan model.[18,19] The tilted structure of the SmC phase is also thought to be the result of favorable packing of mesogens in low energy zigzag conformation (Wulff model).[20] The powder X-ray diffraction profile of an unorientated SmC phase shows a diffuse outer ring and a sharp inner ring at a Bragg angle 2θ corresponding to a layer spacing (***d***), which is normally smaller than the molecular length (***l***) because of the uniform tilt. The SmC phase can be distinguished from the SmA phase based on texture analysis (Figure 1-6 (b) and (c)): a homeotropically aligned sample in the SmA phase gives rise to a Schlieren texture in the SmC phase, while a fan texture in the SmA phase becomes broken in the SmC phase. Transitions from the SmA to the SmC phase are generally second-order

phase in nature with small ΔH on the order of 1 kJ/mol or less, and are often difficult to detect by DSC.

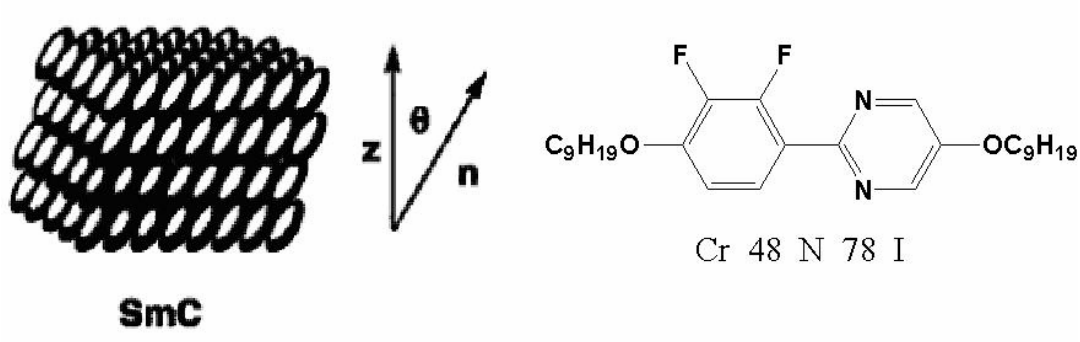

Figure 1-16. The smectic C phase and a typical smectic C mesogen.

1.1.5 Ferroelectric Liquid Crystals

1.1.5.1 Ferroelectric liquid crystals

The achiral SmC phase has three symmetry elements; a C_2 axis of rotation perpendicular to the layer normal, a reflection σ plane congruent with the tilt plane, and an inversion centre. However, Mayer and co-workers predicted that in the chiral SmC phase (SmC*), the elimination of the σ reflection plane would result in a macroscopic electric polarization parallel to the C_2 axis, which is the sum of contributions of transverse dipole moments of the constituent mesogens along the C_2 axis (Figure 1-17). This permanent electric polarization is known as the spontaneous polarization, (P_S), and such SmC* phases are ferroelectric.[21]

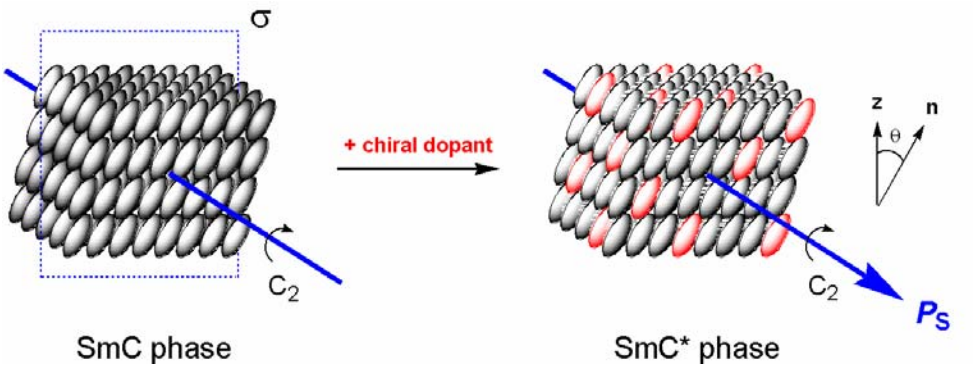

Figure 1-17. Symmetry elements of the achiral SmC and the chiral SmC (SmC*) phases, and the resulting P_S.

In the absence of external constraints, the SmC* phase forms a helical structure (Figure 1-18 (a)), in which the P_S vector rotates from one layer to the next resulting in a net P_S of zero. However, in 1980, Clark and Lagerwall demonstrated that the SmC* helix spontaneously unwinds when the material is aligned between rubbed polyimide-coated glass slides, with a spacing on the order of the helical pitch, p (Figure 1-18(b)).[22] In this aligned state, the SmC* phase is termed a surface-stabilized ferroelectric liquid crystal (SSFLC).

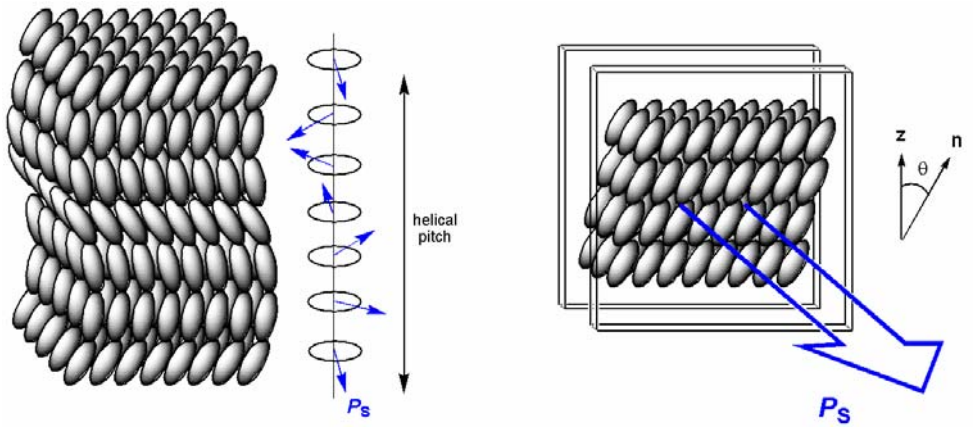

(a) Helical State (Non-Ferroelectric) (b) Surface-Stabilized State (Ferroelectric)

Figure 1-18. (a) Helical structure of the SmC* phase in the absence of external constraints, and (b) the SmC* phase in the ferroelectric surface-stabilized state.

When an external field is applied parallel to the C_2 axis, the tilted mesogens of a SSFLC can be switched from one tilt orientation to another by precession of **n** about **z**. Mesogens go from $+\theta$ tilt orientation to $-\theta$ as the electric field is reversed, thus resulting in an ON/OFF light shutter when the SSFLC film is placed between crossed polarizers (Figure 1-19).

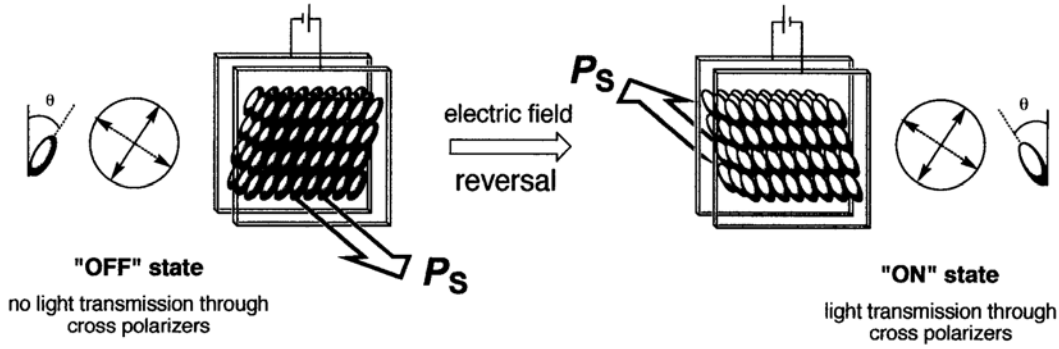

Figure 1-19. Switching ($+\theta$ and $-\theta$ orientations) between opposite applied fields in a SSFLC.

An ideal SmC* material for display applications is one that has a short switching time between $+\theta$ and $-\theta$ tilt orientations under an applied field. The switching time (electro-optical rise time), τ_r, is dependent on the magnitude of P_S, the applied field (E) and the orientational viscosity (η), as described by Equation (1-3).[23]

$$\tau_r \propto \frac{\eta}{|P_S|E} \tag{1-3}$$

Smectic C* liquid crystals consisting solely of chiral mesogens are not suitable for use as ON/OFF light shutters due to their highly viscous nature, which results in slower

switching times. However, Kuszynski and Stegemeyer found that P_S can be induced in an achiral SmC phase after the addition of a chiral polar molecule (or "dopant") that may or may not be mesogenic.[24] Stegemeyer and coworkers extended this work by determining the direct relationship between P_S and the mole fraction of dopant.[25] Commercial devices featuring an ON/OFF light shutter typically consist of a chiral dopant with high polarization power (δ_P) doped into a low viscosity SmC host mixture with a wide temperature range. The ability of a dopant to induce a P_S in an otherwise achiral SmC host mixture is described as its polarization power (Equation (1-4)), where χ_d is the mole fraction of the dopant and P_0 is the reduced polarization, which is normalized for variations in tilt angle θ according to Equation (1-5).[26]

$$\delta_P = [\frac{dP_0(x_d)}{dx_d}]_{x_d \to 0} \tag{1-4}$$

$$P_0 = \frac{P_S}{\sin\theta} \tag{1-5}$$

1.1.5.2 Molecular Origen of P_S

The Boulder model provides a rationale for spontaneous polar ordering at the molecular level.[27] The ordering is described by the Boulder model as a bent-cylinder (binding site) which has a zig-zag shape and is C_2 symmetric, as shown in Figure 1-20. As mesogens adopt this zig-zag shape, with rigid cores more tilted than side-chains in an

all *anti*- conformation, steric coupling between any polar functional group and the chiral centre results in an orientational bias of the corresponding molecular dipole along the C_2 axis that contributes to P_S.

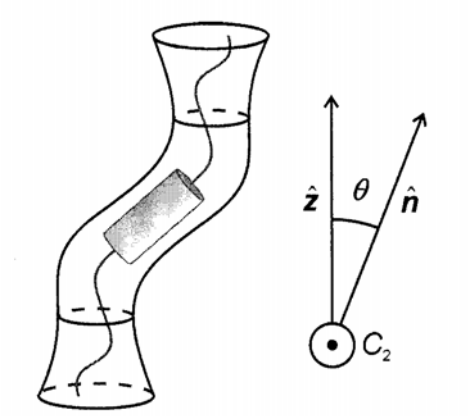

Figure 1-20. The bent-cylinder binding site with a guest molecule in the SmC* phase, according to the Boulder model.

Wand *et al.* used compound **MDW 222** (Scheme 1-1) to illustrate the concept of the Boulder model.[28] This compound consists of many polar functional groups, however, the only group contributing to P_S is that of the chiral ether side-chain. Other functional groups are too far away from the chiral centre to contribute to P_S.

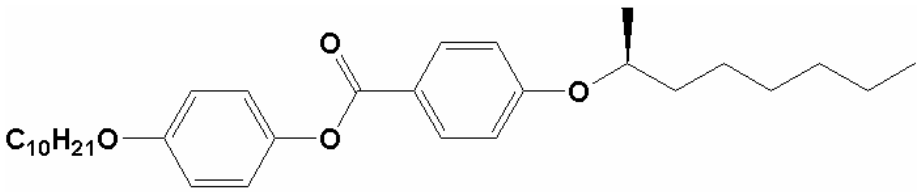

Scheme 1-1

There are three possible conformers for the so-called "stereo-polar unit" of **MDW 222** (Figure 1-21). In conformation **C**, the alkoxy dipole cannot contribute to P_S since it is oriented in the tilt plane. In conformations **A** and **B**, the ether group is *gauche* with respect to the alkyl chain, resulting in equal but opposite dipole contributions along the polar C_2 axis. However, conformation **A** is favored relative to **B** because of the *anti* relationship between the methyl group and alkyl chain corresponding to a net positive polarization, which is consistent with experimental findings by Wand *et al.* in 1991.

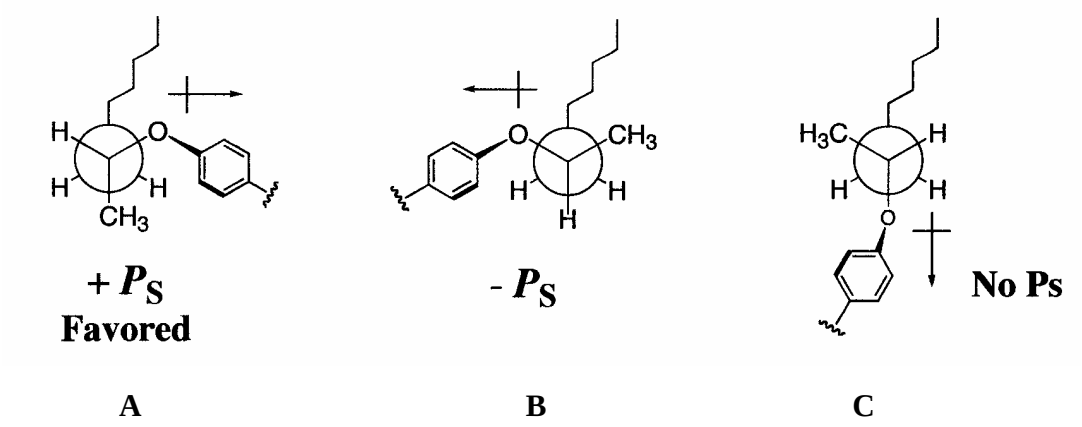

Figure 1-21. Newman projections along the C_2-C_3 bond of the three conformers of MDW 222, according to the Boulder model.

1.1.6 Other Smectic Liquid Crystals

There are several other smectic phases which are all more highly ordered than the SmA and SmC phase, which exhibit short-range positional ordering (layers uncorrelated) but also long-range orientational ordering within the layers.[29] These include the hexatic B (SmB) phase which is similar to the SmA phase but with hexagonal packing. The SmF

and SmI phases are tilted with psuedohexagonal packing; mesogens in the SmF phase tilt to the side of the hexagon while mesogens in the SmI phase tilt to the apex of the hexagon (Figure 1-22).

So-called crystal smectic phases exist, which have both long-range orientational and positional ordering leading to correlated layers, but still lack rotational order about the long molecular axes. These include the crystal B, E, G, H, J and K phases.

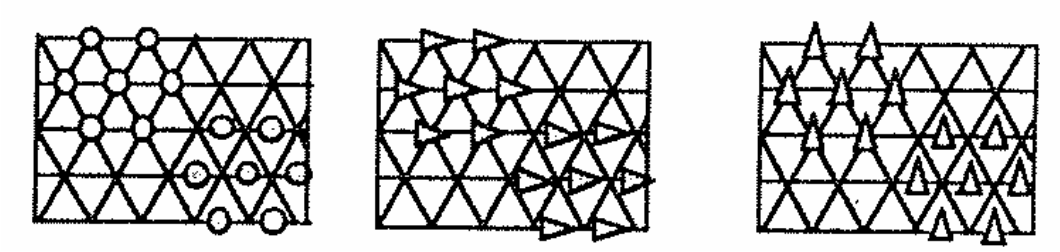

SmB SmI SmF

Figure 1-22. Plan views of the molecular organization with in the SmB, SmI and SmF mesophase structures. The tilt direction is depicted by the direction of the 'triangular' molecules。Reproduced from reference 29.

1.2 Liquid Crystal Photoswitches and Photochromic Systems

1.2.1 Liquid Crystal Photoswitches

Recently, considerable research efforts have focused on the development of ON-OFF LC light shutters triggered by light instead of an electric field. Such optically addressed LC switches have potential applications in optical computing, optical data

storage devices, dynamic holography, and photonics applications. The common requirement of all these applications is the control and manipulation of the flow of light by photons.

There are two general approaches to optically addressed LC switching: extrinsic and intrinsic. An *extrinsic* approach to optically addressed LC switching relies on a photoactive substrate on which the LC film is deposited. An *intrinsic* approach to optically addressed LC switching involves the incorporation of photochromic compounds into LC films. Compounds that can be interconverted photochemically between two forms are referred to as *photochromic* compounds. (Scheme 1-2) Typically, the two different states of the molecule have different UV-visible absorption spectra and often show differences in other physical and chemical properties.[30] The reverse reaction of a photochromic system can be triggered by light, but also frequently proceeds via a thermal (dark) pathway in the absence of light. Irradiation with the appropriate wavelength of light can induce a change at the molecular level that translates into a change in the bulk properties of the liquid crystal film. Such a change in bulk properties can, under the appropriate conditions, result in a switching event.

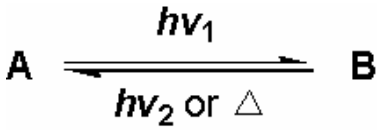

Scheme 1-2. Photochemical conversion from one state to another, and thermal reversion to state A.

For a photochromic system to be useful in devices, there are a number of general requirements. First, it must be possible to photochemically switch between both forms. Second, both photoisomers should be thermally stable; *i.e.* no thermal interconversion of photoisomers should occur over a large temperature range. Third, both photoisomers should be detectable and, furthermore, the detection (or read-out) should be non-destructive. Fourth, photochemical switching should be fast and take place with a high quantum efficiency. Finally, the photoisomers should be highly fatigue resistant, allowing many switching cycles without any thermal or photochemical degradation.

These are important considerations for the development of photochromic systems for device applications. In the following section, examples of photochromic compounds will be briefly discussed in terms of the above considerations.

1.2.2 Examples of Photochromic Systems

Most photochromic compounds fall into three categories based upon the mechanism of switching between photoisomers. These general categories include systems that interconvert *via* a photoinduced *trans*- to *cis*- isomerization, via electrocyclic ring-opening/ring-closure reaction, and by migration of a functional group.[30] Examples of each of these types of photochromic reactions are given below.

Compounds that undergo *trans-cis* isomerization upon irradiation include stilbenes, azobenzene, and thioindigo compounds (Figure 1-23). Both stilbenes and azobenzene absorb ultraviolet light to undergo isomerization about the central C-C double bond. In both types of compounds, the *trans* form is generally more stable than the *cis* form, which reverts thermally to the *trans* form on time scales ranging from milliseconds to months depending upon the particular system.[31] Thioindigo dyes and other indigoids undergo *trans-cis* photoisomerization upon irradiation with visible light. The *cis* form typically absorbs at shorter wavelengths, and also reverts thermally to the thermodynamically more stable *trans* isomer.

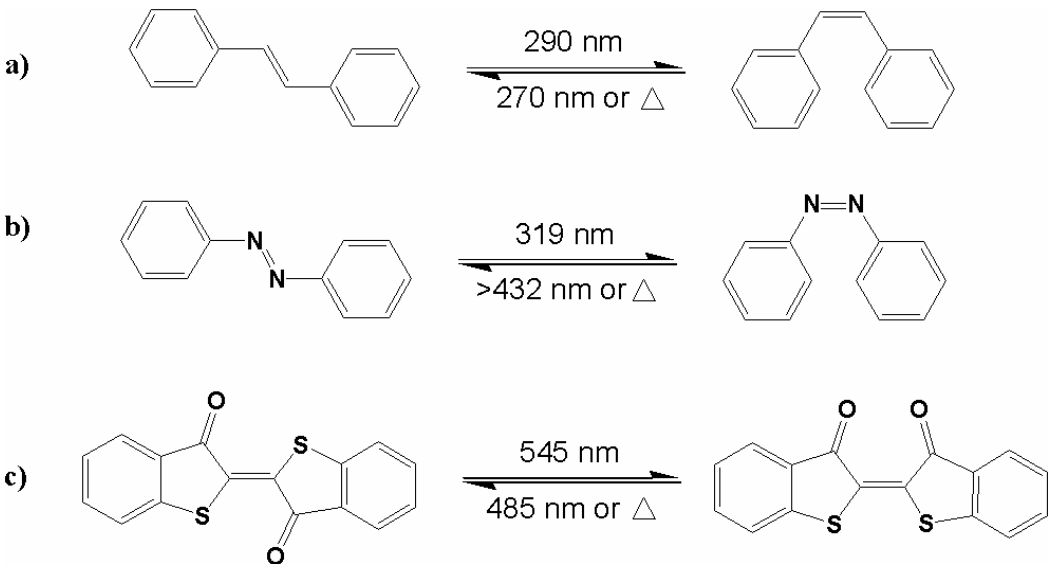

Figure 1-23. Examples of photochromism via *trans-cis* isomerization in a) stilbene, b) azobenzene and c) thioindigo.

Compounds that undergo a photoinduced ring-opening/ring-closure reaction include fulgides, diarylethenes, dihydroazulenes and spiropyrans (Figure 1-24). Upon UV

irradiation, furyl fulgides are converted to ring-closed dihydrobenzo[b]furans via symmetry-allowed conrotatory electrocyclic ring closure. Some ring-closed isomers are thermally stable and can only be converted back to the ring-open fulgide photochemically with visible light.[32] The photochromism of fulgides will be described in further details in following sections. Diarylethenes such as substituted 1,2-dithienylethenes undergo a similar photocyclization with UV light to the ring-closed form and can be converted back to the ring-opened form by visible irradiation.[33] This class of photochromic materials has great potential in applications since both isomeric forms are generally thermally stable, and the photochromic cycle can be repeated many times without degradation. Dihydroazulenes are converted to vinylheptafulvenes by UV irradiation *via* a 10-electron electrocyclic ring-opening.[34] Interestingly, the reverse reaction back to the ring-closed azulene form only takes place thermally. Spiropyrans undergo reversible heterolytic ring-opening to the colored merocyanine form upon UV irradiation.[35] Reversion back to the spiropyran form can be achieved photochemically with visible light or thermally. Limitations of spiropyran systems include low thermal stability of the open form, photochemical side reactions and low fatigue resistance.

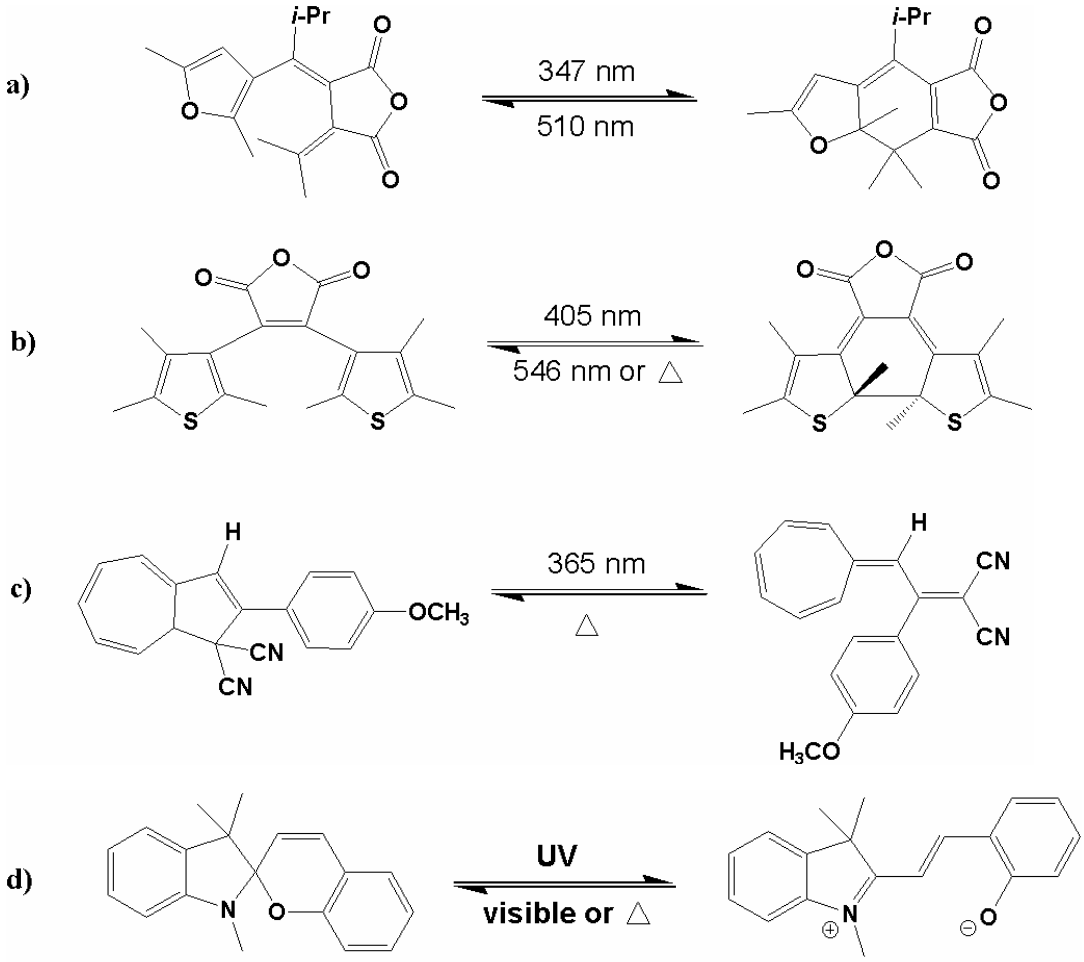

Figure 1-24. Examples of photochromism by ring-opening/ring-closure in a) fulgides, b) diarylethenes, c) dihydroazulenes, and d) spiropyrans.

The final category of photochromic compounds are those which involve photoinduced migration of a proton or functional group. Examples of these include photochromic quinines (Figure 1-25).

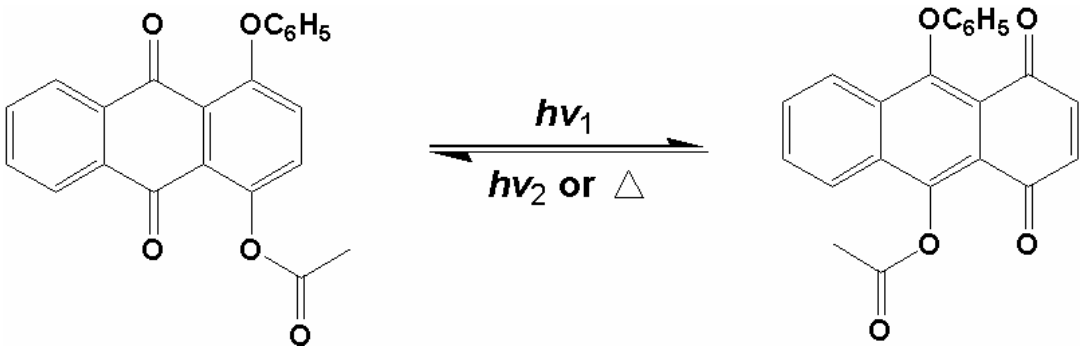

Figure 1-25. Example of photochromism by migration of functional groups in a quinine derivative.

1.3 Photochromic Fulgide and Fulgimide

In 1905, Stobbe first discovered the photochromism of some phenyl-substituted bismethylene succinic anhydrides in the solid state and named them fulgides. The general structure of fulgides is shown in Scheme 1-3.[36] To be photochromic, at least one of the four substituent groups on the fulgide must be an aromatic ring. Subsequently, the related imide derivatives were introduced and named as fulgimide by Heller *et al.* in 1968 (Scheme 1-2).

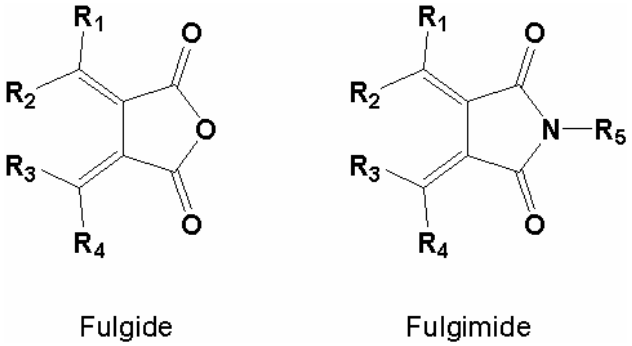

Scheme 1-3

Fulgides like **1** (Scheme 1-4) were shown to undergo thermally reversible cyclization, with some irreversible side reactions.[37] In 1981, Heller *et al.* reported that the ring-closed form of the furylfulgide **2** (Scheme 1-4) does not revert to the ring-opened form via a thermal pathway.[38,39] In addition, the ring-opened form showed few side reactions (hydrogen migration and oxidation to generate an aromatic ring became impossible) and exhibited a high photoconversion to the ring-closed form. This was the first reported example of a thermally bistable photochromic compound. The important modifications to the basic fulgide structure to give **2** were the replacement of all the hydrogen atoms on the photocyclizing carbon framework by methyl groups, and the replacement of the phenyl group by a heterocyclic furan group. By virtue of the bistability afforded by thermal irreversibility, fulgides have long been regarded as prime candidates for photon-mode optical recording materials.[40,41, 42] In addition, fulgides have been used as prototypes to demonstrate the potential applicability of photoswitchable functional materials.

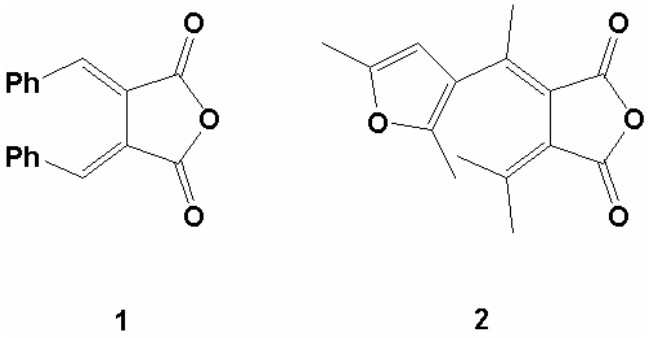

1 2

Scheme 1-4

In general, fulgides exist in three isomeric states as Z-, E- and C- forms (Scheme 1-5).[43] The photochromism of fulgides occurs between the E-forms (the geometry of the double bond connecting the aromatic ring and the succinic anhydride is usually E) and the C-forms. Typical absorption spectra of the E and C forms of fulgide is shown in Figure 1-26. Upon irradiation of the generally colorless (or faintly colored) E-form with UV light, an electrocyclic ring-closure reaction occurs to give the colored C-form. The C-form is almost planar and its extended π-electron system results in a strong and broad absorption band in the visible wavelength range. By exposure to visible light, the reverse reaction to E-forms is achieved. However, there is an additional photochemical E-Z isomerization pathway. The E- and Z-forms can be interconverted reversibly by irradiation with UV light, and both have similar optical properties. The *Z*-form is not considered as an important member of the photochromic system. There has been no report that the *Z*-form cyclizes directly to the C-form by absorbing a single photon.

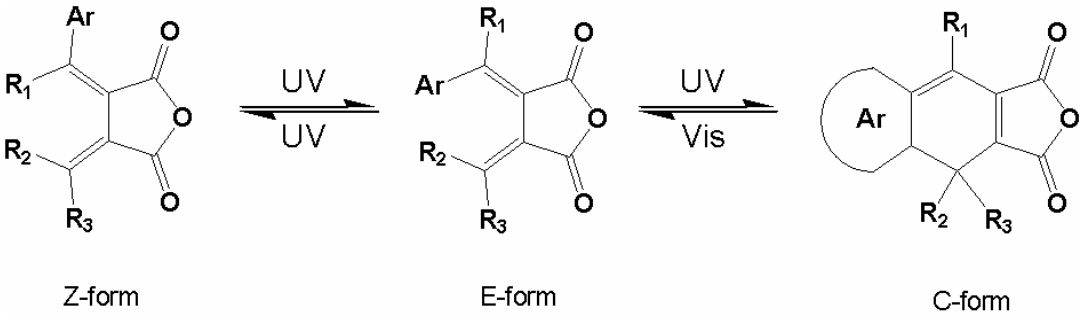

Scheme 1-5

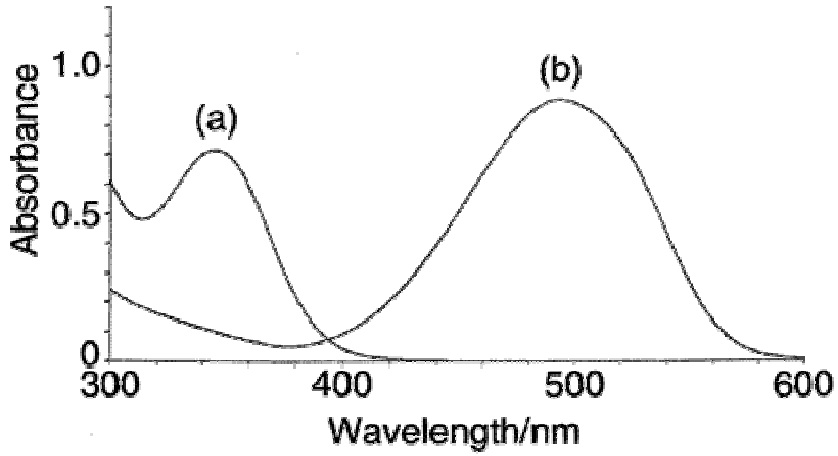

Figure 1-26. Absorption spectra of fulgide: (a) E-form and (b) C-form. Reproduced from Ref. 43.

1.3.1 Mechanism of Fulgide Photochromism

In 1968, Santiago and Becker suggested that the photochromic reaction of fulgide **1** was an intramolecular photocyclization reaction forming a 1,8a-dihydronaphthalene (1,8a-DHN) derivative, as shown in Scheme 1-6.[44] This was further confirmed by later studies of Heller who reported in 1972 and 1974 that the photochromic reaction is an electrocyclic reaction, i.e. the colored form arises from a conrotatory ring closure in accord with the Woodward-Hoffmann selection rules.[45] Heller and Megit also proposed that the photocyclization reaction occurs via a n $\rightarrow$ π^* excitation of one of the carbonyl chromophores in the fulgide molecule. However, in 1986, Becker studied phenyl-substituted fulgides by microsecond and nanosecond laser flash photolysis techniques, and suggested that the photocyclization is caused by $\pi \rightarrow \pi^*$ excitation rather than n $\rightarrow$ π^* excitation, i.e. an excited singlet state $S_1(\pi, \pi^*)$ is the starting point for photochemical

ring closure.[46] Picosecond laser photolysis studies on a furyl fulgide confirmed Becker's statement.[47] In 1992, Zhao *et al.* studied the photochromic mechanism of a pyrryl-substituted fulgide. Their results suggest that the photocyclization of the fulgide does not proceed solely via a concerted reaction, in which the excited singlet state is the starting point for the photocoloration reaction, but also via a stepwise reaction. In other words, the excited triplet state and some intermediates may also be involved.[48]

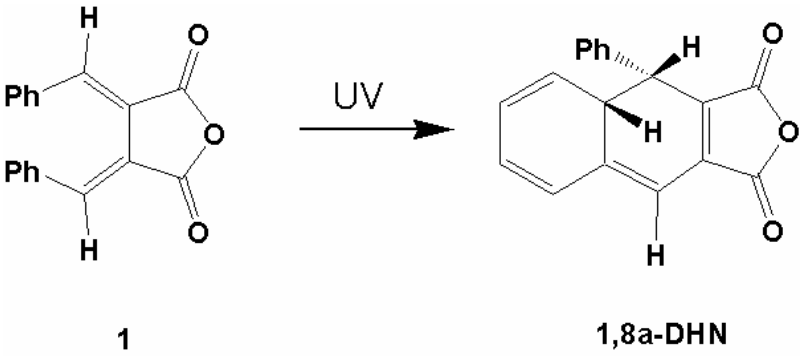

Scheme 1-6

1.3.2 Substituent Effects on the Photochromism of Fulgides

Changes in the molecular structures of fulgides can have dramatic effects on the quantum yield of their photoinduced ring-closure and ring-opening reactions.

1.3.2.1 Steric Effects

The photochromism of fulgides is a reversible photochemical electrocyclization. It requires that three conjugated double bonds lie in an *s-cis-cis-cis* conformation so that the carbon atoms that form the C-C single bond upon photoirradiation are in close proximity.

Therefore, the conformation of fulgides in their ground state influences the quantum yield of photocyclization. One of the factors that governs the conformation is the steric bulk about the hexatriene moiety.

For example, Yokoyama *et al.* examined the steric influence of the alkyl group on the methylene carbon next to the furan ring.[49,50,51] As summarized in Table 1-1, the ring-closing quantum yield upon UV irradiation (Φ_{EC}) became larger and the E-to-Z isomerization quantum yield (Φ_{EZ}) became smaller when the size of the alkyl group was increased. In the case of fulgides with an isopropyl (**6**)[49,50] or *tert*-butyl (**7**)[52] group as the R substituent (Scheme 1-7), E-to-Z photoisomerization was not observed.

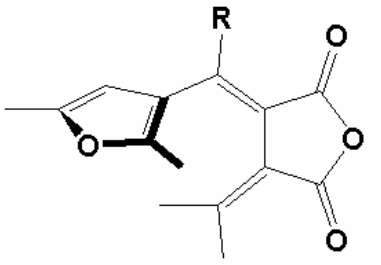

3E. R=Me **4E.** R=Et
5E. R=*n*Pr **6E.** R=*i*Pr
7E. R=*t*Bu

Scheme 1-7

Table 1-1. Quantum Yields of Photoreactions of Furylfulgides. From reference 49-51.

Cpd	Solvent	Φ_{EC}	Φ_{EZ}
3	toluene	0.18	0.13
4	chloroform	0.34	0.06
5	chloroform	0.45	0.04
6	toluene	0.58	0.00
7	toluene	0.79	0.00

1.3.2.2 Electronic Effects

A change of the electronic properties of fulgides generally results in a shift of the absorption bands of both isomers. For example, the introduction of electron-donating substituents such as methoxy, methylthio, and dimethylamino groups at the 5-position of the indole ring of indolylfulgides (Scheme 1-8) resulted in significant shift of the absorption band of the *C*-forms to longer wavelength (Figure 1-27).[53,54]

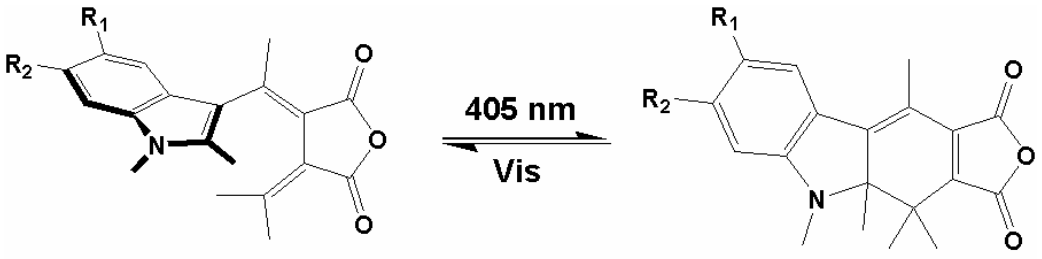

8. R_1=H, R_2=H **9.** R_1=SMe, R_2=H **10.** R_1=OMe, R_2=H
11. R_1=NMe_2,R_2=H **12.** R_1=H, R_2=OMe **13.** R_1=OMe, R_2=OMe

Scheme 1-8

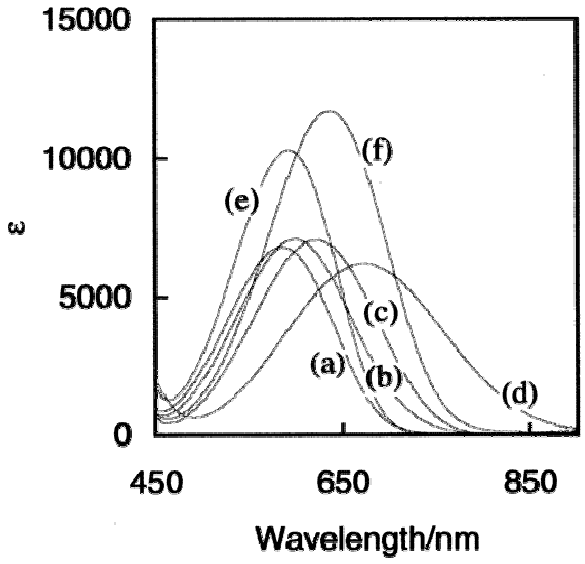

Figure 1-27. Absorption spectra of substituted indolylfulgides in toluene: (a) **8C**, (b) **9C**, (c) **10C**, (d) **11C**, (e) **12C**, and (f) **13C**. Reproduced from Ref. 43.

1.3.3 Comparison of Fulgides and Fulgimides

A comparison of various heteroaromatic fulgides and fulgimides was undertaken by Tomoda *et al.* and Matsushima *et al.*[55,56] It was found that fulgimides have photochromic properties similar to those of corresponding fulgides, and the absorption bands show hypsochromic shifts.

While fulgides generally undergo degradation in solution, fulgimides show high resistance to solvolytic degradation in hydroxylic media. However, it was shown that the *N*-benzylfulgimide **14** (Scheme 1-9) is less fatigue resistant than the corresponding fulgide **2**.

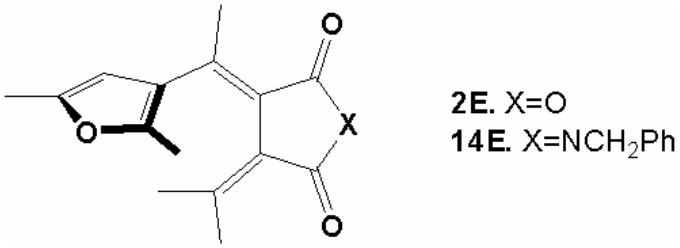

Scheme 1-9

The imide structure of fulgimides allows for the convenient introduction of another substituent at the imide nitrogen, which does not result in significant change of photochromic properties. Hence, fulgimides have been modified by introducing polymers side-chains,[57] fluorescent groups for control of fluorescence,[58] and proteins for regulation of substrate binding[59]. If a long alkyl chain is attached to the imide nitrogen, the resulting fulgimide should be more compatible with liquid crystal hosts than the corresponding fulgide.

1.3.4 Fulgides and Fulgimides as Liquid Crystal Photoswitches

Several groups have attempted to design liquid crystal photoswitches based on fulgides or fulgimides. Ringsdorf *et al.* prepared the liquid crystalline methacrylic and acrylic copolymers **15** and **16** (Scheme 1-10), using monomers having non-mesogenic

fulgimide and mesogenic phenyl benzoate units, and observed that the photochromic properties of the fulgimide unit were preserved in polymer films.[59] Irradiation with UV light to convert the E-form to the C-forms resulted in a higher clearing point of the mesophase. Based on this photoinduced effect, an optically stored image of a photomask was observed by polarized microscopy.

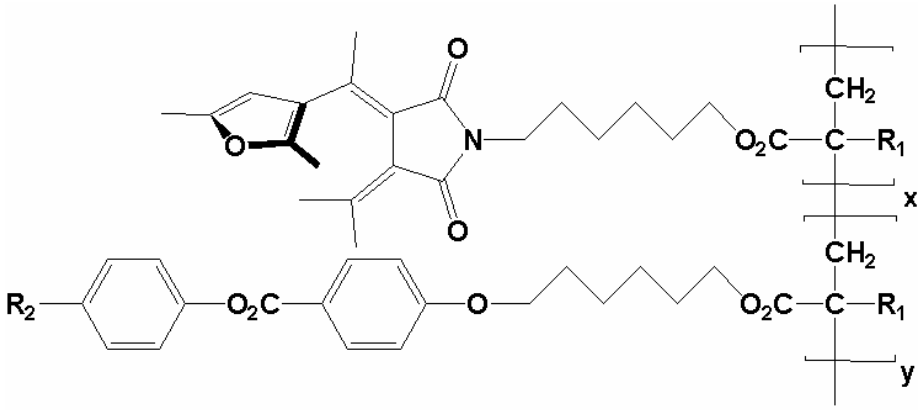

15E. R_1=H, R_2=CN
16E. R_1=Me, R_2=OMe

Scheme 1-10

Gleeson *et al.* mixed the furylfulgide **2** and the thienylfulgide **17** (less than 2% w/w) in the nematic liquid crystal E7 (a mixture of four cyanobiphenyls) (Scheme 1-11) and investigated the changes in phase transition temperature, refractive index and order parameter of the mixture upon photocyclization.[61] Although they had expected a large change of the above properties, little change was observed upon photocyclization. They also examined the change in dielectric and elastic constants upon irradiation of the mixture of **17** (2% w/w) and E7.[62] Their results showed that photocyclization of the

fulgide did not change the elastic constants of the mixture, but did cause a distinct change in the dielectric constant of the mixture. It was found that the change is mostly due to the difference in clearing points between the irradiated and non-irradiated mixtures, and that no significant change was observed when they were compared at the same "reduced temperature", i.e., the same temperature difference relative to the clearing point.

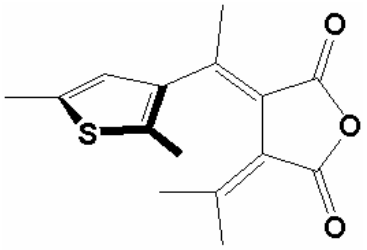

17E

Scheme 1-11

Schuster *et al.* reported that the pitch of a chiral nematic liquid crystal can be altered by the photochromism of a fulgide dopant.[63] They added the indolylfulgide **8** (5.2% w/w) to a chiral nematic liquid crystal formed by a mixture of the chiral cyclic ether ***(R)*-18** (1.35% w/w) and the nematic liquid crystal 5CB (Scheme 1-12). Alternating irradiation of this mixture with visible and UV light produced a reversible change in chiral nematic pitch from 30 to 42μm. In addition, the photochromic states of the mixture were thermally stable under the conditions tested, and the mixture did not show fatigue during the course of the experiments.

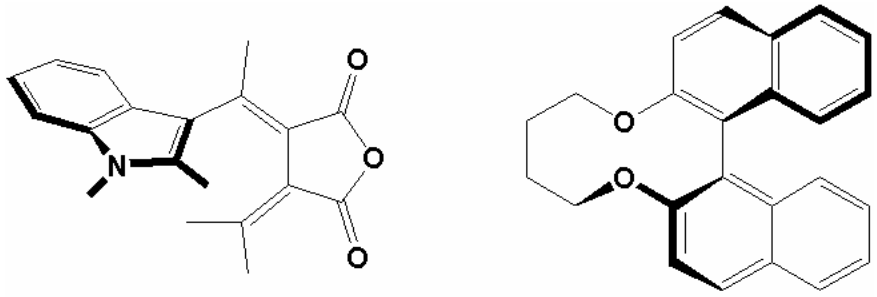

8E ***(R)*-18**

Scheme 1-12

Yokoyama *et al.* showed that doping either the (*R*)-binaphthol-condensed indolylfulgides **19** or **20** or an enantiomer of resolved indolylfulgide **21** in **5CB** resulted in the formation of a chiral nematic phase (Scheme 1-13). Irradiation of the dopants **19** and **20** resulted in a dramatic and reversible change in helical pitch.[64,65] For example, with only 1.1 mol % **19** present, photocyclization caused a change of pitch from 15.8 to 2.6μm, at the photostationary state. The change in pitch was reproducible, as shown in Figure 1-28. Interestingly, the resolved indolylfulgide **(P)-21** produced much smaller changes in pitch than **19** and **20**, and the helical pitch sense of **(P)-21** was different from **19** and **20**, although the helicity of the fulgide core was the same.

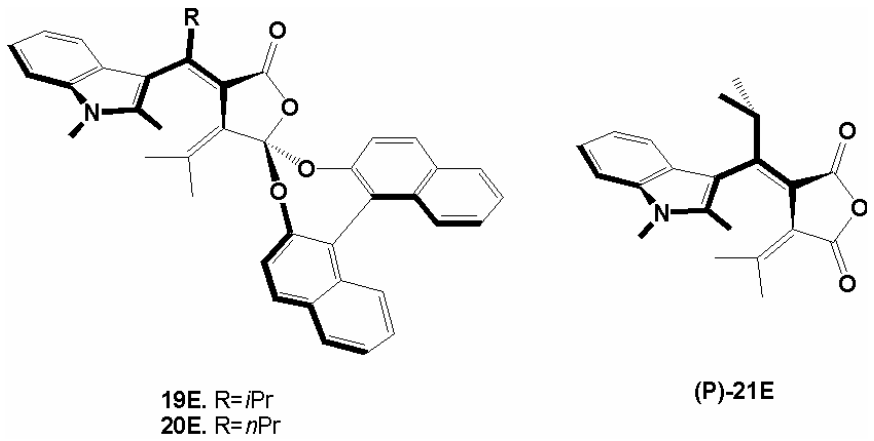

Scheme 1-13

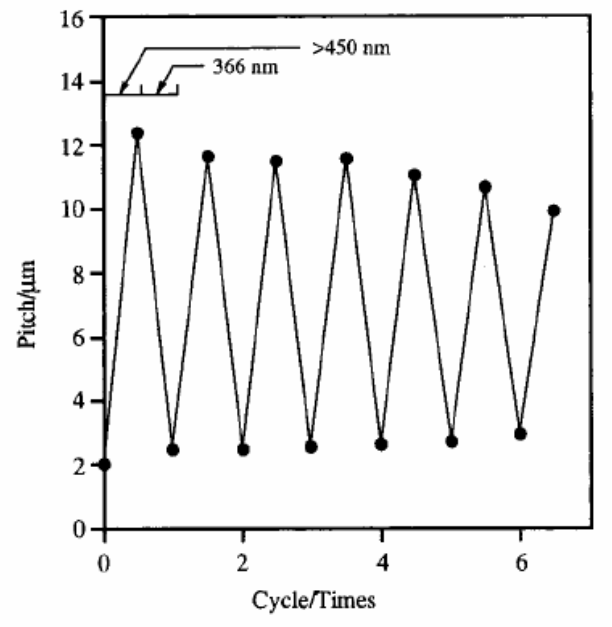

Figure 1-28. Reversible changes of the cholesteric pitch of a mixture of **5CB** and **20**, by photochromism of **20**.

1.4 Improving Compatibility of Photochromic Dopants with Liquid Crystal Hosts Using Siloxane End-groups

In some cases, the compability of a photochromic dopant with a liquid crystal host is very poor. For example, previous studies in the Lemieux group showed that the phase

diagrams of phenylpyrimidine and phenyl benzoate smectic liquid crystals doped with the non-mesogenic dithienylethene **22** (Scheme 1-14) have broad smectic/isotropic biphasic regions at dopant mole fractions greater than 3 mol%.[66] In principle, dopant-host compatibilization can be achieved by introducing the non-mesogenic molecule as a side-chain in a liquid crystalline copolymer. In such cases, compatibility is attained at the expense of electrooptic switching performance because polymeric liquid crystal materials tend to have higher viscosities and are more difficult to align than low-molecular-weight liquid crystal materials.

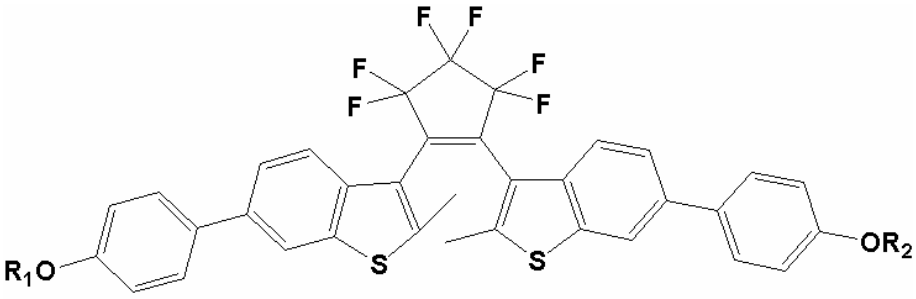

22. R_1, $R_2=C_7H_{15}$

23. $R_1=$ —Si(CH$_3$)$_2$—O—Si(CH$_3$)$_2$—(CH$_2$)$_{11}$—, $R_2=C_7H_{15}$

Scheme 1-14

A compromise solution to this problem was described by Coles and co-workers using low-molecular weight LC materials terminated with short siloxane oligomers.[67,68] The addition of oligomeric siloxane end-groups to mesogenic materials has been shown to promote lamellar organization and the formation of smectic phases due to the tendency of siloxane and paraffinic moieties to nanosegregate into distinct sublayers within a

lamellar structure (Figure 1-29). The formation of this so-called "virtual siloxane backbone" confers some of the mechanical stability of side-chain polysiloxane LC materials to low molecular weight organosiloxane LC materials without significantly compromising their electro-optical switching performance and ease of alignment.

Hence, dye molecules bearing a siloxane end-group can be doped into an organosiloxane liquid crystal host in relatively high concentrations by behaving like a pendant group on a side-chain polysiloxane liquid crystal (Figure 1-29). One advantage of this approach over conventional side-chain polysiloxanes is that the dye molecule is ''grafted'' on the virtual backbone simply by mixing the organosiloxane materials. For example, Coles showed that addition of a trisiloxane end group to a non-mesogenic dichroic dye such as 4-hydroxy-4'-nitrostilbene, **24** (Scheme 1-15) gives a liquid crystalline material with SmA and SmC phases which forms homogeneous mixtures with organosiloxane LC hosts over a wide range of concentrations.[69]

Following Cole's approach, previous work in the Lemieux group focused on the addition of a siloxane end-group to diarylethene compounds in order to improve their compability with siloxane-terminated liquid crystal hosts. Various diarylethene compounds (with or without siloxane end-groups, compounds **22**, **23, 25-28**, Scheme 1-14, 1-16) were doped into **Br11-Si$_3$**,[70] and phase diagrams were constructed in order to evaluate the effect of the siloxane end-group on the compatibility between dopants and

the LC host (see Figure 1-30). However, all phase diagrams indicate that the dithienylethene dopants (with or without siloxane end-groups) are incompatible with siloxane-terminated hosts, and the compounds with siloxane end-groups are actually somewhat less compatible than compounds without siloxane end-groups. This incompatibility is attributed to the significant lateral bulk of the diarylethene core, which in turn strongly destabilizes the layer structure of the SmC phase. The marginally better solubility of the dopants without siloxane end-groups has been attributed to a higher degree of out-of-layer fluctuations, which can relieve the unfavourable core-core interactions. (Figure 1-31)

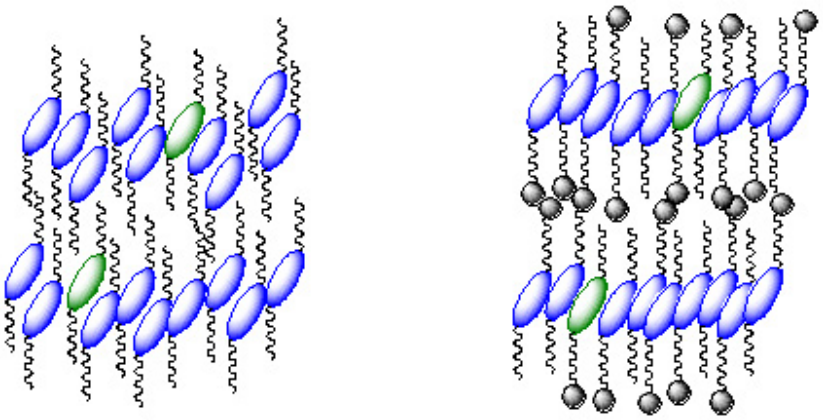

Figure 1-29. A combination of dopant and smectic host molecules terminated with short siloxane oligomers (circles) is known to significantly increase the miscibility and promote the formation of lamellar smectic phases due to the tendency of siloxane and paraffinic groups to nanosegregate into distinct sublayers. Blue: host molecules; Red: dopant molecules.

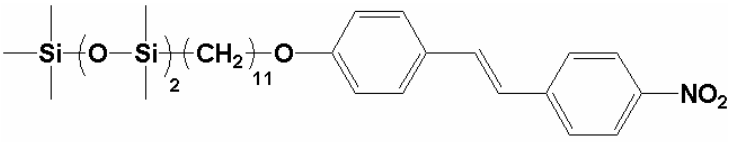

NO_2-11-Si_3

24

Scheme 1-15

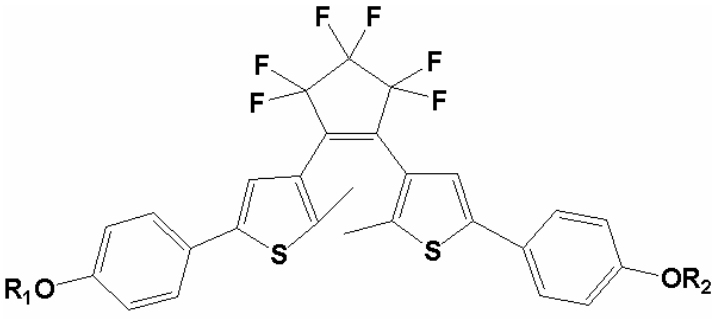

25. R_1, R_2=C_7H_{15}

26. R_1= 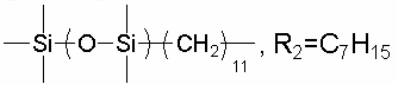 , R_2=C_7H_{15}

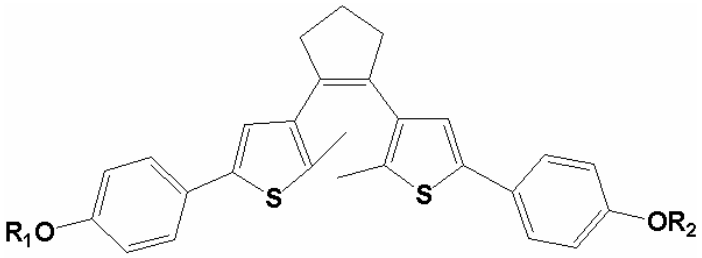

27. R_1, R_2=C_7H_{15}

28. R_1= 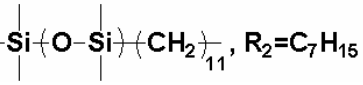 , R_2=C_7H_{15}

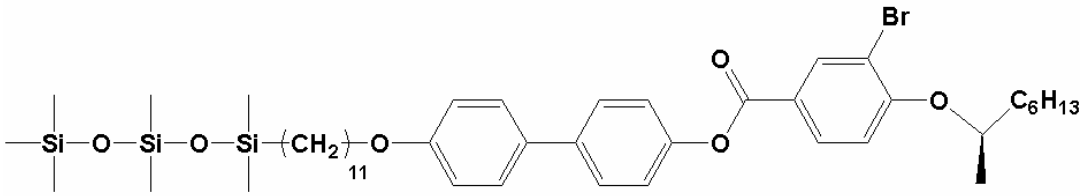

Br11-Si_3 Cr 42 SmC* 89 I

Scheme 1-16

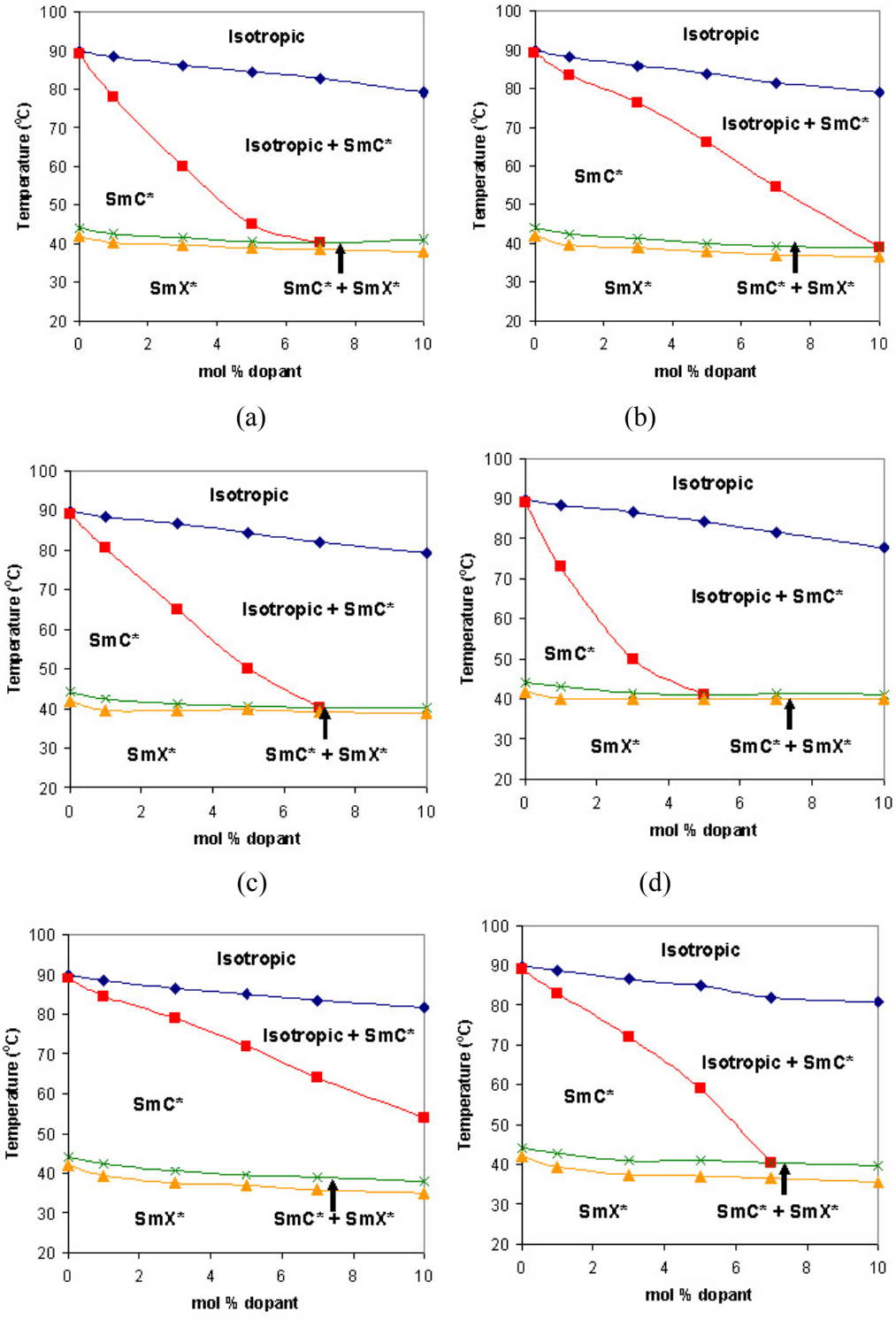

Figure 1-30. Phase diagrams of compound **22**(a), **23**(b)**, 25**(c)**, 26**(d)**, 27**(e), and **28**(f) in **Br11-Si$_3$**.

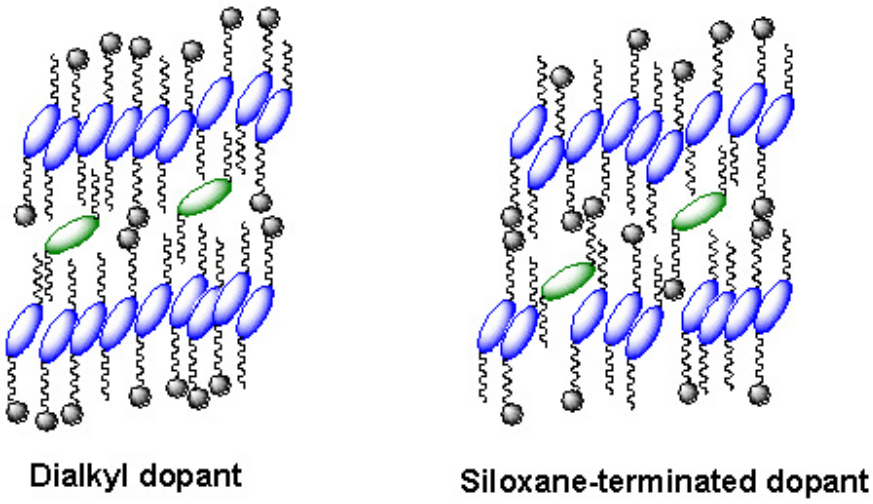

Figure 1-31. The dopants without siloxane end-groups should have a higher degree of out-of-layer fluctuations, which can relieve the unfavourable core-core interactions.

Bistable photochromic compounds which have a smaller core size relative to diarylethene may solve the compatibility problem. Fulgimide are such compounds and therefore siloxane-terminated fulgimide dopants are expected to have a better compatibility with siloxane-terminated liquid crystal hosts.

1.5 Outline of Research Project

The first goal of this thesis is to design smectic liquid crystal hosts and photochromic dopants terminated with short siloxane oligomers, in order to produce homogeneous liquid crystal mixtures containing a photochromic component for ferroelectric liquid crystal photoswitches. Based on the notion that nanosegregation of siloxane end-groups may also promote the formation of 'de Vries'-type SmA phases, the siloxane-terminated liquid crystal hosts reported herein were also assessed in term of their layer contraction

from the SmA to SmC phase in an effort to minimize the formation of chevrons and zigzag defects that severely degrade the quality of electro-optic devices.

Surprisingly, despite the ubiquitous nature of phenylpyrimidine liquid crystals in liquid crystal mixture formulations, examples of siloxane-terminated phenylpyrimidine mesogens have yet to be reported. The first section focuses on the synthesis and characterization of siloxane-terminated phenylpyrimidine liquid crystal hosts, and the effect of 1) variation of chain length, 2) variation of number of siloxy units 3) exchanging positions of chains, and 4) addition of a terminal halogen atom to the alkyloxy chain on the phase behaviour of siloxane-terminated phenylpyrimidine liquid crystals (compound series **29** to **34**, Scheme 1-17). Techniques such as differential scanning calorimetry, polarized microscopy and X-ray powder diffraction were used to characterize the LC phases.

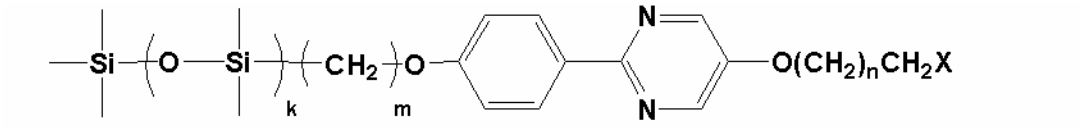

29. **a.** n=3, m=11, k=2, X=H; **b.** n=6, m=11, k=2, X=H; **c.** n=7, m=11, k=2, X=H
d. n=8, m=11, k=2, X=H; **e.** n=9, m=11, k=2, X=H; **f.** n=11, m=11, k=2, X=H
30. **a.** n=3, m=6, k=2, X=H; **b.** n=6, m=6, k=2, X=H; **c.** n=7, m=6, k=2, X=H
d. n=8, m=6, k=2, X=H; **e.** n=9, m=6, k=2, X=H; **f.** n=11, m=6, k=2, X=H
31. n=3, m=11, k=1, X=H
33. **a.** n=7, m=11, k=2, X=Cl; **b.** n=7, m=6, k=2, X=Cl; **c.** n=7, m=6, k=2, X=Br;

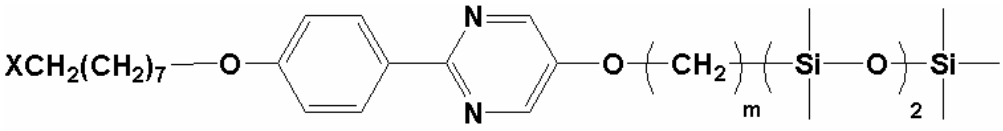

32. **a.** m=11, X=H; **b.** m=6, X=H
34. **a.** m=11, X=Cl; **b.** m=6, X=Cl

Scheme 1-17

Next, as an extension of results of the first project, we studied the properties of siloxane-terminated liquid crystals with the biphenyl benzoate and phenyl benzoate cores. Using differential scanning calorimetry, polarized microscopy and X-ray powder diffraction, we investigated the effect of the same structural variations as in the phenylpyrimidine series (compound series **35** to **40,** Scheme 1-18).

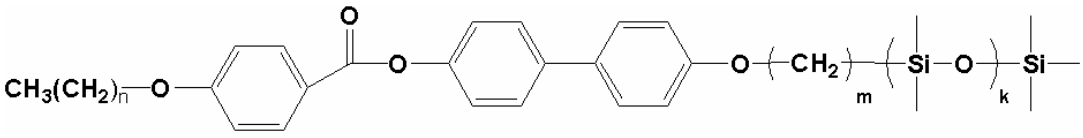

35. a. n=3, m=11, k=2; **b.** n=6, m=11, k=2; **c.** n=7, m=11, k=2;
d. n=8, m=11, k=2; **e.** n=9, m=11, k=2; **f.** n=11, m=11, k=2.
36. n=7, m=6, k=2.
37. n=7, m=11, k=1.

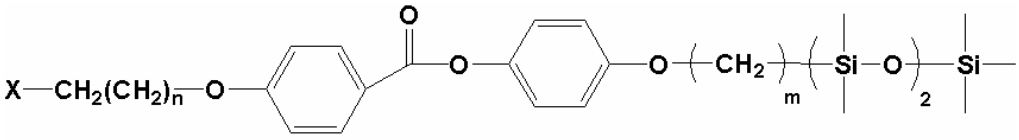

38. n=7, m=11, X=H;
39. a. n=7, m=6, X=H; **b.** n=8, m=6, X=H ; **c.** n=9, m=6, X=H;
d. n=11, m=6, X=H.
40. a. n=7, m=11, X=Cl; **b.** n=7, m=6, X=Cl.

Scheme 1-18

Finally, siloxane-terminated fulgides and fulgimides were designed as dopants in an attempt to improve solubility into siloxane-terminated LC hosts. Compound **41** was designed and synthesized successfully in 12 steps (Scheme 1-19). However, this compound proved to be an oil at room temperature, which made it difficult to purify and unsuitable for mixing with liquid crystal hosts. The low melting point of compound **41** was attributed to a combination of the siloxane tail and long alkyl chain in the compound. We therefore turned our attention to the fulgide precusors **42, 43a** and **44b** which are solids at room temperature (Scheme 1-19). One of the key requirements of photochromic system for the development of a liquid crystal photoswitch is that fast switching must be achieved, so the photochemical process must occur rapidly and with high quantum

efficiency. Compound **42**, **43a** and **44b** were assessed as photochromic dopants in terms of this requirement, and their photophysical properties were studied in solution using HPLC and UV-vis spectroscopy.

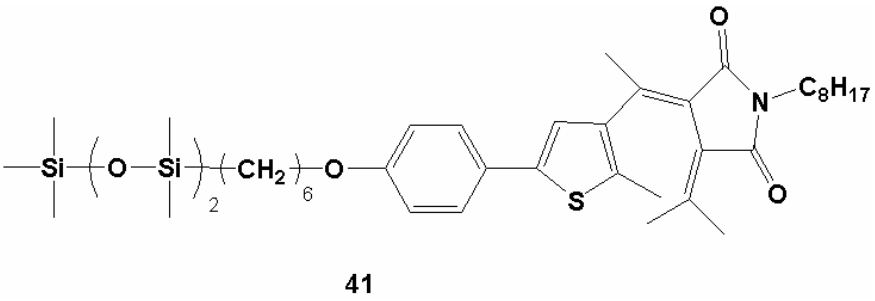

41

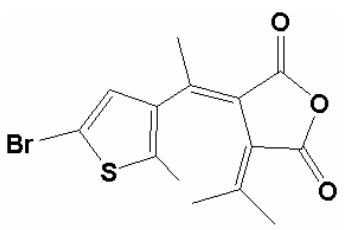

42

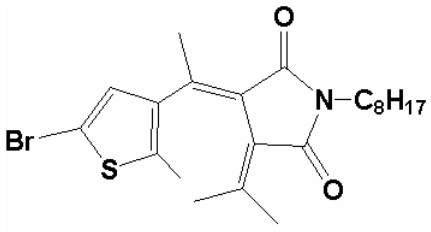

43a

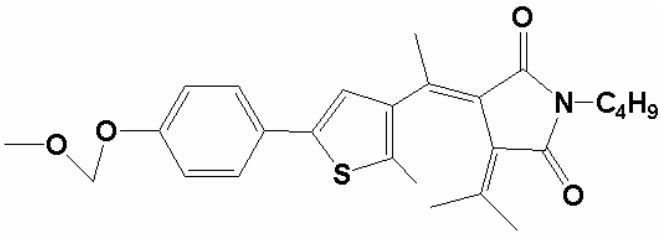

44b

Scheme 1-19

1.6 References

(1) Reinitzer, F. M.; *Chem* **1888**, 9, 421.

(2) *Handbook of Liquid Crystals.*; Kelker, H.; Hatz, R.; Verlag Chemie, Weinheim, Fed. Rep. Ger.; **1980**.

(3) Tschierske, C.; *J. Mater. Chem.* **1998**, 8, 1485.

(4) Demus, D.; *Chemical Structure and Mesogenic Properties, in Handbook of liquid Crystals: Fundamentals;* Demus, D., Goodby, J.; Gray, G. W.; Spiess, H. W.; Vill, V. Ed.; Wiley-VCH: New York, **1998**; Vol.1.

(5) Grandjean, F.; *Compt. rend. Acad. Sci. (Paris)* **1917**, 166, 165.

(6) Dierking, I.; Textures of Liquid Crystals; Dierking, I. Ed.; Wiley-VCH: New York, **2003**.

(7) Friedel, G. ; *Ann. Physique* **1922**, 18, 273.

(8) Walba, D. M.; Slater, S. C.; Thurmes, W. N.; Clark, N. A.; Handschy, M. A.; Supon, F.; *J. Am. Chem. Soc.* **1986**, 108, 5210.

(9) Lagerwall, P. F. J.; Giesselmann, F.; *ChemPhysChem* **2006**, 7, 20.

(10) Lagerwall, P. F. J.; Giesselmann, F.; Radcliffe, M. D.; *Phys. Rev. E* **2002**, 66, 031703.

(11) Selinger, V. J.; Collings, J. P.; Shashidhar, R.; *Phys. Rev. E* **2001**, 64, 061705.

(12) Rossle, M.; Zentel, R.; Lagerwall, J.; Giesselmann, F.; *Liq. Cryst.* **2004**, 31, 883.

(13) de Vries, A.; *J. Chem. Phys.* **1979**, 71, 25.

(14) de Vries, A.; Ekachai, A.; Spielberg, N.; *Mol. Cryst. Liq. Cryst. Lett.* **1979**, 49,143.

(15) Giesselmann, F.; Lagerwall, P. F. J.; Andersson, G.; Radcliffe, M. D.; *Phys. Rev. E* **2002**, 66, 051704.

(16) a) Gorkunov, V. M.; Osipov, A. M.; Lagerwall, P. F. J.; Giesselmann, F.; *Phys. Rev. E* **2007**, 76, 051706; b) Gorkunov, V. M.; Giesselmann, F.; Lagerwall, P. F. J.; Sluckin, J. T.; Osipov, A. M.; *Phys. Rev. E* **2007**, 75, 060701.

(17) a) Saunders, K.; Hernandez, D.; Pearson, S.; Toner, J.; *Phys. Rev. Lett.* **2007**, 98, 197801. b) Saunders, K.; *Phys. Rev. E* **2008**, 77, 061708.

(18) McMillan, W. L.; *Phys. Rev. A* **1973**, 8, 1921.

(19) Meyer, R. B.; McMillan, W. L.; *Phys. Rev. A* **1974**, 9, 899.

(20) Wulf, A.; *Phys. Rev. A* **1975**, 11, 365.

(21) Meyer, R.B.; Liebert, L.; Strzelecki, L.; Keller, P.; *J. Phys. (Paris) Lett.* **1975**, 36, L69.

(22) Clark, N. A.; Lagerwall, S. T.; *Appl. Phys. Lett.* **1980**, 36, 899.

(23) Handschy, M. A.; Clark, N. A.; *Appl. Phys. Lett.* **1982**, 41, 39.

(24) Kuczynski, W.; Stegemeyer, H.; *Chem. Phys. Lett.* **1980**, 70, 123.

(25) Stegemeyer, H.; Meister, R.; Hoffmann, U.; Sprick, A.; Becker, A.; *J. Mater. Chem.* **1995**, 5, 2183.

(26) Siemensmeyer, K.; Stegemeyer, H.; *Chem. Phys. Lett.* **1988**, 148, 409.

(27) Walba, D. M.; Slater, S. C.; Thusmes, W. N.; Clark, N. A.; Handschy, M. A.; Supon, F.; *J. Am. Chem. Soc.* **1986**, 108, 5210.

(28) Wand, M. D.; Vohra, R.; Walba, D. M.; Clark, N. A.; Shao, R.; *Mol. Cryst. Liq. Cryst.* **1991**, 202, 183.

(29) *An Introduction to Liquid Crystals: Chemistry and Physics.*; Collings, P.; Hird, M. Ed.; Taylor & Francis: London, **1997**.

(30) Crano, J. C.; Guglielmetti, R. J.; *Organic Photochromic and Thermochromic Compounds*; Katritzky, A. R.; Sabongi, G. J. Ed.; Plenum Press: New York, **1999**.

(31) Ross, D. L.; Blanc, J.; *Photochromism by Cis-trans Isomerization*; Brown, G. H. Ed.; Wiley-Interscience: New York, **1971**; Vol. III, pp471-556.

(32) Kurita, Y.; Goto, T.; Inoue, T.; Yokoyama, M.; Yokoyama, Y.; *Chem. Lett.* **1988**, 1049.

(33) Irie, M.; Mori, M. J.; *Org. Chem.* **1988**, 53, 803.

(34) Daub, J.; Knochel, T.; Mannschreck, A.; *Angew. Chem. Int. Ed. Engl.* **1984**, 23, 960.

(35) Ando, E.; Miyazaki, J.; Morimoto, K.; Nakahara, H.; Fukuda, K.; *Thin Solid Films* **1985**, 133, 21.

(36) Stobbe, H.; *Ber. Dtsch. Chem. Ges.* **1905**, 38, 3673.

(37) a) Heller, H. G.; Auld, D.; Salisbury, K.; *J. Chem. Soc. C* **1967**, 682. b) Hastings, J. S.; Heller, H. G.; Tucker, H.; Smith, K.; *J. Chem. Soc., Perkin Trans.*

1 **1975**, 1545. c) Heller, H. G.; Oliver, S.; Shawe, M.; *J. Chem. Soc., Perkin Trans. 1* **1979**, 154.

(38) Heller, H. G.; Oliver, S.; *J. Chem. Soc., Perkin Trans. 1* **1981**,197.

(39) Darcy, P. J.; Heller, H. G.; Strydom, P. J.; Whittall, J.; *J. Chem. Soc., Perkin Trans. 1* **1981**, 202.

(40) Heller, H. G.; *Spec. Publ., R. Soc. Chem., Fine Chem. Electron. Ind.* **1986**, 60, 120.

(41) Heller, H. G.; *Photochromics for the Future. In ElectronicMaterials, from Silicon to Organics*; Miller, L. S., Mullin, J. B., Ed.; Plenum Publishing: New York, **1991**; Chapter 31, pp 471.

(42) Feringa, B. L.; Jager, W. F.; de Lange, B.; *Tetrahedron* **1993**, *49*, 8267.

(43) Yokoyama, Y.; *Chem. Rev.* **2000,** *100,* 1717.

(44) Santiago, A.; Becker, S. R.; *J. Am. Chem. Soc.* **1968**, 90, 3654.

(45) Heller, G. H.; Szewczyk, M.; *J. Chem. Soc., Perkin. Trans. 1* **1974**, 1483.

(46) Lenoble, C.; Becker, S. R.; *J. Phys. Chem.* **1986**, 90, 2651.

(47) a) Ilge, -D. H.; Paetzold, R.; *J. Prake. Chem.* **1984**, 326, 705. b) Ilge, -D. H.; Kaschke, M.; Khechinashvili, D.; *J. Photochem.* **1986**, 33, 349.

(48) Zhao, W.; Ming, Y.; Zhu, Z.; Fan, M.; *J. Photochem. Photobiol. A: Chem.* **1992**, 63, 235.

(49) Yokoyama, Y.; Goto, T.; Inoue, T.; Yokoyama, M.; Kurita, Y.; *Chem. Lett.* **1988**, 1049.

(50) Yokoyama, Y.; Inoue, T.; Yokoyama, M.; Goto, T.; Iwai, T.; Kera, N.; Hitomi, I.; Kurita, Y.; *Bull. Chem. Soc. Jpn.* **1994**, 67, 3297.

(51) Yokoyama, Y.; Kurita, Y.; *Mol. Cryst. Liq. Cryst., Sect. A* **1994**, 246, 87.

(52) Kiji, J.; Okano, T.; Kitamura, H.; Yokoyama, Y.; Kubota, S.; Kurita, Y.; *Bull. Chem. Soc. Jpn.* **1995**, 68, 616.

(53) Yokoyama, Y.; Kurita, Y.; *Mol. Cryst. Liq. Cryst., Sect. A* **1994**, 246, 87.

(54) Yokoyama, Y.; Tanaka, T.; Yamane, T.; Kurita, Y.; *Chem. Lett.* **1991**, 1125.

(55) Tomoda, A.; Tsuboi, H.; Kaneko, A.; Matsushima, R.; *Nippon Kagaku Kaishi* **1993**, 209.

(56) Matsushima, R.; Sakaguchi, H.; *J. Photochem. Photobiol., A* **1997**, 108, 239.

(57) a) Deblauwe, V.; Smets, G.; *Makromol. Chem.* **1988**, 189, 2503. b) Cabrera, I.; Dittrich, A.; Ringsdorf, H.; *Angew. Chem., Int. Ed. Engl.* **1991**, 30, 76.

(58) Walz, J.; Ulrich, K.; Port, H.; Wolf, H. C.; Wonner, J.; Effenberger, F.; *Chem. Phys. Lett.* **1993**, 213, 321.

(59) a) Willner, I.; Rubin, S.; Wonner, J.; Effenberger, F.; Bauerle, P.; *J. Am. Chem. Soc.* **1992**, 114, 3150. b) Willner, I.; Lion-Digan, M.; Rubin, S.; Wonner, J.; Effenberger, F.; Bauerle, P.; *Photochem. Photobiol.* **1994**, 59, 491.

(60) Cabrera, I.; Dittrich, A.; Ringsdorf, H.; *Angew. Chem., Int. Ed. Engl.* **1991**, 30, 76.

(61) Allinson, H.; Gleeson, H. F.; *Liq. Cryst.* **1993**, 14, 1469.

(62) (a) Allinson, H.; Gleeson, H. F.; *Liq. Cryst.* **1995**, 19, 421. (b) Allinson, H.; Gleeson, H. F.; *J. Mater. Chem.* **1995**, 5, 2139.

(63) Janicki, S. Z.; Schuster, G. B.; *J. Am. Chem. Soc.* **1995**, 117, 8524.

(64) (a) Yokoyama, Y.; Sagisaka, T.; *Chem. Lett.* **1997**, 687. (b) Sagisaka, T.; Yokoyama, Y.; *Bull. Chem. Soc. Jpn.* **2000**, 73, 191.

(65) Yokoyama, Y.; Uchida, S.; Yokoyama, Y.; Sagisaka, T.; Uchida, Y.; Inada, T.; *Enantiomer* **1998**, 3, 123.

(66) Maly, K.; Synthesis and characterization of photochromic thioindigo and dithienylethene dopants designed to photomodulate the spontaneous polarization of ferroelectric liquid crystals; Ph.D. Thesis; Published: Kingston, Ontario: **2002**.

(67) Shoosmith, E. D.; Remnant, A.; Perkins, S. P.; Coles, H. J.; *Ferroelectrics* **2000**, 243, 75.

(68) Robinson, K. W.; Carboni, C.; Kloess, P.; Perkins P. S.; Coles, J. H.; *Liq. Cryst.* **1998**, 25, 301.

(69) Shoosmith, D.; Carboni, C.; Perkins, S.; Meyer, S.; Coles, J. H.; *Mol. Cryst. Liq. Cryst.* **1999**, 331, 181.

(70) a) Maly, E. K.; Zhang, P.; Wand, D. M.; Buncel, E.; Lemieux, P. R.; *J. Mater. Chem.* **2004**, 14, 2806. b) Maly, E. K.; Wand, D. M.; Lemieux, P. R.; *J. Am. Chem. Soc.* **2002**, 124, 7898. c) Zhang, P.; Buncel, E.; Lemieux, P. R.; *Adv. Mater.* **2005**, 17, 567.

Chapter 2. Design and Synthesis of Siloxane-terminated Phenylpyrimidine Liquid Crystals

2.1 Siloxane-terminated phenylpyrimidine liquid crystals

2.1.1 Synthesis

All siloxane-terminated phenylpyrimidine liquid crystals were prepared by sequential alkylations of 2-(4-hydroxyphenyl)-5-pyrimidinol. As shown in Scheme 2-1, the synthesis of compounds **29a-f** and **30a-e** began with the selective alkylation of 2-(4-hydroxyphenyl)-5-pyrimidinol under basic conditions to give the 2-(4-hydroxyphenyl)-5-alkoxypyrimidine precursors **46a-f** in 61–65% yield. The siloxane-terminated alcohols **45a-c** were prepared from 10-undecen-1-ol and 5-hexen-1-ol via a platinum-catalyzed hydrosilation reaction using 1,1,1,3,3,5,5-heptamethyltrisiloxane or 1,1,1,3,3-pentamethyldisiloxane and either dicyclopentadienylplatinum(II) chloride or Karstedt's catalyst (platinum(0)-1,3-divinyl-1,1,3,3-tetramethyldisiloxane complex) in 80–95% yield, and then combined with **46a-f** via a Mitsunobu reaction to give **29a-f** and **30a-e** in yields ranging from 46 to 52%. The 'inverted' phenylpyrimidine liquid crystals **32a** and **32b** were prepared by simply reversing the alkylation sequence shown in Scheme 2-2. All compounds were recrystallized from EtOH prior to mesophase characterization.

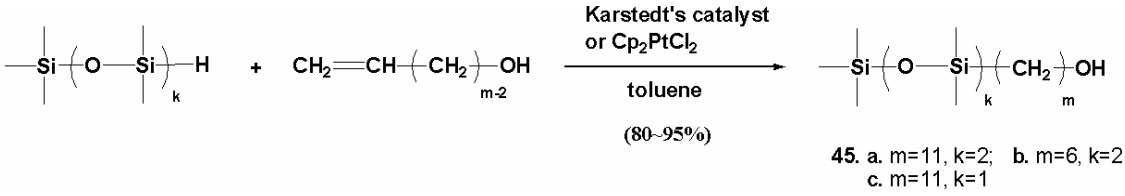

45. **a.** m=11, k=2; **b.** m=6, k=2
c. m=11, k=1

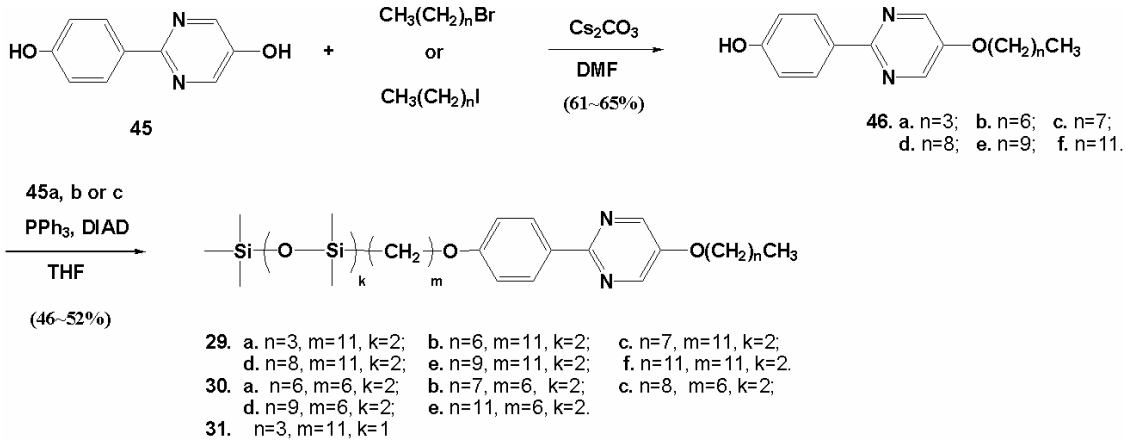

46. **a.** n=3; **b.** n=6; **c.** n=7;
d. n=8; **e.** n=9; **f.** n=11.

29. **a.** n=3, m=11, k=2; **b.** n=6, m=11, k=2; **c.** n=7, m=11, k=2;
d. n=8, m=11, k=2; **e.** n=9, m=11, k=2; **f.** n=11, m=11, k=2.
30. **a.** n=6, m=6, k=2; **b.** n=7, m=6, k=2; **c.** n=8, m=6, k=2;
d. n=9, m=6, k=2; **e.** n=11, m=6, k=2.
31. n=3, m=11, k=1

Scheme 2-1

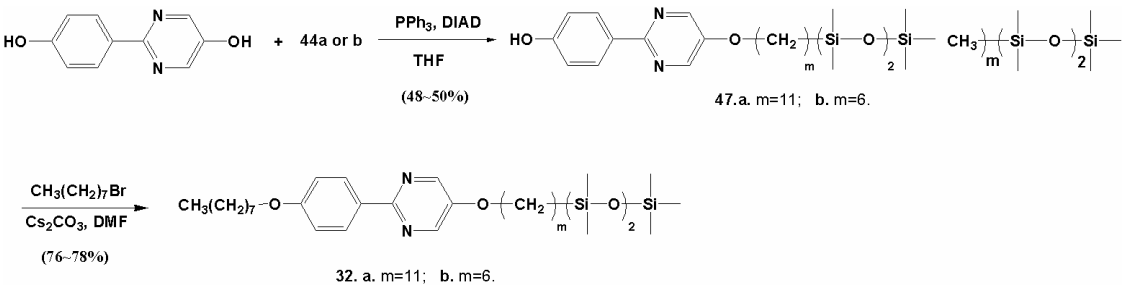

47.a. m=11; **b.** m=6.

32. **a.** m=11; **b.** m=6.

Scheme 2-2

2.2 Mesophase characterization

The mesophases formed by compounds **29a-f**, **30a-e**, **31**, **32a**, **32b**, **33a-c**, **34a** and **34b** were characterized by polarized optical microscopy (POM), differential scanning calorimetry (DSC) and powder X-ray diffraction (XRD). Compounds **29a-f** and **31** form a single mesophase showing both broken fan and Schlieren textures by POM, which are characteristic of a tilted SmC phase (Figure 2-1). Their transition temperatures and enthalpies of transitions are shown graphically in Figure 2-3 and Table 2-1. DSC analysis revealed, in some cases, a second melting transition (Cr–Cr') on heating (Figure 2-5), which has been previously attributed to the melting of siloxane domains separate from that of paraffinic domains.[1,2] The clearing point (SmC-I) in series **29a-f** generally increases with increasing alkoxy chain length *n*, whereas the clearing point (SmC-I) of **29a** with three siloxy units is lower by 2K than that of **31** with two siloxy units.

Shortening the alkyl spacer linking the siloxane end-group to the phenylpyrimidine core *m* (series **30a-e**) resulted in the formation of a very narrow SmA phase along with the broader SmC phase (Figure 2-4 and Table 2-1). These results are consistent with normally observed trends showing a stabilization of the SmC phase at the expense of the SmA phase with increasing chain length.[4] The SmA phase was distinguished from the SmC phase by POM observations of coexisting domains with fan and homeotropic textures (SmA) which turned into broken fan and Schlieren textures

upon transition to the SmC phase (Figure 2-2). The SmA-SmC phase transition is normally second order in nature, which is difficult to detect by DSC. However, with **30a-d**, the SmA-SmC transition produced a small endotherm peak (ΔH=0.8-1.0 kJ/mol), which suggests that the SmA-SmC transition is weakly first order in nature (Figure 2-6).

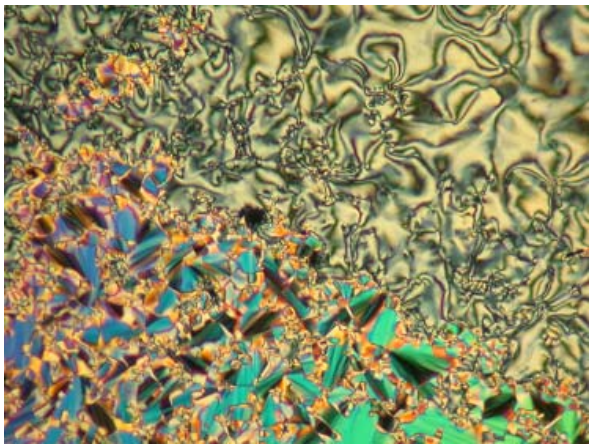

Figure 2-1. Polarized photomicrograph of compound **29a** taken on cooling as a representative example: in the SmC phase at 52^{o}C. (100X Magnification)

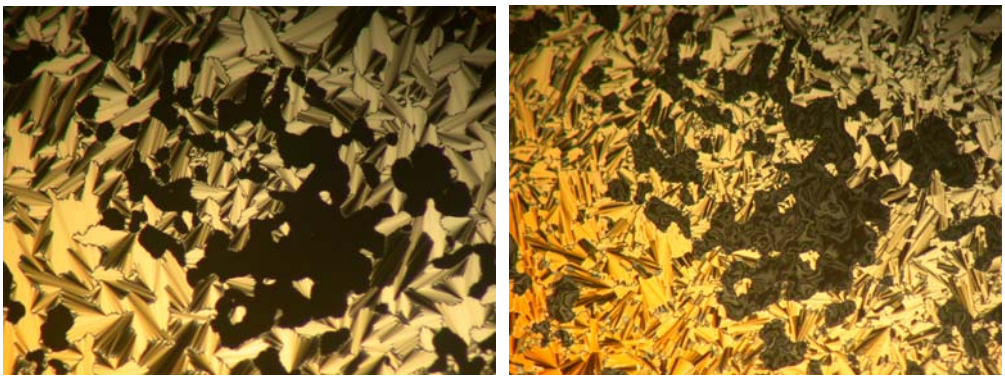

(a) (b)

Figure 2-2. Polarized photomicrographs of compound **30c** on cooling as a representative example: (a) in the SmA phase at 70^{o}C, and (b) in the SmC phase at 50^{o}C. (100X Magnification)

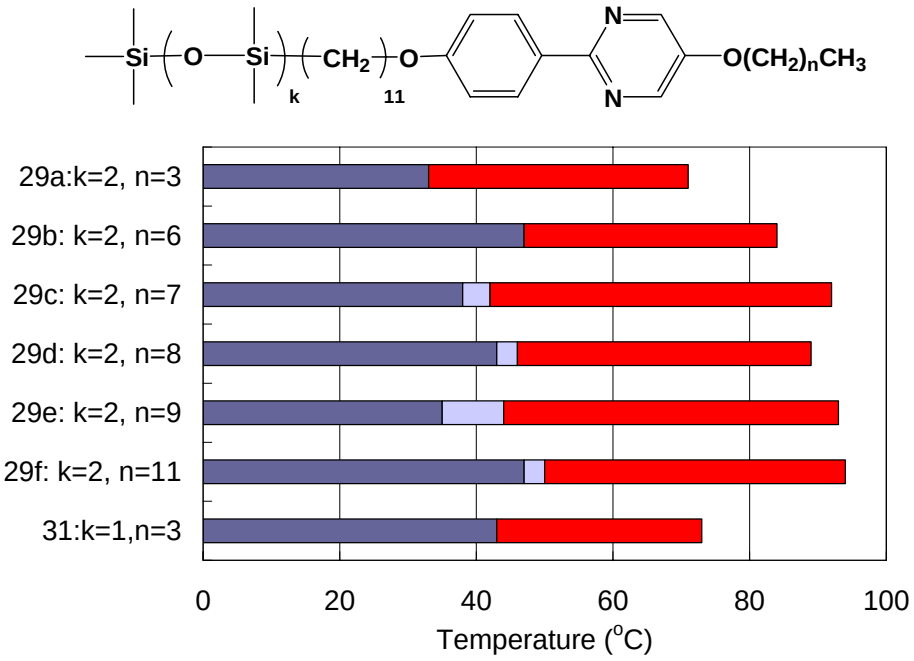

Figure 2-3. Phase transition temperatures for compounds **29a-f** and **31** measured by DSC on heating. Dark blue: Cr; light blue: Cr'; red: SmC.

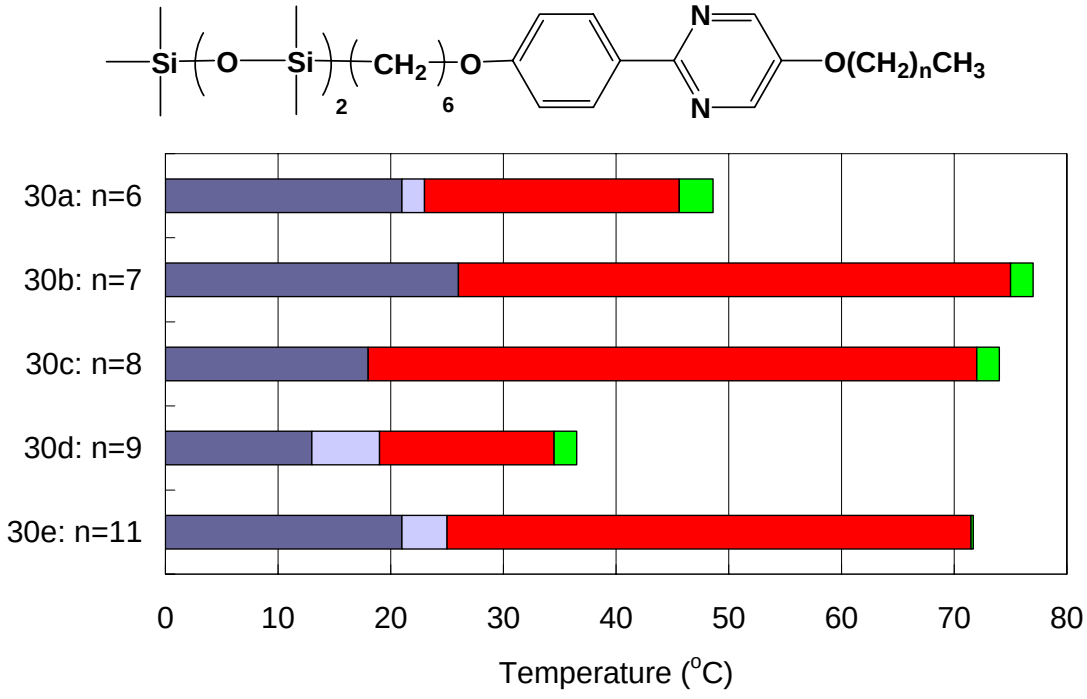

Figure 2-4. Phase transition temperatures for compounds **30a-e** measured by DSC on heating. Dark blue: Cr; light blue: Cr'; red: SmC; green: SmA phase.

Table 2-1. Transition temperatures (°C) and enthalpies of transitions (kJ/mol, in parentheses) for compounds **29a-f** , **30a-e** and **31**.

Cpd	Cr		Cr'		SmC		SmA		I
29a	•	33(35.9)			•	71(7.4)			•
29b	•	47(51.6)			•	84(9.3)			•
29c	•	38	•	42(46.6)[a]	•	92(11.5)			•
29d	•	43	•	46(37.2)[a]	•	89(11.0)			•
29e	•	35	•	44(33.0)[a]	•	93(12.7)			•
29f	•	47	•	50(24.1)[a]	•	94(14.6)			•
30a	•	21	•	23(13.6)[a]	•	71(0.8)	•	74(5.3)	•
30b	•	26(13.9)			•	75(1.0)	•	77(5.4)	•
30c	•	18(13.6)			•	72(1.0)	•	74(4.3)	•
30d	•	13	•	19(10.1)[a]	•	71	•	73(8.9)[b]	•
30e	•	21	•	25(30.4)[a]	•	70.7[c]	•	71(6.6)	•
31	•	43(25.1)			•	73(6.0)			•

[a]ΔH derived from overlapping peaks for Cr-Cr' and Cr'-SmC transitions. [b]ΔH derived from overlapping peaks for SmA-I and SmC-SmA transitions. [c]Measured by polarized microscopy on cooling.

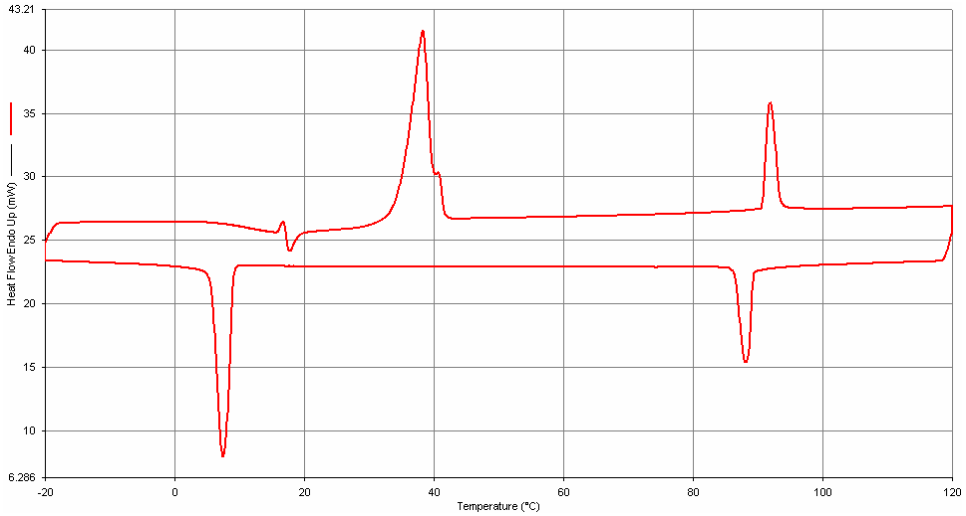

Figure 2-5. Differential scanning calorimetry (DSC) trace for compound **29c** taken at a scan rate of 5K/min as a representative example.

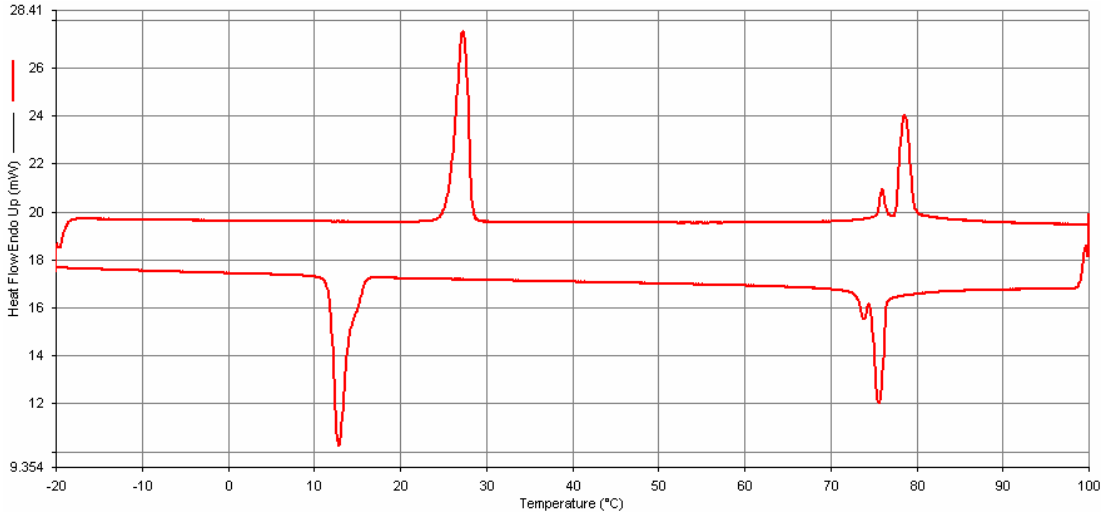

Figure 2-6. Differential scanning calorimetry (DSC) trace for compound **30b** taken at a scan rate of 5K/min as a representative example.

The powder XRD profiles of these compounds are consistent with a disordered smectic phase; they show first and second-order Bragg diffraction peaks in the small-angle region corresponding to the smectic layer structure, together with a pair of diffuse bands in the wide-angle region corresponding to the disordered lateral arrangement of paraffinic chains (4.5Å) and siloxane groups (6.9Å) within each layer (for a representative example, see Figure 2-7).[3]

In the case of compound **29c**, the Bragg angle ($2\theta = 2.2^{o}$) in the small-angle region corresponds to a layer spacing *d* of 43.5Å according to equation 2-1.

$$2d \sin\theta = n\lambda \qquad (2\text{-}1)$$

This layer spacing *d* is slightly longer than the molecular length *l* of **29c** (Table 2-2), which is inconsistent with a tilted lamellar structure. The same observation was made for

the C6 analogues, with the *d* spacing in the SmA phase of compound **30b** even longer than the calculated molecular length by 3.9 Å (Table 2-2). Such a discrepancy between the X-ray data and POM observations has been previously reported for other siloxane-terminated liquid crystals, and rationalized by the formation of a partially bilayered SmC structure.[2,3]

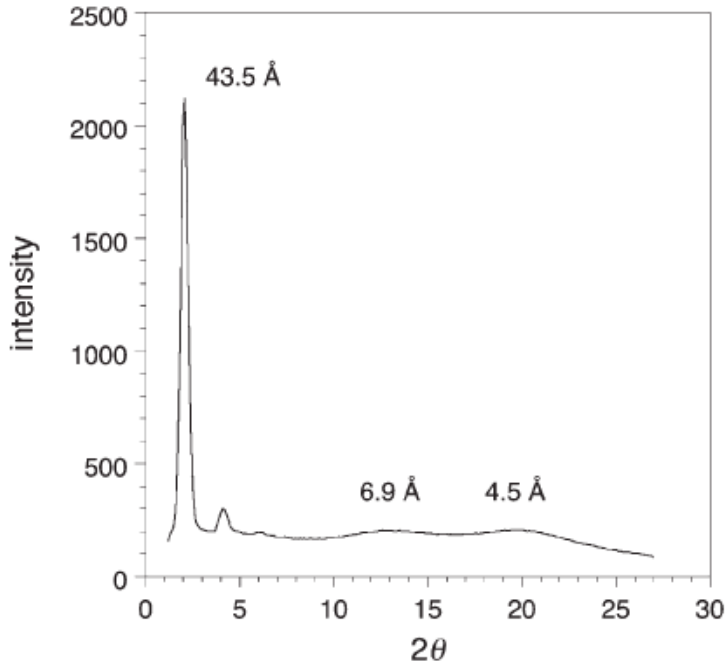

Figure 2-7. Powder X-ray diffraction profile for compound **29c** in the SmC phase.

Table 2-2. Smectic layer spacings in the SmA phase (d_A) and SmC phase (d_C) at T-T_C = -10K and molecular lengths derived from AM1 molecular modeling (l) for compounds **29c**, **30b**, **32a** and **32b**.

Cpd	d_A/Å	d_C/Å	l/Å
29c	--	43.5	42.3
30b	39.6	36.9	35.7
32a	--	35.8	42.3
32b	--	28.3	35.7

We attempted to measure the optical tilt angle of the SmC phase as a function of temperature by POM using a sample of **29c** doped with the chiral siloxane **Br11-Si$_3$** (2 mol%),[2] but were unable to achieve a uniform alignment of the SmC* mixture in conventional polyimide coated ITO cells (ca. 4 μm spacing, E.H.C. Co., Japan). Elvamide®-coated ITO cells were fabricated in-house and attempts were made to align the liquid crystal mixture in this type of cells, but with no improvement over the polyamide-coated cells (Figure 2-8 (a)). Unlike the case of **29c**, we were able to achieve a uniform alignment of a 1 mol% mixture of **Br11-Si$_3$** in **30b** in an ITO cell with rubbed Elvamide® alignment layers (Figure 2-8 (b)), which enabled the measurement by POM of an optical tilt angle of 36^o at T-T_C=-10 K (Figure 2-9).

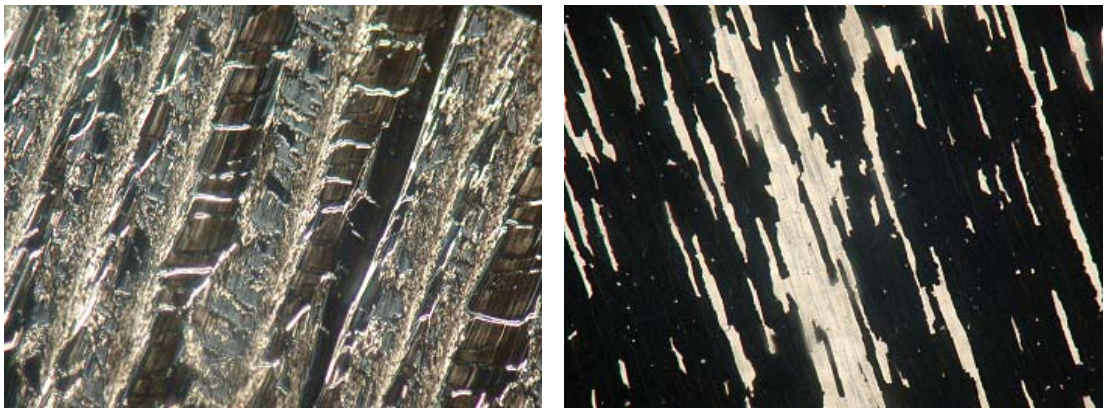

(a) (b)

Figure 2-8. Alignment in Elvamide®-coated ITO cells: (a) 2 mol% of **Br11-Si$_3$** in **29c**, (b) 1 mol% of **Br11-Si$_3$** in **30b**. (100X Magnification)

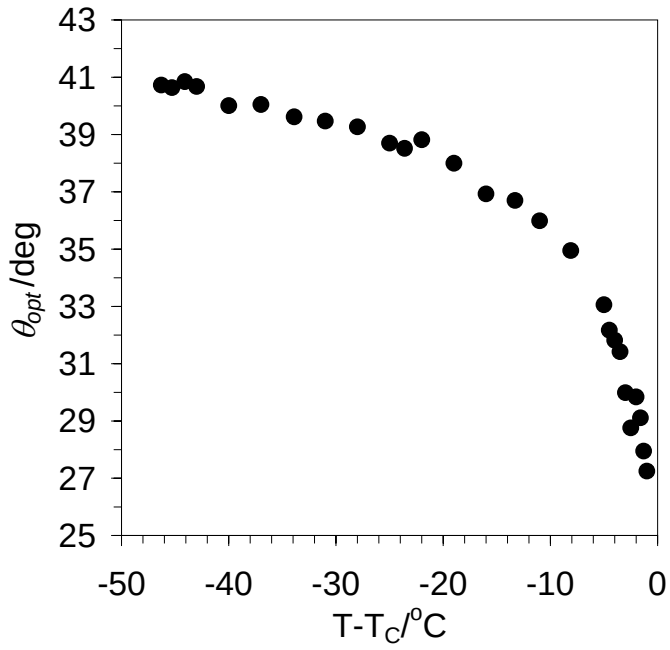

Figure 2-9. Optical tilt angle θ_{opt} *vs.* reduced temperature $T–T_C$ for compounds **30b**.

An accurate measurement of smectic layer spacing as a function of temperature by powder X-ray diffraction was carried out for compound **30b**. As shown in Figure 2-10,

the SmA–SmC phase transition results in a maximum layer shrinkage of 7.6%, which is within the range of conventional materials with this phase sequence.[5]

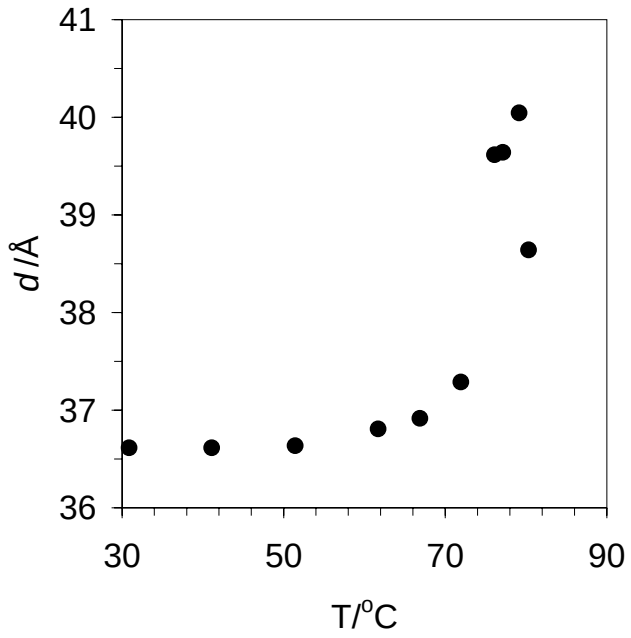

Figure 2-10. Smectic layer spacing *d vs.* temperature T for compounds **30b**.

Inverting the orientation of the phenylpyrimidine core in compounds **32a** and **32b**, resulted in a complete suppression of the SmA phase (Figure 2-11 and Table 2-3) and a reduction in layer spacing d_C (Table 2-2), which is remarkable considering the fact that both side-chains are linked to the core via alkoxy groups, and that their conformational hypersurfaces should therefore remain unaffected by the inversion. The reduced layer spacing may reflect an increase in tilt angle, although we were unable to measure θ_{opt} with samples doped with **Br11-Si$_3$** due to extremely poor alignment of the SmC* phases in ITO cells with either rubbed polyimide or rubbed Elvamide® alignment layers. It may

also reflect specific core–core interactions in the intercalated bilayer structure that are controlled primarily by π-stacking of the electron-poor pyrimidine rings, thus causing a shift in offset upon inverting the orientation of the cores.

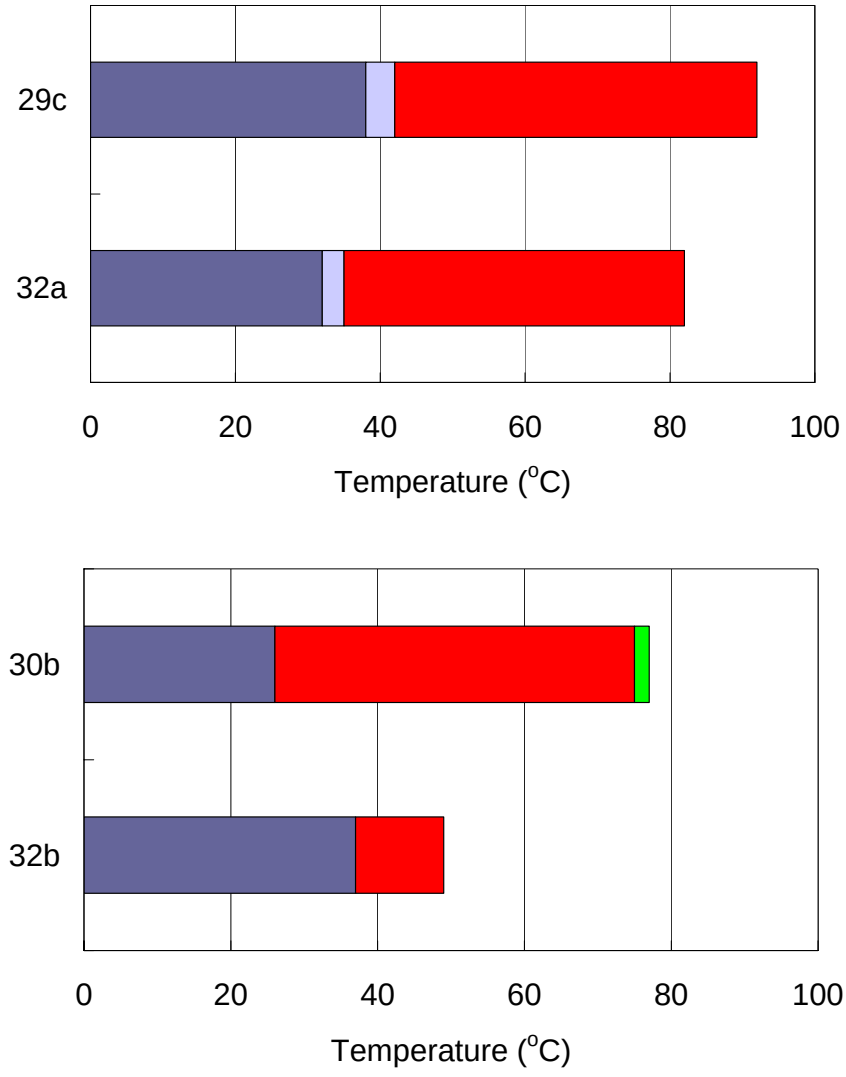

Figure 2-11. Phase transition temperatures for compounds **29c**, **30b**, **32a** and **32b** measured by DSC on heating. Dark blue: Cr; light blue: Cr'; red: SmC; green: SmA phase.

Table 2-3. Transition temperatures (°C) and enthalpies of transitions (kJ/mol, in parentheses) for compounds **32a** and **32b**.

Cpd	Cr		Cr'		SmC		I
32a	•	32	•	35(20.9)[a]	•	82(12.2)	•
32b	•	37(12.7)			•	49(8.5)	•

[a] Measured with samples containing 1 mol% of **Br11-Si$_3$**.

2.3 Siloxane-terminated phenylpyrimidine liquid crystals with halogen end-groups

2.3.1 Synthesis

We sought to modify the molecular structure of the compounds described in Section 2.1 to broaden the temperature range of the SmA phase because of the proven potential of siloxane-terminated mesogens to form 'de Vries'-type SmA phases, and the observation by Giesselmann and co-workers of an inverse correlation between the temperature range of the SmA phase and the degree of layer shrinkage upon SmA-SmC phase transition.[5-10] Based on a recent report by Cowlings *et al.* that the addition of a terminal halogen atom in the side-chain of a calamitic mesogen promotes the formation of a SmA phase,[11] we modified the side-chains of both **30a** and **30b** to give the chloro-terminated mesogens **33a** and **33b** and the bromo-terminated mesogen **33c**.

The chloro-terminated and bromo-terminated mesogens **33a**, **33b** and **33c** were

prepared by alkylation of 2-(4-hydroxyphenyl)-5-pyrimidinol via a Mitsunobu reaction with 8-chloro-1-octanol or 8-bromo-1-octanol in 53-54% yield, followed by alkylation with either **45a** or **45b** (Scheme 2-3). The inverted analogues **34a** and **34b** were prepared by reversing the alkylation sequence (Scheme 2-4). All compounds were recrystallized from EtOH prior to mesophase characterization.

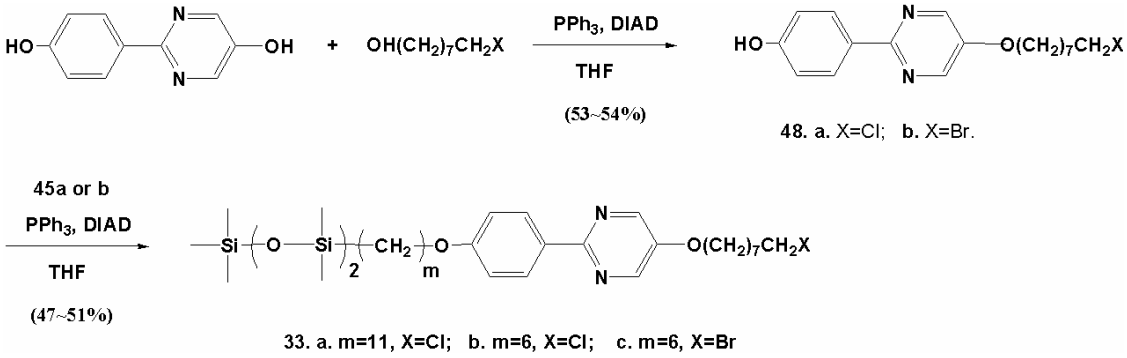

Scheme 2-3

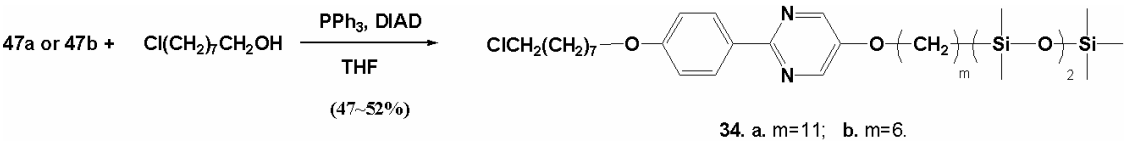

Scheme 2-4

2.3.2 Mesophase characterization

As shown in Figure 2-12 and Table 2-4, the inclusion of a terminal chloro substituent resulted in a narrower SmC temperature range, and a broader SmA

temperature range of 9 K. Interestingly, having a terminal bromo-substituent instead of chloro made no difference in terms of the temperature range of the SmA phase.

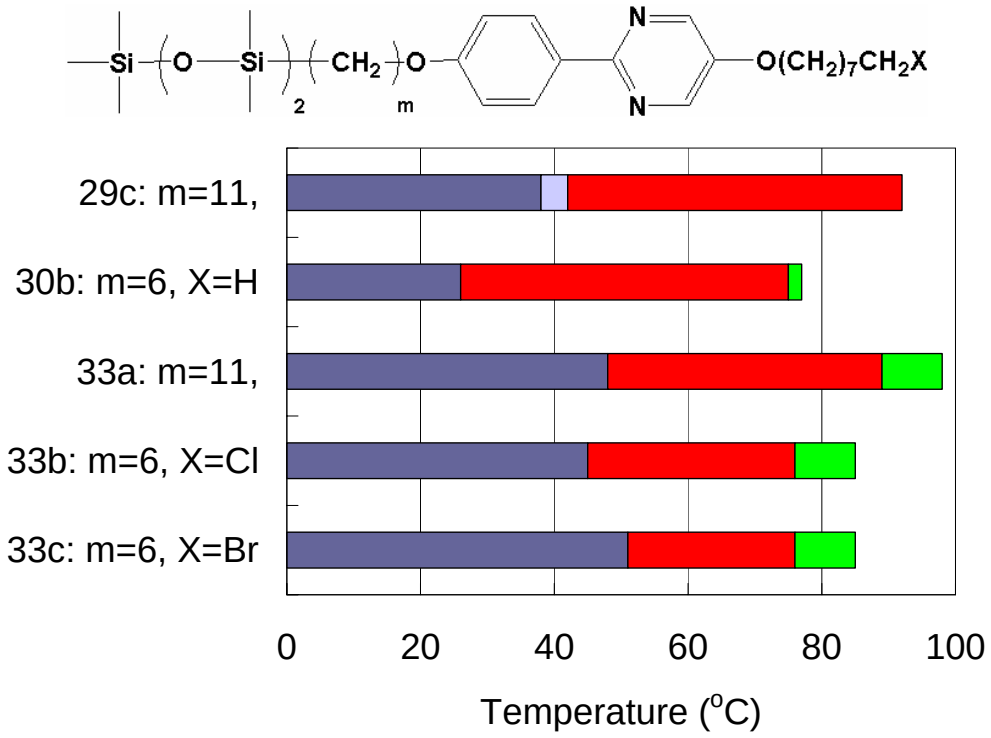

Figure 2-12. Phase transition temperatures for compounds **29c**, **30b**, **33a**, **33b** and **33c** measured by DSC on heating. Dark blue: Cr; light blue: Cr'; red: SmC; green: SmA phase.

Table 2-4. Transition temperatures (°C) and enthalpies of transitions (kJ/mol, in parentheses) for compounds **33a**, **33b** and **33c**.

Cpd	Cr		SmC		SmA		I
33a	•	48(45.4)	•	89(0.2)	•	98(10.7)	•
33b	•	45(51.1)	•	76(0.6)	•	85(7.7)	•
33c	•	51(51.3)	•	76(0.6)	•	85(7.5)	•

As observed with series **29a-f** and **30a-e**, the layer spacings in the orthogonal SmA and tilted SmC phases are greater than the corresponding molecular lengths (Table 2-5 and Figure 2-13), which is consistent with the assignment of partially intercalated bilayer structures. The SmA–SmC phase transition results in a maximum layer shrinkage of 4.2% for compound **33b** and only 1.6% for compound **33a**, although the d_C spacing of **33a** increases with decreasing temperature to such an extent that $d_C = d_A$ near the SmC–Cr transition temperature (Figure 2-8). The *d(T)* profile for compound **33a** is very similar to that reported for the perfluorinated material **3M8422** (see Figure 1-13) with a 'de Vries' SmA*–SmC* transition that results in a maximum layer shrinkage of 0.8%.[12] A common characteristic of these two profiles is the negative thermal expansion of the SmA phase layer spacing, which appears to continue in the SmC phase. In conventional materials such as **PhP1**, any such negative thermal expansion is less profound, and usually saturates before the SmA-SmC phase transition. The effect of the terminal chloro substituent in promoting an orthogonal layer structure is reflected in the smaller optical tilt angles θ_{opt} of 24° and 26° at $T-T_C$=-10 K in the SmC phases of **33a** and **33b**, respectively (Figure 2-14), which were measured by POM in rubbed Elvamide cells as previously described for **30b**. This is consistent with the SmA-promoting effect previously observed by Cowlings et. al.

Table 2-5. Smectic layer spacings in the SmA phase (d_A) and SmC phase (d_C) at T-T_C = -10K and molecular lengths derived from AM1 molecular modeling (l) for compounds **33a** and **33b**.

Cpd	d_A/Å	d_C/Å	l/Å
33a	48.4	47.7	42.8
33b	40.4	38.9	36.2

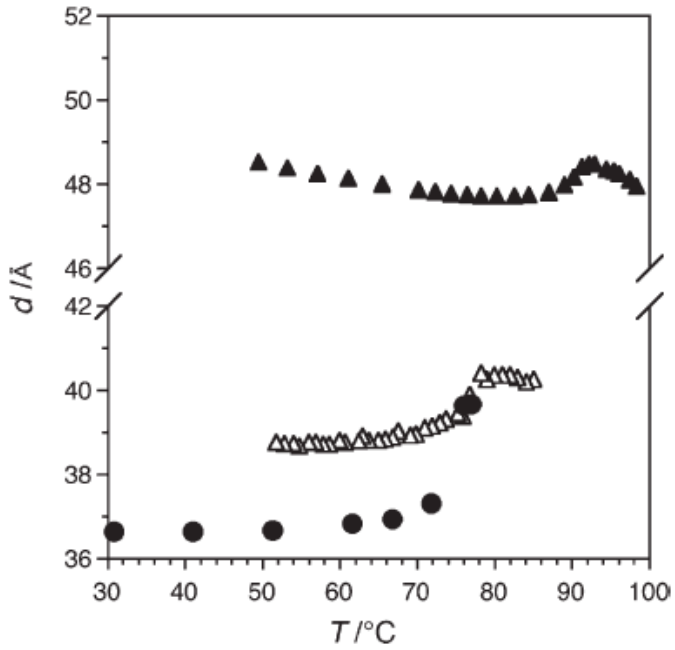

Figure 2-13. Smectic layer spacing *d vs.* temperature T for compounds **30b** (circles), **33a** (filled triangles) and **33b** (open triangles).

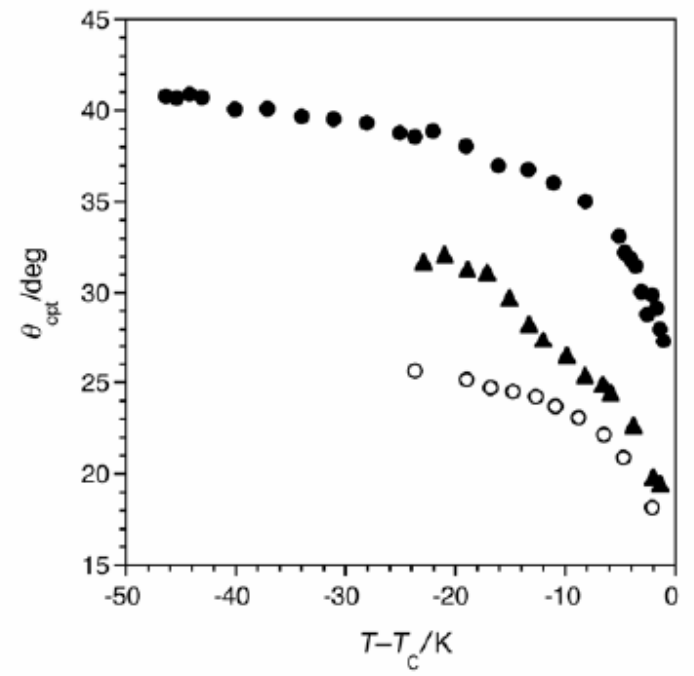

Figure 2-14. Optical tilt angle θ_{opt} *vs.* reduced temperature $T–T_C$ for compounds **30b** (filled circles), **33a** (open circles) and **33b** (triangles).

We also observed significant changes in interference colors in the fan/broken fan textures of both **33a** and **33b** upon cooling from the SmA to the SmC phase (Figure 2-15 and Figure 2-16). These color changes are consistent with an increase in birefringence that is expected in a 'de Vries' phase transition from random to ordered molecular tilt (*vide infra*).[5]

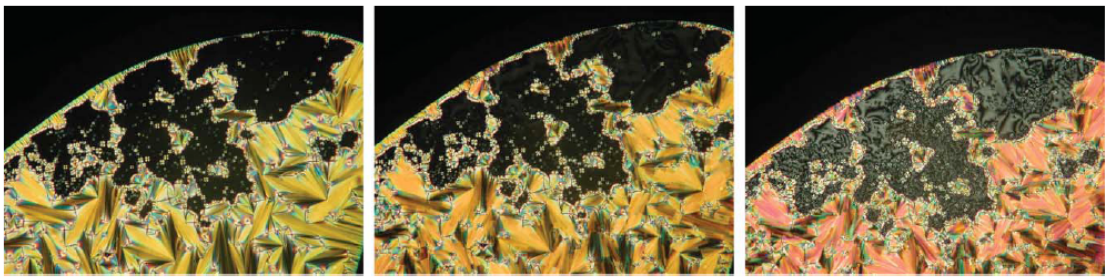

(a) (b) (c)

Figure 2-15. Polarized photomicrographs of compound **33a** on cooling: (a) in the SmA phase at 91°C, (b) just below the SmA–SmC phase transition at 86°C, and (c) in the SmC phase at 82°C. (100X Magnification)

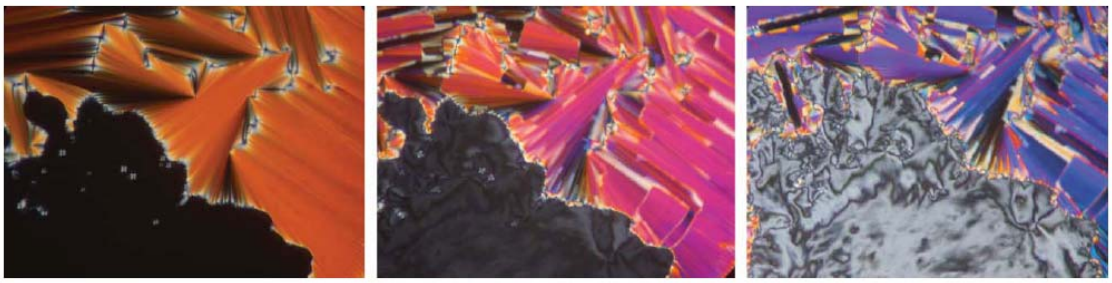

(a) (b) (c)

Figure 2-16. Polarized photomicrographs of compound **33b** on cooling: (a) in the SmA phase at 82°C, (b) just below the SmA–SmC phase transition at 73°C, and (c) in the SmC phase at 62 °C. (100X Magnification)

To assess whether the decrease in layer shrinkage achieved by introducing a terminal chloro substituent in the side-chain of **30b** is due to an increase in 'de Vries' character, one must consider the difference in tilt angle in the SmC phases formed by these materials. The description of any SmA–SmC phase transition may be found somewhere along a continuum between two limiting cases, the classic rigid rod model and the diffuse cone model proposed by de Vries (Figure 1.9 and 1-14).[5,13] According to the first model, in which rigid rod molecules are uniformly oriented along a director **n**

and tilted at an angle θ with respect to the layer normal z, the relationship between d_C and d_A is expressed by Equation 2-2, and the layer shrinkage $(d_A\text{-}d_C)/d_A$ is a function of the tilt angle θ according to Equation 2-3. In order to attribute any decrease in layer shrinkage to an increase in 'de Vries' character based on the diffuse cone model, we normalize the layer shrinkage with respect to θ by dividing the observed $(d_A\text{-}d_C)/d_A$ by $1\text{-}\cos\theta$, where θ is approximated as the optical tilt angle θ_{opt} measured by POM (Equation 2-4). Using this expression, the 'de Vries' coefficient C_{dV} of any given material can range from 0 (classic rigid rod model with maximum layer shrinkage) to 1 (pure 'de Vries' SmA–SmC transition with no layer shrinkage).

$$d_C = d_A \cos\theta \tag{2-2}$$

$$(d_A - d_C)d_A = 1 - \cos\theta \tag{2-3}$$

$$C_{dV} = 1 - [(d_A - d_C)/(d_A(1 - \cos\theta))] \tag{2-4}$$

C_{dV} values were calculated for compounds **30b**, **33a** and **33b** using the maximum d_A value at T_C. As shown in Figure 2-17, the C_{dV} of compound **30b** shows little variance with temperature, with values ranging from 0.63 to 0.67. The $C_{dV}(T\text{-}T_C)$ profile of compound **33b** is steeper than that of **30b**, which reflects the higher negative thermal expansion in the SmC phase for **33b**, although C_{dV} values are fairly similar in the $T\text{-}T_C$ range of -5 to -15 K. At $T\text{-}T_C$=-10K (Table 2-6), the two compounds **30b** and **33b** have

nearly the same C_{dV} value despite the large difference in layer shrinkage (6.8% *vs*. 3.7%, respectively) because of the difference in tilt angle (36^{o} *vs.* 26^{o}, respectively). A comparison of C_{dV} value for **30b** with the non-siloxane analogue **PhP1** (Scheme 2-5) suggests that the trisiloxane end-group does impart some 'de Vries' character to the SmA–SmC transition of compounds **30a-e**.[15] However, addition of a chloro end-group to **30b** to **33b** does not increase 'de Vries' character, as the decrease in layer shrinkage can be accounted for by the decrease in tilt angle.

The C_{dV} ($T-T_C$) profile of compound **33a** is similar to that of **33b**, but features significantly higher C_{dV} values. Compound **33a** shows a maximum layer shrinkage of 1.6% and a C_{dV} of 0.89 at $T-T_C$=-10K, which is comparable to those of known 'de Vries' materials, **TSiKN65**[16] and **3M8422**[17] (Table 2-6). Compound **33a** may be considered a bona fide 'de Vries' material with a SmA-SmC transition approaching that described by the diffuse cone model.[6-10, 18-19] However, given the partially bilayered structure of the smectic phases formed by these compounds, one cannot rule out a variation in the degree of bilayer intercalation as a contributor to the observed reductions in layer shrinkage. Nevertheless, the results show that addition of terminal chlorine on the alkyl side-chain results in a C_{dV} value of 0.89 in **33a**. This suggests that the combination of a structural element that promotes the formation of a SmC phase (trisiloxane-terminated C11 side-chain) with one that strongly promotes the formation of a SmA phase (chloro-terminated side-chain) results in 'de Vries'-type SmA material.[14]

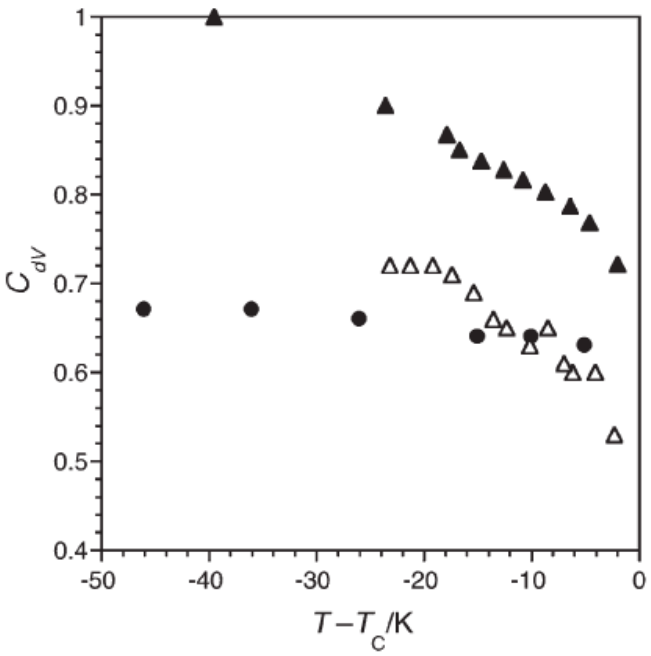

Figure 2-17. de Vries coefficient C_{dV} *vs.* reduced temperature T-T_C for compounds **30b** (filled circles), **33a** (filled triangles) and **33b** (open triangles).

Table 2-6. Optical tilt angles (θ_{opt}) measured by POM, and de Vries coefficients (C_{dV}) at T-T_C=-10K for compounds **30b**, **33a**, **33b**, **PPh1**[15], **TSiKN65**[16] and **3M8422**[17].

Cpd	θ_{opt}/deg	C_{dV}[b]
30b	36[a]	0.64
33a	24[a]	0.89
33b	26[a]	0.63
PPh1	--	0.4
TSiKN65	34	0.96
3M8422	25	0.95

[a] Measured with samples containing 1 mol% of **Br11-Si$_3$**. [b] Calculated using equation 2-3 and maximum d_A value at T_C.

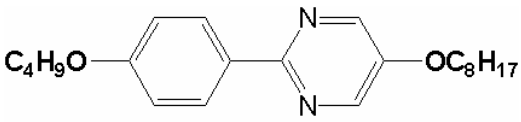

PhP1: Cr 58 SmC 85 SmA 95 N 98 I

Scheme 2-5

As shown in Figure 2-18 and Table 2-7, inverting the orientation of the phenylpyrimidine core in compounds **34a** and **34b**, again resulted in a complete suppression of the SmA phase, as in the case of the non-chlorine-terminated analogues.

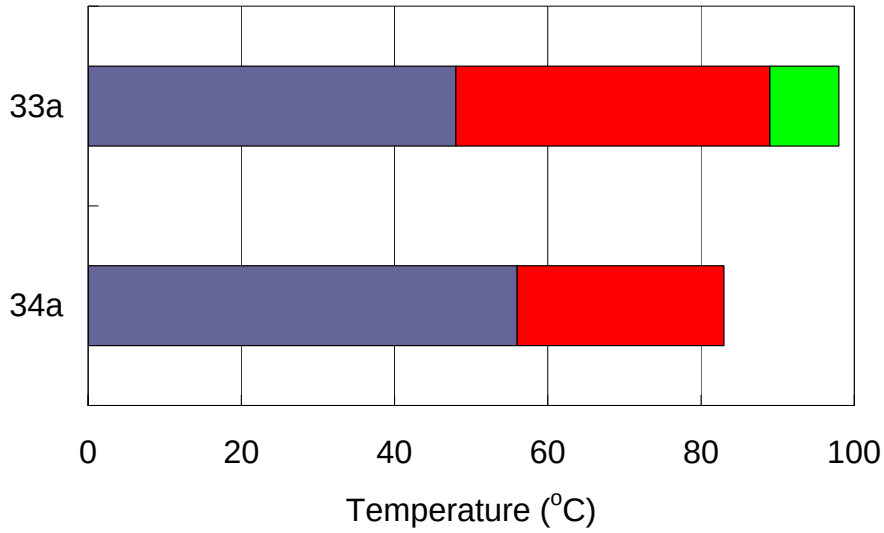

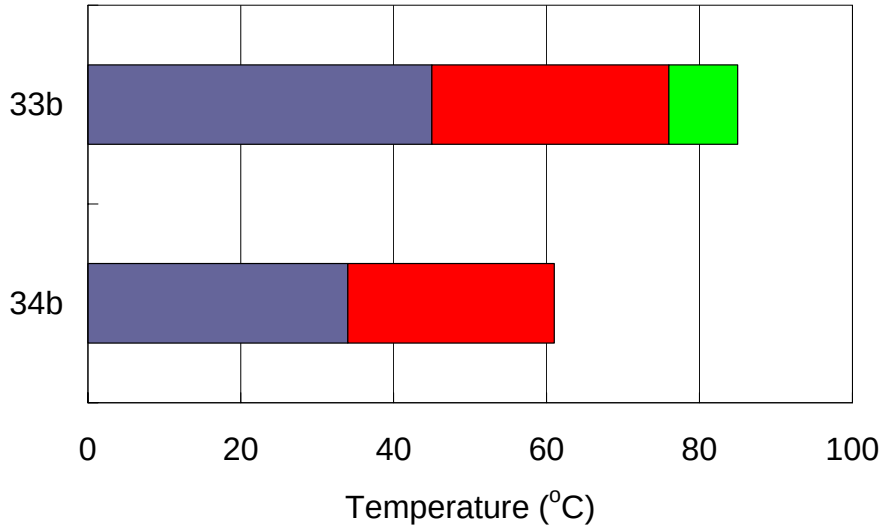

Figure 2-18. Phase transition temperatures for compounds **33a**, **33b**, **34a** and **34b** measured by DSC on heating. Dark blue: Cr; red: SmC; green: SmA phase.

Table 2-7. Transition temperatures (°C) and enthalpies of transitions (J/g, in parentheses) for compounds **34a** and **34b**.

Cpd	Cr		SmC		I
34a	•	56(57.5)	•	83(11.4)	•
34b	•	34(37.1)	•	61(10.2)	•

2.4 Conclusion

The addition of a siloxane end-group on one side-chain of a dialkoxyphenylpyrimidine mesogen results in the formation of a broad SmC phase and, in some cases, a narrower SmA phase. The temperature range of the SmA phase may be broadened by the addition of a terminal halogen substituent on the other alkoxy side-chain. Comparison of siloxane-terminated phenylpyrimidine liquid crystals with the non-

siloxane analogue **PhP1** revealed that the trisiloxane end-groups cause the SmA–SmC transitions of these compounds to be more 'de Vries'-like. This is consistent with the notion that nanophase segregation plays a significant role in the manifestation of 'de Vries' behavior, whether it is achieved with amphiphilic mesogens,[6-10, 16-17] or with side-chain siloxane copolymers.[14] Further addition of terminal chlorine on the alkyl side-chain results in a bona fide 'de Vries' material, 2-(4-(11-(1,1,1,3,3,5,5-heptamethyltrisiloxanyl)undecyloxy)phenyl)-5-(1-chlorooctyloxy)pyrimidine (**33a**), which is characterized by a maximum layer shrinkage of only 1.6% and a C_{dV} value of 0.89 at $T-T_C$=-10K. The C_{dV} value is comparable to those of known 'de Vries' materials, **TSiKN65**[16] and **3M8422**[17]. The results suggest that the combination of a structural element that promotes the formation of a SmC phase (trisiloxane-terminated side-chain) with one that promotes the formation of a SmA phase (chloro-terminated sidechain) results in 'de Vries'-type SmA material.[14]

2.5 References

(1) Newton, J.; Coles, H.; Hodge, P.; Hannington, J.; *J. Mater. Chem.* **1994**, 4, 869.

(2) Corsellis, E.; Guillon, D.; Kloess, P.; Coles, H.; *Liq. Cryst.* **1997**, 23, 235.

(3) Ibn-Elhaj, M.; Skoulios, A.; Guillon, D.; Newton, J.; Hodge, P.; Coles, H. J.; *J. Phys. II* **1996**, 6, 271.

(4) *An Introduction to Liquid Crystals: Chemistry and Physics.;* Collings, P.; Hird, M. Ed.; Taylor & Francis: London, **1997**.

(5) Lagerwall, P. F. J.; Giesselmann, F.; *ChemPhysChem* **2006**, 7, 20.

(6) Spector, S. M.; Heiney, A. P.; Naciri, J. B.; Weslowski, T.; Holt, B. D.; Shashidhar, R.; *Phys. Rev. E* **2000**, 61, 1579.

(7) Naciri, J.; Carboni, C.; George, K. A.; *Liq. Cryst.* **2003**, 30, 219.

(8) Panarina, E. O.; Panarin, P. Y.; Vij, K. J.; Spector, S. M.; Shashidhar, R.; *Phys. Rev. E* **2003**, 67, 051709.

(9) Hayashi, N.; Kato, T.; Fukuda, A.; Vij, K. J.; Panarin, P.Y.; Naciri, J.; Shashidhar, R.; Kawada, S.; Kondoh, S.; *Phys. Rev. E* **2005**, 71, 041705.

(10) Panarina, E. O.; Panarin, P. Y.; Antonelli, F.; Vij, K. J.; Reihmann, M.; Galli, G.; *J. Mater. Chem.* **2006**, 16, 842.

(11) Cowling, J. S.; Goodby, W. J.; Hall, W. A.; Cosquer, Y. G.; Sia, S.; presented at 10th Conference on Ferroelectric Liquid Crystals, Stare Jablonki, Poland, September **2005**.

(12) Lagerwall, P. F. J.; Giesselmann, F.; Radcliffe, D. M;. *Phys. Rev. E* **2002**, 66, 031703.

(13) de Vries, A.; *J. Chem. Phys.* **1979**, 71, 25.

(14) Rossle, M.; Zentel, R.; Lagerwall, P. F. J.; Giesselmann, F.; *Liq. Cryst.* **2004**, 31, 883.

(15) Hartley, S. C.; Kapernaum, N.; Roberts, J. C.; Giesselmann, F.; Lemieux, P. R.; *J. Mater. Chem.* **2006**, 16, 2329.

(16) Spector, S. M.; Heiney, A. P.; Naciri, J.; Weslowski, T. B.; Holt, B. D.; Shashidhar, R.; *Phys. Rev. E* **2000**, 61, 1579.

(17) Radcliffe, D. M.; Brostrom, L. M.; Spstein, A. K.; Rappaport, G. A.; Thomas, N. B.; Shao, R.; Clark, A. N.; *Liquid Crystals* **1999**, 26, 789.

(18) Vlahakis, J. Z.; Maly, E. K.; Lemieux, P. R.; *J. Mater. Chem.* **2001**, 11, 2459.

(19) Radcliffe, M. D.; Brostrom, M. L.; Epstein, K. A.; Rappaport, A. G.; Thomas, B. N.; Shao, R.; Clark, A. N.; *Liq. Cryst.* **1999**, 26, 789.

Chapter 3. Design and Synthesis of Siloxane-terminated Biphenyl Benzoate and Phenyl Benzoate Liquid Crystals

3.1 Siloxane-terminated biphenyl benzoate liquid crystals

3.1.1 Synthesis

The general synthetic approach to compounds **35a-f**, **36** and **37** is shown in Scheme 3-1. The trisiloxane-terminated side-chains precursors **45a** and **45b** were derived from the commercially available alcohols 10-undecen-1-ol and 5-hexen-1-ol *via* Pt-catalyzed hydrosilation reactions with 1,1,1,3,3,5,5-heptamethyltrisiloxane in the presence of dicyclopentadienylplatinum(II) chloride or Karstedt's catalyst in 95% and 80% yield respectively. The disiloxane-terminated side-chain precursor **45c** was obtained in a similar manner in 87% yield. Monoalkylation of 4,4′-dihydroxybiphenyl with **45a-c** via Mitsunobu reactions gave **49a-c** in 35-48% yields. Finally, reaction of **49a-c** with the appropriate alkoxybenzoic acid in the presence of DCC and DMAP gave **35a-f, 36** and **37** in yields ranging from 78 to 85% yield. All compounds were recrystallized from EtOH prior to mesophase characterization.

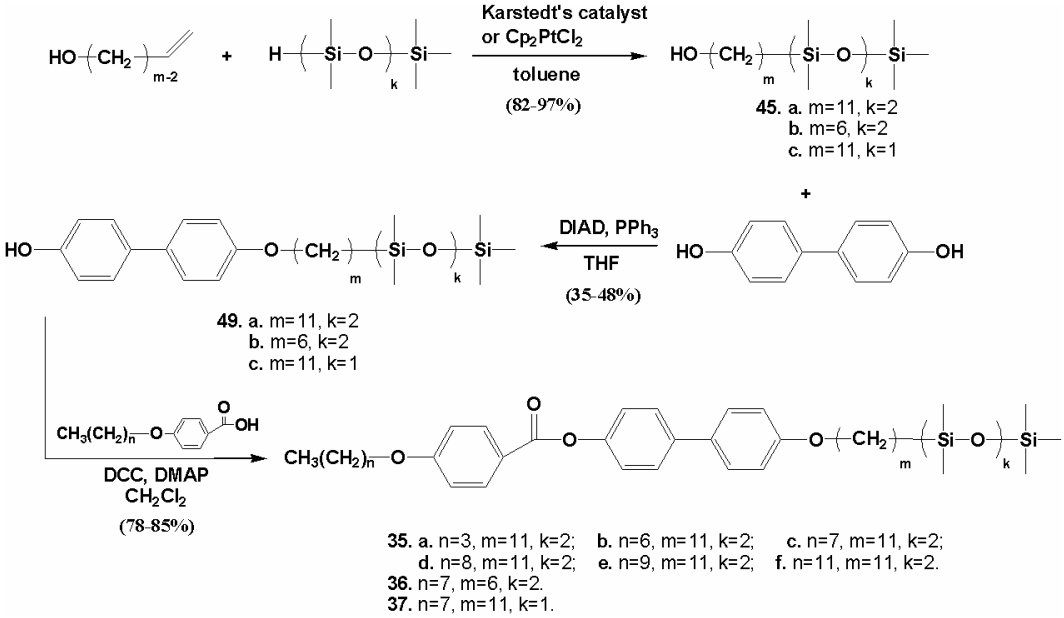

Scheme 3-1

3.1.2 Mesophase characterization

The mesophases formed by compounds **35a-f, 36** and **37** were characterized by polarized optical microscopy (POM) and differential scanning calorimetry (DSC). Furthermore, compound **35c** was analyzed by wide-angle powder X-ray diffraction to confirm the mesophase assignment. The phase transition temperatures and enthalpies of transition are listed in Table 3-1.

Compounds **35a-e** form a single mesophase showing both broken fan and Schlieren textures by POM, which are characteristic of a tilted SmC phase (see Figure 3-1 (a) as a representative example). Upon cooling, the SmC fan domains become threaded, and the

Schlieren domains transform into uniform domains consisting of overlapping platelets. These are reminiscent of the texture displayed by the crystal E phase (Figure 3-1 (b)), which is consistent with previous observations made by Coles *et al.* for a ferrocene-containing siloxane-terminated liquid crystal material. [1]

Table 3-1. Transition temperatures (^{o}C) and enthalpies of transitions (kJ/mol, in parentheses) for compounds **35a-f**, **36** and **37**.

Cpd	Cr		X		SmC		I
35a	•	127(27.3)			•	167(9.6)	•
35b	•	109(25.7)			•	164(11.7)	•
35c	•	102(23.8)			•	163(10.8)	•
35d	•	93(24.2)			•	160(12.3)	•
35e	•	81(19.7)			•	160(11.7)	•
35f	•	62(7.8)	•	90(4.2)	•	156(12.1)	•
36	•	72(18.1)			•	149(8.4)	•
37	•	107(25.9)			•	167(11.1)	•

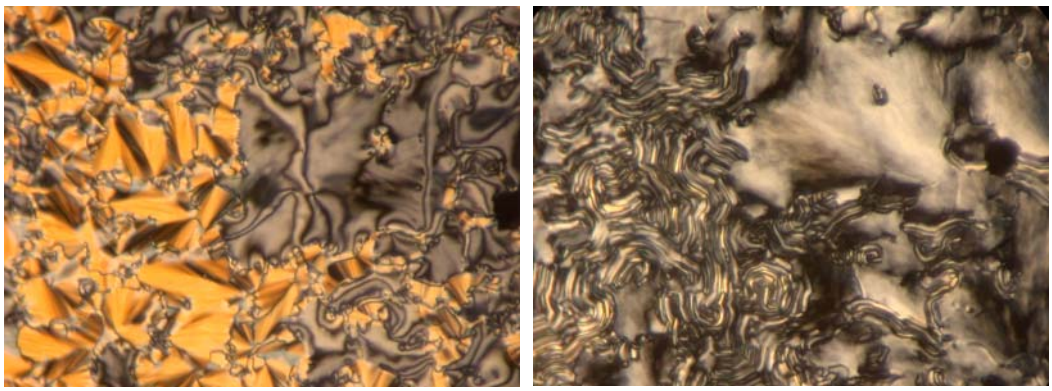

(a) (b)

Figure 3-1. Textures of compound **35a** observed by polarized microscopy on cooling: (a) SmC phase at 140 ^{o}C, and (b) Cr phase at 82 ^{o}C (100X Magnification).

DSC profiles show endotherm peaks on heating with enthalpies of transitions consistent with a Cr-SmC phase transition (ΔH=10-60 kJ/mol) and a SmC-I phase transition (ΔH=5-15 kJ/mol) (see Figure 3-2 and Table 3-1). The power X-ray diffraction profile of **35c** is consistent with a disordered smectic phase; it shows first and second-order Bragg diffraction peaks in the small-angle region corresponding to the periodic smectic layer structure, together with a pair of diffuse bands in the wide-angle region corresponding to the disordered lateral arrangement of paraffinic side-chains and siloxane groups within each layer (Figure 3-3). The Bragg angle ($2\theta = 2.2^{o}$) in the small-angle region corresponds to a layer spacing *d* of approximately 39.3 Å. According to molecular mechanics calculations (MM2 force field), the molecular lengths *l* of **35c** is 48.2 Å, which suggests that the organosiloxane mesogens **35** do not form a particaly intercalated bilayer structure. Hence, assuming a normal monolayer structure, the combined layer spacing *d* and molecular length *l* correspond to a tilt angle $\theta = \cos^{-1}(d/l) = 35^{o}$ (Figure 3-4).

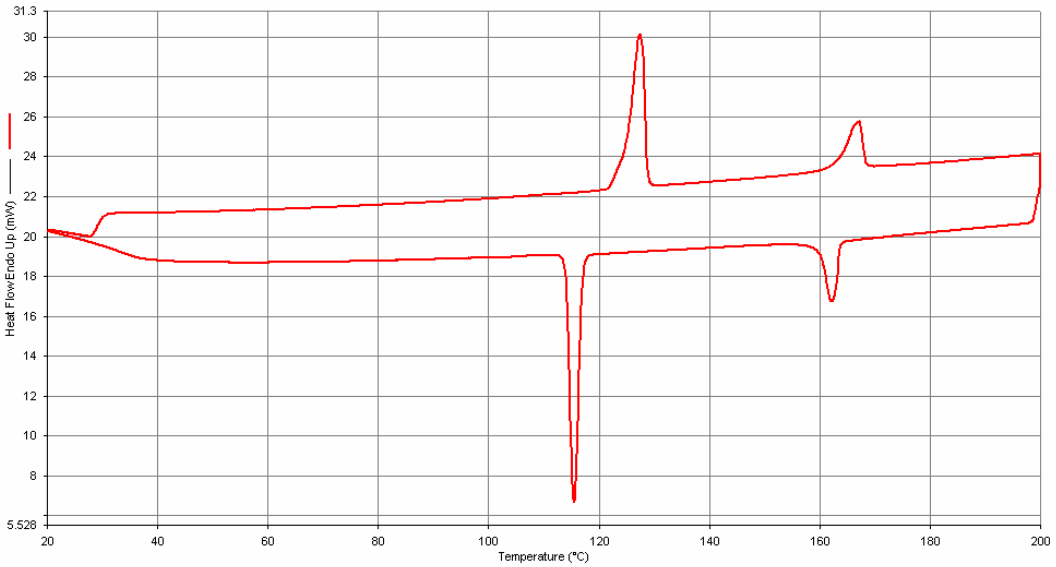

Figure 3-2. Differential scanning calorimetry (DSC) profile for compound **35a** taken at a scan rate of 5K/min as a representative example.

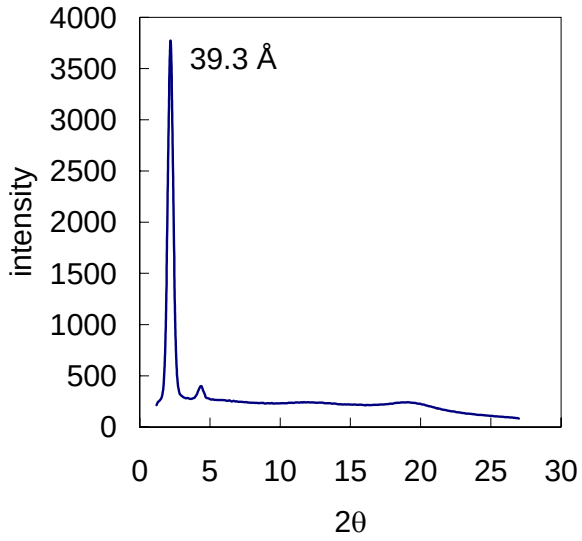

Figure 3-3. Powder X-ray diffraction profile for compound **35c** in the SmC phase at 130 ^{o}C.

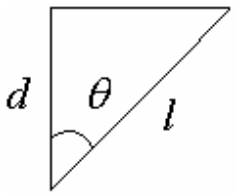

Figure 3-4. Relationship between layer spacing *d*, molecular length *l* and tilt angle *θ*.

Compound **35f** shares the same characteristics as compounds **35a-e** except that it forms one additional phase as shown by an extra peak on the DSC profile (Figure 3-5). The texture observed by POM (Figure 3-6) suggests that it is another crystalline phase and is simply listed as X. No further analysis of this phase was conducted.

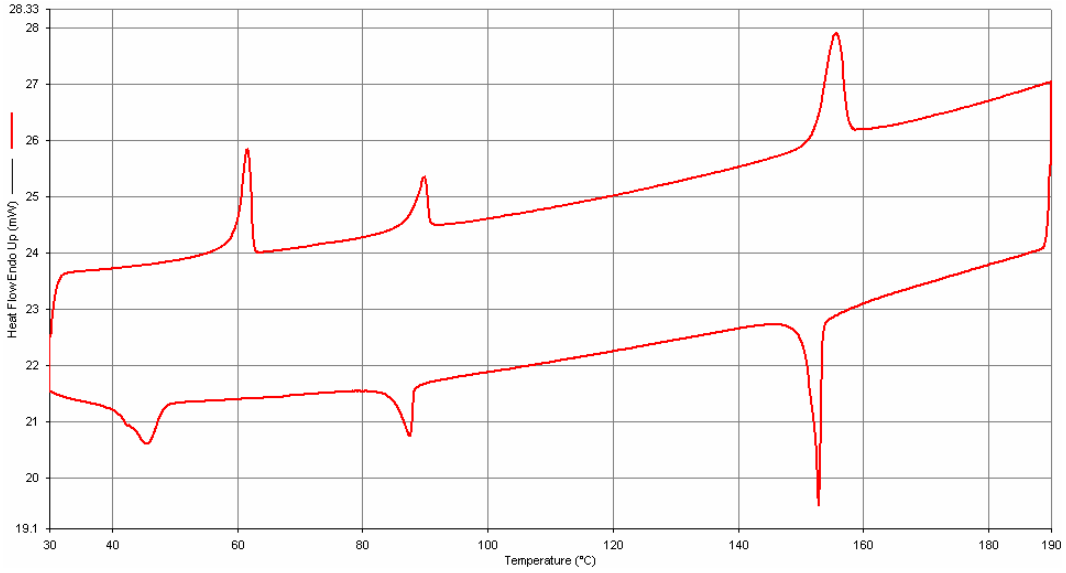

Figure 3-5. Differential scanning calorimetry (DSC) profile for compound **35f** taken at a scan rate of 5K/min.

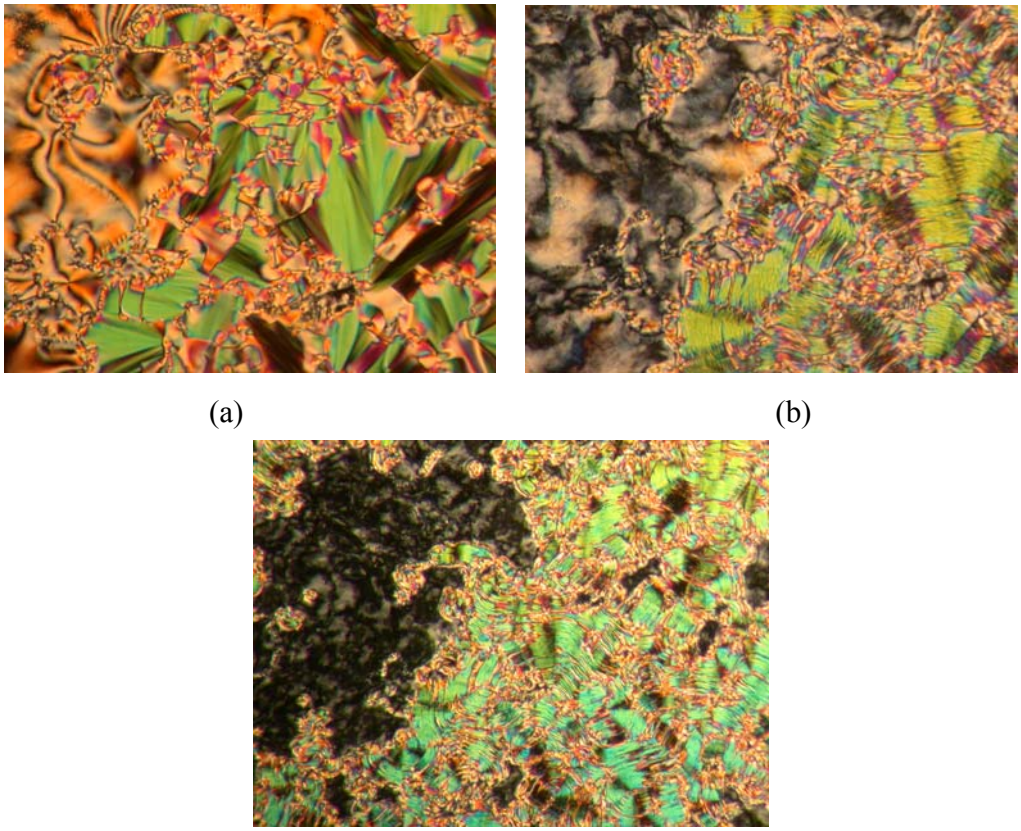

Figure 3-6. Textures of compound **35f** observed by polarized microscopy on cooling: (a) SmC phase at 135 ^{o}C, (b) X phase at 75 ^{o}C, and (c) Cr phase at 45 ^{o}C (100X Magnification).

In general, increasing the alkoxy chain length *n* resulted in a broadening of the temperature range of the SmC phase formed by compounds **35a-f** (Figure 3-7 and Table 3-1), which is consistent with normally observed trends.[2] One exception is compound **35f** which shows a decrease in SmC temperature range compared to **35e**.

To be suitable for display application purposes, the SmC range should extend to room temperature. As shown in Figure 3-7 and Table 3-1, the SmC ranges of **35a-f** are all

well above room temperature. Hence, we sought to modify the molecular structure of these compounds to lower the temperature range of the SmC phase. By changing the number of siloxyl units *k+1* from 3 (compound **35c**) to 2, we obtained compound **37**, which forms only a SmC phase with higher transition temperatures than the trisiloxane analogue (Figure 3-8). Shortening the alkyl spacer linking the trisiloxane end-group to the biphenyl core *m* from 11 (compound **35c**) to 6 (compound **36**) resulted in a SmC phase with somewhat lower transition temperatures (Figure 3-8), although still well above room temperature.

In general, mesophase transition temperatures tend to decrease with a decreasing number of aromatic rings in the core structure.[2] Therefore, a series of siloxane-terminated phenyl benzoate mesogens were prepared and their synthesis and mesophase characterization are presented in the next section.

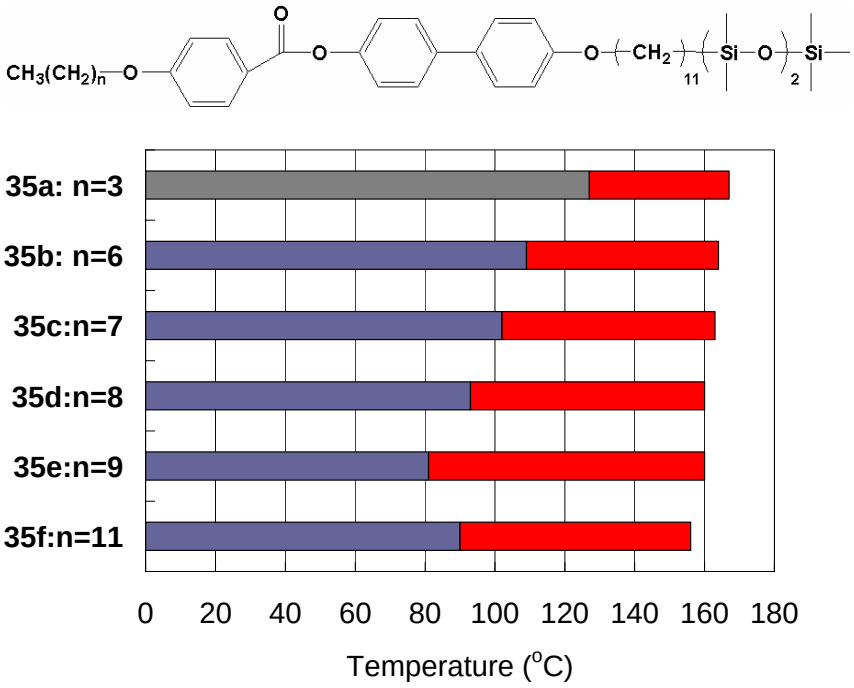

Figure 3-7. Phase transition temperatures for compound **35a-f** measured by DSC on heating. Blue: Cr phase; grey: Cr phase and X phase; Red: SmC phase.

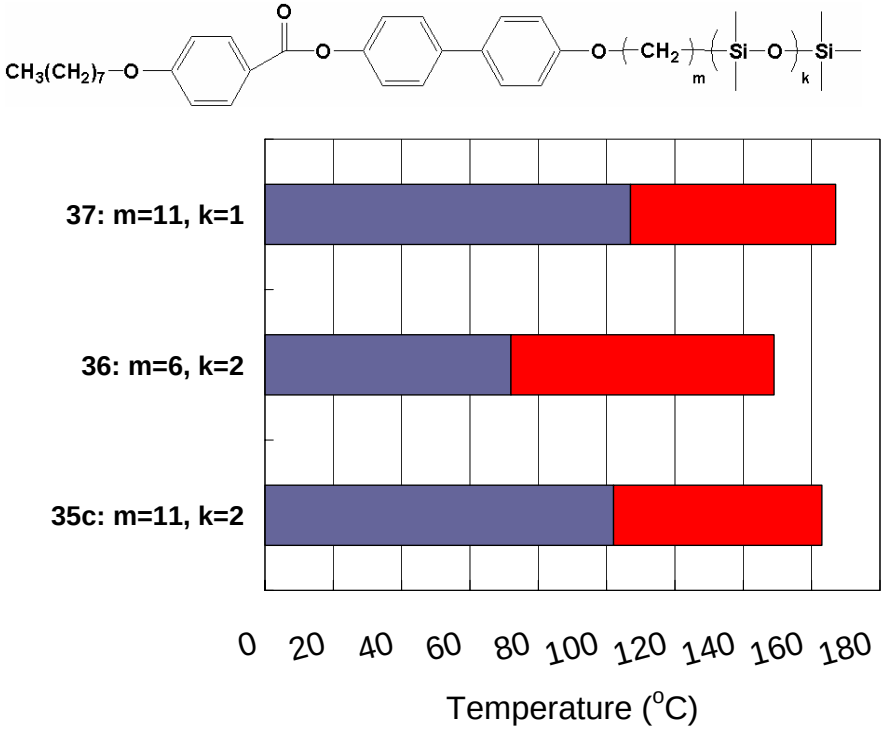

Figure 3-8. Phase transition temperatures for compounds **35c**, **36** and **37** measured by DSC on heating. Red: SmC phase; blue: Cr phase.

3.2 Siloxane-terminated phenyl benzoate liquid crystals

3.2.1 Synthesis

We attempted to use the same synthetic approach as for compounds **35a-f** to prepare compounds **38** and **39a-f** (Scheme 3-2). Surprisingly, the Mitsunobu reaction of hydroquinone with **45b** didn't work, and only starting material was recovered. Therefore, an alternative route to prepare these compounds was considered.

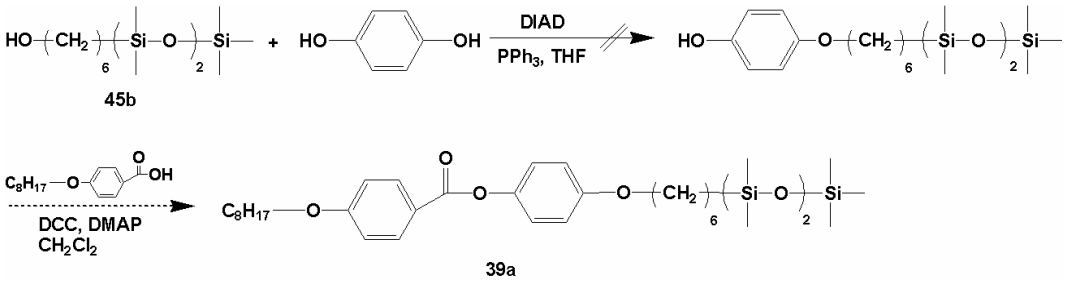

Scheme 3-2

It was found that the reaction of hydroquinone with bromo-substituted alkenes under basic condition proceeded to give the alkenyloxyphenol **50a** and **50b** in 40% and 42% yield, respectively (Scheme 3-3). Hence, a synthetic route was sought which involves preparing **51a** and **51b** first, followed by hydrosilation reaction of the vinyl end-group. This synthetic approach is outlined in Scheme 3-3.

For example, the synthesis of compound **39b** began with the monoalkylation of hydroquinone with 6-bromo-1-hexene under basic condition to give **50b** in 42% yield**.**

Compound **50b** was then esterified with 4-nonyloxybenzoic acid in the presence of DCC and DMAP to give **53b** in 83% yield. Hydrosilation of compound **52b** with 1,1,1,3,3,5,5-heptamethyltrisiloxane using Karstedt's catalyst gave **39b** in 87% yield. All compounds were recrystallized from EtOH prior to mesophase characterization.

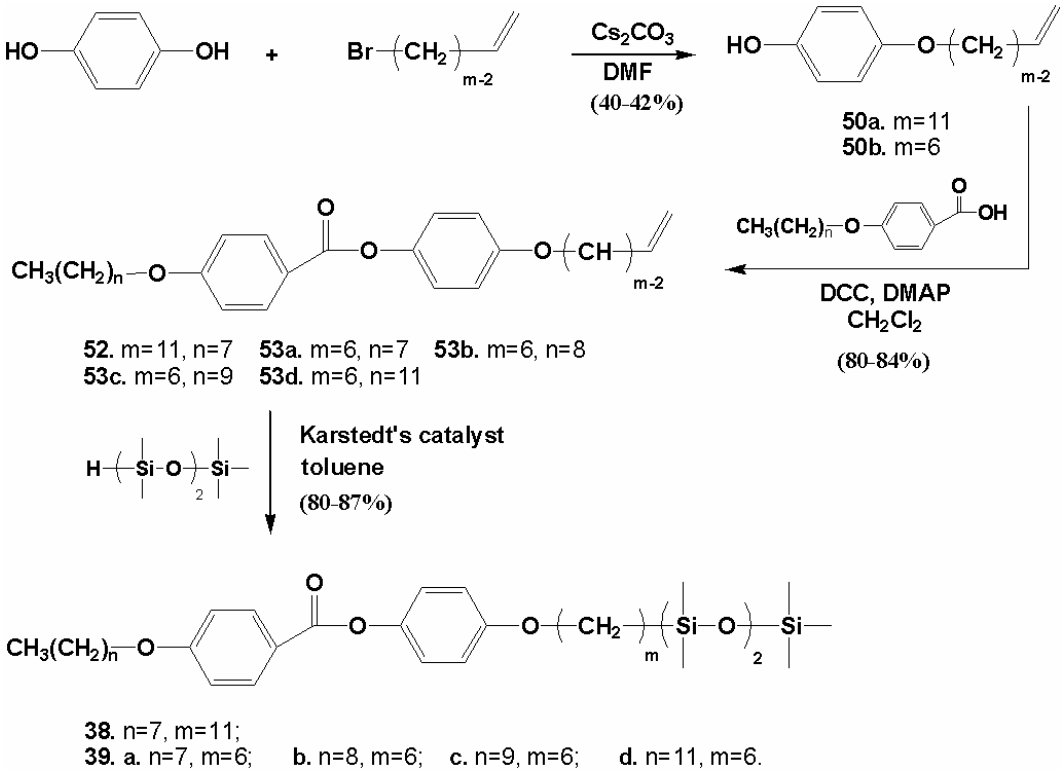

Scheme 3-3

3.2.2 Mesophase characterization

Compound **38** forms only a SmC phase as shown by the broken fan/Schlieren texture observed by POM (Figure 3-9 and Table 3-2). As expected, the SmC temperature range

of **38** is significantly lower than that of the biphenyl benzoate siloxane-terminated liquid crystals **35c** (Figure 3-10).

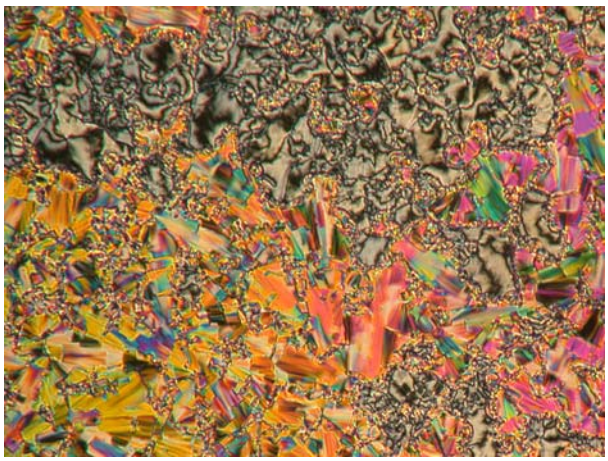

Figure 3-9. Textures of compound **38** observed by polarized microscopy on cooling: SmC phase at 58 ^{o}C. (100 X Magnification)

Table 3-2. Transition temperatures (^{o}C) and enthalpies of transitions (kJ/mol, in parentheses) for compounds **38** and **39a-d**.

Cpd	Cr		SmI		SmC		SmA		I
38	•	41(34.2)			•	82(10.5)			•
39a	•	9(15.7)			•	63(0.3)	•	69(8.3)	•
39b	•	9(16.1) [a]		10	•	62(0.3)	•	66(7.0)	•
39c	•	15(17.3)	•	22(2.0)	•	64(0.3)	•	68(8.5)	•
39d	•	31(20.5)			•	64(0.5)	•	67(7.3)	•

[a] ΔH derived from overlapping peaks for Cr-SmI and SmI-SmC transitions.

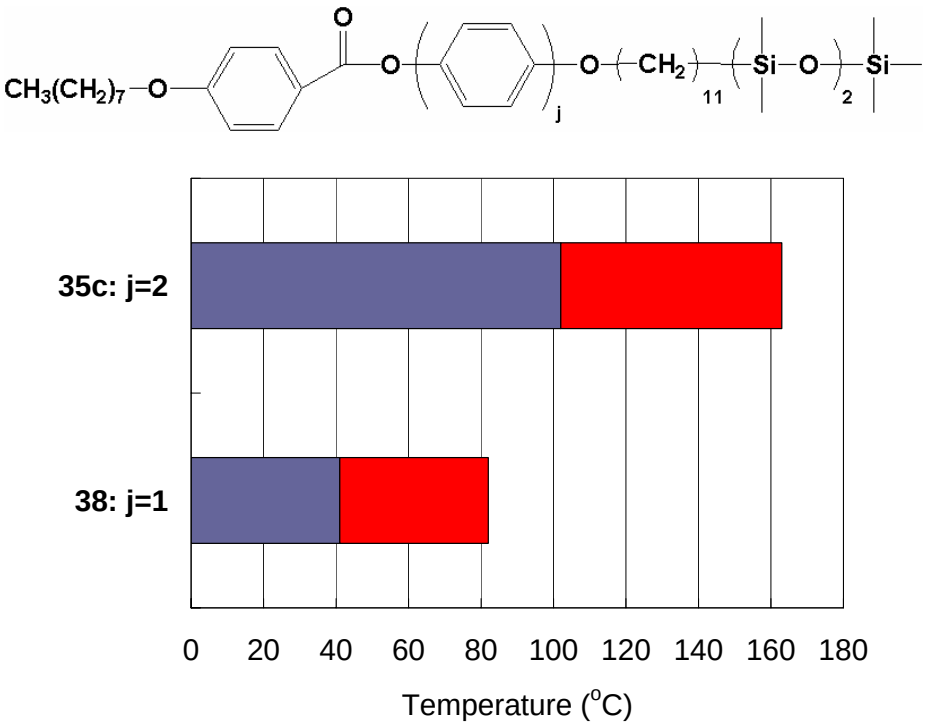

Figure 3-10. Phase transition temperatures for compounds **35c** and **38** measured by DSC on heating. Red: SmC phase; blue: Cr phase.

All four homologues of **39a** to **39d** form SmA and SmC phases on heating; compounds **39b** and **39c** also form a hexatic SmI phase on heating. All four homologues form SmA, SmC and SmI phases on cooling (Table 3-2 and Figure 3-13). Compounds **39a-c** form a SmC phase at room temperature. Increasing the alkoxy chain length *n* causes the SmA range to become narrower.

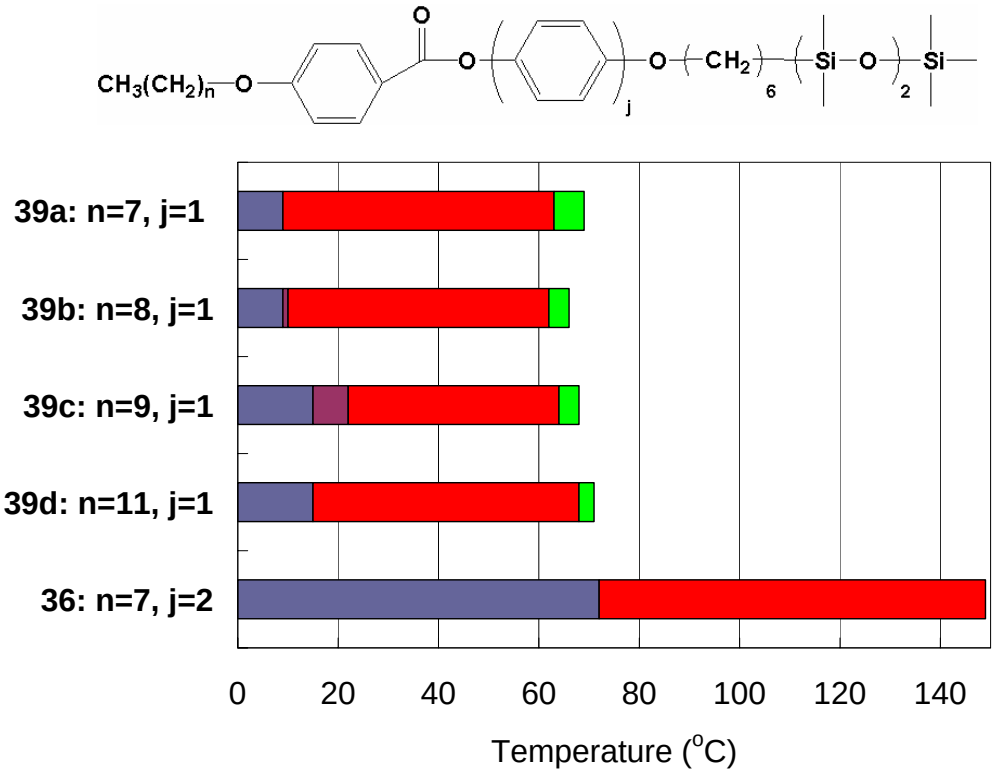

Figure 3-11. Phase transition temperatures for compounds **39a-d** and **36** measured by DSC on heating. Grey: Cr phase; Purple: SmI phase; Red: SmC phase; Green: SmA phase.

Representative POM textures are shown in Figure 3-12 for compound **39b**. On cooling from the isotropic liquid phase, the SmA phase of compound **39b** starts to form at 60°C, showing coexisting domains with fan and homeotropic textures. At 57°C, the textures change to broken fan and Schlieren textures, respectively, which is consistent with a transition to the SmC phase. On further cooling, a change in texture is apparent around 5°C, in which the broken fan domains turn into a sharper mosaic-like texture while the schlieren texture becomes somewhat less pronounced. This texture change

corresponds to a small exotherm on the DSC profile of **39b** (Figure 3-13), and is consistent with a hexatic SmI phase.[3] At -14°C, the crystal phase is formed.

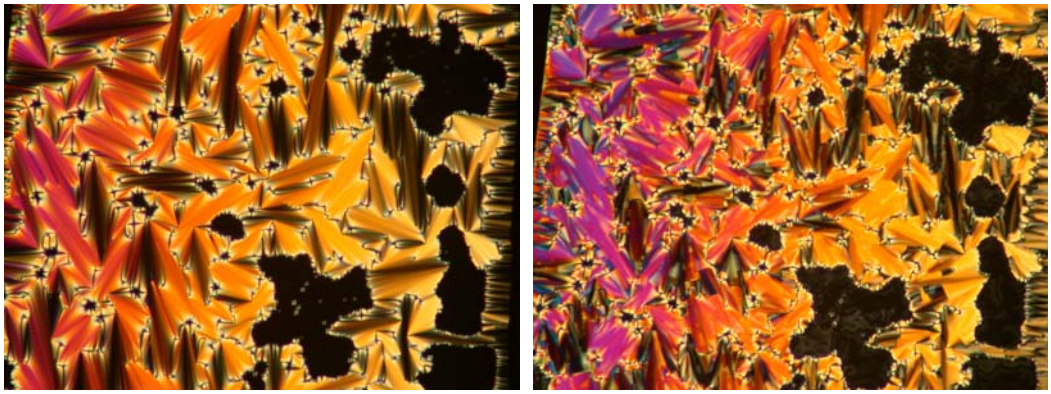

(a) (b)

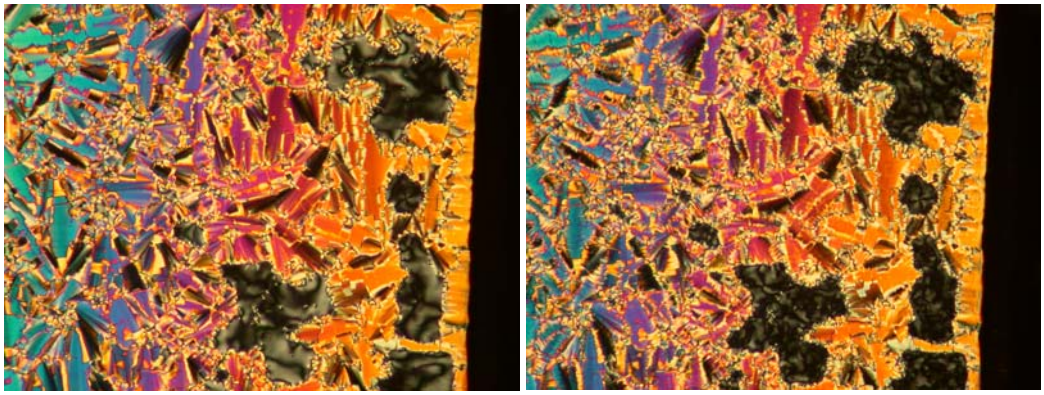

(b) (d)

Figure 3-12. Textures of compound **39b** observed by polarized microscopy on cooling: (a) SmA phase at 60°C, (b) SmC phase at 57°C, (c) SmI phase at 5°C, and (d) Cr phase at -14°C. (100 X Magnification)

A representative DSC profile is shown in Figure 3-13 for compound **39b**. The SmA-SmC phase transition is normally second order in nature, which is difficult to detect by DSC. However, with **39a-d**, the SmA-SmC transition produced a small endotherm peak

(ΔH=0.3-0.5 kJ/mol), which suggests that the SmA-SmC transition is weakly first order in nature. A small peak is observed near the melting point on heating **39b-c**, which is assigned to a SmI-SmC phase transition.

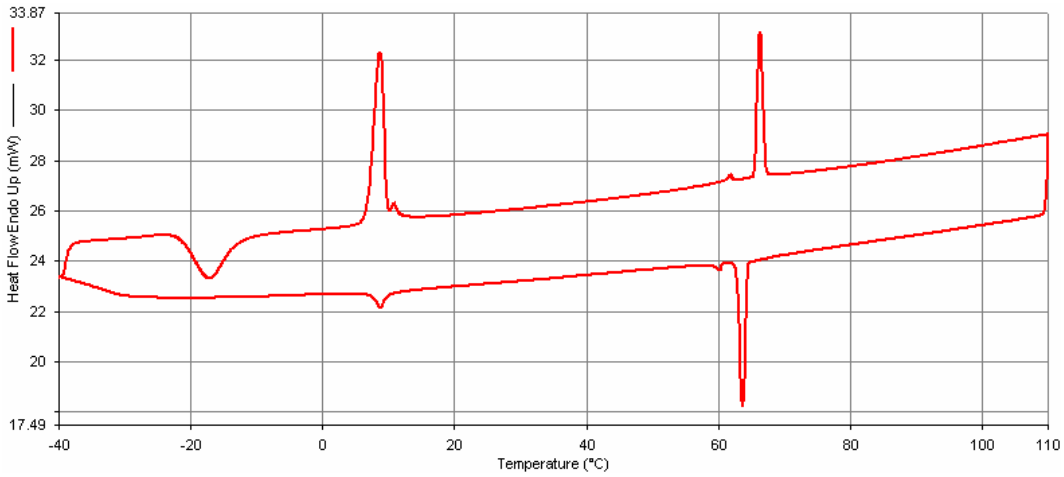

Figure 3-13. Differential scanning calorimetry (DSC) trace for compound **39b** taken at a scan rate of 5K/min.

To determine whether these compounds exhibit 'de Vries'-type behavior, the change in smectic layer spacing as a function of temperature was determined by small-angle powder X-ray diffraction for compounds **39a** and **39d**. The analyses show that the SmA-SmC phase transitions result in a maximum layer shrinkage of 5.5% in both cases, which is within the range of conventional materials with this phase sequence (Figure 3-14).

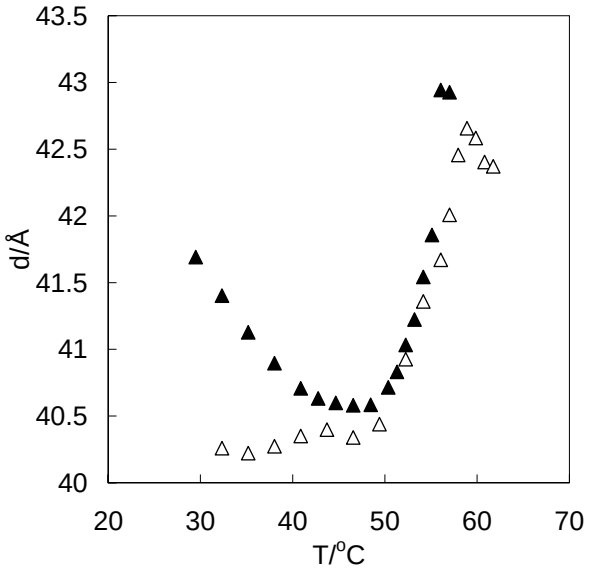

Figure 3-14. Smectic layer spacing *d vs.* temperature T for compounds **39a** (open triangles) and **39d** (filled triangles).

3.3 Siloxane-terminated phenyl benzoate liquid crystals with halogen end-group

The SmA temperature ranges of compounds **39a-d** (n=6) are relatively narrow (3-6K), as in the case of siloxane-terminated phenylpyrimidine liquid crystals. We used the strategies of incorporating a terminal chlorine atom into the side chain of **38** to possibly induce a SmA phase, and that of **39a** to broaden the SmA phase temperature range, and perhaps enhance its 'de Vries' character.

3.3.1 Synthesis

We attempted to use the similar synthetic approach as compound **39a-d** to prepare **40a** and **40b** (Scheme 3-4). Protection of the carboxylic acid group in 4-hydroxybenzoic

acid using methanol under acid condition gave methyl 4-hydroxybenzoate (**53**) in 87% yield. Mitsunobu reaction of **53** with 8-chloro-1-octanol afforded compound **54** in 55% yield. However, subsequent hydrolysis of the ester didn't give the desired compound, since under basic condition the desired compound reacts with itself to form a polyester. Therefore, an alternative synthetic route was sought as shown in Scheme 3-5.

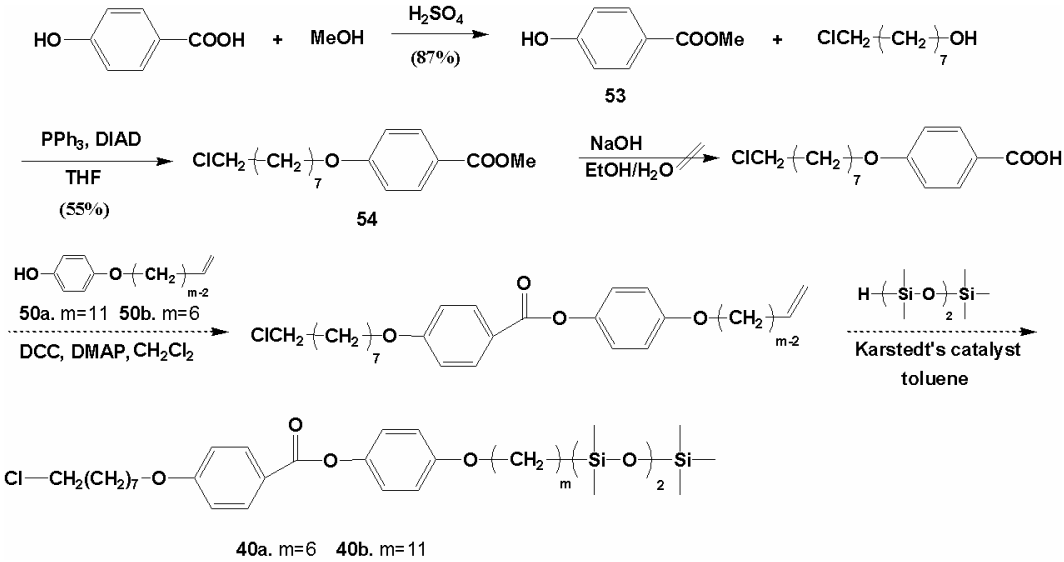

Scheme 3-4

The synthesis began with monoalkylation of hydroquinone with 11-bromo-1-undecene and 6-bromo-1-hexene under basic conditions to give **50a** and **50b** in 40% and 42% yield, respectively**.** Reaction of **50a** and **50b** with 4-hydroxybenzoic acid in the presence of DCC and DMAP gave **55a** and **55b** in 18% and 20% yield, respectively. Compound **55a** and **55b** were converted to **56a** and **56b** in 66% and 60% yield via a Mitsunobu reaction with 8-chloro-1-octanol in the presence of DIAD and PPh_3. The desired product **40a** and **40b** were then obtained from **56a** and **56b** in 85% and 80% yield

by platinum-catalyzed hydrosilation with 1,1,1,3,3,5,5-heptamethyltrisiloxane using Karstedt's catalyst. All compounds were recrystallized from EtOH prior to mesophase characterization.

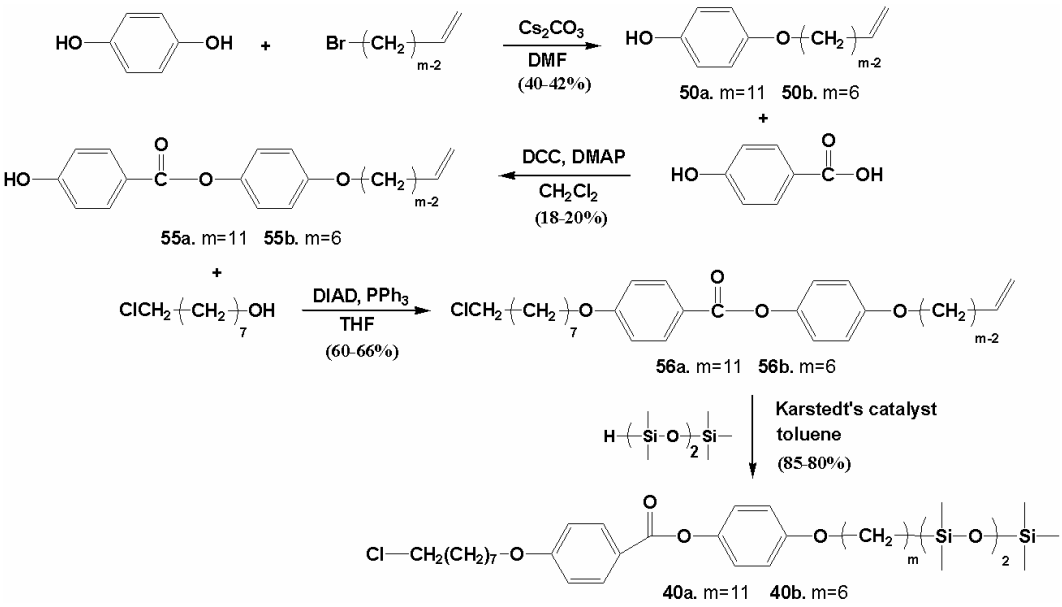

Scheme 3-5

3.3.2 Mesophase characterization

In the case of compound **40b**, DSC analysis shows that, the inclusion of a terminal chloro substituent results in a SmI phase on heating, a narrower SmC temperature range, and broader SmA range of 16K (Figure 3-15 and Table 3-3). The results are consistent with our previous results for siloxane-terminated phenylpyrimidine liquid crystals, except for the formation of SmI phase. We also observed a significant change in interference colors in the fan/broken fan textures upon cooling from the SmA to the SmC phase, which is consistent with an increase in birefringence and suggests that the SmA phase has

some ‘de Vries’ character (Figure 3-16). Results of layer spacing measurements by small-angle powder X-ray diffraction show a maximum layer shrinkage of only 1.7% for compound **40b** at the SmA-SmC phase transition, which is within the range of ‘de Vries’-type materials (Figure 3-17). The optical tilt angle θ_{opt} was measured by POM as a function of temperature using a 2.5% mixture of the chiral dopant **57** (Scheme 3-6) in **40b** by Dr. Jeff Robert and the results are shown in Figure 3-18. The de Vries coefficient C_{dv} for **40b** was calculated to be 0.72 at $T-T_C=-11K$, and therefore compound **40b** exhibits some ‘de Vries’ character. Comparing to the C_{dv} values of 0.96 and 0.95 for the known ‘de Vries’ materials **TSiKN65** and **3M8422**, the C_{dv} of **40b** is relatively small.

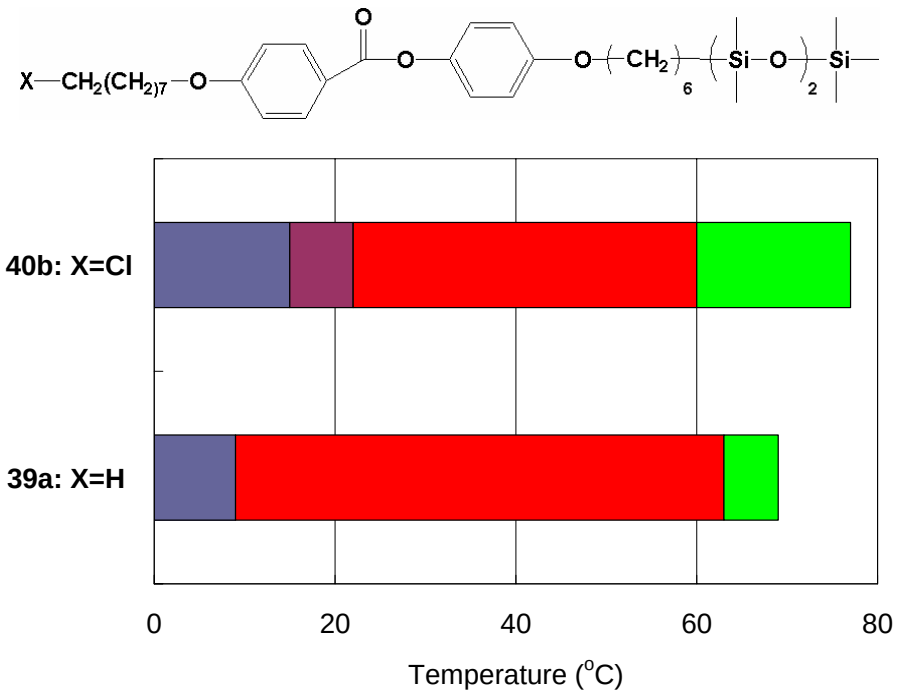

Figure 3-15. Phase transition temperatures for compounds **40b** and **39a** measured by DSC on heating. Grey: Cr phase; Purple: SmI phase; Red: SmC phase; Green: SmA phase.

Table 3-3. Transition temperatures (°C) and enthalpies of transitions (kJ/mol, in parentheses) for compounds **40a** and **40b**.

Cpd	Cr		SmI		SmC		SmA		I
40a	•					42(38.1)	•	91(10.6)	•
40b	•	15(15.0)	•	21(1.8)	•	59(0.1)	•	76(8.5)	•

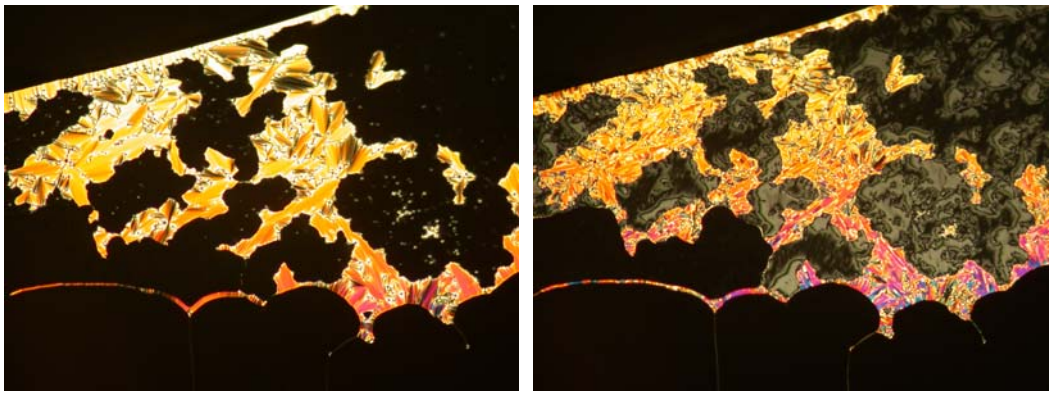

(a) (b)

Figure 3-16. Textures of compound **40b** observed by polarized microscopy on cooling: (a) SmA phase at 61°C, (b) SmC phase at 43°C. (100 X Magnification)

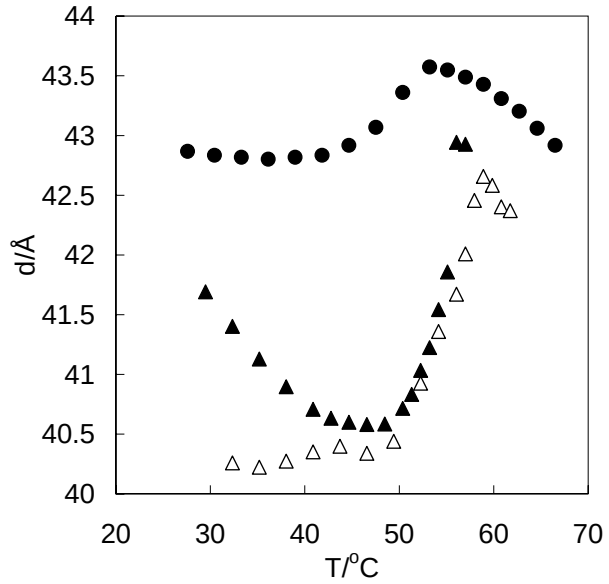

Figure 3-17. Smectic layer spacing *d vs.* temperature T for compounds **39a** (open triangles), **39d** (filled triangles) and **40b** (circles).

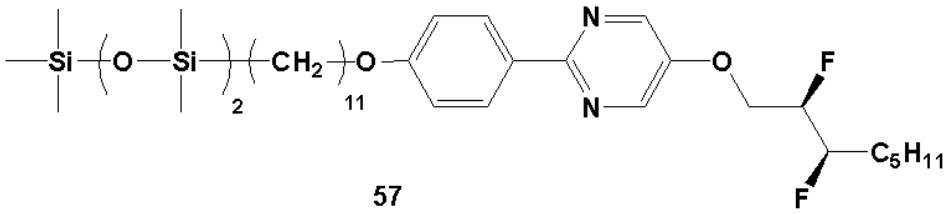

57

Scheme 3-6

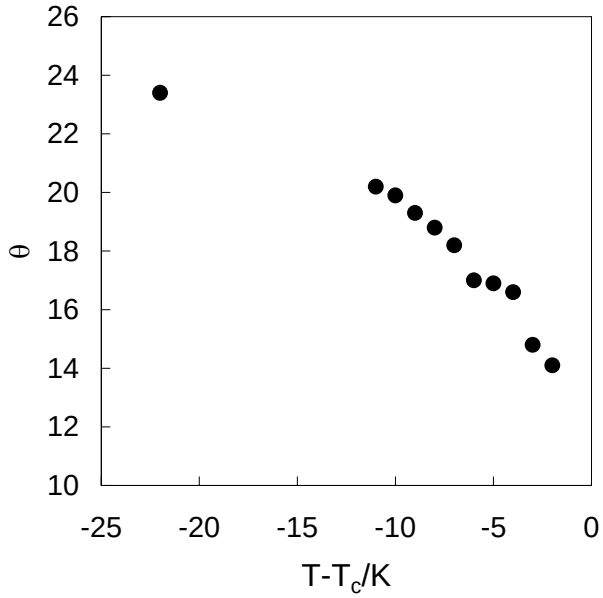

Figure 3-18. Optical tilt angle θ_{opt} *vs.* reduced temperature $T–T_C$ for compounds **40b**.

Remarkably, introducing a terminal chloro-substituent in **38** to give **40a** caused the SmC phase to vanish, forming the SmA phase exclusively, as shown by the sharp fan texture and homeotropic domains in Figure 3-18. This is inconsistent with previously observed trends showing that a larger alkyl spacer favors the formation of a SmC phase.

Figure 3-19. Textures of compound **40a** observed by polarized microscopy on cooling: SmA phase at 85 ^{o}C. (100X Magnification)

3.3 Conclusion

The influence of variations in chain length, number of siloxy units, chloro substitution and structure of aromatic cores on the phase behavior of siloxane-terminated benzoate-type liquid crystals has been presented. Siloxane-terminated biphenyl benzoate liquid crystals studied here form a SmC phase only. Siloxane-terminated phenyl benzoate liquid crystals also form a SmC phase, and in some cases SmA and SmI phases, with significantly lower SmC temperature ranges than siloxane-terminated biphenyl benzoate liquid crystals. The temperature range of the SmA phase may be broadened by the addition of a terminal chloro substituent on the alkoxy side-chain. In some cases, incorporation of a terminal chloro substituent affects not only the mesophase thermal stability, but also the nature of the mesophase formed. The compound 4-[6-(1,1,1,3,3,5,5-Heptamethyltrisiloxanyl)hexanoyloxy]phenyl 4-(8-chlorooctyloxy)benzoate (**40b**) is characterized by a maximum layer shrinkage of only 1.7% at SmA-SmC phase transition,

and its de Vries coefficient C_{dv} was calculated to be 0.72 at $T-T_C$=-11K. Comparing to the C_{dv} values of 0.96 and 0.95 for the known 'de Vries' materials **TSiKN65** and **3M8422**, the C_{dv} of **40b** is relatively small. Compound **40b** may be considered to possess some 'de Vries' character.

3.5 References

(1) Coles, H. J.; Meyer, S.; Lehmann, P.; Deschenaux, R.; Jauslin, I.; *J. Mater. Chem.* **1999**, 9, 1085.

(2) *An Introduction to Liquid Crystals: Chemistry and Physics.;* Collings, P.; Hird, M. Ed.; Taylor & Francis: London, **1997**.

(b) *Textures of liquid crystals*; Dierking, I. Ed.; Wiley-VCH: Weinheim, **2003**.

Chapter 4. Synthesis and Photochemistry of Fulgide and Fulgimide Dopants

Previous work in the Lemieux group focused on the addition of a siloxane end-group to diarylethene compounds in order to improve their compability with siloxane-terminated liquid crystal hosts. However, it was found that the dithienylethene dopants (with or without siloxane end-groups) are incompatible with siloxane-terminated hosts, and the compounds with siloxane end-groups are actually somewhat worse than compounds without siloxane end-groups. This incompatibility was attributed to the significant lateral bulk of the diarylethene core, which in turn strongly destabilizes the layer structure of the SmC phase. Bistable photochromic compounds which have a smaller core size relative to diarylethene may solve this compatibility problem. Fulgimide are such compounds, and the siloxane-terminated fulgimide dopants **41** was first designed to have a better compatibility with siloxane-terminated liquid crystal hosts (Scheme 4-1).

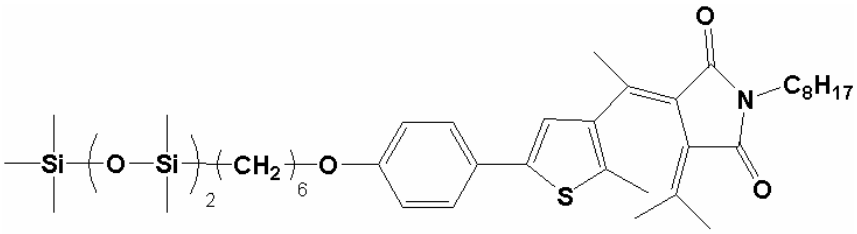

41

Scheme 4-1

4.1 Synthesis

4.1.1 Stobbe Condensation Route

The route used most frequently to prepare fulgide and derivatives employs the "Stobbe condensation reaction", which was first carried out by Stobbe, a pioneer of fulgide chemistry (Scheme 4-2).[2,3]

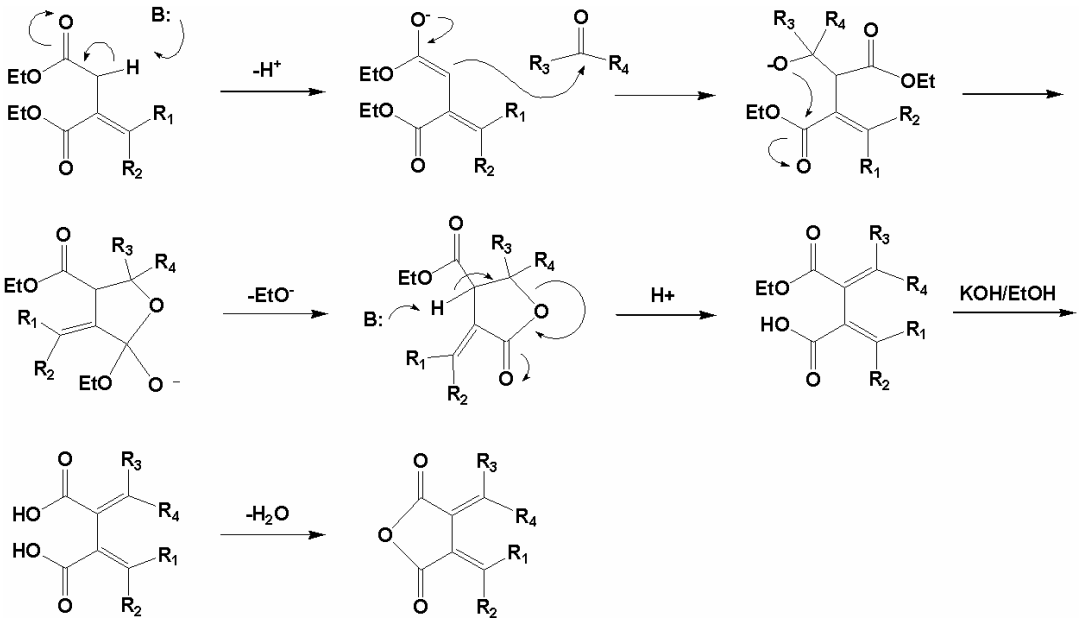

Scheme 4-2

Initially, we followed the Stobbe condensation approach to synthesize the fulgimide **41**, as shown in Scheme 4-3. Bromination of 2-methylthiophene gave 3,5-dibromo-methylthiophene (**58**) in 88% yield. 4-Bromoanisole was converted to the boronic acid **59** in 89% yield via metal-halogen exchange with n-butyllithium and trapped with triisopropyl borate. Then, Suzuki cross-coupling of **58** with **59** in the presence of

$Pd(PPh_3)_4$ gave **60** in 81% yield. Another metal-halogen exchange reaction with n-butyllithium and trapping with carbon dioxide gave compound **61** in 85% yield. Conversion of the carboxylic acid group in **61** to an acetyl group was achieved by nucleophilic addition of methyl lithium to give **62** in 51% yield. However, the subsequent Stobbe condensation of **62** with isopropylidene diethyl succinate **63** to prepare the corresponding fulgide was unsuccessful. Compound **63** was treated with lithium diisopropylamide (LDA) in THF and added to a suspension of cerium chloride in THF followed by addition of the ketone **62**, but the reaction only gave the starting material back. The condensation reaction was also performed using NaH as base but the reaction still didn't proceed. This is likely due to the enolate not being nucleophilic enough to achieve nucleophilic addition to the ketone. Therefore, an alternative route to prepare the fulgide was considered.

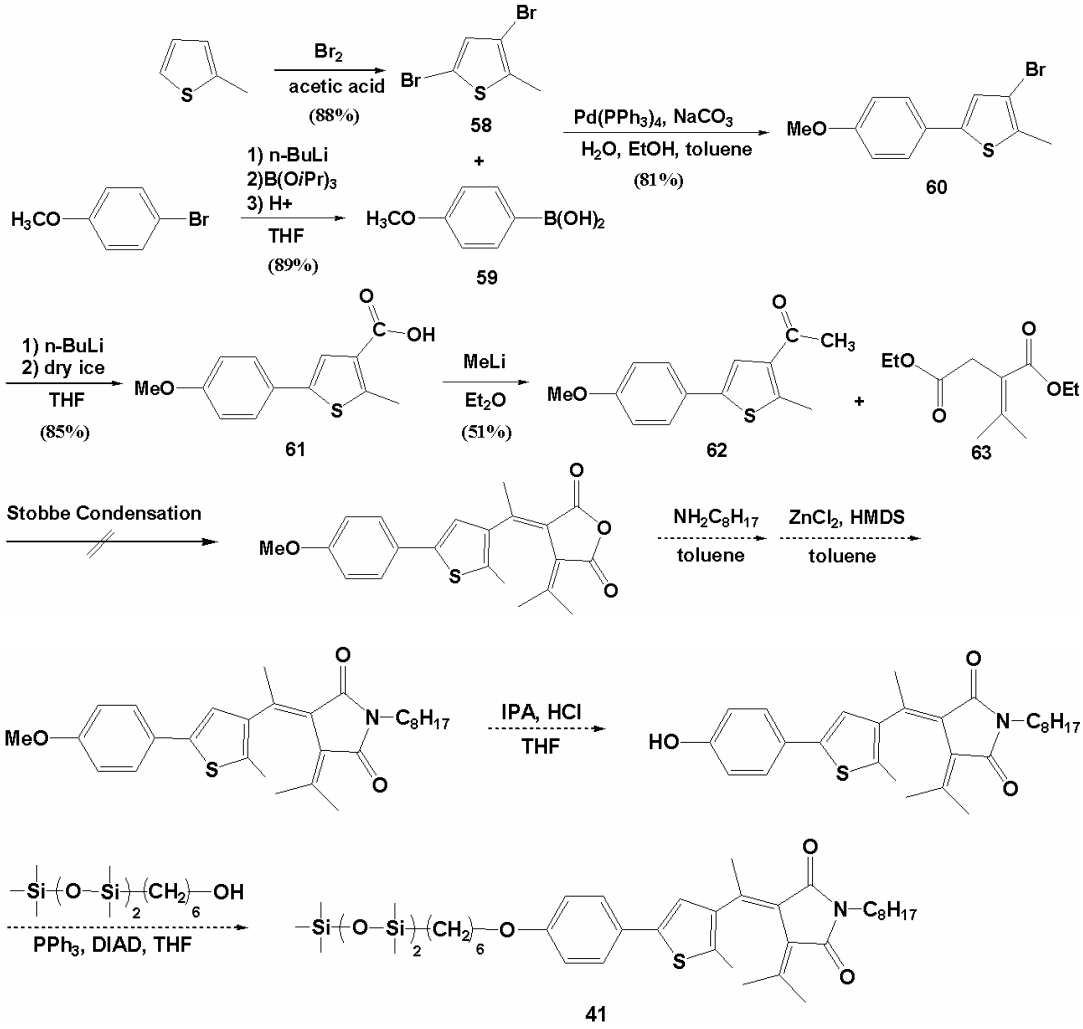

Scheme 4-3

4.1.2 Pd-catalyzed Carbonylation Route

Kiji *et al.* reported that the reaction of substituted 1,4-butynediol with carbon monoxide in the presence of a Pd catalyst, under elevated temperature and high pressure, afforded the corresponding fulgide and the corresponding fulgenic acid.[4,5,6] This method was reported to be useful for the synthesis of sterically congested fulgides. While the Stobbe condensation of 2,5-dimethyl-3-pivaloylfuran with diethyl

isopropylidenesuccinate using LDA as base failed to proceed,[7] the Pd-catalyzed route was reported to give the corresponding fulgide in 59% yield, together with the diacid in ca. 20% yield.[4] One limitation is that this reaction was not effective for the synthesis of fulgides with a strongly electron-donating aryl groups such as indolylfulgides with an *N*-methyl group. However, *N*-tosylindolylfulgide was synthesized in ca. 30% yield by this method.[5] The mechanism of the Pd-catalyzed carbonylation is shown in Scheme 4-4.

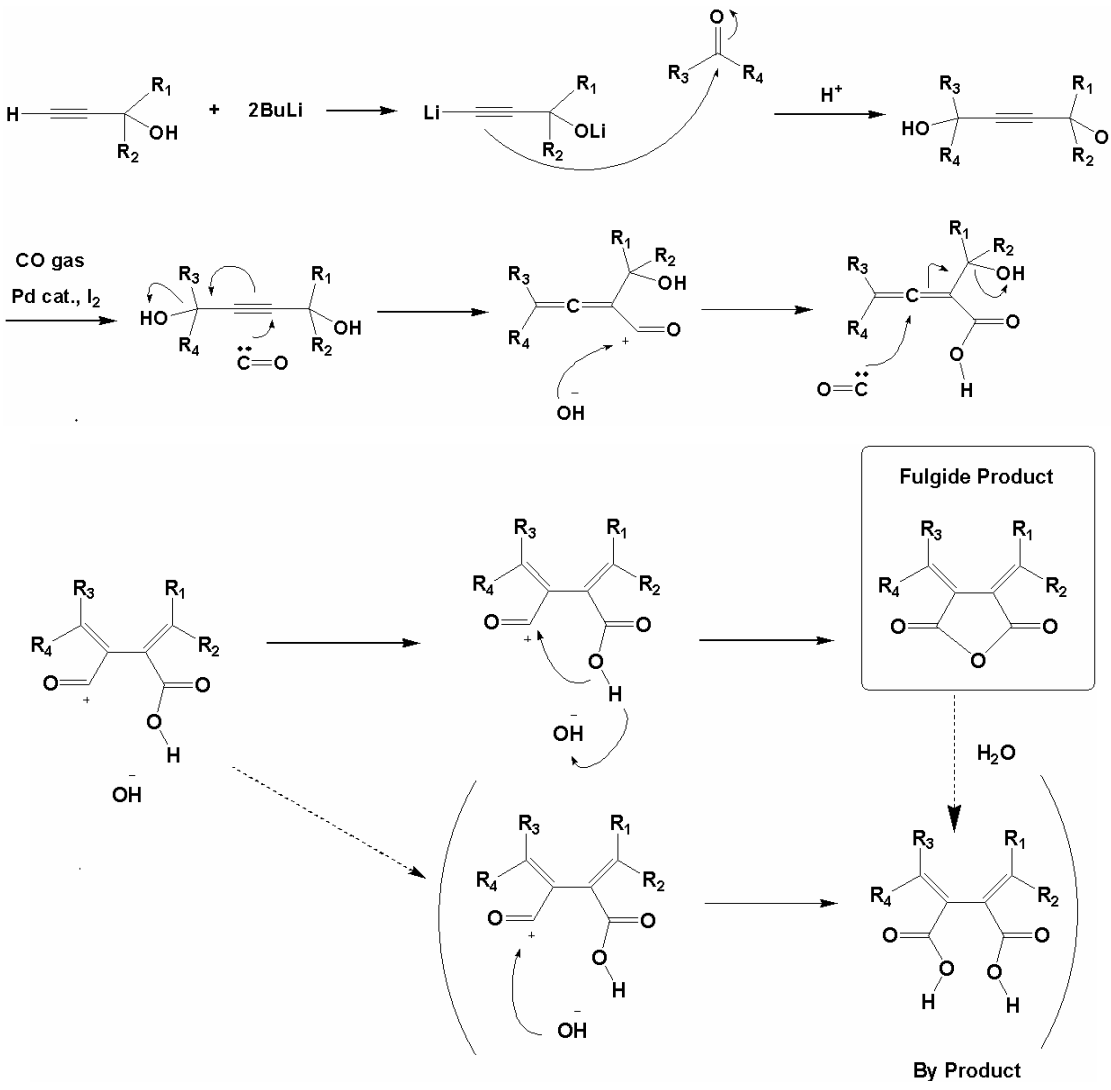

Scheme 4-4

The initial step of the carbonylation method is a nucleophilic addition reaction which is similar to the Stobbe condensation method. However, the alkynyl lithium in the carbonylation method is more nucleophilic than the enolate in the Stobbe condensation method, and the carbonylation method is therefore expected to give better results. Compound **62** was treated with the dilithium species, as shown in Scheme 4-5 (a), but the reaction still didn't proceed and only starting material was isolated.

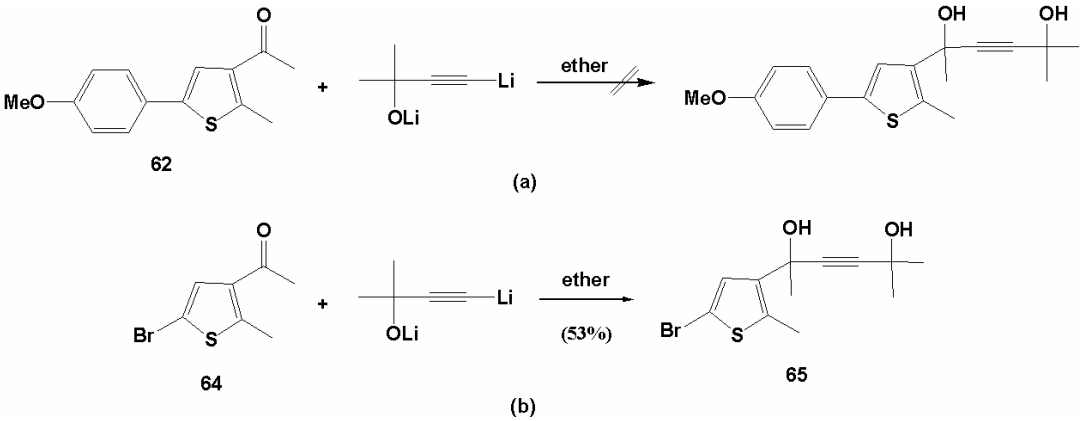

Scheme 4-5

Failure of this reaction may be due to the low electrophilicity of the carbonyl carbon in **62**, given the presence of the 4-methoxyphenyl substituent on the thiophene ring. The same reaction was then performed using **64**, which is more electrophilic given the electron-withdrawing bromo group on the thiophene ring, and the reaction did produce the diol **65** in 53% yield. (Scheme 4-5 (b)). Hence, an alternative synthetic route was sought which involves nucleophilic addition onto **64** first, followed by conversion of the bromo substituent to a methoxyphenyl group via a Suzuki cross-coupling reaction. This synthetic approach is outlined in Scheme 4-6.

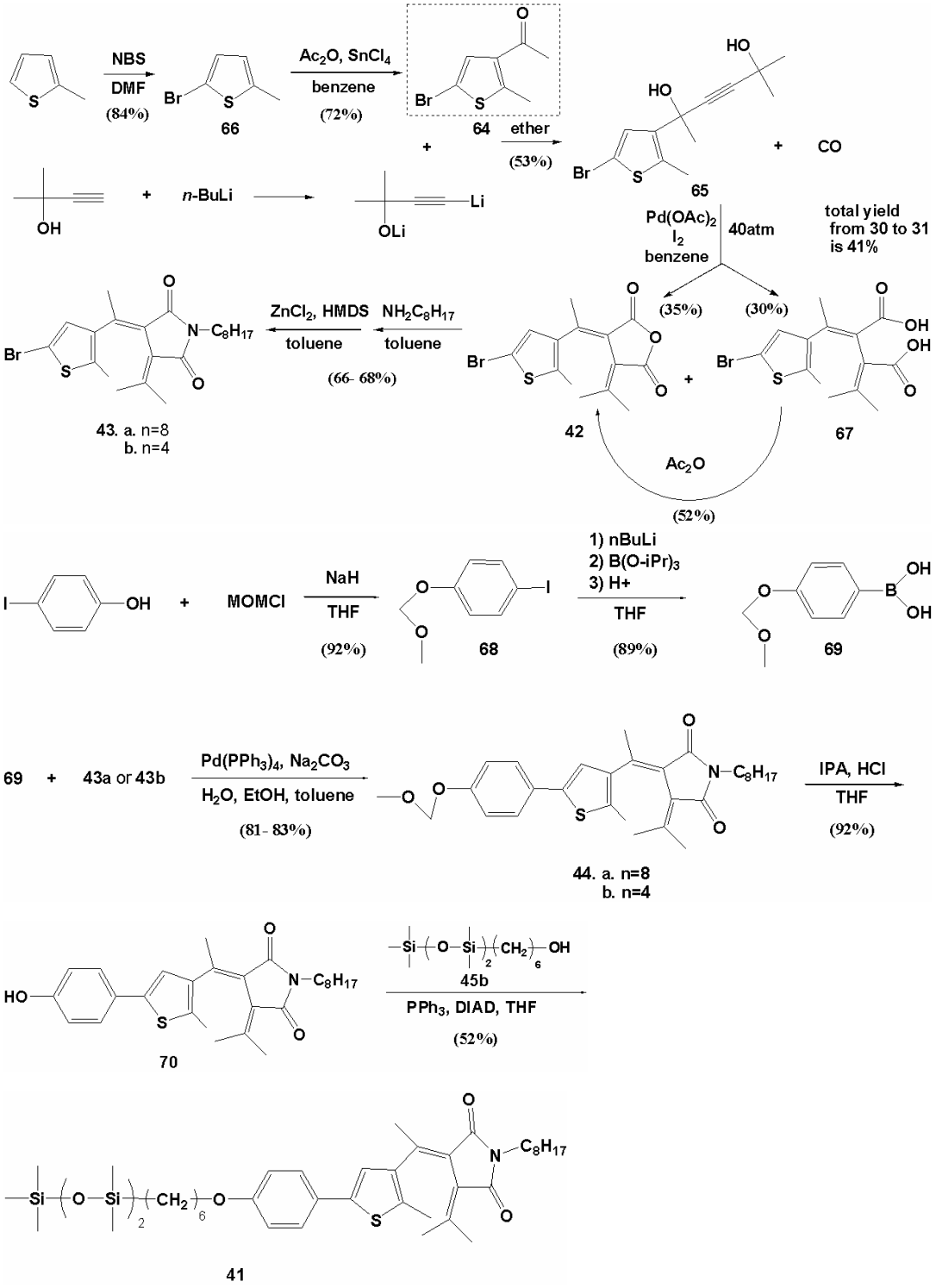
NBS
DMF
(84%)
66
Ac2O, SnCl4
benzene
(72%)
64
ether
(53%)
65
CO
n-BuLi
Pd(OAc)2
I2
benzene
40atm
total yield from 30 to 31 is 41%
(35%)
(30%)
42
67
Ac2O
(52%)
ZnCl2, HMDS
toluene
NH2C8H17
toluene
(66- 68%)
43. a. n=8
b. n=4
1) nBuLi
2) B(O-iPr)3
3) H+
THF
(89%)
NaH
THF
(92%)
68
69
MOMCl
69 + 43a or 43b
Pd(PPh3)4, Na2CO3
H2O, EtOH, toluene
(81- 83%)
IPA, HCl
THF
(92%)
44. a. n=8
b. n=4
45b
PPh3, DIAD, THF
(52%)
70
41

Scheme 4-6

Bromination of 2-methylthiophene with N-bromosuccinimide (NBS) gave 2-bromo-5-methylthiophene (**66**) in 84% yield, and Friedel-Crafts acylation with acetic anhydride in the presence of tin(IV) chloride gave 3-acetyl-2-bromo-5-methylthiophene (**64**) in 72% yield. Compound **64** was then treated with the alkynyl lithium species to give the diol **65** in 53% yield. The carbonylation reaction of **65** gave the fulgide **42** and by-product diacid **43** in 35% and 30% yield respectively. The by-product **43** was converted to the fulgide **42** by condensation in the presence of acetic anhydride in 52% yield. The total yield of fulgide **42** from **65** was 41%. The fulgide **42** then underwent a one-pot reaction with octylamine promoted by zinc chloride as a Lewis acid and hexamethyldisilazane (HMDS) to form the N-substituted fulgimide **43** in 68% yield, according to Liang *et. al*.[8] The hydroxy group in 4-iodophenol was protected with a MOM group under basic condition to give **68** in 92% yield. Subsequent metal-halogen exchange reaction using n-butyllithium and trapping with triisopropyl borate gave 4-(methoxymethoxy)phenylboronic acid **69** in 89% yield. A Suzuki cross-coupling reaction between **69** and **43a** in the presence of $Pd(PPh_3)_4$ gave the fulgimide **44a** in 83% yield. Deprotection of the hydroxy group with hydrochloric acid and IPA gave compound **70** in 92% yield, which was then condensed with **45b** via a Mitsunobu reaction to give the final compound **41** in 52% yield. The synthetic approach prepared the final compound **41** in 12 steps in an overall yield of 3% from 2-methylthiophene.

Unfortunately, compound **41** proved to be an oil at room temperature, which made it difficult to purify and unsuitable for mixing with liquid crystal hosts. The low melting point of compound **41** was attributed to a combination of the siloxane tail and long alkyl chain in the compound. We therefore turned our attention to the fulgide precusors **42, 43a** and **44b** which are solids at room temperature (Scheme 4-6). One of the key requirements of photochromic system for the development of a liquid crystal photoswitch is that fast switching must be achieved, so the photoisomerization must occur rapidly and with high quantum efficiency. Compound **42**, **43a** and **44b** were assessed as photochromic dopants in terms of this requirement, and their photophysical properties were studied in solution.

4.2 Photoisomerization in Isotropic Solution

The E-, Z- and C-forms of fulgide derivatives show different NMR spectra. For example, Ulrich *et al.* reported that, in the E-form of compound **71** (Scheme 4-7), the methyl group α-CH_3 (1.30 ppm) is shielded by the thiophene ring, while in the Z-form the α-CH_3 (2.13 ppm) is outside of the shielding zone of the thiophene ring. Compared to that of E- (6.56 ppm) and Z-forms (6.35 ppm), the resonance of β-H in the C-form is at higher field (6.18 ppm).[9] After compound **42**, **43a** and **44b** were synthesized and purified by column chromatography, their NMR spectra showed only one set of peaks (Figure 4-1). This suggests that only one isomer X was obtained.

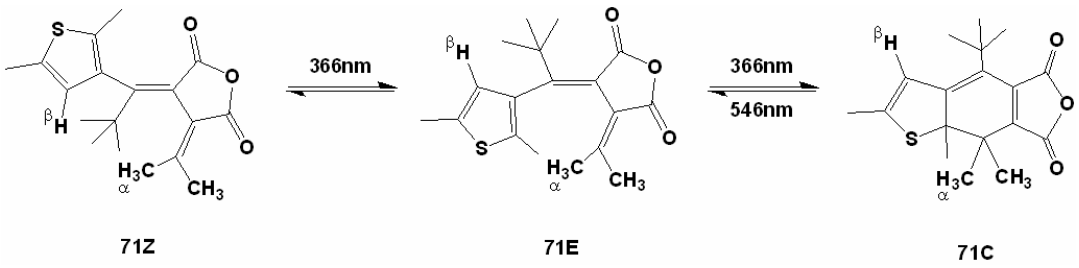

Scheme 4-7

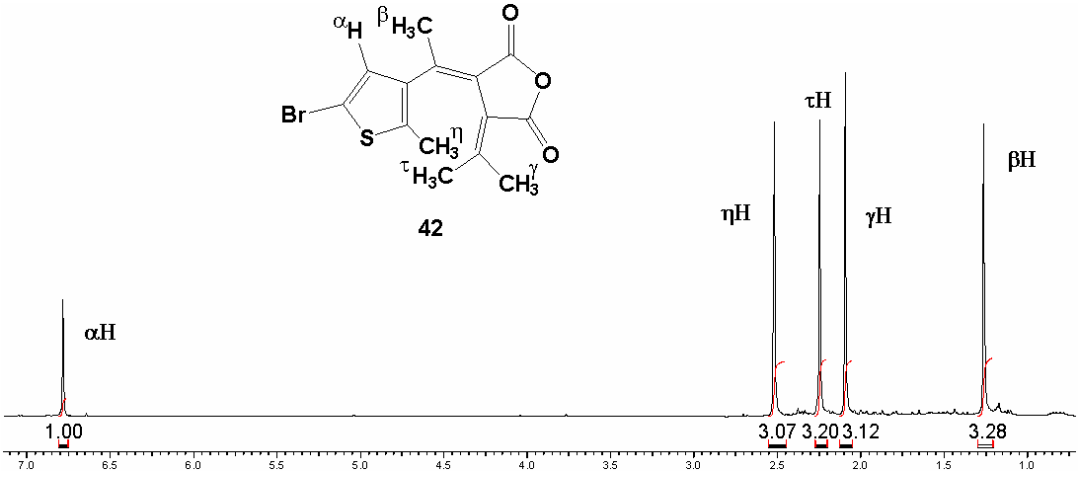

Figure 4-1. NMR spectrum of compound **42** in $CDCl_3$ after synthesis and purification by column chromatography.

A PTI A6000 450W Xe arc lamp (25A, 18V) fitted with a water filter (to cut off the infrared output) was used as the light source for the photoisomerization process. When hexanes solutions of the isomer X (corresponding to State A, Scheme 4-8) of compound **42** and **43a** were irradiated with UV light (365nm or 313nm), the initial colorless solution became yellow (the photostationary state, pss, corresponds to State B). When isomer X of compound **44b** was irradiated with UV light (365nm or 313nm), the colorless solution became purple. These are consistent with the formation of the ring-closed C-forms from

either the E-forms or Z-forms. Irradiation with visible light (λ>450nm) caused the color to disappear (pss corresponding to State C), which is consistent with the regeneration of the ring open isomers.

Scheme 4-8

Figure 4-2 shows the UV-vis spectra of compound **43**, **43a** and **44b** in States A, B and C respectively. The spectra of fulgimide **43a** are red-shifted in all of the three states relative to its parent fulgide **42,** which is consistent with what was reported in the literature.[10] Replacement of the electron-withdrawing bromo substituent on the thiophene ring in **43a** with the electron-donating 4-methoxyphenyl group in **44b** results in a red-shift of the absorption of the C-form. This electronic effect is in good agreement with the previously reported observations,[11,12,13] which suggests that the excited states of both the E- and C-forms arises from a charge transfer from the aromatic ring to the anhydride group.

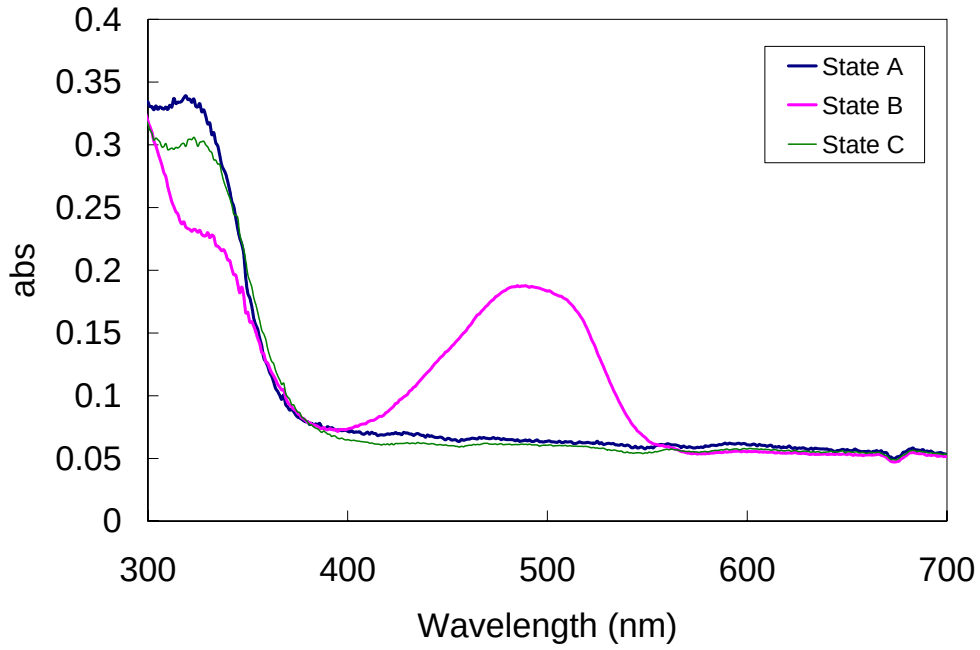
0.4
0.35
0.3
0.25
0.2
0.15
0.1
0.05
0
abs
300
400
500
600
700
Wavelength (nm)
State A
State B
State C

(a)

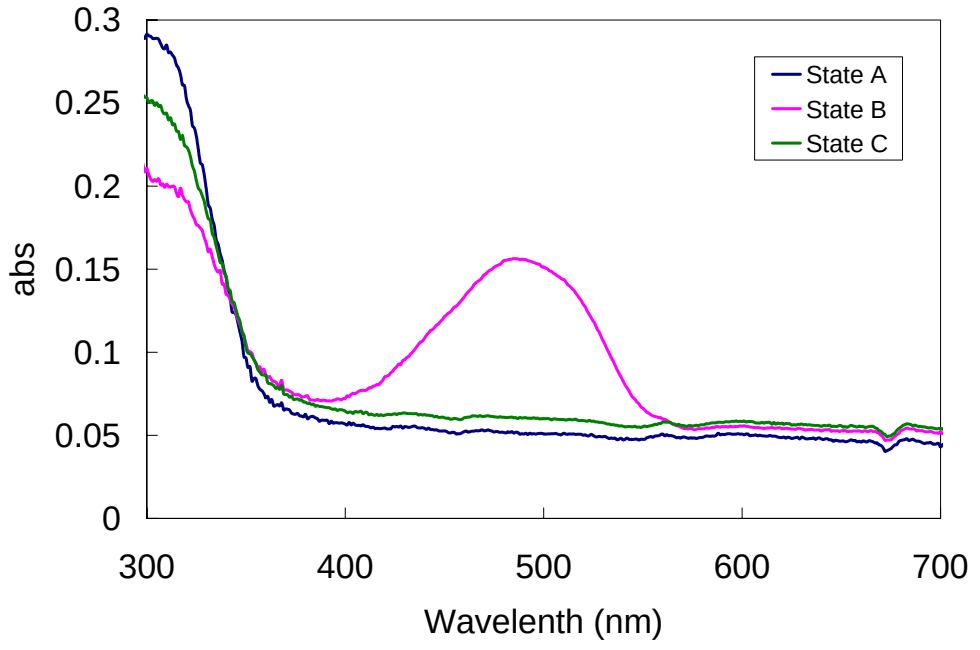
0.3
0.25
0.2
0.15
0.1
0.05
0
abs
300
400
500
600
700
Wavelenth (nm)
State A
State B
State C

(b)

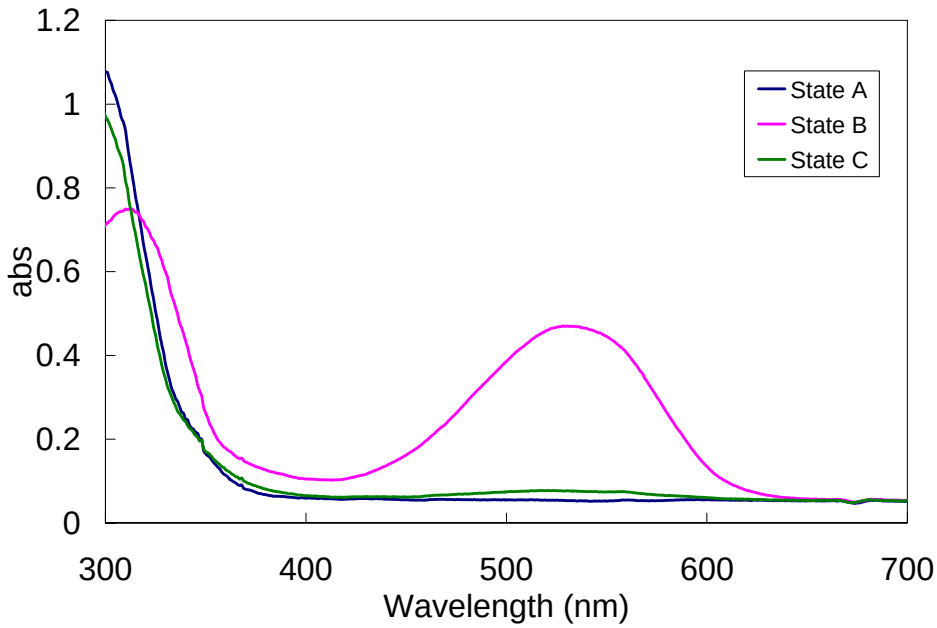

(c)

Figure 4-2. (a) State A, B and C of 0.37 mM of **42** in hexanes, (b) State A, B and C of 0.34 mM of **43a** in hexanes, and (c) State A, B and C of 0.43 mM of **44b** in hexanes.

The UV-vis absorption spectra change of **44b** from State A to State B and from State B to State C (*λ=313nm*) are shown in Figure 4-3 (a) and (b), respectively as an representative example. Upon irradiation of **44b** at 313nm, a broad absorption band in the visible range (λ_{max}=530nm) appears, concomitant with a decrease in the absorption at 300nm. Upon irradiation at λ>450nm, the visible absorption band disappears, and the absorption at around 300nm reappears. Irradiation using *λ=365nm* and λ>450nm light gave similar results (Figure 4-4 (a) and (b)).

The absorption of compound **44b** at λ_{max} in the visible range (at ~520nm) was plotted versus time for the coloration and decoloration process, respectively (Figure 4-3(c) and

(d), Figure 4-4 (c) and (d)). Table 4-1 lists the observed half-lives for compound **43**, **43a** and **44b**, which are comparable to half-lives reported in the literature for similar compounds.[9, 10] It was found that, for all three compounds, the coloration process (λ=313nm or 365nm) is slower than the decoloration process (λ>450nm). The difference between coloration and decoloration rate may be attributed, at least partially, to the spectral overlap. Thus, in the case of decoloration, a relatively large fraction of the visible light is absorbed by the C-form and a small fraction by the E-form, thus allowing for selective excitation of the C-form. In the case of coloration, on the other hand, selective excitation of the E -form is less effective at 313nm and 365nm, where a significant fraction of the light is absorbed by the colored C-form as the reaction proceeds, thus causing to lower the observed coloration rate. It was also found that coloration with 313nm light allows the pss to be reached faster than with 365nm light.

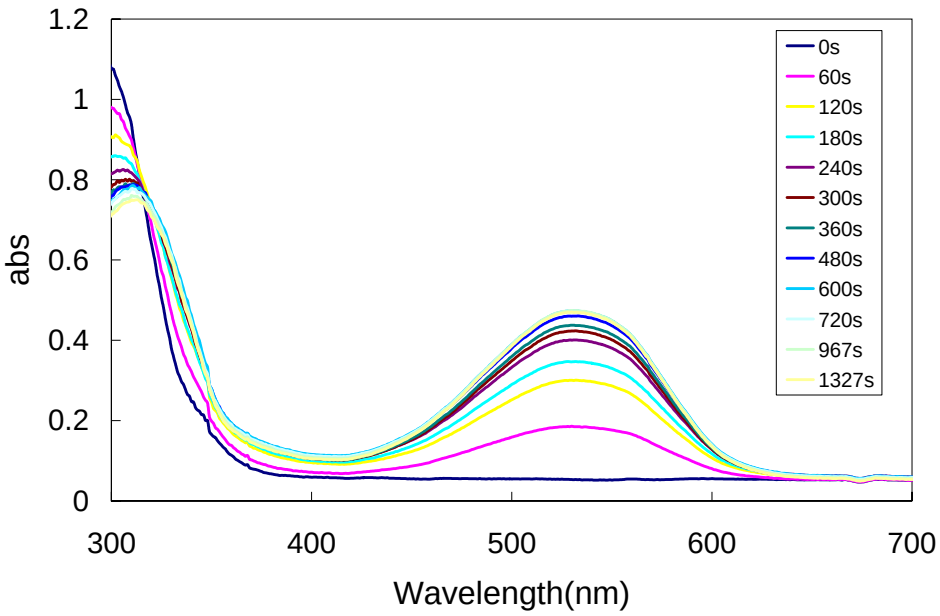
1.2
1
0.8
0.6
0.4
0.2
0
abs
300
400
500
600
700
Wavelength(nm)
0s
60s
120s
180s
240s
300s
360s
480s
600s
720s
967s
1327s

(a)

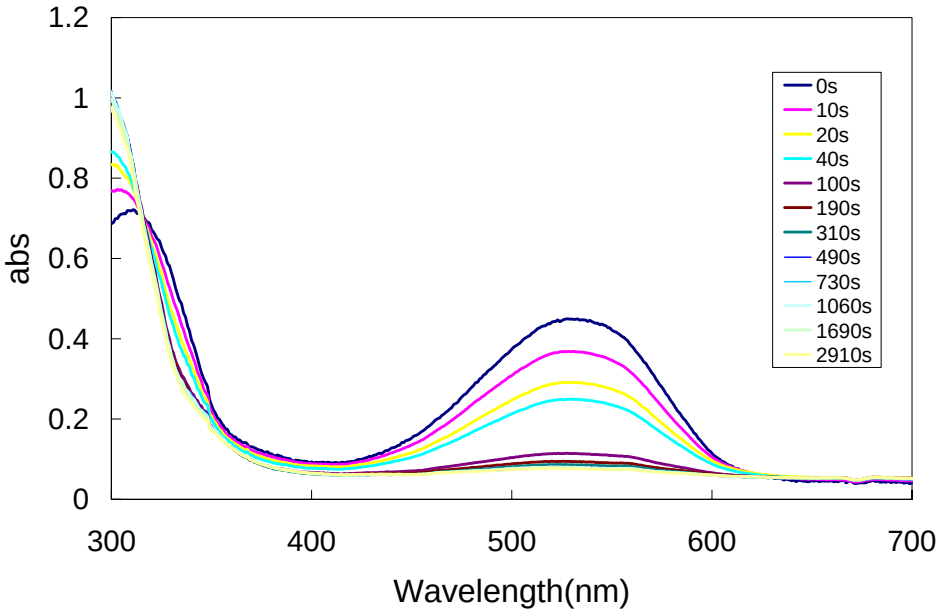
1.2
1
0.8
0.6
0.4
0.2
0
abs
300
400
500
600
700
Wavelength(nm)
0s
10s
20s
40s
100s
190s
310s
490s
730s
1060s
1690s
2910s

(b)

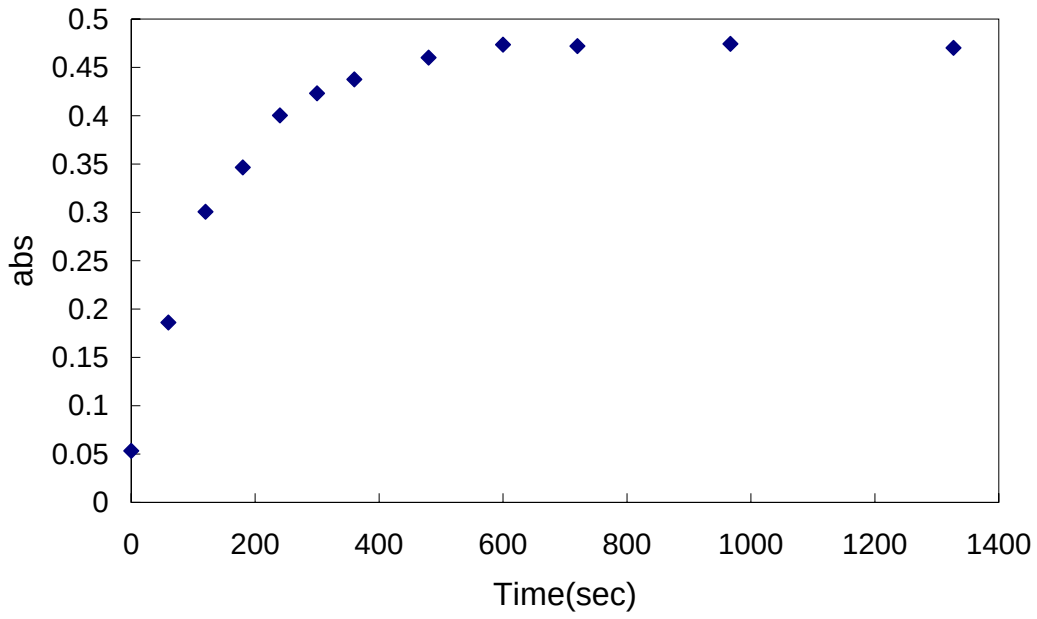

(c)

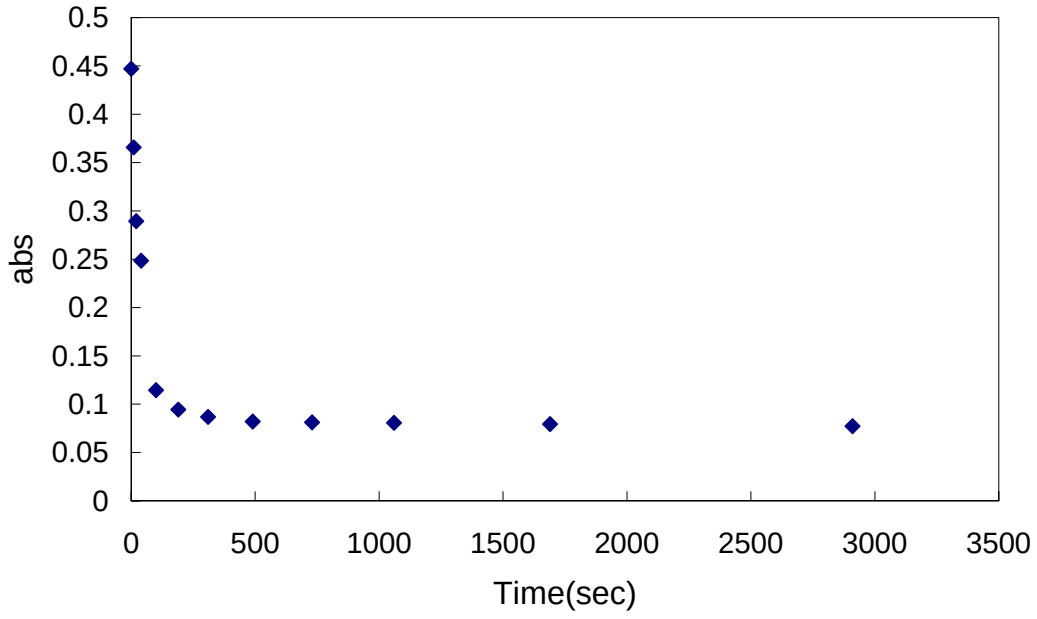

(d)

Figure 4-3. Fulgimide **44b** in 0.43 mM hexanes solution: (a) photochemical coloration of State A with *λ=313nm* light, (b) decoloration of State B with λ>450nm light, (c) plot of absorbance *versus* time at 530nm for the coloration, (d) plot of absorbance *versus* time at 523nm for the decoloration. A PTI A6000 450W Xe arc lamp (25A, 18V) fitted with a water filter (to cut off the infrared output) was used as the light source.

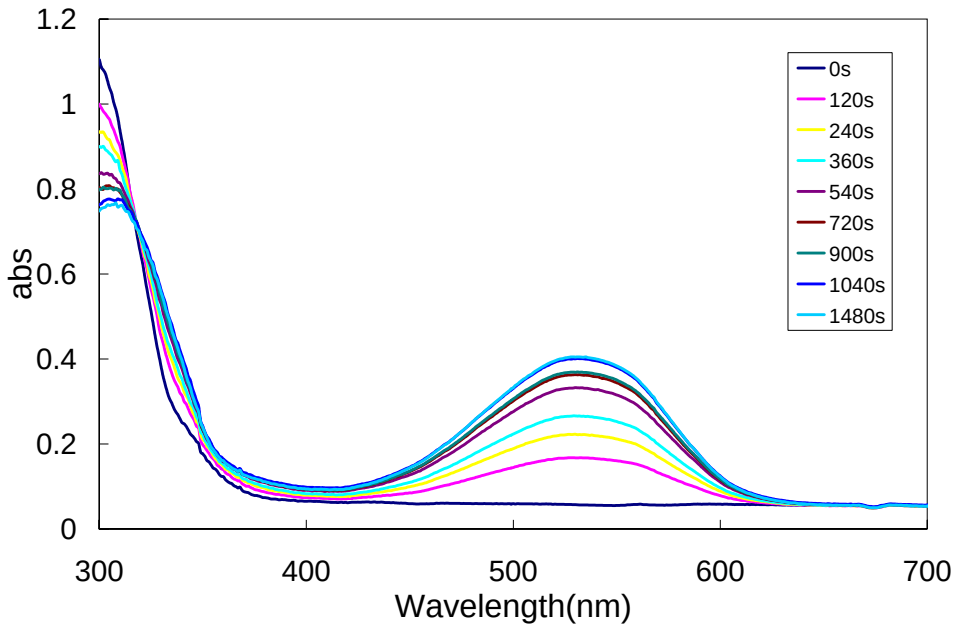
1.2
1
0.8
0.6
0.4
0.2
0
abs
300
400
500
600
700
Wavelength(nm)
0s
120s
240s
360s
540s
720s
900s
1040s
1480s

(a)

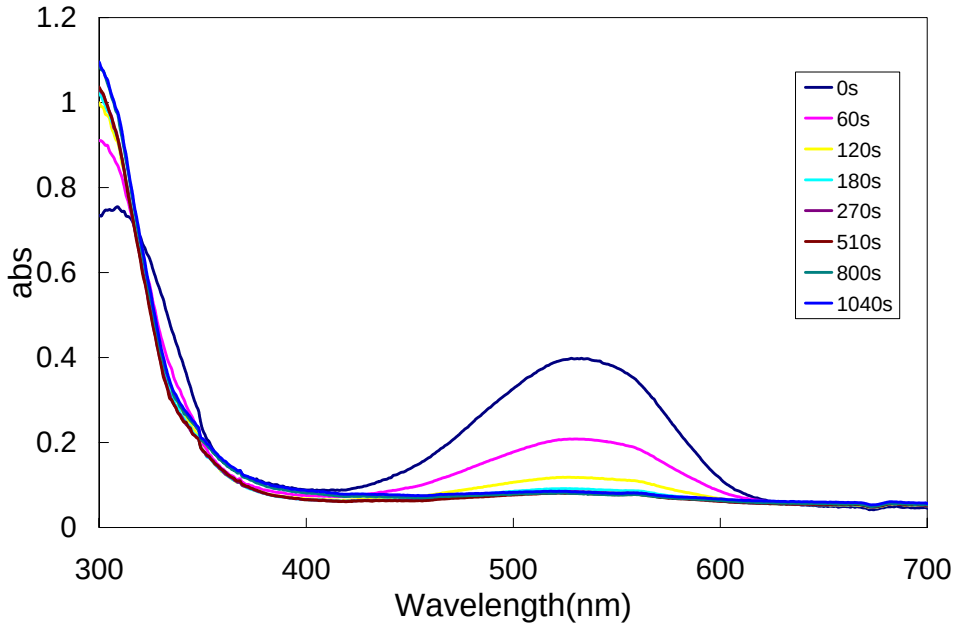
1.2
1
0.8
0.6
0.4
0.2
0
abs
300
400
500
600
700
Wavelength(nm)
0s
60s
120s
180s
270s
510s
800s
1040s

(b)

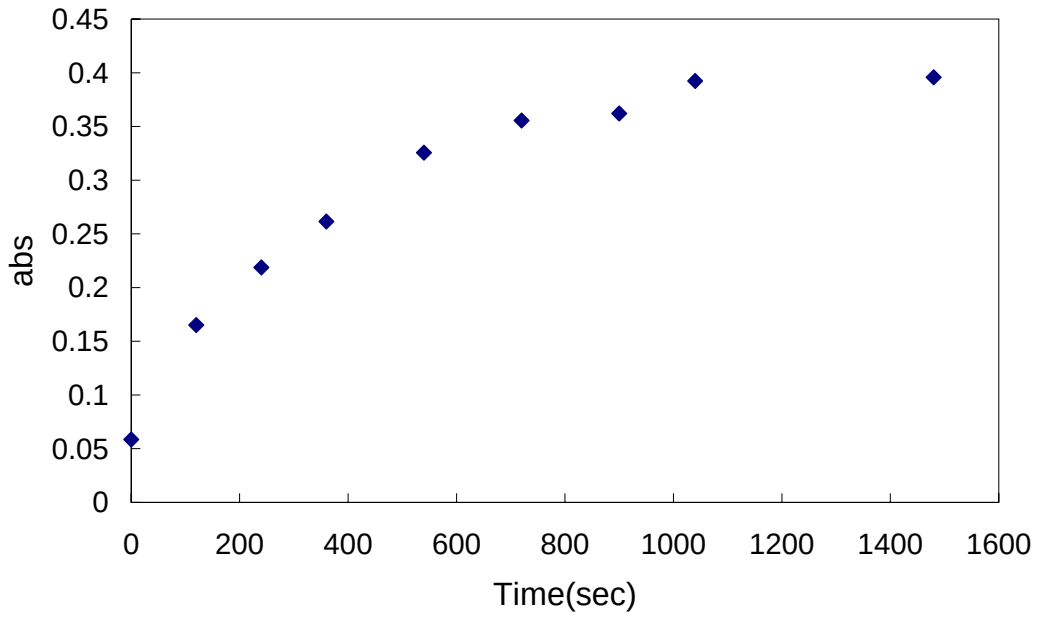

(c)

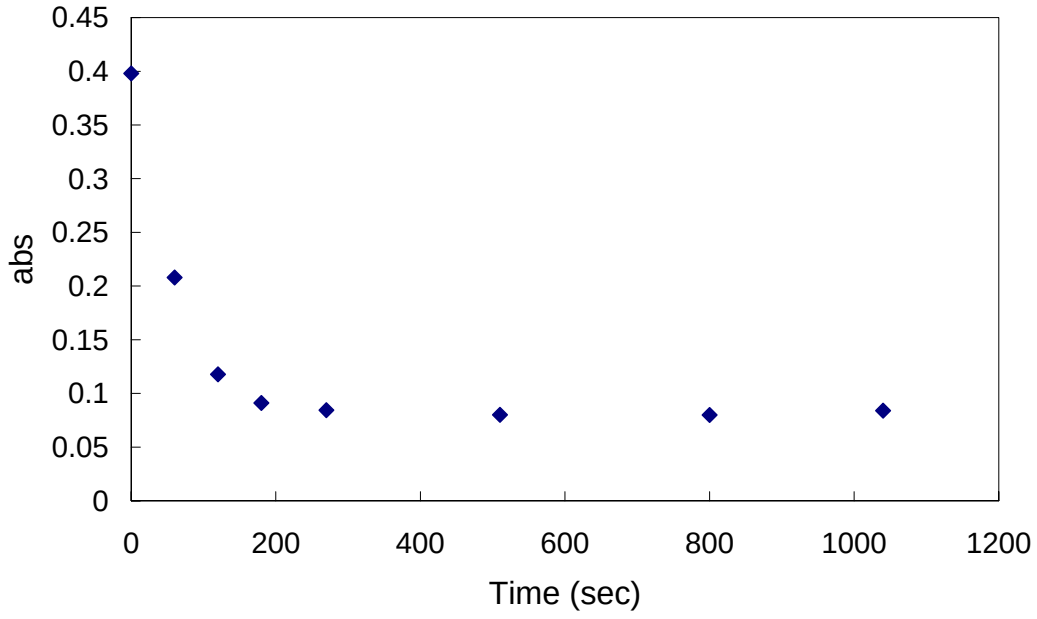

(d)

Figure 4-4. Fulgimide **44b** in 0.43mM hexanes solution: (a) photochemical coloration of State A with *λ=365nm* light, (b) decoloration of State B with λ>450nm light, (c) plot of absorbance *versus* time at 520nm for the coloration, (d) plot of absorbance *versus* time at 528nm for the decoloration. A PTI A6000 450W Xe arc lamp (25A, 18V) fitted with a water filter (to cut off the infrared output) was used as the light source.

Table 4-1. Observed half-lives for photoisomerization of **42**, **43a** and **44b** measured in hexanes at ambient temperature. A PTI A6000 450W Xe arc lamp (25A, 18V) fitted with a water filter (to cut off the infrared output) was used as the light source.

	Half-life (sec)		
Irradiation	0.37 mM of **42** in hexanes	0.34 mM of **43a** in hexanes	0.43 mM of **44b** in hexanes
λ=313nm	72	40	93
λ>450	7	12	25
λ=365nm	120	220	220
λ>450	5	13	32

To assess the efficiency of E-C photoisomerization, we have also determined the isomer compositions of State A, B and C for compound **42**, **43a**, and **44b** by HPLC. Baseline resolution of the isomers of these compounds was achieved using either 49:1 hexanes/EtOAc or 24:1 hexanes/EtOAc as eluant (1 mL/min) on a silica gel column. Figure 4-5 shows the HPLC traces for compound **43a** as a representative example. Only one peak was observed for State A (Peak 2), which is consistent with the NMR spectrum suggesting that there is only one isomer. In State B, two new peaks appear (Peak 1 and Peak 3), and in State C, only Peak 2 and Peak 3 are observed.

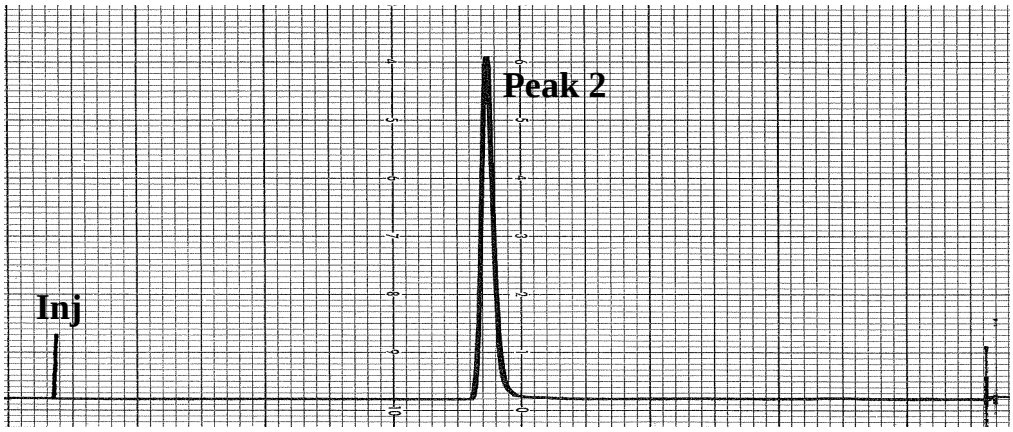

(a)

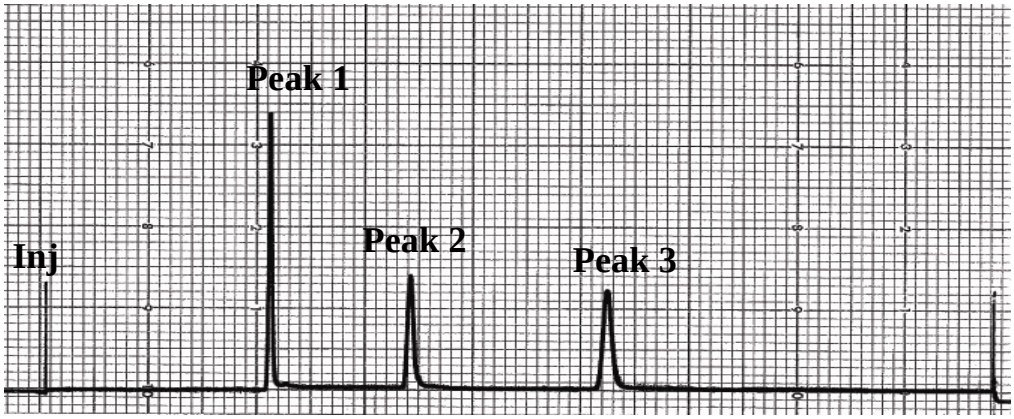

(b)

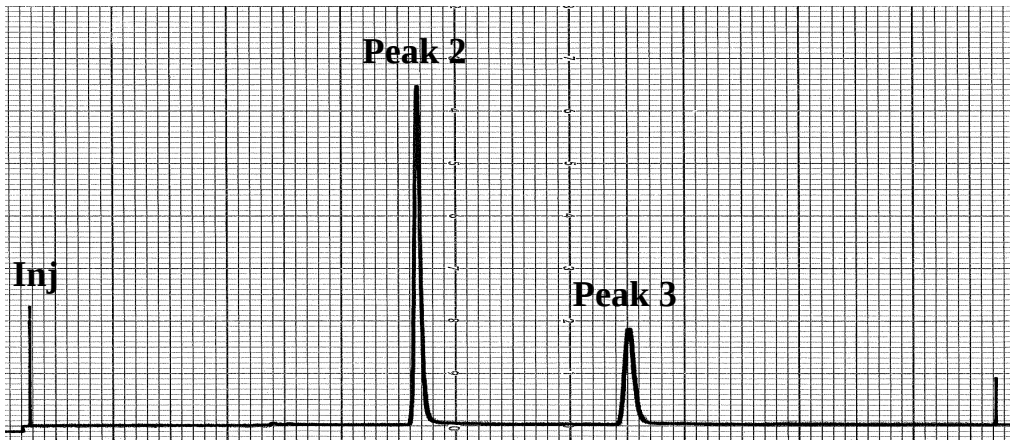

(c)

Figure 4-5. HPLC traces for the photoisomerization of 0.34mM hexanes solution of fulgimide **43a**: (a) State A; (b) State B, coloration with λ=313nm light; (c) State C, decoloration with λ>450nm light. A mixture of 24:1 hexanes/EtOAc was used as the eluant (1 mL/min). Wavelength of detector was 256nm.

Of the three isomers, only the C-form absorbs visible light, and therefore irradiation of the C-form (or pps) by visible light induces only the transformation from the C-form to the E-form, until the C-form disappears completely. Hence, the absence of Peak 1 in State C suggests that Peak 1 represents the ring-closed C-form. If peak 2 represents the E-form, then UV light irradiation should cause the amount of E-form to decrease and the amounts of both Z-form and C-form to increase，following the pattern (a) shown in Figure 4-6. If peak 2 corresponds to the Z-form, then, with UV light irradiation, the amount of Z-form should decrease, the amount of E-form first go up and then decline, concomitant with an increase in C-form, following the pattern (b) in Figure 4-6. To figure out which isomer Peak 2 corresponds to, a solution of **43a** was irradiated with 313nm light and the change of isomer composition was monitored by HPLC. It was found that pattern (a) is followed (Figure 4-7) which suggests that peak 2 is the E form. Therefore, in the HPLC traces Peak 1, Peak 2 and Peak 3 correspond to the C-form, E-form, and Z-form, respectively.

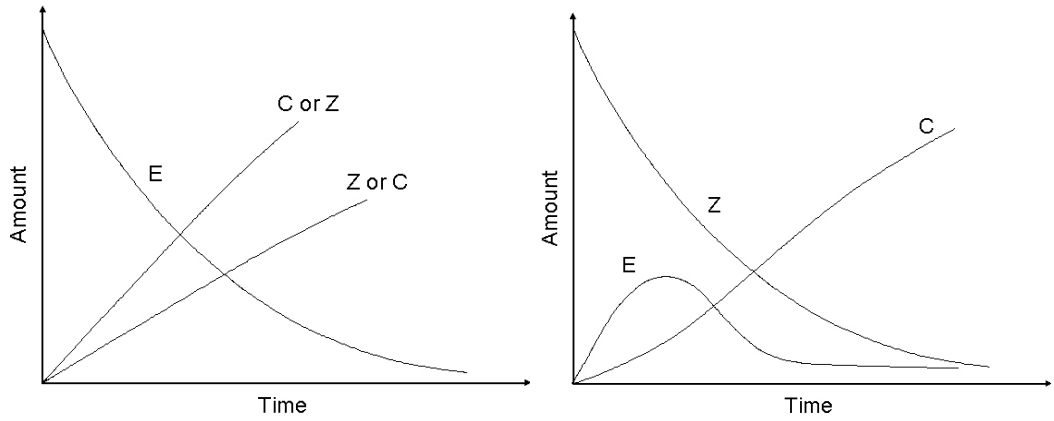

Figure 4-6. Change of isomer composition upon UV irradiation.

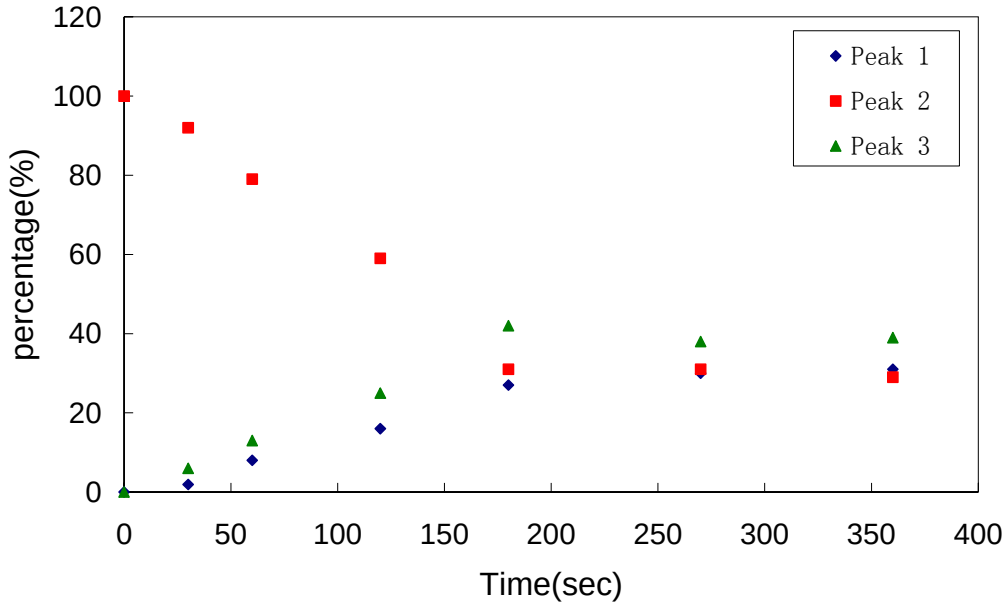

Figure 4-7. Change of the percentage of Peak 1, 2 and 3 in the mixture during irradiation of 0.34 mM hexanes solution of fulgimide **43a** with λ=313nm light.

Table 4-2 summarizes the isomer composition of States A, B and C of compounds **42**, **43a** and **44b**, and shows that, upon UV light irradiation, the pure E-form was converted to a mixture of three isomers. Generally the conversion from E to C-form is low with C-

form in State B ranging from 7% to 57%. The competition from E-Z isomerization is high, with Z-form in State B ranging from 18% to 60%. Among the three compounds, State B of **44b** is more enriched with C-form and less with Z-form than **42** and **43a**. It was also found that irradiation with 365nm light generally results in less Z-form content in State B than 313nm light. Upon visible light irradiation，the amount of Z-form in the mixture stayed about the same, and the C-form is almost completely converted to E-form. Overall, the results suggest that the competition from E-Z isomerization is likely too high, that is, the cyclization quantum yield (Φ_{EC}) is too low for compounds **42**, **43a** and **44b** to be suitable as photochromic dopants for photoswitches.

Table 4-2. Composition of State A, B and C of **42**, **43a** and **44b**. A PTI A6000 450W Xe arc lamp (25A, 18V) fitted with a water filter (to cut off the infrared output) was used as the light source.

Solution	Photostationary State					
		313nm			365nm	
	State A	State B	State C	State A	State B	State C
0.37 mM of **42** in hexanes	100%E	30%E, 60%Z, 10%C	42%E, 58%Z, 0%C	100%E	50%E，35%Z，14%C	68%E，35%Z，0%C
0.34 mM of **43a** in hexanes	100%E	30%E, 40%Z, 30%C	65%E, 35%Z, 0%C	100%E	70%E，23%Z 7%C	75%E，25%Z，0%C
0.43 mM of **44b** in hexanes	100%E	21%E, 22%Z, 57%C	73%E，25%Z, 2%C	100%E	43%E，18%Z, 39%C	81%E, 19%Z, 0%C

4.4 Conclusion

The siloxane-terminated fulgimide **41** was designed and synthesized successfully in 12 steps as dopant into siloxane-terminated LC hosts. However, this compound proved to be an oil at room temperature, which made it difficult to purify and unsuitable for mixing with liquid crystal hosts. Attention was turned to the fulgide precusors **42, 43a** and **44b** which are solids at room temperature. Compound **42**, **43a** and **44b** were assessed as photochromic dopants in terms of fast switching and high quantum yield requirements for the development of a liquid crystal photoswitch, and their photophysical properties were studied in solution. The observed half-lives for compound **42**, **43a** and **44b** by UV-vis spectroscopy are comparable to half-lives reported in the literature for similar compounds. The isomer composition of the pss determined by HPLC suggests that the competition from E-Z isomerization is likely too high, that is, the cyclization quantum yield (Φ_{EC}) is too low for compounds **42**, **43a** and **44b** to be suitable as photochromic dopants for photoswitches.

4.5 References

(1) (a) Shoosmith, E. D.; Remnant, A.; Perkins, S. P.; Coles, H. J.; *Ferroelectrics* **2000**, 243, 75. (b) Robinson, K. W.; Carboni, C.; Kloess, P.; Perkins P. S.; Coles, J. H.; *Liq. Cryst.* **1998**, 25, 301. (c) Shoosmith, D.; Carboni, C.; Perkins, S.; Meyer, S.; Coles, J. H.; *Mol. Cryst. Liq. Cryst.* **1999**, 331, 181.

(2) *Name Reactions and Reagents in Organic Synthesis*; Munday, B. P.; Ellerd, M. G. Ed.; John Wiley and Sons: New York, **1988**; pp 204-205.

(3) Fan, M.; Yu, L.; Zhao, W.; *Fulgide Family Compounds: Synthesis, Photochromism, and Applications. In Organic Photochromic and Thermochromic Compounds, Vol. 1, Main Photochromic Families*; Crano, J. C.; Guglielmetti, R.; Ed.; Plenum Publishers: New York, **1999**; Chapter 4, pp 141-206.

(4) Hastings, J. S.; Heller, H. G.; Tucker, H.; Smith, K.; *J. Chem. Soc., Perkin Trans. 1* **1975**, 1545.

(5) Uchida, S.; Yokoyama, Y.; Kiji, J.; Okano, T.; Kitamura, H.; *Bull. Chem. Soc. Jpn.*, **1995**, 68, 2961.

(6) Kiji, J.; Konishi, H.; Okano, T.; Kometani, S.; Iwasa, A.; *Chem. Lett.* **1987**, 313.

(7) Yokoyama, Y.; Goto, T.; Inoue, T.; Yokoyama, M.; Kurita, Y.; *Chem. Lett.* **1988**, 1049.

(8) Liang, Y.; Dvornikov, S. A.; Rentzepis, M. P.; *J. Mater. Chem.* **2000**, 10, 2477.

(9) Ulrich, K.; Port, H.; Wolf, C. H.; *Chem. Phys.* **1991**, 154, 311.

(10) Matsushima, R.; Sakaguchi, H.; *J. Photochem. Photobio. A: Chemistry* **1997**, 108, 239.

(11) Yokoyama, Y.; Tanaka, T.; Yamane T.; Kurita, Y.; *Chem. Lett.* **1991**, 1125.

(12) Kaneko, A.; Tomoda, A.; Ishizuka, M.; Suzuki, H.; Matsushima, R.; *Bull. Chem. Soc. Jpn.* **1988**, 61, 3569.

(13) Liang, Y.; Dvornikov, A. S.; Rentzepis, P. M.; *Tetrahedron Lett.* **1999**, 40, 8067.

Chapter 5. Conclusions and Future Work

5.1 Conclusions and Future Work

The goal of this thesis is to design photochromic dopants and liquid crystal hosts terminated with short siloxane oligomers, in order to produce homogeneous liquid crystal mixtures containing a bistable photochromic component for liquid crystal photoswitches.

In the first section, the synthesis and characterization of siloxane-terminated liquid crystals with 2-phenylpyrimidine cores were performed. These compounds form a broad SmC phase and, in some cases, a SmA phase. The temperature range of the SmA phase may be broadened by the addition of a terminal halogen substituent on the alkoxy side-chain. One such derivative, 2-(4-(11-(1,1,1,3,3,5,5-heptamethyltrisiloxanyl) undecyloxy)phenyl)-5-(1-chlorooctyloxy)pyrimidine (**33a**) undergoes SmA-SmC transition with a maximum layer contraction of 1.6% and shows a C_{dV} value of 0.89 at T-T_C=-10K, which is comparable to those of known 'de Vries' materials, **TSiKN65** and **3M8422**. Compounds **33a** maybe considered as a bona fide 'de Vries' material. These results are consistent with a general design strategy for 'de Vries-like' materials that consists of combining in a mesogen a structural element that promotes the formation of a SmC phase (trisiloxane-terminated side-chain) with one that promotes the formation of a SmA phase (chloro-terminated sidechain).

Further addition of terminal chlorine on the alkyl side-chain results in a bona fide 'de Vries' material, 2-(4-(11-(1,1,1,3,3,5,5-heptamethyltrisiloxanyl)undecyloxy)phenyl)-5-(1-chlorooctyloxy)pyrimidine (**33a**), which is characterized by a maximum layer shrinkage of only 1.6% and a C_{dV} value of 0.89 at $T-T_C$=-10K. The C_{dV} value is comparable to those of known 'de Vries' materials, **TSiKN65**[16] and **3M8422**[17].

To test this hypothesis, and validate our design strategy for "de Vries'-type liquid crystals, Dr. Jeff Robert designed and characterized the liquid crystal properties of another trisiloxane-terminated mesogen in which the SmA-promoting element is a nonplanar 5-phenylpyrimidine core, **72** (Scheme 5-1).[1] Compound **72** forms both SmA and SmC phases and, upon SmA-SmC phase transition, shows a maximum layer contraction of 1.2%. The C_{dV} value of compound **72** is comparable to those of **3M 8422** and **TSiKN65**, which are considered to be among the best 'de Vries'-type materials reported heretofore.[2]

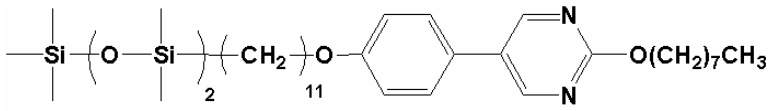

72

Scheme 5-1

In the second section, as an extension of result of the first project, siloxane-terminated biphenyl benzoate and phenyl benzoate liquid crystals were synthesized and their liquid crystal properties studied. These compounds form SmC phase, and in some

cases SmA and SmI phases. The temperature range of the SmA phase may be broadened by the addition of a terminal chloro substituent on alkoxy side-chain. In some cases, incorporation of a terminal chloro substituent affects not only the mesophase thermal stability, but also the nature of the mesophase formed. Compound 4-[6-(1,1,1,3,3,5,5-heptamethyltrisiloxanyl)hexanoyloxy]phenyl 4-(8-chlorooctyloxy)benzoate (**40b**) is characterized by a maximum layer shrinkage of only 1.7% at SmA-SmC phase transition, and its de Vries coefficient C_{dv} was calculated to be 0.72 at $T-T_C$=-11K, and is therefore considered to exhibit some 'de Vries' character. Investigation of the effect of inverting the orientation of the benzoate core, as in the case of siloxane-terminated phenylpyrimidine liquid crystals will be carried out in the future, as well as a systematic investigation of homologous Cl-terminated series of phenyl phenylpyrimidine and phenyl benzoate siloxane derivatives. Future 'de Vries'-type liquid crystal designs might include other types of nanosegregating structural elements that strongly promote lamellar order such as partially fluorinated side-chains.

Finally, siloxane-terminated fulgimide compounds were designed to use as photochromic dopants for liquid crystal photoswitches. Compound **41** was designed and synthesized successfully in 12 steps. However, this compound proved to be an oil at room temperature, which made it difficult to purify and unsuitable for mixing with liquid crystal hosts. Attention was turned to the fulgide precusors **42, 43a** and **44b** which are solids at room temperature. Compound **42**, **43a** and **44b** were assessed as photochromic

dopants in terms of fast switching and high quantum yield requirements for the development of a liquid crystal photoswitch, and their photophysical properties were studied in solution. The observed half-lives for compound **42**, **43a** and **44b** by UV-vis spectroscopy are comparable to half-lives reported in the literature for similar compounds. The isomer composition of the pss obtained by HPLC suggests that the competition from E-Z isomerization is likely too high, that is, the cyclization quantum yield (Φ_{EC}) is too low for compounds **42**, **43a** and **44b** to be suitable as photochromic dopants for photoswitches.

Incorporation of bulky alkyl groups about the hexatriene moiety is known to increase the cyclization quantum yield (Φ_{EC}) and decreases the E-Z isomerization quantum yield (Φ_{EZ}) of fulgide derivatives.[5,6,7,8] The effect of bulkyl substituent (for example, *i*-propyl, *t*-butyl and adamantylidene group) on the photochromic properties of our fulgide/fulgimide system could be explored.

Within the fulgide family, indolyl fulgides are particularly attractive due to their enhanced photochemical and thermal stability and the shift of their E-form wavelength maxima into the near visible region of the spectrum relative to other heteroaromatic fulgides.[5,6,7] It would be interesting, for example, to prepare compound **73a** (Scheme 5-2) and determine the effect of the indole subsituent on our system. However, a previous synthetic approach by Dr. Naohiko Ikuma in the Lemieux group to make **74** or **75**

following either the Stobbe condensation or the Pd-catalyzed carbonylation route was unsuccessful (Scheme 5-3). This was attributed to the strong electron-donating nature of methoxy indole ring.

Indolyl fulgide substituted with electron-withdrawing trifluoromethyl group **73b** could be an easier candidate to prepare (Scheme 5-4). In addition, Yokoyama *et al.* recently reported that the trifluoromethyl derivative of an indolyl-based fulgide, **76** ($R=CF_3$), possessed the most promising combination of photochromic properties recorded to date (Scheme 5-5).[9] Among these properties were a large increase in photochemical stability relative to the methyl derivative **8** ($R=CH_3$) and a red shift of the absorption maximum which places the absorbance of the E-form further into the visible region (426 nm) than any other fulgide.

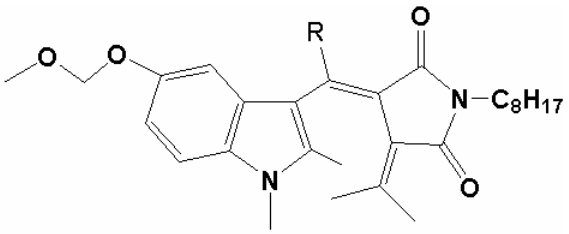

73. a. $R=CH_3$
b. $R=CF_3$

Scheme 5-2

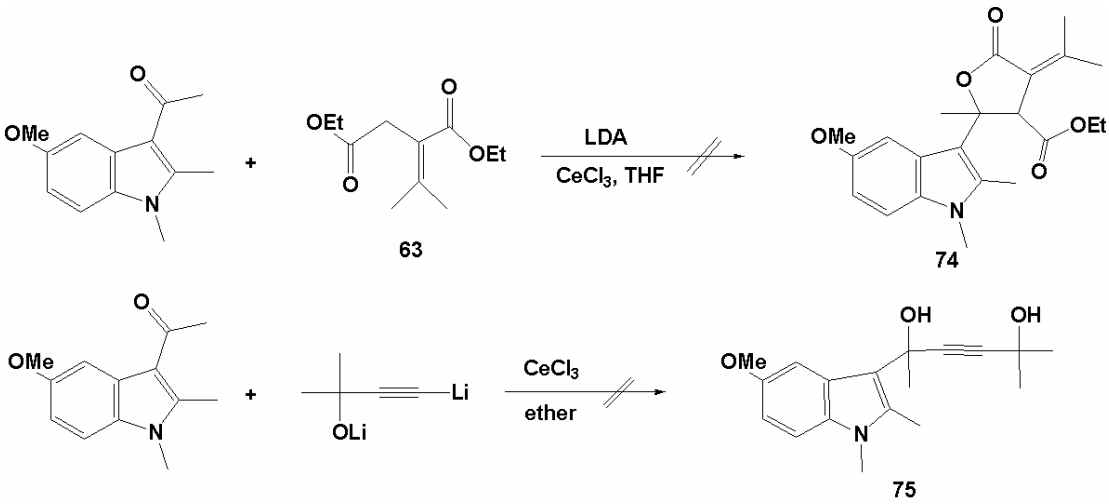

Scheme 5-3

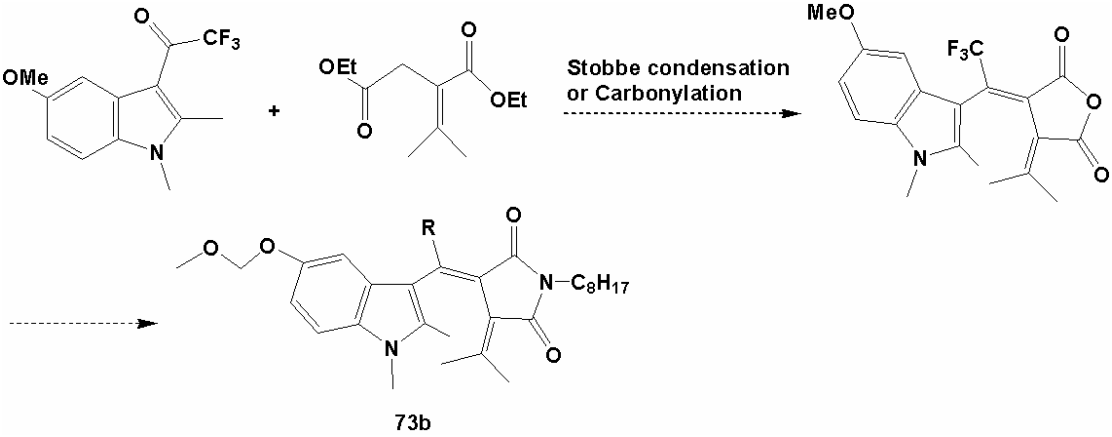

Scheme 5-4

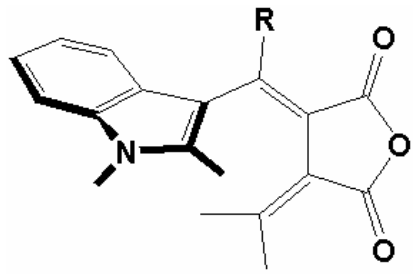

76E. R=CF_3
8E. R=CH_3

Scheme 5-5

5.2 References

(1) Roberts, C. J.; Kapernaum, N.; Giesselmann, F.; Lemieux, R. P.; *J. Am. Chem. Soc.* **2008**, 130, 13842.

(2) Lagerwall, J. P. F.; Giesselmann, F. *ChemPhysChem.* **2006**, *7*, 20–45.

(3) Thurmes, N. W.; Wand, D. M.; Vohra, T. R.; More, M. K.; Walba, M. D.; *Liq. Cryst.*, **1993**, 14, 1061.

(4) Roberts, C. J.; Kapernaum, N.; Giesselmann, F.; Wand, M. D.; Lemieux, P. R.; *J. Mater. Chem.* **2008**, 18, 5301.

(5) Yokoyama, Y.; Goto, T.; Inoue, T.; Yokoyama, M.; Kurita, Y.; *Chem. Lett.* **1988**, 1049.

(6) Yokoyama, Y.; Inoue, T.; Yokoyama, M.; Goto, T.; Iwai, T.; Kera, N.; Hitomi, I.; Kurita, Y.; *Bull. Chem. Soc. Jpn.* **1994**, 67, 3297.

(7) Yokoyama, Y.; Kurita, Y.; *Mol. Cryst. Liq. Cryst., Sect. A* **1994**, 246, 87.

(8) Kiji, J.; Okano, T.; Kitamura, H.; Yokoyama, Y.; Kubota, S.; Kurita, Y.; *Bull. Chem. Soc. Jpn.* **1995**, 68, 616.

(9) Yokoyama, Y.; Takahashi, K.; *Chem. Lett.* **1996**, 1037.

Chapter 6. Experimental

6.1 Synthesis and Characterization

6.1.1 General

^{1}H, ^{13}C, and ^{29}Si NMR spectra were recorded on Bruker Avance 400 and 500 spectrometers in deuterated chloroform, deuterated acetone, or deuterated DMSO. The chemical shifts are reported in δ (ppm) relative to tetramethylsilane as internal standard. Low- and high-resolution EI mass spectra were recorded on a Micromass GC-TOF mass spectrometer; low- and high-resolution ES spectra were recorded on an Applied Biosystems/MDS Sciex Q-TOF QSTAR XL mass spectrometer with electrospray ionization source; low- and high-resolution MALDI spectra were recorded on a Applied Biosystems Voyager DE-STR MALDI-TOF mass spectrometer equipped with a UV laser (337 nm). Peaks are reported as m/z (% intensity relative to the base peak) for low resolution mass spectra. Wide-angle powder X-ray diffraction analyses were performed at the Centre de Recherche en Sciences et Ingénierie des Macromolécules (CERSIM) of Université Laval using a Siemens/Bruker Kristalloflex 760 diffractometer (Cu-K_α radiation, λ=1.5418 Å) fitted with a Hi-Star bidimensional detector. Measurements of *d* spacings as a function of temperature were performed at the Liquid Crystal Materials Research Center of the University of Colorado (Boulder) using a Rigaku UltraX-18 rotating anode generator (Cu-K_α radiation, λ =1.5418 Å) and a Crismatec Scintiflex point

detector mounted on a Huber four-circle goniometer. Temperature control of the powder samples was achieved using a Instec STC200 hot stage. The diffraction peaks, fit to a Gaussian, show an error in layer spacing of roughly 2 x 10^{-4} Å, and the machine resolution is $q_{res} \sim 2.6 \times 10^{-3}$ $Å^{-1}$ in the configuration used for the experiment. Molecular modeling calculations were performed at the semi-empirical AM1 level using Spartan '04, v. 1.0.3 (Wavefunction Inc.). Melting points were measured on a Fisher-Johns melting point apparatus and are uncorrected. UV-vis absorption spectra were recorded on a Varian Cary-3 UV-visible spectrometer in HPLC grade hexanes. HPLC analyses and separations were performed on a system consisting of a Waters 501 single piston pump, a Supelguard C18 LC-Si silica guard column (2 cm X 4.0 mm i.d.), a Supelcosil LC-SI semiprep HPLC column (25 cm X 5 μm i.d.), and a D-Star DWW-10 variable-wavelength UV detector. Solvent mixtures of hexanes/EtOAc (49:1 or 24:1) were used as the eluant (1 mL/min). Phase transition temperatures for LC compounds were determined by differential scanning calorimetry (DSC) and/or polarized optical microscopy (POM) and are reported in ^{o}C. DSC analyses were performed on a Perkin-Elmer DSC-7 instrument with a scanning rate of 5 $Kmin^{-1}$ using the second heating and cooling curves. Liquid crystal texture analyses were performed using a Nikon Eclipse E600 POL polarized microscope fitted with a Nikon Coolpix 995 digital camera, and a Linkam LTS 350 hot stage. Tilt angles (θ) were measured by polarized microscopy as half the rotation between two extinction positions corresponding to opposite signs of the applied field.

Nylon-coated ITO glass cells with 1 μm spacing were prepared in the Lemieux group and were used for all tilt angle measurements. Alignment of the SmC* phase was achieved by slow cooling (0.1 K/min) from the isotropic phase while applying a triangular AC field (3 Hz, 4 V/μm) across the film.

6.1.2 Materials

All reagents and chemicals were obtained from commercial sources and used without further purification unless otherwise noted. Anhydrous CH_2Cl_2, toluene, ethyl ether, DMF and THF were obtained by passing through two columns containing activated alumina and copper using a PureSolv 400 solvent purification system (Innovative Technology Inc.); Anhydrous benzene was purchased from commercial sources. N-Butyllithium (hexane solution) were purchased from commercial sources and titrated against s-butanol with N-benzylbenzamide as an indicator. Flash chromatography was performed using 40–63 mm (230–400 mesh) silica gel (Silicycle Inc.). 11-(1,1,1,3,3,5,5-heptamethyltrisiloxanyl)undecanol (**45a**)[1], 11-(1,1,1,3,3-pentamethyldisiloxanyl) undecanol (**45c**)[1], 2-(4-hydroxyphenyl)-5-octyloxypyrimidine (**46c**)[2], 2-(4-hydroxyphenyl)-5-decyloxypyrimidine (**46e**)[3], 4-(11-undecenyloxy)phenol (**50a**)[4], 4-(5-hexenyloxy)phenol (**50b**)[5], 4-(5-hexenyloxy)phenyl 4-(octyloxy)benzoate (**52a**)[6], 3,5-dibromo-2-methylthiophene (**58**)[7], 4-methoxyphenylboronic acid (**59**)[7], 5-(4-methoxyphenyl)-2-methylthiophene-3-carboxylic acid (**60**)[7], diethyl 2-(propan-2-ylidene)succinate (**63**)[8], 2-bromo-5-methyl-thiophene (**66**)[9], 3-acetyl-2-bromo-5-

methylthiophene (**64**)[10],1-iodo-4-(methoxymethoxy)benzene (**68**)[11], and 4-(methoxymethoxy)phenylboronic acid (**69**)[12] were prepared according to published procedures and shown to have the expected physical and spectral properties.

6.1.3 Synthetic Procedures

6-(1,1,1,3,3,5,5-Heptamethyltrisiloxanyl)hexanol (45b) Under an argon atmosphere, a 3 wt% solution of platinum(0)-1,3-divinyl-1,1,3,3-tetramethyldisiloxane complex in xylenes (264 μL, 0.026 mmol) was added to a solution of 5-hexen-1-ol (172 mg, 1.75 mmol), and 1,1,1,3,3,5,5-heptamethyltrisiloxane (584 mg, 2.63 mmol) in toluene (12 mL). The mixture was stirred at room temperature overnight, then concentrated, and the residue purified by flash chromatography on silica gel (EtOAC) to give **45b** (463 mg, 82%) as a clear liquid: ^{1}H NMR (400 MHz, $CDCl_3$3.66 (t,) δ *J* = 6.6 Hz, 2 H), 1.58 (m, 2 H), 1.46-1.35 (m, 8 H), 0.55 (t, *J* = 7.3 Hz, 2 H), 0.10 (s, 9 H), 0.08 (s, 6 H), 0.04 (s, 6 H); ^{13}C NMR (100 MHz, $CDCl_3$63.0, 33.2, 32.7, 25.5, 23.2, 18.2, 1.8, 1.2, 0.2;) δ ^{29}Si NMR (99 MHz, $CDCl_3$-20.9, 7.2, 7.6; MS (ES) m/z 323 ([M+H]+, 27),) δ 281(14), 233(98), 159(36), 149(100); HRMS (ES) calcd for $C_{13}H_{35}O_3Si_3$ ([M+H]+): 323.1894, found 323.1886.

2-(4-Hydroxyphenyl)-5-butyloxypyrimidine (46a) Under an Ar atmosphere, 1-iodobutane (508 mg, 2.75 mmol) was added to a solution of 2-(4-hydroxyphenyl)-5-pyrimidinol (604 mg, 3.21 mmol) and dry Cs_2CO_3 (902 mg, 2.77 mmol) in anhydrous

DMF (80 mL). After the mixture was stirred at room temperature overnight, water was added and the mixture was washed twice with ether, and twice with brine. The organic layer was dried ($MgSO_4$) and concentrated to a yellow oil. Purification by flash chromatography on silica gel (4:1 hexanes/EtOAc) gave **46a** (410 mg, 61%) as a white solid: mp 134-135 °C; ^{1}H NMR (400 MHz, $CDCl_3$) δ 8.45 (s, 2H), 8.19 (d, *J*=8.3Hz, 2H), 6.90 (d, *J*=8.3Hz, 2H), 4.14 (t, *J*=6.3Hz, 2H), 1.80 (m, 2H), 1.48 (m, 2H), 1.31 (t, *J*=7.3Hz, 3H); ^{13}C NMR (100 MHz, $CDCl_3$) δ 158.0, 157.5, 151.2, 143.9, 129.5, 129.4, 115.7, 68.8, 31.1, 19.1, 13.8; MS (EI) m/z 244 (M+, 60), 188(100), 132(20), 119(48); HRMS (EI) calcd for $C_{14}H_{16}N_2O_2$: 244.1212, found 244.1216.

2-(4-Hydroxyphenyl)-5-heptyloxypyrimidine (46b) The procedure described for the synthesis of **46a** was repeated with 1-bromoheptane (263 mg, 1.46 mmol) and 2-(4-hydroxyphenyl)-5-pyrimidinol (331 mg, 1.76 mmol) to give **46b** (272 mg, 65%) as a white solid: mp 105-106 °C; ^{1}H NMR (400 MHz, $CDCl_3$) δ 8.44 (s, 2H), 8.14 (d, *J*=8.3Hz, 2H), 6.86 (d, *J*=8.3Hz, 2H), 4.07 (t, *J*=6.6Hz, 2H), 1.82 (m, 2H), 1.47 (m, 2H), 1.32 (m, 6H), 0.91 (t, *J*=7.1Hz, 3H); ^{13}C NMR (100 MHz, $CDCl_3$) δ 158.3, 157.6, 151.2, 143.9, 129.4, 129.3, 115.7, 69.1, 31.7, 29.1, 29.0, 25.8, 22.6, 14.1; MS (EI) m/z 286 (M+, 35), 188(100), 119(6); HRMS (EI) calcd for $C_{17}H_{22}N_2O_2$: 286.1681, found 286.1682.

2-(4-Hydroxyphenyl)-5-nonyloxypyrimidine (46d) The procedure described for the synthesis of **46a** was repeated with 1-bromononane (378 mg, 1.83 mmol) and 2-(4-

hydroxyphenyl)-5-pyrimidinol (416 mg, 2.21 mmol) to give **46d** (367 mg, 62%) as a white solid: mp 114-115 °C; ^{1}H NMR (400 MHz, $CDCl_3$) δ 8.44 (s, 2H), 8.19 (d, *J*=8.6Hz, 2H), 6.89 (d, *J*=8.6Hz, 2H), 4.08 (t, *J*=6.6Hz, 2H), 1.83 (m, 2H), 1.48 (m, 2H), 1.30 (m, 10H), 0.90 (t, *J*=6.2Hz, 3H); ^{13}C NMR (100 MHz, $CDCl_3$) δ 158.3, 157.7, 151.2, 143.9, 129.4, 129.3, 115.7, 69.1, 31.9, 29.5, 29.3, 29.2, 29.1, 25.8, 22.7, 14.1; MS (EI) m/z 314 (M+, 80), 188(100), 159(3), 132(5), 119(14); HRMS (EI) calcd for $C_{19}H_{26}N_2O_2$: 314.1994, found 314.1985.

2-(4-Hydroxyphenyl)-5-dodecyloxypyrimidine (46f) The procedure described for the synthesis of **46a** was repeated with 1-bromododecane (542 mg, 2.17 mmol) and 2-(4-hydroxyphenyl)-5-pyrimidinol (481 mg, 2.55 mmol) to give **46f** (490 mg, 64%) as a white solid: mp 74-75 °C; ^{1}H NMR (400 MHz, $CDCl_3$) δ 8.43 (s, 2H), 8.21 (d, *J*=7.0Hz, 2H), 6.94 (d, *J*=7.0Hz, 2H), 4.08 (t, *J*=5.9Hz, 2H), 1.83 (m, 2H), 1.48 (m, 2H), 1.28 (m, 16H), 0.89 (t, *J*=5.8Hz, 3H); ^{13}C NMR (100 MHz, $CDCl_3$) δ 162.8, 158.5, 157.6, 151.1, 143.8, 129.3, 115.7, 69.0, 36.6, 31.9, 31.6, 29.6, 29.5, 29.3, 29.1, 25.9, 22.7, 14.1; MS (EI) m/z 356 (M+, 39), 314(3), 219(4), 188(100), 119(7); HRMS (EI) calcd for $C_{22}H_{32}N_2O_2$: 356.2464, found 356.2468.

2-(4-Hydroxyphenyl)-5-(8-chlorooctyloxy)pyrimidine (48a) Under an Ar atmosphere, diisopropylazodicarboxylate (182 mg, 0.90 mmol) was added dropwise to a stirred solution of 8-chloro-1-octanol (141 mg, 0.86 mmol), 2-(4-hydroxyphenyl)-5-pyrimidinol

(193 mg, 1.03 mmol), and triphenylphosphine (209 mg, 0.80 mmol) in anhydrous THF (12 mL). The mixture was stirred at room temperature for 24 h, and then concentrated to a yellow oil. Purification by flash chromatography on silica gel (2:1 hexanes/EtOAc) and recrystallization from 1:15 hexane/acetonitrile gave **48a** (107 mg, 54%) as a colorless solid: mp 109-110 °C; ^{1}H NMR (400 MHz, $CDCl_3$) δ 8.43 (s, 2H), 8.13 (d, *J*=8.6Hz, 2H), 6.85 (d, *J*=8.6Hz, 2H), 4.06 (t, *J*=6.3Hz, 2H), 3.54 (t, *J*=6.7Hz, 2H), 1.84-1.36 (m, 12H); ^{13}C NMR (100 MHz, $CDCl_3$) δ 158.4, 157.7, 151.2, 143.9, 129.4, 129.2, 115.7, 69.0, 45.1, 32.6, 29.1, 28.8, 26.8, 25.7, 21.9; MS (EI) m/z 334 (M+, 56), 188(48), 119(22), 105(18), 86(100); HRMS (EI) calcd for $C_{18}H_{23}N_2O_2Cl$: 334.1448, found 334.1448.

2-(4-Hydroxyphenyl)-5-(8-bromooctyloxy)pyrimidine (48b) The procedure described for the synthesis of **48a** was repeated with diisopropylazodicarboxylate (186 mg, 0.92 mmol), 8-bromo-1-octanol (181 mg, 0.87 mmol), 2-(4-hydroxyphenyl)-5-pyrimidinol (196 mg, 1.04 mmol), and triphenylphosphine (221 mg, 0.81 mmol) in anhydrous THF (12 mL) to give **48b** (164 mg, 53%) as a colorless solid: mp 81-82 °C; ^{1}H NMR (400 MHz, $CDCl_3$) δ 8.43 (s, 2H), 8.14 (d, *J*=8.3Hz, 2H), 6.86 (d, *J*=8.3Hz, 2H), 4.05 (t, *J*=6.2Hz, 2H), 3.41 (t, *J*=6.6Hz, 2H), 1.85-1.25 (m, 12H); ^{13}C NMR (100 MHz, $CDCl_3$) δ 158.4, 157.7, 151.1, 143.9, 129.4, 129.2, 115.7, 68.9, 34.0, 32.8, 29.1, 28.6, 28.1, 25.7, 21.9; MS (EI) m/z 378(M+, 1), 188(13), 83(100); HRMS (EI) calcd for $C_{18}H_{23}N_2O_2Br$: 378.0943, found 378.0941.

2-(4-Hydroxyphenyl)-5-[11-(1,1,1,3,3,5,5-heptamethyltrisiloxanyl) undecyloxy]pyrimidine (47a) Under an Ar atmosphere, diisopropylazodicarboxylate (225 mg, 1.11 mmol) was added dropwise to a stirred solution of **45a** (416 mg, 1.06 mmol), 2-(4-hydroxyphenyl)-5-pyrimidinol (241 mg, 1.28 mmol), and triphenylphosphine (286 mg, 1.09 mmol) in anhydrous THF (15 mL). The mixture was stirred at room temperature for 24 h, and then concentrated to a yellow oil. Purification by flash chromatography on silica gel (5:1 hexanes/EtOAc) gave **47a** (284 mg, 48 %) as a white solid: mp 50-51 °C; ^{1}H NMR (400 MHz, $CDCl_3$) δ 8.43 (s, 2H), 8.14 (d, *J*=8.7Hz, 2H), 6.85 (d, *J*=8.7Hz, 2H), 4.06 (t, *J*=6.2Hz, 2H), 1.82 (m, 2H), 1.83-1.29 (m, 16H), 0.54 (t, *J*=7.2Hz, 2H), 0.10 (s, 9H), 0.07 (s, 6H), 0.04 (s, 6H); ^{13}C NMR (100 MHz, $CDCl_3$) δ 158.3, 157.7, 151.2, 143.9, 129.4, 129.3, 115.7, 69.1, 33.5, 29.6, 29.5, 29.4, 29.3, 29.1, 25.9, 23.2, 18.3, 1.8, 1.3, 0.2; MS (EI) m/z 562 (M+, 17), 547(22), 472(2), 398(4), 221(100), 188(12); HRMS (EI) calcd for $C_{28}H_{50}N_2O_4Si_3$: 562.3078, found 562.3064.

2-(4-Hydroxyphenyl)-5-[11-(1,1,1,3,3,5,5-heptamethyltrisiloxanyl) hexyloxy]pyrimidine (47b) The procedure described for the synthesis of **47a** was repeated with diisopropylazodicarboxylate (579 mg, 2.87 mmol), **45b** (889 mg, 2.76 mmol), 2-(4-hydroxyphenyl)-5-pyrimidinol (625 mg, 3.31 mmol), and triphenylphosphine (728 mg, 2.78 mmol) in anhydrous THF (40 mL). to give **47b** (676 mg, 50 %) as a white solid: mp 75-76 °C; ^{1}H NMR (400 MHz, $CDCl_3$) δ 8.41 (s, 2H),

8.12 (d, *J*=8.7Hz, 2H), 6.85 (d, *J*=8.7Hz, 2H), 4.02 (t, *J*=6.2Hz, 2H), 1.79 (m, 2H), 1.80-1.39 (m, 6H), 0.57 (t, *J*=7.3Hz, 2H), 0.11 (s, 9H), 0.09 (s, 6H), 0.05 (s, 6H); ^{13}C NMR (100 MHz, $CDCl_3$) δ 158.7, 157.7, 151.2, 143.8, 129.5, 128.9, 115.8, 69.0, 33.0, 29.0, 25.6, 23.1, 18.2, 1.8, 1.3, 0.2; MS (EI) m/z 492 (M+, 39), 477(15), 393(17), 221(100), 188(5); HRMS (EI) calcd for $C_{23}H_{40}N_2O_4Si_3$: 492.2296, found 492.2298.

2-{4-[11-(1,1,1,3,3,5,5-Heptamethyltrisiloxanyl)undecyloxy]phenyl}-5-butyloxypyrimidine (29a) Under an Ar atmosphere, diisopropylazodicarboxylate (111 mg, 0.55 mmol) was added dropwise to a stirred solution of **45a** (169 mg, 0.57 mmol), **46a** (112 mg, 0.46 mmol), and triphenylphosphine (147 mg, 0.56mmol) in anhydrous THF (10 mL). The mixture was stirred at room temperature for 30 h, and then concentrated to a yellow oil. Purification by flash chromatography on silica gel (30:1 hexanes/EtOAc) gave **29a** (142 mg, 50%) as a white solid, which was further purified by recrystallization from EtOH after filtration through a 0.45 mm PTFE filter: ^{1}H NMR (400 MHz, $CDCl_3$) δ 8.44 (s, 2H), 8.29 (d, *J*=7.7Hz, 2H), 6.98 (d, *J*=7.7Hz, 2H), 4.11 (t, *J*=6.2Hz, 2H), 4.03 (t, *J*=6.3Hz, 2H), 1.95 –1.08 (m, 22H), 1.01 (t, *J*=7.3Hz, 3H), 0.54 (t, *J*=7.2Hz, 2H), 0.10 (s, 9H), 0.07 (s, 6H), 0.03 (s, 6H); ^{13}C NMR (100 MHz, $CDCl_3$) δ 160.8, 157.6, 151.1, 143.8, 129.9, 129.0, 114.5, 68.7, 68.1, 33.5, 31.1, 29.7, 29.6, 29.4, 29.3, 26.1, 23.2, 19.1, 18.3, 13.8, 1.8, 1.3, 0.2; MS (EI) m/z 618 (M+, 100), 603(36), 243(43), 221(88), 187(48); HRMS (EI) calcd for $C_{32}H_{58}N_2O_4Si_3$: 618.3704, found 618.3698.

2-(4-(11-(1,1,1,3,3,5,5-Heptamethyltrisiloxanyl)undecyloxy)phenyl)-5-heptyloxypyrimidine (29b) The procedure described for the synthesis of **29a** was repeated with **45a** (192 mg, 0.49 mmol), **46b** (117 mg, 0.41 mmol) to give **29b** (140 mg, 52%) as a white solid, which was further purified by recrystallization from EtOH after filtration through a 0.45 mm PTFE filter: ^{1}H NMR (400 MHz, $CDCl_3$) δ 8.44 (s, 2H), 8.29 (d, *J*=8.0Hz, 2H), 6.99 (d, *J*=8.0Hz, 2H), 4.10 (t, *J*=6.4Hz, 2H), 4.04 (t, *J*=6.6Hz, 2H), 1.84-1.30 (m, 28H), 0.92 (t, *J*=6.2Hz, 3H), 0.55 (t, *J*=7.3Hz, 2H), 0.11 (s, 9H), 0.08 (s, 6H), 0.04 (s, 6H); ^{13}C NMR (100 MHz, $CDCl_3$) δ 160.7, 157.6, 151.1, 143.8, 130.0, 129.0, 114.4, 69.0, 68.1, 33.5, 31.7, 30.9, 29.7, 29.6, 29.5, 29.4, 29.3, 29.1, 29.0, 26.1, 25.8, 23.2, 22.6, 18.3, 14.1, 1.8, 1.3, 0.2; MS (EI) m/z 660 (M+, 53), 647(29), 287(27), 221(100), 188(63); HRMS (EI) calcd for $C_{35}H_{64}N_2O_4Si_3$: 660.4174, found 660.4186.

2-(4-(11-(1,1,1,3,3,5,5-Heptamethyltrisiloxanyl)undecyloxy)phenyl)-5-octyloxypyrimidine (29c) The procedure described for the synthesis of **29a** was repeated with **45a** (180 mg, 0.46 mmol) and **46c** (114 mg, 0.38 mmol) to give **29c** (125 mg, 49%) as a white solid, which was further purified by recrystallization from EtOH after filtration through a 0.45 mm PTFE filter: ^{1}H NMR (400 MHz, $CDCl_3$) δ 8.43 (s, 2H), 8.29 (d, *J*=8.5 Hz, 2H), 6.98 (d, *J*=8.5Hz, 2H), 4.09 (t, *J*=6.3Hz, 2H), 4.03 (t, *J*=6.4Hz, 2H), 1.90-1.31 (m, 30H), 0.91 (t, *J*=6.3Hz, 3H), 0.54 (t, *J*=7.6Hz, 2H), 0.10 (s, 9H), 0.07 (s, 6H), 0.03 (s, 6H); ^{13}C NMR (100 MHz, $CDCl_3$) δ 160.7, 157.7, 151.1, 143.8, 130.1, 129.0, 114.4, 68.9, 68.1, 33.5, 31.8, 29.7, 29.6, 29.5, 29.4, 29.3, 29.2, 29.1, 26.1, 25.9, 23.3, 22.7,

18.6, 18.3, 14.1, 1.8, 1.7, 1.3; MS (EI) m/z 674 (M+, 100), 659(25), 300(13), 221(49), 188(22); HRMS (EI) calcd for $C_{36}H_{66}N_2O_4Si_3$: 674.4330, found 674.4326.

2-(4-(11-(1,1,1,3,3,5,5-Heptamethyltrisiloxanyl)undecyloxy)phenyl)-5-nonyloxypyrimidine (29d) The procedure described for the synthesis of **29a** was repeated with **45a** (169 mg, 0.43 mmol) and **46d** (113 mg, 0.36 mmol) to give **29d** (126 mg, 51%) as a white solid, which was further purified by recrystallization from EtOH after filtration through a 0.45 mm PTFE filter: ^{1}H NMR (400 MHz, $CDCl_3$) δ 8.44 (s, 2H), 8.29 (d, *J*=8.5Hz, 2H), 6.99 (d, *J*=8.5Hz, 2H), 4.10 (t, *J*=6.6Hz, 2H), 4.04 (t, *J*=6.6Hz, 2H), 1.83-1.30 (m, 32H), 0.91 (t, *J*=7.0Hz, 3H), 0.55 (t, *J*=7.0Hz, 2H), 0.11 (s, 9H), 0.08 (s, 6H), 0.04 (s, 6H); ^{13}C NMR (100 MHz, $CDCl_3$) δ 160.8, 157.6, 151.1, 143.8, 129.9, 129.0, 114.5, 69.0, 68.1, 33.5, 31.9, 29.7, 29.6, 29.5, 29.4, 29.3, 29.2, 29.1, 26.1, 25.9, 23.2, 22.7, 18.3, 14.1, 1.8, 1.3, 0.2; MS (EI) m/z 688 (M+, 16), 673(6), 221(100), 207(64), 149(36); HRMS (EI) calcd for $C_{37}H_{68}N_2O_4Si_3$: 688.4487, found 688.4482.

2-(4-(11-(1,1,1,3,3,5,5-Heptamethyltrisiloxanyl)undecyloxy)phenyl)-5-decyloxypyrimidine (29e) The procedure described for the synthesis of **29a** was repeated with **45a** (188 mg, 0.48 mmol) and **46e** (137 mg, 0.40 mmol) to give **29e** (134 mg, 48%) as a white solid, which was further purified by recrystallization from EtOH after filtration through a 0.45 mm PTFE filter: ^{1}H NMR (400 MHz, $CDCl_3$) δ 8.44 (s, 2H), 8.29 (d, *J*=8.6Hz, 2H), 6.99 (d, *J*=8.6Hz, 2H), 4.10 (t, *J*=6.4Hz, 2H), 4.04 (t, *J*=6.6Hz,

2H), 1.83-1.30 (m, 34H), 0.91 (t, *J*=6.2Hz, 3H), 0.55 (t, *J*=7.3Hz, 2H), 0.11 (s, 9H), 0.08 (s, 6H), 0.04 (s, 6H); ^{13}C NMR (100 MHz, $CDCl_3$) δ160.8, 157.5, 151.1, 143.8, 129.9, 129.0, 114.5, 69.0, 68.1, 33.5, 31.9, 29.7, 29.6, 29.5, 29.4, 29.3, 29.1, 26.1, 25.9, 23.2, 22.7, 18.3, 14.1, 1.8, 1.3, 0.2; MS (EI) m/z 702 (M+, 81), 687(34), 221(100), 188(50); HRMS (EI) calcd for $C_{38}H_{70}N_2O_4Si_3$: 702.4643, found 702.4631.

2-(4-(11-(1,1,1,3,3,5,5-Heptamethyltrisiloxanyl)undecyloxy)phenyl)-5-dodecyloxypyrimidine (29f) The procedure described for the synthesis of **29a** was repeated with **45a** (169 mg, 0.43 mmol) and **46f** (121 mg, 0.34 mmol) to give **29f** (117 mg, 47%) as a white solid, which was further purified by recrystallization from EtOH after filtration through a 0.45 mm PTFE filter: ^{1}H NMR (400 MHz, $CDCl_3$) δ 8.45 (s, 2H), 8.30 (d, *J*=8.6Hz, 2H), 6.99 (d, *J*=8.6Hz, 2H), 4.10 (t, *J*=6.6Hz, 2H), 4.03 (t, *J*=6.6Hz, 2H), 1.89 –1.20 (m, 38H), 0.90 (t, *J*=7.0Hz, 3H), 0.54 (t, *J*=7.6Hz, 2H), 0.10 (s, 9H), 0.07 (s, 6H), 0.03 (s, 6H); ^{13}C NMR (100 MHz, $CDCl_3$) δ 160.7, 157.6, 151.1, 143.8, 130.0, 129.0, 114.4, 69.0, 68.1, 33.5, 31.9, 29.7, 29.6, 29.5, 29.4, 29.3, 29.1, 26.1, 25.9, 23.2, 22.7, 18.3, 14.1, 1.8, 1.3, 0.2; MS (EI) m/z 730(M+, 100), 715(18), 221(32); HRMS (EI) calcd for $C_{40}H_{74}N_2O_4Si_3$: 730.4949, found 730.4956.

2-(4-(11-(1,1,1,3,3,5,5-Heptamethyltrisiloxanyl)undecyloxy)phenyl)-5-(1-chlorooctyloxy)pyrimidine (33a) The procedure described for the synthesis of **29a** was repeated with **45a** (223 mg, 0.67 mmol) and **48a** (193 mg, 0.66 mmol). Purification by

flash chromatography on silica gel (9:1 hexanes/EtOAc) gave **33a** (238mg, 51%) as a white solid, which was further purified by recrystallization from EtOH after filtration through a 0.45 mm PTFE filter: ^{1}H NMR (400 MHz, $CDCl_3$) δ 8.43 (s, 2H), 8.28 (d, *J*=8.8Hz, 2H), 6.98 (d, *J*=8.8Hz, 2H), 4.09 (t, *J*=6.4Hz, 2H), 4.03 (t, *J*=6.6Hz, 2H), 3.56 (t, *J*=6.7Hz, 3H), 1.88 –1.29 (m, 30H), 0.54 (t, *J*=7.6Hz, 2H), 0.10 (s, 9H), 0.07 (s, 6H), 0.03 (s, 6H); ^{13}C NMR (100 MHz, $CDCl_3$) δ 160.8, 157.7, 151.1, 143.8, 130.0, 129.0, 114.5, 68.9, 68.1, 45.1, 33.5, 32.6, 29.7, 29.6, 29.4, 29.3, 29.2, 29.1, 28.8, 26.8, 25.8, 23.2, 18.3, 1.8, 1.3, 0.2; MS (EI) m/z 708(M+, 40), 693(8), 672(4), 334(6), 221(100), 188(35); HRMS (EI) calcd for $C_{36}H_{65}N_2O_4Si_3Cl$: 708.3941, found 708.3973.

2-(4-(6-(1,1,1,3,3,5,5-Heptamethyltrisiloxanyl)hexyloxy)phenyl)-5-heptyloxypyrimidine (30a) The procedure described for the synthesis of **29a** was repeated with **45b** (155 mg, 0.48 mmol) and **46b** (114 mg, 0.40 mmol) to give **30a** (113 mg, 48%) as a white solid, which was further purified by recrystallization from EtOH after filtration through a 0.45 mm PTFE filter: ^{1}H NMR (400 MHz, $CDCl_3$) δ 8.36 (s, 2H), 8.29 (d, *J*=8.7Hz, 2H), 6.95 (d, *J*=8.7Hz, 2H), 3.97 (m, 4H), 1.80-1.30 (m, 18H), 0.90 (t, *J*=6.3Hz, 3H), 0.57 (t, *J*=7.7Hz, 2H), 0.11 (s, 9H), 0.09 (s, 6H), 0.05 (s, 6H); ^{13}C NMR (100 MHz, $CDCl_3$) δ 160.7, 157.5, 151.0, 143.6, 130.1, 129.0, 114.3, 68.8, 68.0, 33.2, 31.7, 29.2, 29.1, 29.0, 25.8, 23.2, 22.6, 18.2, 14.1, 1.8, 1.3, 0.2; MS (ES) m/z 591([M+H]+, 100); HRMS (ES) calcd for $C_{30}H_{55}N_2O_4Si_3$ ([M+H]+): 591.3470, found 591.3453.

2-(4-(6-(1,1,1,3,3,5,5-Heptamethyltrisiloxanyl)hexyloxy)phenyl)-5-octyloxypyrimidine (30b) The procedure described for the synthesis of **29a** was repeated with **45b** (141 mg, 0.44 mmol) and **46c** (111 mg, 0.37 mmol) to give **30b** (112 mg, 50%) as a white solid, which was further purified by recrystallization from EtOH after filtration through a 0.45 mm PTFE filter: ^{1}H NMR (400 MHz, $CDCl_3$) δ 8.43 (s, 2H), 8.29 (d, *J*=8.7Hz, 2H), 6.99 (d, *J*=8.7Hz, 2H), 4.09 (t, *J*=6.4Hz, 2H), 4.03 (t, *J*=6.6Hz, 2H), 1.83-1.32 (m, 20H), 0.91 (t, *J*=6.4Hz, 3H), 0.57 (t, *J*=7.6Hz, 2H), 0.11 (s, 9H), 0.09 (s, 6H), 0.04 (s, 6H); ^{13}C NMR (100 MHz, $CDCl_3$) δ 160.7, 157.6, 151.1, 143.8, 130.0, 129.0, 114.4, 69.0, 68.1, 33.2, 31.8, 29.3, 29.2, 29.1, 25.9, 25.8, 23.2, 22.7, 18.2, 14.1, 1.8, 1.3, 0.2; MS (ES) m/z 605([M+H]+, 100); HRMS (ES) calcd for $C_{31}H_{57}N_2O_4Si_3$ ([M+H]+): 605.3626, found 605.3618.

2-(4-(6-(1,1,1,3,3,5,5-Heptamethyltrisiloxanyl)hexyloxy)phenyl)-5-nonyloxypyrimidine (30c) The procedure described for the synthesis of **29a** was repeated with **45b** (145 mg, 0.45 mmol) and **46d** (119 mg, 0.38 mmol) to give **30c** (117 mg, 50%) as a white solid, which was further purified by recrystallization from EtOH after filtration through a 0.45 mm PTFE filter: ^{1}H NMR (400 MHz, $CDCl_3$) δ 8.45 (s, 2H), 8.30 (d, *J*=8.3Hz, 2H), 6.99 (d, *J*=8.3Hz, 2H), 4.10 (t, *J*=6.3Hz, 2H), 4.03 (t, *J*=6.3Hz, 2H), 1.85-1.27 (m, 22H), 0.90 (t, *J*=7.0Hz, 3H), 0.54 (t, *J*=7.6Hz, 2H), 0.10 (s, 9H), 0.07 (s, 6H), 0.03 (s, 6H); ^{13}C NMR (100 MHz, $CDCl_3$) δ 160.7, 157.6, 151.1, 143.8, 130.0, 129.0, 114.4, 68.9, 68.1, 33.2, 31.9, 29.7, 29.5, 29.3, 29.2, 29.1, 25.9, 25.8, 23.2, 22.7,

18.2, 14.1, 1.8, 1.3, 1.2; MS (ES) m/z 619([M+H]+, 100); HRMS (ES) calcd for $C_{32}H_{59}N_2O_4Si_3$ ([M+H]+): 619.3783, found 619.3763.

2-(4-(6-(1,1,1,3,3,5,5-Heptamethyltrisiloxanyl)hexyloxy)phenyl)-5-decyloxypyrimidine (30d) The procedure described for the synthesis of **29a** was repeated with **45b** (142 mg, 0.44 mmol) and **46e** (116 mg, 0.34 mmol) to give **30d** (112 mg, 52%) as a white solid, which was further purified by recrystallization from EtOH after filtration through a 0.45 mm PTFE filter: ^{1}H NMR (400 MHz, $CDCl_3$) δ 8.43 (s, 2H), 8.29 (d, *J*=8.9Hz, 2H), 6.99 (d, *J*=8.9Hz, 2H), 4.09 (t, *J*=6.4Hz, 2H), 4.04 (t, *J*=6.6Hz, 2H), 1.88 –1.30 (m, 24H), 0.91 (t, *J*=6.2Hz, 3H), 0.57 (t, *J*=7.2Hz, 2H), 0.11 (s, 9H), 0.09 (s, 6H), 0.05 (s, 6H); ^{13}C NMR (100 MHz, $CDCl_3$) δ 160.7, 157.7, 151.1, 143.8, 130.1, 129.0, 114.4, 68.9, 68.1, 33.2, 31.9, 29.5, 29.3, 29.2, 29.1, 25.8, 23.2, 22.7, 18.2, 14.1, 1.8, 1.3, 0.2; MS (EI) m/z 632(M+, 50), 533(10), 221(100), 207(32), 188(9); HRMS (EI) calcd for $C_{33}H_{60}N_2O_4Si_3$: 632.3861, found 632.3850.

2-(4-(6-(1,1,1,3,3,5,5-Heptamethyltrisiloxanyl)hexyloxy)phenyl)-5-dodecyloxypyrimidine (30e) The procedure described for the synthesis of **29a** was repeated with **45b** (122 mg, 0.38 mmol) and **46f** (112 mg, 0.31 mmol) to give **30e** (104 mg, 51%) as a white solid, which was further purified by recrystallization from EtOH after filtration through a 0.45 mm PTFE filter: ^{1}H NMR (400 MHz, $CDCl_3$) δ 8.43 (s, 2H), 8.29 (d, *J*=8.6Hz, 2H), 6.99 (d, *J*=8.6Hz, 2H), 4.10 (t, *J*=6.4Hz, 2H), 4.04 (t, *J*=6.4Hz,

2H), 1.83-1.29 (m, 28H), 0.90 (t, *J*=6.3Hz, 3H), 0.57 (t, *J*=7.5Hz, 2H), 0.11 (s, 9H), 0.09 (s, 6H), 0.05 (s, 6H); ^{13}C NMR (100 MHz, $CDCl_3$) δ 160.7, 157.6, 151.1, 143.8, 130.0, 129.0, 114.4, 69.0, 68.1, 33.2, 31.9, 29.7, 29.6, 29.5, 29.4, 29.3, 29.2, 29.1, 25.9, 25.8, 23.2, 22.7, 18.2, 14.1, 1.8, 1.3, 0.2; MS (ES) m/z 661([M+H]+, 100); HRMS (ES) calcd for $C_{35}H_{65}N_2O_4Si_3$ ([M+H]+): 661.4252, found 661.4255.

2-(4-(6-(1,1,1,3,3,5,5-Heptamethyltrisiloxanyl)hexyloxy)phenyl)-5-(8-chlorooctyloxy)pyrimidine (33b) The procedure described for the synthesis of **29a** was repeated with **45b** (122 mg, 0.38 mmol) and **46b** (94 mg, 0.28 mmol). Purification by flash chromatography on silica gel (9:1 hexanes/EtOAc) gave **33b** (84 mg, 47%) as a white solid, which was further purified by recrystallization from EtOH after filtration through a 0.45 mm PTFE filter: ^{1}H NMR (400 MHz, $CDCl_3$) δ 8.41 (s, 2H), 8.24 (d, *J*=8.9Hz, 2H), 6.97 (d, *J*=8.9Hz, 2H), 4.07 (t, *J*=6.4Hz, 2H), 4.01 (t, *J*=6.4Hz, 2H), 3.54 (t, *J*=6.7Hz, 2H), 2.20-1.38 (m, 20H), 0.55 (t, *J*=7.7Hz, 2H), 0.08 (s, 9H), 0.06 (s, 6H), 0.02 (s, 6H); ^{13}C NMR (100 MHz, $CDCl_3$) δ 160.7, 157.7, 151.0, 143.8, 132.2, 129.0, 114.4, 68.8, 68.1, 45.1, 33.2, 32.6, 29.2, 29.1, 28.8, 26.8, 25.8, 23.2, 18.2, 1.8, 1.3, 0.2; MS (EI) m/z 638(M+, 91), 539(8), 334(7), 221(100), 188(29), 149(23); HRMS (EI) calcd for $C_{31}H_{55}N_2O_4Si_3Cl$: 638.3158, found 638.3141.

2-{4-[6-(1,1,1,3,3,5,5-Heptamethyltrisiloxanyl)hexyloxy]phenyl}-5-(8-bromooctyloxy)pyrimidine (33c) The procedure described for the synthesis of **33b** was

repeated with **45b** (129 mg, 0.40 mmol), **48b** (117 mg, 0.31 mmol) to give **33c** (104mg, 49%) as a white solid, which was further purified by recrystallization from EtOH after filtration through a 0.45 mm PTFE filter: ^{1}H NMR (400 MHz, $CDCl_3$) δ 8.43 (s, 2H), 8.29 (d, *J*=8.8Hz, 2H), 6.99 (d, *J*=8.8Hz, 2H), 4.09 (t, *J*=6.3Hz, 2H), 4.03 (t, *J*=6.4Hz, 2H), 3.43 (t, *J*=6.7Hz, 2H), 1.92-1.40 (m, 20H), 0.57 (t, *J*=7.6Hz, 2H), 0.10 (s, 9H), 0.08 (s, 6H), 0.04 (s, 6H); ^{13}C NMR (100 MHz, $CDCl_3$) δ 160.8, 157.6, 151.0, 143.8, 129.9, 129.0, 114.5, 68.9, 68.1, 33.9, 33.2, 32.8, 29.2, 29.1, 28.7, 28.1, 25.8, 23.2, 18.2, 1.8, 1.3, 0.2; MS (EI) m/z 684(M+, 59), 534(28), 393(15). 221(100), 188(39); HRMS (EI) calcd for $C_{31}H_{55}N_2O_4Si_3Br$: 682.2653, found 682.2643.

2-{4-[11-(1,1,1,3,3-Pentamethyldisiloxanyl)undecyloxy]phenyl}-5-butyloxypyrimidine (31) The procedure described for the synthesis of **29a** was repeated with **45c** (234 mg, 0.73 mmol) and **46a** (139 mg, 0.57 mmol) to give **31** (153mg, 51%) as a white solid, which was further purified by recrystallization from EtOH after filtration through a 0.45 mm PTFE filter: ^{1}H NMR (400 MHz, $CDCl_3$) δ 8.44 (s, 2H), 8.30 (d, *J*=8.5Hz, 2H), 6.99 (d, *J*=8.5Hz, 2H), 4.11 (t, *J*=6.3Hz, 2H), 4.04 (t, *J*=6.4Hz, 2H), 1.84-1.30 (m, 22H), 1.02 (t, *J*=7.3Hz, 3H), 0.52 (t, *J*=6.6Hz, 2H), 0.08 (s, 9H), 0.06 (s, 6H); ^{13}C NMR (100 MHz, $CDCl_3$) δ 160.7, 157.7, 151.1, 143.8, 130.1, 129.0, 114.4, 68.6, 68.1, 33.4, 31.1, 29.7, 29.6, 29.5, 29.4, 29.3, 26.1, 23.3, 19.1, 18.4, 13.8, 2.0, 0.4; MS (EI) m/z 544(M+, 73), 529(23), 244(40), 188(69), 147(76), 84(100); HRMS (EI) calcd for $C_{29}H_{49}N_2O_3Si_2$ ([M-CH_3]+): 529.3282, found 529.3298.

2-(4-Octyloxyphenyl)-5-[11-(1,1,1,3,3,5,5-heptamethyltrisiloxanyl)undecyloxy]pyrimidine (32a) Under an Ar atmosphere, 1-bromooctane (57 mg, 0.30 mmol) was added to a solution of **46b** (118 mg, 0.21 mmol) and dry Cs_2CO_3 (85 mg, 0.26 mmol) in anhydrous DMF (14 mL). After the mixture was stirred at room temperature overnight, water was added and the mixture was extracted twice with ether. The combined organic layers were washed with brine, dried ($MgSO_4$) and concentrated to a white solid. Purification by flash chromatography on silica gel (13:1 hexanes/EtOAc) gave **32a** (107 mg, 76%) as a white solid, which was further purified by recrystallization from EtOH after filtration through a 0.45 mm PTFE filter: ^{1}H NMR (400 MHz, $CDCl_3$) δ 8.44 (s, 2H), 8.29 (d, *J*=8.2Hz, 2H), 6.99 (d, *J*=8.2Hz, 2H), 4.10 (t, *J*=5.8Hz, 2H), 4.04 (t, *J*=6.2Hz, 2H), 1.83-1.30 (m, 30H), 0.91 (t, *J*=5.5Hz, 3H), 0.55 (t, *J*=7.0Hz, 2H), 0.11 (s, 9H), 0.08 (s, 6H), 0.04 (s, 6H); ^{13}C NMR (100 MHz, $CDCl_3$) δ160.7, 157.6, 151.1, 143.8, 129.9, 129.0, 114.4, 69.0, 68.1, 33.5, 31.8, 29.6, 29.4, 29.3, 29.1, 26.1, 25.9, 23.2, 22.7, 18.3, 14.1, 1.8, 1.3, 0.2; MS (ES) m/z 675([M+H]+, 100), 365(12), 337(7); HRMS (ES) calcd for $C_{36}H_{67}N_2O_4Si_3$ ([M+H]+): 675.4409, found 675.4396.

2-(4-(8-Chlorooctyloxy)phenyl)-5-(11-(1,1,1,3,3,5,5-heptamethyltrisiloxanyl)undecyloxy)pyrimidine (34a) Under an argon atmosphere, diisopropylazodicarboxylate (73 mg, 0.36 mmol) was added dropwise to a stirred solution of 8-chloro-1-octanol (54 mg, 0.33 mmol), **46b** (173 mg, 0.31 mmol), and

triphenylphosphine (94 mg, 0.36 mmol) in anhydrous THF (12 mL). The mixture was stirred at room temperature for 24 h, and then concentrated to a yellow oil. Purification by flash chromatography on silica gel (4:1 hexanes/EtOAc) gave **34a** (103 mg, 47%) as a white solid, which was further purified by recrystallization from EtOH after filtration through a 0.45 mm PTFE filter: ^{1}H NMR (400 MHz, $CDCl_3$) δ 8.43 (s, 2H), 8.29 (d, *J*=8.6Hz, 2H), 6.98 (d, *J*=8.6Hz, 2H), 4.09 (t, *J*=6.4Hz, 2H), 4.03 (t, *J*=6.4Hz, 2H), 3.56 (t, *J*=6.7Hz, 2H), 1.88 –1.30 (m, 30H), 0.54 (t, *J*=7.4Hz, 2H), 0.10 (s, 9H), 0.08 (s, 6H), 0.04 (s, 6H); ^{13}C NMR (100 MHz, $CDCl_3$) δ 160.7, 157.6, 151.1, 143.8, 130.1, 129.0, 114.4, 69.0, 68.0, 45.2, 33.5, 32.6, 29.6, 29.4, 29.2, 29.1, 28.8, 26.8, 26.0, 23.2, 18.3, 1.8, 1.3, 0.2; MS (ES) m/z 709([M+H]+, 84), 528(96), 500(44), 345(96), 186(100); HRMS (ES) calcd for $C_{36}H_{66}N_2O_4Si_3Cl$ ([M+H]+): 709.4018, found 709.4053.

2-(4-Octyloxyphenyl)-5-(6-(1,1,1,3,3,5,5-heptamethyltrisiloxanyl)hexyloxy)pyrimidine (32b) The procedure described for the synthesis of **32a** was repeated with **47a** (113 mg, 0.23 mmol) to give **32b** (108 mg, 78%) as a white solid, which was further purified by recrystallization from EtOH after filtration through a 0.45 mm PTFE filter: ^{1}H NMR (400 MHz, $CDCl_3$) δ 8.44 (s, 2H), 8.29 (d, *J*=8.6Hz, 2H), 6.99 (d, *J*=8.6Hz, 2H), 4.10 (t, *J*=6.4Hz, 2H), 4.04 (t, *J*=6.4Hz, 2H), 1.83-1.31 (m, 20H), 0.91 (t, *J*=6.0Hz, 3H), 0.57 (t, *J*=7.5Hz, 2H), 0.11 (s, 9H), 0.09 (s, 6H), 0.04 (s, 6H); ^{13}C NMR (100 MHz, $CDCl_3$) δ 160.8, 157.6, 151.1, 143.8, 129.9, 129.0, 114.5, 69.0, 68.1, 33.1, 31.8, 30.9, 29.4, 29.3, 29.1, 26.1, 25.6, 23.2, 22.7, 18.2, 14.1, 1.8,

1.3, 0.2; MS (EI) m/z 604(M+, 100), 589(11), 221(54), 188(13); HRMS (EI) calcd for $C_{31}H_{56}N_2O_4Si_3$: 604.3548, found 604.3547.

2-[4-(8-Chlorooctyloxy)phenyl]-5-[6-(1,1,1,3,3,5,5-heptamethyltrisiloxanyl)hexyloxy]pyrimidine (34b) The procedure described for the synthesis of **34a** was repeated with **47a** (123 mg, 0.25 mmol) to give **34b** (83 mg, 52%) as a white solid, which was further purified by recrystallization from EtOH after filtration through a 0.45 mm PTFE filter:: ^{1}H NMR (400 MHz, $CDCl_3$) δ 8.43 (s, 2H), 8.29 (d, *J*=8.7Hz, 2H), 6.98 (d, *J*=8.7Hz, 2H), 4.09 (t, *J*=6.3Hz, 2H), 4.03 (t, *J*=6.3Hz, 2H), 3.55 (t, *J*=6.7Hz, 2H), 1.58 –1.40 (m, 20H), 0.57 (t, *J*=7.5Hz, 2H), 0.10 (s, 9H), 0.08 (s, 6H), 0.04 (s, 6H); ^{13}C NMR (100 MHz, $CDCl_3$) δ 160.6, 157.6, 151.1, 143.8, 130.1, 129.0, 114.4, 68.9, 68.0, 45.1, 33.1, 32.6, 29.2, 29.1, 28.8, 26.8, 26.0, 25.6, 23.2, 18.2, 1.8, 1.3, 0.2; MS (EI) m/z 638(M+, 24), 602(19), 221(100), 188(17); HRMS (EI) calcd for $C_{31}H_{55}N_2O_4Si_3Cl$: 638.3158, found 638.3143.

4-[11-(1,1,1,3,3,5,5-Heptamethyltrisiloxanyl)undecyloxy]-4'-hydroxybiphenyl (49a) Under an argon atmosphere, a solution of diisopropylazodicarboxylate (105 mg, 0.52 mmol), 4,4′-dihydroxybiphenyl (122 mg, 0.66 mmol), **45a** (202 mg, 0.52 mmol), and triphenylphosphine (135 mg, 0.52 mmol) in anhydrous THF (8 mL) was stirred at room temperature for 24 h, and then concentrated to a yellow oil. Purification by flash chromatography on silica gel (5:1 hexanes/EtOAc) gave **49a** (135 mg, 48%) as a white

solid: mp 78–79 ^{o}C; ^{1}H NMR (400 MHz, acetone-d6) δ 7.47-7.40 (m, 4H), 6.94-6.88 (m, 4H), 3.97 (t, *J*=6.5 Hz, 2H), 1.79-1.31 (m, 18H), 0.58 (t, *J*=7.7 Hz, 2H), 0.11 (s, 9H), 0.09 (s, 6H), 0.04(s, 6H); ^{13}C NMR (100 MHz, acetone-d6) δ 159.6, 157.9, 134.7, 133.5, 128.8, 117.0, 116.0, 69.0, 34.7, 30.9, 30.8, 30.7, 30.6, 30.4, 30.2, 29.8, 27.4, 24.5, 19.4, 2.6, 2.1, 1.0; MS (EI) m/z 560(M+, 100), 391(8), 221(73), 186(62); HRMS (EI) calcd for $C_{30}H_{52}O_4Si_3$: 560.3173, found 560.3151.

4-[6-(1,1,1,3,3,5,5-Heptamethyltrisiloxanyl)hexyloxy]-4'-hydroxybiphenyl (49b) The procedure described for the synthesis of **49a** was repeated with 4,4′-dihydroxybiphenyl (140 mg, 0.75 mmol) and **45b** (182 mg, 0.56 mmol) to give **49b** (106 mg, 39%) as a white solid: mp 75–76 ^{o}C; ^{1}H NMR (400 MHz, acetone-d6) δ 7.46-7.41 (m, 4H), 6.96-6.87 (m, 4H), 3.99 (t, *J*=6.4 Hz, 2H), 1.84-1.39 (m, 8H), 0.57 (t, *J*=7.2 Hz, 2H), 0.11 (s, 9H), 0.09 (s, 6H), 0.04(s, 6H); ^{13}C NMR (100 MHz, acetone-d6) δ 159.1, 157.4, 157.3, 134.2, 133.3, 133.0, 128.3, 128.2, 116.5, 115.6, 69.0, 34.0, 30.4, 26.6, 24.0, 18.9, 2.1, 1.6, 0.6; MS (EI) m/z 490(M+, 99), 391(32), 221(100), 186(98); HRMS (EI) calcd for $C_{25}H_{42}O_4Si_3$: 490.2391, found 490.2390.

4-Hydroxy-4'-[11-(1,1,1,3,3-Pentamethyldisiloxanyl)undecyloxy]biphenyl (49c) The procedure described for the synthesis of **49a** was repeated with 4,4′-dihydroxybiphenyl (148 mg, 0.79 mmol) and **45c** (215 mg, 0.68 mmol) to give **49c** (123 mg, 35%) as a white solid: mp 77-78 ^{o}C; ^{1}H NMR (400 MHz, acetone-d6) δ 7.48-7.41

(m, 4H), 6.96-6.88 (m, 4H), 3.99 (t, *J*=6.6 Hz, 2H), 1.81-1.31 (m, 18H), 0.54 (t, *J*=7.6 Hz, 2H), 0.07 (s, 9H), 0.05(s, 6H); ^{13}C NMR (100 MHz, acetone-d6) δ 159.6, 157.9, 134.7, 133.5, 128.8, 128.6, 117.0, 116.1, 69.0, 34.6, 30.7 30.5, 30.4, 30.2, 29.8, 27.3, 24.5, 19.5, 2.6, 1.1; MS (EI) m/z 486(M+, 100), 317(4), 186(50), 147(77); HRMS (EI) calcd for $C_{28}H_{46}O_3Si_2$: 486.2986, found 486.2997.

4-(4-Butoxybenzoyloxy)-4-[11-(1,1,1,3,3,5,5-heptamethyltrisiloxanyl)undecyloxy]biphenyl (35a) Under an argon atmosphere, a mixture of **49a** (99 mg, 0.18 mmol), 4-butoxybenzoic acid (44 mg, 0.23 mmol), DCC (47 mg, 0.24 mmol) and DMAP (9 mg, 0.075 mmol) in anhydrous CH_2Cl_2 (10 mL) was stirred at room temperature for 24 h, and then concentrated to a white solid. Purification by flash chromatography on silica gel (30:1 hexanes/EtOAc) gave **35a** (104 mg, 78%) as a white solid, which was further purified by recrystallization from EtOH after filtration through a 0.45 mm PTFE filter: ^{1}H NMR (400 MHz, $CDCl_3$) δ 8.18 (d, *J*=8.6 Hz, 2H), 7.60 (d, *J*=8.6 Hz, 2H), 7.53 (d, *J*=8.6 Hz, 2H), 7.27 (d, *J*=8.6 Hz, 2H), 7.01-6.98 (m, 4H), 4.08 (d, *J*=6.4 Hz, 2H), 4.02 (d, *J*=6.6 Hz, 2H), 1.87-1.32 (m, 22H), 1.02 (t, *J*=7.5 Hz, 3H), 0.55 (t, *J*=7.1 Hz, 2H), 0.11 (s, 9H), 0.08 (s, 6H), 0.04 (s, 6H); ^{13}C NMR (100 MHz, $CDCl_3$) δ 165.3, 163.8, 159.0, 150.2, 138.8, 133.0, 132.5, 128.3, 127.9, 122.2, 121.8, 115.0, 114.5, 68.3, 68.2, 33.7, 31.4, 29.9, 29.8, 29.7, 29.6, 26.3, 23.5, 19.4, 18.5, 14.1, 2.0, 1.5, 0.4; MS (MALDI) m/z 759([M+Na]+, 100); HRMS (MALDI) calcd for $C_{41}H_{64}O_6NaSi_3$: 759.3908, found 759.3900.

4-[11-(1,1,1,3,3,5,5-Heptamethyltrisiloxanyl)undecyloxy]-4'-(4-heptyloxybenzoyloxy)biphenyl (35b) The procedure described for the synthesis of **35a** was repeated with **49a** (62 mg, 0.11 mmol) and 4-heptyloxybenzoic acid (34 mg, 0.14 mmol) to give **35b** (72 mg, 82%) as a white solid, which was further purified by recrystallization from EtOH after filtration through a 0.45 mm PTFE filter: ^{1}H NMR (400 MHz, $CDCl_3$) δ 8.18 (d, *J*=8.8 Hz, 2H), 7.60 (d, *J*=8.6 Hz, 2H), 7.53 (d, *J*=8.7 Hz, 2H), 7.26 (d, *J*=8.7 Hz, 2H), 6.99-6.97 (m, 4H), 4.06 (d, *J*=6.6 Hz, 2H), 4.01 (d, *J*=6.6 Hz, 2H), 1.88-1.31 (m, 28H), 0.93 (t, *J*=6.7 Hz, 3H), 0.56 (t, *J*=7.5 Hz, 2H), 0.12 (s, 9H), 0.09 (s, 6H), 0.05 (s, 6H); ^{13}C NMR (100 MHz, $CDCl_3$) δ 165.3, 163.8, 159.0, 150.2, 138.7, 133.0, 132.5, 128.3, 127.9, 122.2, 121.8, 115.0, 114.5, 68.5, 68.3, 33.7, 32.0, 29.9, 29.8, 29.7, 29.6, 29.3, 26.3, 26.2, 23.5, 22.8, 18.5, 14.3, 2.0, 1.5, 0.4; MS (MALDI) m/z 801([M+Na]+, 100); HRMS (MALDI) calcd for $C_{44}H_{70}O_6NaSi_3$: 801.4377, found 801.4418.

4-[11-(1,1,1,3,3,5,5-Heptamethyltrisiloxanyl)undecyloxy]-4'-(4-octyloxybenzoyloxy)biphenyl (35c) The procedure described for the synthesis of **35a** was repeated with **49a** (68 mg, 0.12 mmol) and 4-octyloxybenzoic acid (39 mg, 0.16 mmol) to give **35c** (81 mg, 83%) as a white solid, which was further purified by recrystallization from EtOH after filtration through a 0.45 mm PTFE filter: ^{1}H NMR (400 MHz, $CDCl_3$) δ 8.19 (d, *J*=8.6 Hz, 2H), 7.61 (d, *J*=8.1 Hz, 2H), 7.53 (d, *J*=8.3 Hz, 2H), 7.27 (d, *J*=8.3 Hz, 2H), 7.01-6.99 (m, 4H), 4.07 (d, *J*=6.4 Hz, 2H), 4.02 (d, *J*=6.3 Hz, 2H),

1.89-1.33 (m, 30H), 0.93 (t, *J*=6.6 Hz, 3H), 0.56 (t, *J*=7.3 Hz, 2H), 0.12 (s, 9H), 0.09 (s, 6H), 0.05 (s, 6H); ^{13}C NMR (100 MHz, $CDCl_3$) δ 165.3, 163.8, 159.0, 150.2, 138.8, 133.0, 132.5, 128.3, 127.9, 122.2, 121.8, 115.0, 114.5, 68.6, 68.3, 33.7, 32.0, 29.9, 29.8, 29.7, 29.6, 29.5, 29.3, 26.3, 26.2, 23.5, 22.9, 18.5, 14.3, 2.0, 1.5, 0.4; MS (MALDI) m/z 815([M+Na]+, 100); HRMS (MALDI) calcd for $C_{45}H_{72}O_6NaSi_3$: 815.4534, found 815.4531.

4-[11-(1,1,1,3,3,5,5-Heptamethyltrisiloxanyl)undecyloxy]-4'-(4-nonyloxybenzoyloxy)biphenyl (35d) The procedure described for the synthesis of **35a** was repeated with **49a** (75 mg, 0.13 mmol) and 4-nonyloxybenzoic acid (49 mg, 0.17 mmol) to give **35d** (95 mg, 80%) as a white solid, which was further purified by recrystallization from EtOH after filtration through a 0.45 mm PTFE filter: ^{1}H NMR (400 MHz, $CDCl_3$) δ 8.16 (d, *J*=8.8 Hz, 2H), 7.57 (d, *J*=8.6 Hz, 2H), 7.50 (d, *J*=8.5 Hz, 2H), 7.24 (d, *J*=8.5 Hz, 2H), 6.98-6.95 (m, 4H), 4.03-3.97 (m, 4H), 1.84-1.31 (m, 32H), 0.91 (t, *J*=6.6 Hz, 3H), 0.56 (t, *J*=6.9 Hz, 2H), 0.12 (s, 9H), 0.09 (s, 6H), 0.05 (s, 6H); ^{13}C NMR (100 MHz, $CDCl_3$) δ 165.2, 163.7, 158.9, 150.2, 138.7, 132.9, 132.5, 128.2, 127.8, 122.2, 121.8, 115.0, 114.5, 68.5, 68.2, 33.7, 32.1, 29.9, 29.8, 29.7, 29.6, 29.5, 29.3, 26.3, 26.2, 23.4, 22.9, 18.5, 14.3, 2.0, 1.5, 0.4; MS (MALDI) m/z 829([M+Na]+, 100); HRMS (MALDI) calcd for $C_{46}H_{74}O_6NaSi_3$: 829.4691, found 829.4681.

4-(4-Decyloxybenzoyloxy)-4'-[11-(1,1,1,3,3,5,5-heptamethyltrisiloxanyl)undecyloxy]biphenyl (35e) The procedure described for the synthesis of **35a** was repeated with **49a** (75 mg, 0.13 mmol) and 4-decyloxybenzoic acid (49 mg, 0.17 mmol) to give **35e** (95 mg, 84%) as a white solid, which was further purified by recrystallization from EtOH after filtration through a 0.45 mm PTFE filter: ^{1}H NMR (400 MHz, $CDCl_3$) δ 8.19 (d, *J*=7.8 Hz, 2H), 7.61 (d, *J*=7.3 Hz, 2H), 7.53 (d, *J*=7.7 Hz, 2H), 7.27 (d, *J*=7.7 Hz, 2H), 7.10-6.99 (m, 4H), 4.07 (t, *J*=6.4 Hz, 2H), 4.02 (t, *J*=6.3 Hz, 2H), 1.88-1.32 (m, 34H), 0.92 (t, *J*=5.7 Hz, 3H), 0.56 (t, *J*=6.5 Hz, 2H), 0.12 (s, 9H), 0.09 (s, 6H), 0.05 (s, 6H); ^{13}C NMR (100 MHz, $CDCl_3$) δ 165.3, 163.8, 159.0, 150.2, 138.8, 133.0, 132.5, 128.3, 127.9, 122.2, 121.8, 115.0, 114.5, 68.6, 68.3, 33.7, 32.1, 29.9, 29.8, 29.7, 29.6, 29.5, 29.3, 26.3, 26.2, 23.5, 22.9, 18.5, 14.3, 2.0, 1.5, 0.4; MS (MALDI) m/z 843([M+Na]+, 100); HRMS (MALDI) calcd for $C_{47}H_{76}O_6NaSi_3$: 843.4847, found 843.4858.

4-(4-Dodecyloxybenzoyloxy)-4'-[11-(1,1,1,3,3,5,5-heptamethyltrisiloxanyl)undecyloxy]biphenyl (35f) The procedure described for the synthesis of **35a** was repeated with **49a** (112 mg, 0.20 mmol) and 4-dodecyloxybenzoic acid (80 mg, 0.26 mmol) to give **35f** (1.46 mg, 84%) as a white solid, which was further purified by recrystallization from EtOH after filtration through a 0.45 mm PTFE filter: ^{1}H NMR (400 MHz, $CDCl_3$) δ 8.18 (d, *J*=8.8 Hz, 2H), 7.60 (d, *J*=8.3 Hz, 2H), 7.53 (d, *J*=8.6 Hz, 2H), 7.27 (d, *J*=8.6 Hz, 2H), 7.01-6.98 (m, 4H), 4.07 (t, *J*=6.6 Hz, 2H), 4.02 (t, *J*=6.6

Hz, 2H), 1.88-1.28 (m, 38H), 0.91 (t, *J*=6.6 Hz, 3H), 0.56 (t, *J*=7.4 Hz, 2H), 0.11 (s, 9H), 0.09 (s, 6H), 0.05 (s, 6H); ^{13}C NMR (100 MHz, CDCl3) δ 165.3, 163.8, 159.0, 150.2, 138.8, 133.0, 132.5, 128.3, 127.9, 122.2, 121.8, 115.0, 114.5, 68.6, 68.3, 33.7, 32.1, 29.9, 29.8, 29.7, 29.6, 29.5, 29.3, 26.3, 26.2, 23.5, 22.9, 18.5, 14.3, 2.0, 1.5, 0.4; MS (MALDI) m/z 872([M+Na]+, 100); HRMS (MALDI) calcd for $C_{49}H_{80}O_6NaSi_3$: 871.5160, found 871.5186.

4-[6-(1,1,1,3,3,5,5-Heptamethyltrisiloxanyl)hexanoyloxy-4'-(4-octyloxybenzoyloxy)]biphenyl (36) The procedure described for the synthesis of **35a** was repeated with **49b** (139 mg, 0.29 mmol) and 4-octyloxybenzoic acid (93 mg, 0.37 mmol) to give **36** (168 mg, 85%) as a white solid, which was further purified by recrystallization from EtOH after filtration through a 0.45 mm PTFE filter: ^{1}H NMR (400 MHz, $CDCl_3$) δ 8.19 (d, *J*=8.8 Hz, 2H), 7.60 (d, *J*=8.6 Hz, 2H), 7.53 (d, *J*=8.6 Hz, 2H), 7.27 (d, *J*=8.6 Hz, 2H), 7.01-6.99 (m, 4H), 4.07 (t, *J*=6.6 Hz, 2H), 4.02 (t, *J*=6.6 Hz, 2H), 1.88-1.33 (m, 20H), 0.93 (t, *J*=6.8 Hz, 3H), 0.59 (t, *J*=7.8 Hz, 2H), 0.13 (s, 9H), 0.10 (s, 6H), 0.06 (s, 6H); ^{13}C NMR (100 MHz, $CDCl_3$) δ 165.3, 163.8, 159.0, 150.2, 138.8, 133.0, 132.5, 128.3, 127.9, 122.2, 121.8, 115.0, 114.5, 68.5, 68.3, 33.4, 32.0, 29.4, 29.3, 26.2, 26.0, 23.4, 22.9, 18.5, 14.3, 2.0, 1.5, 0.4; MS (MALDI) m/z 745([M+Na]+, 100); HRMS (MALDI) calcd for $C_{40}H_{62}O_6NaSi_3$: 745.3751, found 745.3741.

4-[11-(1,1,1,3,3-Pentamethyldisiloxanyl)undecyloxy]-4'-(4-octyloxybenzoyloxy)biphenyl (37) The procedure described for the synthesis of **35a** was repeated with **49c** (139 mg, 0.29 mmol) and 4-octyloxybenzoic acid (93 mg, 0.37 mmol) to give **37** (168 mg, 82%) as a white solid, which was further purified by recrystallization from EtOH after filtration through a 0.45 mm PTFE filter: ^{1}H NMR (400 MHz, $CDCl_3$) δ 8.19 (d, *J*=7.6 Hz, 2H), 7.61 (d, *J*=7.3 Hz, 2H), 7.53 (d, *J*=7.3 Hz, 2H), 7.27 (d, *J*=8.3 Hz, 2H), 7.01-6.99 (m, 4H), 4.07 (t, *J*=6.5 Hz, 2H), 4.02 (t, *J*=6.4 Hz, 2H), 1.88-1.32 (m, 30H), 0.93 (t, *J*=6.8 Hz, 3H), 0.53 (t, *J*=6.9 Hz, 2H), 0.09 (s, 9H), 0.07 (s, 6H); ^{13}C NMR (100 MHz, $CDCl_3$) δ 165.3, 163.8, 159.0, 150.2, 138.8, 133.0, 132.5, 128.3, 127.9, 122.2, 121.8, 115.0, 114.5, 68.6, 68.3, 33.7, 32.0, 29.9, 29.8, 29.7, 29.6, 29.5, 29.4, 29.3, 26.3, 26.2, 23.5, 22.9, 18.6, 14.3, 2.2, 1.6; MS (MALDI) m/z 741([M+Na]+, 100); HRMS (MALDI) calcd for $C_{43}H_{66}O_5NaSi_2$: 741.4346, found 741.4335.

4-(Undec-10-enyloxy)phenyl 4-octyloxybenzoate (51) Under an argon atmosphere, a mixture of **50a** (131 mg, 0.50 mmol), 4-octyloxybenzoic acid (163 mg, 0.65 mmol), DCC (130 mg, 0.63 mmol) and DMAP (13 mg, 0.11 mmol) in anhydrous CH_2Cl_2 (10 mL) was stirred at room temperature for 24 h, and then concentrated to a white solid. Purification by flash chromatography on silica gel (12:1 hexanes/EtOAc) gave **51** (148 mg, 80 %) as a white solid, which was further purified by recrystallization from EtOH after filtration through a 0.45 mm PTFE filter: ^{1}H NMR (400 MHz, $CDCl_3$) δ 8.15 (d, *J*=9.1 Hz, 2H), 7.12 (d, *J*=9.1 Hz, 2H), 6.99-6.93 (m, 4H), 5.84 (m, 1H), 4.99 (m, 2H), 4.06 (t, *J*=6.6 Hz,

2H), 3.97 (t, *J*=6.5 Hz, 2H), 2.07 (m, 2H), 1.87-1.32 (m, 26H), 0.92 (t, *J*=6.8 Hz, 3H); ^{13}C NMR (100 MHz, $CDCl_3$) δ 165.6, 163.7, 157.0, 144.6, 139.5, 132.4, 122.7, 121.9, 115.3, 115.0, 114.5, 68.6, 68.5, 34.0, 32.0, 29.7, 29.6, 29.5, 29.4, 29.3, 29.1, 26.3, 22.9, 14.3; MS (MALDI) m/z 369 ($[M+H]_+$, 100); HRMS (MALDI) calcd for $C_{23}H_{29}O_4$: 369.2066, found 369.2079.

4-(Hex-5-enyloxy)phenyl 4-nonyloxybenzoate (52b) The procedure described for the synthesis of **51** was repeated with **50b** (42 mg, 0.39 mmol) and 4-nonyloxybenzoic acid (123 mg, 0.46 mmol) to give **52b** (141 mg, 83%) as a white solid, which was further purified by recrystallization from EtOH after filtration through a 0.45 mm PTFE filter: ^{1}H NMR (400 MHz, $CDCl_3$) δ 8.15 (d, *J*=7.8 Hz, 2H), 7.12 (d, *J*=7.6 Hz, 2H), 6.99-6.93 (m, 4H), 5.86 (m, 1H), 5.03 (m, 2H), 4.06 (t, *J*=5.6 Hz, 2H), 3.99 (t, *J*=4.8 Hz, 2H), 2.16 (m, 2H), 1.83-1.31 (m, 18H), 0.91 (t, *J*=5.6 Hz, 3H); ^{13}C NMR (100 MHz, $CDCl_3$) δ 165.6, 163.7, 156.9, 144.6, 138.8, 132.4, 122.7, 121.9, 115.3, 115.0, 114.5, 68.5, 68.4, 33.7, 32.1, 29.7, 29.6, 29.5, 29.3, 28.9, 26.2, 25.5, 22.9, 14.3; MS (MALDI) m/z 439([M+H]+, 100); HRMS (MALDI) calcd for $C_{28}H_{39}O_4$: 439.2848, found 439.2861.

4-(Hex-5-enyloxy)phenyl 4-decyloxybenzoate (52c) The procedure described for the synthesis of **51** was repeated with **50b** (60 mg, 0.31 mmol) and 4-decyloxybenzoic acid (103 mg, 0.36 mmol) to give **52c** (118 mg, 84%) as a white solid, which was further purified by recrystallization from EtOH after filtration through a 0.45 mm PTFE filter: ^{1}H

NMR (400 MHz, $CDCl_3$) δ 8.15 (d, *J*=9.1 Hz, 2H), 7.12 (d, *J*=9.1 Hz, 2H), 6.99-6.92 (m, 4H), 5.86 (m, 1H), 5.03 (m, 2H), 4.06 (t, *J*=6.6 Hz, 2H), 3.99 (t, *J*=6.5 Hz, 2H), 2.16 (m, 2H), 1.87-1.30 (m, 20H), 0.91 (t, *J*=6.8 Hz, 3H); ^{13}C NMR (100 MHz, $CDCl_3$) δ 165.6, 163.7, 156.9, 144.7, 138.8, 132.5, 122.7, 121.9, 115.3, 115.0, 114.5, 68.5, 68.4, 33.7, 32.1, 29.8, 29.6, 29.5, 29.3, 28.9, 26.2, 25.6, 22.9, 14.3; MS (EI) m/z 452(M+, 1), 261(100), 121(7); HRMS (EI) calcd for $C_{29}H_{40}O_4$: 452.2927, found 452.2905.

4-(Hex-5-enyloxy)phenyl 4-dodecyloxybenzoate (52d) The procedure described for the synthesis of **51** was repeated with **50b** (53 mg, 0.28 mmol) and 4-dodecyloxybenzoic acid (102 mg, 0.33 mmol) to give **52d** (107 mg, 80%) as a white solid, which was further purified by recrystallization from EtOH after filtration through a 0.45 mm PTFE filter: ^{1}H NMR (400 MHz, $CDCl_3$) δ 8.15 (d, *J*=8.6 Hz, 2H), 7.12 (d, *J*=9.1 Hz, 2H), 6.99-6.93 (m, 4H), 5.86 (m, 1H), 5.03 (m, 2H), 4.06 (t, *J*=6.6 Hz, 2H), 3.99 (t, *J*=6.4 Hz, 2H), 2.16 (m, 2H), 1.83-1.29 (m, 24H), 0.91 (t, *J*=6.8 Hz, 3H); ^{13}C NMR (100 MHz, $CDCl_3$) δ 165.5, 163.7, 156.9, 144.6, 138.7, 132.4, 122.7, 121.9, 115.3, 115.0, 114.5, 68.5, 68.4, 33.6, 32.1, 29.9, 29.8, 29.6, 29.3, 28.9, 26.2, 25.5, 22.9, 14.3; MS (EI) m/z 480(M+, 1), 289(100), 121(14); HRMS (EI) calcd for $C_{31}H_{44}O_4$: 480.3240, found 480.3229.

4-[11-(1,1,1,3,3,5,5-Heptamethyltrisiloxanyl)undecyloxy]phenyl 4-octyloxybenzoate (38) Under an argon atmosphere, a 3 wt% solution of platinum(0)-1,3-divinyl-1,1,3,3-tetramethyldisiloxane complex in xylenes (25 μL, 0.0025 mmol) was added to a solution

of **51** (86 mg, 0.17 mmol), and 1,1,1,3,3,5,5-heptamethyltrisiloxane (58 mg, 0.28 mmol) in toluene (6 mL). The mixture was stirred at room temperature overnight, then concentrated, and the residue purified by flash chromatography on silica gel (30:1 Hexanes: EtOAC) to give **38** (107 mg, 87%) as a white solid, which was further purified by recrystallization from EtOH after filtration through a 0.45 mm PTFE filter: ^{1}H NMR (400 MHz, $CDCl_3$ 8.17 (d,) δ *J* = 8.8 Hz, 2 H), 7.14 (d, *J*=9.1 Hz, 2 H), 7.00-6.94 (m, 4 H), 4.05 (t, *J* = 6.4 Hz, 2 H), 3.98 (t, *J* = 6.6 Hz, 2 H), 1.89-1.34 (m, 30H), 0.95 (t, *J*=6.5 Hz, 3H), 0.59 (t, *J*=7.7 Hz, 2H), 0.15 (s, 9H), 0.12 (s, 6H), 0.08 (s, 6H); ^{13}C NMR (100 MHz, $CDCl_3$ 165.4, 163.6, 157.0, 144.6, 132.4, 122.6,) δ 121.9, 115.2, 114.4, 68.5, 68.4, 33.7, 32.0, 29.9, 29.8, 29.6, 29.5, 29.4, 29.3, 26.3, 26.2, 23.4, 22.9, 18.5, 14.3, 2.0, 1.5, 0.4; MS (MALDI) m/z 739([M+Na]+, 100), 553(1); HRMS (MALDI) calcd for $C_{39}H_{68}O_6NaSi_3$: 739.4221, found 739.4204.

4-[6-(1,1,1,3,3,5,5-Heptamethyltrisiloxanyl)hexanoyloxy]phenyl 4-octyloxybenzoate (39a). The procedure described for the synthesis of **38** was repeated with a 3 wt% solution of platinum(0)-1,3-divinyl-1,1,3,3-tetramethyldisiloxane complex in xylenes (25 μL, 0.0029 mmol), **52a** (95 mg, 0.21 mmol), and 1,1,1,3,3,5,5-heptamethyltrisiloxane (64 mg, 0.29 mmol) to give **39a** (102 mg, 82%) as a white solid, which was further purified by recrystallization from EtOH after filtration through a 0.45 mm PTFE filter: ^{1}H NMR (400 MHz, $CDCl_3$ 8.15 (d,) δ *J* = 8.8 Hz, 2 H), 7.12 (d, *J*=8.8 Hz, 2 H), 6.99-6.92 (m, 4 H), 4.06 (t, *J* = 6.4 Hz, 2 H), 3.97 (t, *J* = 6.4 Hz, 2 H), 1.87-1.32 (m, 20H), 0.92 (t, *J*=6.4

Hz, 3H), 0.57 (t, *J*=7.6 Hz, 2H), 0.11 (s, 9H), 0.09 (s, 6H), 0.05 (s, 6H); ^{13}C NMR (100 MHz, $CDCl_3$165.6, 163.7, 157.0,) δ 144.6, 132.4, 122.7, 121.9, 115.3, 114.5, 68.7, 68.5, 33.4, 32.0, 29.5, 29.4, 29.3, 26.2, 26.0, 23.4, 22.9, 18.5, 14.3, 2.0, 1.5, 0.4; MS (ES) m/z 647([M+H]+, 5), 664(5), 557(10), 483(100), 233(10); HRMS (ES) calcd for $C_{34}H_{59}O_6Si_3$: 647.3619, found 647.3630.

4-[6-(1,1,1,3,3,5,5-Heptamethyltrisiloxanyl)hexanoyloxy]phenyl 4-nonyloxybenzoate (39b). The procedure described for the synthesis of **38** was repeated with a 3 wt% solution of platinum(0)-1,3-divinyl-1,1,3,3-tetramethyldisiloxane complex in xylenes (27 μL, 0.0027 mmol), **52b** (80 mg, 0.18 mmol), and 1,1,1,3,3,5,5-heptamethyltrisiloxane (61 mg, 0.27 mmol) to give **39b** (105 mg, 87%) as a white solid, which was further purified by recrystallization from EtOH after filtration through a 0.45 mm PTFE filter: ^{1}H NMR (400 MHz, $CDCl_3$8.15 (d,) δ *J* = 8.8 Hz, 2 H), 7.12 (d, *J*=8.9 Hz, 2 H), 6.99-6.93 (m, 4 H), 4.06 (t, *J* = 6.6 Hz, 2 H), 3.98 (t, *J* = 6.4 Hz, 2 H), 1.88-1.32 (m, 22H), 0.91 (t, *J*=6.7 Hz, 3H), 0.58 (t, *J*=7.6 Hz, 2H), 0.12 (s, 9H), 0.10 (s, 6H), 0.05 (s, 6H); ^{13}C NMR (100 MHz, $CDCl_3$ 165.6, 163.7, 157.0,) δ 144.6, 132.4, 122.7, 121.9, 115.3, 114.5, 68.7, 68.5, 33.4, 32.1, 29.7, 29.6, 29.5, 29.3, 26.2, 26.0, 23.4, 22.9, 18.5, 14.3, 2.0, 1.5, 0.4; MS (ES) m/z 661([M+H]+, 3), 571(7), 497(100), 247(5); HRMS (ES) calcd for $C_{35}H_{61}O_6Si_3$: 661.3776, found 661.3805.

4-[6-(1,1,1,3,3,5,5-Heptamethyltrisiloxanyl)hexanoyloxy]phenyl 4-decyloxybenzoate (39c). The procedure described for the synthesis of **38** was repeated with a 3 wt% solution of platinum(0)-1,3-divinyl-1,1,3,3-tetramethyldisiloxane complex in xylenes (33 μL, 0.0033 mmol), **52c** (94 mg, 0.21 mmol), and 1,1,1,3,3,5,5-heptamethyltrisiloxane (69 mg, 0.31 mmol) to give **39c** (119 mg, 82%) as a white solid, which was further purified by recrystallization from EtOH after filtration through a 0.45 mm PTFE filter: ^{1}H NMR (400 MHz, $CDCl_3$) 8.15 (d,δ *J* = 8.8 Hz, 2 H), 7.12 (d, *J*=9.0 Hz, 2 H), 6.99-6.92 (m, 4 H), 4.06 (t, *J* = 6.6 Hz, 2 H), 3.97 (t, *J* = 6.5 Hz, 2 H), 1.87-1.34 (m, 24H), 0.92 (t, *J*=7.2 Hz, 3H), 0.57 (t, *J*=7.5 Hz, 2H), 0.11 (s, 9H), 0.09 (s, 6H), 0.05 (s, 6H); ^{13}C NMR (100 MHz, $CDCl_3$) 165.6, 163.7, 157.0, 144.6, 132.4, 122.7, 121.9, 115.3, 114.5, 68.7, 68.2,δ 33.4, 31.8, 29.7, 29.6, 29.5, 29.3, 26.2, 26.0, 23.4, 22.8, 18.5, 14.3, 2.0, 1.5, 0.4; MS (MALDI) m/z 697([M+Na]+, 100), 511(43); HRMS (MALDI) calcd for $C_{36}H_{62}O_6NaSi_3$: 697.3751, found 697.3730.

4-[6-(1,1,1,3,3,5,5-Heptamethyltrisiloxanyl)hexanoyloxy]phenyl 4-dodecyloxybenzoate (39d). The procedure described for the synthesis of **38** was repeated with a 3 wt% solution of platinum(0)-1,3-divinyl-1,1,3,3-tetramethyldisiloxane complex in xylenes (34 μL, 0.0033 mmol), **52d** (116 mg, 0.24 mmol), and 1,1,1,3,3,5,5-heptamethyltrisiloxane (74 mg, 0.33 mmol) to give **39d** (129 mg, 80%) as a white solid, which was further purified by recrystallization from EtOH after filtration through a 0.45 mm PTFE filter: ^{1}H NMR (400 MHz, $CDCl_3$8.15 (d,) δ *J* = 8.8 Hz, 2 H), 7.12 (d, *J*=9.1

Hz, 2 H), 6.99-6.92 (m, 4 H), 4.06 (t, *J* = 6.4 Hz, 2 H), 3.97 (t, *J* = 6.6 Hz, 2 H), 1.87-1.29 (m, 28H), 0.90 (t, *J*=6.7 Hz, 3H), 0.57 (t, *J*=7.7 Hz, 2H), 0.11 (s, 9H), 0.09 (s, 6H), 0.05 (s, 6H); ^{13}C NMR (100 MHz, $CDCl_3$ 165.5, 163.7, 157.0, 144.6, 132.4, 122.7,) δ 121.9, 115.3, 114.5, 68.7, 68.5, 33.4, 32.1, 29.9, 29.8, 29.6, 29.4, 29.3, 26.2, 26.0, 23.4, 22.9, 18.4, 14.3, 2.0, 1.5, 0.4; MS (MALDI) m/z 725([M+Na]+, 100), 659(22), 648(25), 520(19); HRMS (MALDI) calcd for $C_{38}H_{66}O_6NaSi_3$: 725.4064, found 725.4058.

4-[11-(1,1,1,3,3,5,5-Heptamethyltrisiloxanyl)undecyloxy]phenyl 4-(8-chlorooctyloxy)benzoate (40a). The procedure described for the synthesis of **38** was repeated with a 3 wt% solution of platinum(0)-1,3-divinyl-1,1,3,3-tetramethyldisiloxane complex in xylenes (15 μL, 0.0015 mmol), **56a** (53 mg, 0.10 mmol), and 1,1,1,3,3,5,5-heptamethyltrisiloxane (33 mg, 0.15 mmol). Purification by flash chromatography on silica gel (20:1 hexanes:EtOAC) gave **40a** (64 mg, 85%) as a white solid, which was further purified by recrystallization from EtOH after filtration through a 0.45 mm PTFE filter: ^{1}H NMR (400 MHz, $CDCl_3$) 8.15 (d,δ *J* = 8.1 Hz, 2 H), 7.12 (d, *J*=8.1 Hz, 2 H), 6.99-6.93 (m, 4 H), 4.06 (t, *J* = 6.3 Hz, 2 H), 3.97 (t, *J* = 6.4 Hz, 2 H), 3.56 (t, *J* = 6.7 Hz, 2 H), 1.88-1.31 (m, 30H), 0.55 (t, *J*=7.1 Hz, 2H), 0.11 (s, 9H), 0.08 (s, 6H), 0.05 (s, 6H); ^{13}C NMR (100 MHz, $CDCl_3$) δ 165.5, 163.6, 157.0, 144.6, 132.4, 122.7, 122.0, 115.3, 114.4, 68.6, 68.4, 45.3, 33.7, 32.8, 29.9, 29.8, 29.6, 29.5, 29.4, 29.3, 29.0, 27.0, 26.3, 26.1, 23.4, 18.5, 2.0, 1.5, 0.4; MS (ES) m/z 751([M+H]+, 100); HRMS (ES) calcd for $C_{39}H_{68}O_6Si_3Cl$: 751.4012, found 751.4064.

4-[6-(1,1,1,3,3,5,5-Heptamethyltrisiloxanyl)hexanoyloxy]phenyl 4-(8-chlorooctyloxy)benzoate (40b). The procedure described for the synthesis of **40a** was repeated with a 3 wt% solution of platinum(0)-1,3-divinyl-1,1,3,3-tetramethyldisiloxane complex in xylenes (20 μL, 0.0020 mmol), **56b** (60 mg, 0.13 mmol), and 1,1,1,3,3,5,5-heptamethyltrisiloxane (45 mg, 0.20 mmol) to give **40b** (72 mg, 80%) as a white solid, which was further purified by recrystallization from EtOH after filtration through a 0.45 mm PTFE filter: ^{1}H NMR (400 MHz, $CDCl_3$) 8.16 (d,δ *J* = 8.9 Hz, 2 H), 7.13 (d, *J*=8.9 Hz, 2 H), 7.00-6.94 (m, 4 H), 4.06 (t, *J* = 6.4 Hz, 2 H), 3.98 (t, *J* = 6.6 Hz, 2 H), 3.56 (t, *J* = 6.7 Hz, 2 H), 1.88-1.40 (m, 20H), 0.59 (t, *J*=7.7 Hz, 2H), 0.13 (s, 9H), 0.11 (s, 6H), 0.07 (s, 6H); ^{13}C NMR (100 MHz, $CDCl_3$) δ 165.5, 163.6, 157.0, 144.6, 132.4, 122.6, 121.9, 115.2, 114.4, 68.6, 68.4, 45.2, 33.3, 32.8, 29.4, 29.2, 29.0, 27.0, 26.1, 26.0, 23.4, 18.4, 2.0, 1.5, 0.4; MS (ES) m/z 681([M+H]+, 100); HRMS (ES) calcd for $C_{34}H_{58}O_6Si_3Cl$: 681.3229, found 681.3174.

4-(Undec-10-enyloxy)phenyl 4-hydroxybenzoate (55a). Under an argon atmosphere, a mixture of **50a** (490 mg, 1.87 mmol), 4-hydroxybenzoic acid (530 mg, 3.84 mmol), DCC (640 mg, 3.11 mmol) and DMAP (182 mg, 1.49 mmol) in anhydrous CH_2Cl_2 (10 mL) was stirred at room temperature for 50 h, and then concentrated to a white solid. Purification by flash chromatography on silica gel (4:1 hexanes/EtOAc) gave **55a** (132 mg, 18%) as a white solid: mp 116-117 ^{o}C; ^{1}H NMR (400 MHz, $CDCl_3$8.08 (d,) δ *J* = 8.6 Hz, 2 H), 7.12 (d, *J*=9.1 Hz, 2 H), 6.95-6.86 (m, 4 H), 5.85 (m, 1H), 4.99 (m, 2H),

3.96 (t, *J* = 6.6 Hz, 2 H), 2.10-1.33 (m, 16H); ^{13}C NMR (100 MHz, $CDCl_3$) δ 166.2, 161.3, 157.1, 144.4, 139.4, 132.7, 122.6, 121.5, 115.7, 115.4, 114.3, 68.7, 34.0, 31.2, 29.7, 29.6, 29.4, 29.3, 29.1, 26.2; MS (ES) m/z 383([M+H]+, 100); HRMS (ES) calcd for $C_{24}H_{31}O_4$: 383.2222, found 383.2198.

4-(Hex-5-enyloxy)phenyl 4-hydroxybenzoate (55b). The procedure described for the synthesis of **55a** was repeated with **50b** (445 mg, 2.31 mmol), 4-hydroxybenzoic acid (650mg, 4.71 mmol), DCC (791 mg, 3.92 mmol) and DMAP (119 mg, 0.97 mmol) to give **55b** (144 mg, 20%) as a white solid: mp 120-121 ^{o}C; ^{1}H NMR (400 MHz, $CDCl_3$) 8.10 (d,δ *J* = 8.6 Hz, 2 H), 7.11 (d, *J*=9.1 Hz, 2 H), 6.94-6.89 (m, 4 H), 5.85 (m, 1H), 5.03 (m, 2H), 3.98 (t, *J* = 6.4 Hz, 2 H), 2.18-1.55 (m, 6H); ^{13}C NMR (100 MHz, $CDCl_3$) δ 165.8, 160.8, 157.0, 144.5, 138.7, 132.8, 122.7, 122.0, 115.6, 115.3, 115.0, 68.4, 33.6, 28.9, 25.5; MS (ES) m/z 313([M+H]+, 100); HRMS (ES) calcd for $C_{19}H_{21}O_4$: 313.1439, found 313.1430.

4-(Undec-10-enyloxy)phenyl 4-(8-chlorooctyloxy)benzoate (56a) Under an argon atmosphere, a solution of diisopropylazodicarboxylate (131 mg, 0.65 mmol), 8-chloro-1-octanol (105 mg, 0.64 mmol), **55a** (114 mg, 0.30 mmol) and triphenylphosphine (144 mg, 0.54 mmol) in anhydrous THF (8 mL) was stirred at room temperature for 26 h, and then concentrated to a yellow oil. Purification by flash chromatography on silica gel (12:1 hexanes/EtOAc) gave **56a** (105 mg, 66%) as a white solid, which was further purified by

recrystallization from EtOH after filtration through a 0.45 mm PTFE filter: ^{1}H NMR (400 MHz, $CDCl_3$) 8.16 (d,δ *J* = 7.8 Hz, 2 H), 7.13 (d, *J*=8.8 Hz, 2 H), 6.99-6.93 (m, 4 H), 5.85 (m, 1H), 5.00 (m, 2H), 4.05 (t, *J* = 6.4 Hz, 2 H), 3.97 (t, *J* = 6.4 Hz, 2 H), 3.56 (t, *J* = 6.7 Hz, 2 H), 2.10-1.34 (m, 28H); ^{13}C NMR (100 MHz, $CDCl_3$) δ 165.4, 163.5, 156.9, 144.5, 139.3, 132.3, 122.6, 121.9, 115.2, 114.4, 114.3, 68.5, 68.3, 45.2, 34.0, 32.7, 29.7, 29.6, 29.5, 29.4, 29.3, 29.2, 29.1, 28.9, 26.9, 26.2, 26.0; MS (ES) m/z 529([M+H]+, 100), 425(94); HRMS (ES) calcd for $C_{32}H_{46}O_4Cl$: 529.3084, found 529.3124.

4-(Hex-5-enyloxy)phenyl 4-(8-chlorooctyloxy)benzoate (56b). The procedure described for the synthesis of **56a** was repeated with diisopropylazodicarboxylate (157 mg, 0.78 mmol), 8-chloro-1-octanol (127 mg, 0.77 mmol), **55b** (108 mg, 0.35 mmol) and triphenylphosphine (120 mg, 0.45 mmol) in anhydrous THF (5 mL) to give **56b** (96 mg, 60%) as a white solid, which was further purified by recrystallization from EtOH after filtration through a 0.45 mm PTFE filter: ^{1}H NMR (400 MHz, $CDCl_3$8.16 (d,) δ *J* = 8.9 Hz, 2 H), 7.13 (d, *J*=9.1 Hz, 2 H), 6.99-6.93 (m, 4 H), 5.05 (m, 1H), 5.00 (m, 2H), 4.05 (t, *J* = 6.4 Hz, 2 H), 3.98 (t, *J* = 6.3 Hz, 2 H), 3.56 (t, *J* = 6.7 Hz, 2 H), 2.19-1.40 (m, 18H); ^{13}C NMR (100 MHz, $CDCl_3$) δ 165.4, 163.5, 156.8, 144.5, 138.6, 132.3, 122.6, 121.8, 115.1, 114.9, 114.3, 68.3, 68.2, 45.2, 33.5, 32.7, 29.3, 29.2, 28.9, 28.8, 26.9, 26.0, 25.4; MS (ES) m/z 459([M+H]+, 100), 355(25); HRMS (ES) calcd for $C_{27}H_{36}O_4Cl$: 459.2302, found 459.2268.

5-(4-Methoxyphenyl)-2-methylthiophene-3-carboxylic acid (61) Under an argon atmosphere, a 1.4M solution of *n*-butyllithium in hexanes (1.6 mL, 2.24 mmol) was added dropwise to a solution of **60** (534 mg, 1.89 mmol) in anhydrous THF (12 mL) at –78 ^{o}C. The reaction mixture was stirred for 1.5 hrs at –78 ^{o}C, then an excess of dry ice was added. After the mixture was slowly warmed to room temperature and stirred overnight, it was quenched with water, and concentrated to a yellowish solid. The residue was purified by flash chromatography on silica gel ($CHCl_3$) to give **61** (193 mg, 78%) as a white solid: mp 350 ^{o}C (dec); ^{1}H NMR (400 MHz, DMSO-d6) δ 7.58 (d, *J* = 8.9 Hz, 2 H), 7.54 (s, 1H), 7.00 (d, *J*=8.8 Hz, 2 H), 3.85(s, 3H), 2.74 (s, 3H); ^{13}C NMR (100 MHz, DMSO-d6) δ 164.6, 159.0, 146.0, 138.3, 130.5, 126.5, 125.7, 123.7, 114.5, 55.2, 15.1; MS (EI) m/z 248(M+, 100), 233(43); HRMS (EI) calcd for $C_{13}H_{12}O_3S$: 248.0507, found 248.0498.

1-[5-(4-Methoxyphenyl)-2-methylthiophen-3-yl]ethanone (62) Under an argon atmosphere, a mixture of **61** (148 mg, 0.60 mmol) and methyllithium (0.39 mL, 0.62 mmol, 1.6M solution in diethyl ether) in anhydrous ether (75 mL) was heated to reflux for 2 days, and then quenched with ice water. The aqueous phase was extracted with ether, dried ($MgSO_4$), and concentrated. The residue was purified by flash chromatography on silica gel (10:1 hexanes:EtOAc) to give **62** (125 mg, 51%) as a white solid: mp 224-225 ^{o}C; ^{1}H NMR (400 MHz, $CDCl_3$ 7.49 (d,) δ *J* = 8.6 Hz, 2 H), 7.41(s, 1H), 6.93 (d, *J*=8.8 Hz, 2 H), 3.85(s, 3H), 2.75 (s, 3H), 2.54(s, 3H); ^{13}C NMR (100 MHz,

$CDCl_3$) δ 194.3, 159.6, 147.7, 139.6, 137.0, 127.1, 126.5, 123.3, 114.6, 55.5, 30.0, 16.4; MS (EI) m/z 246(M+, 5), 231(5), 84(100); HRMS (EI) calcd for $C_{14}H_{14}O_2S$: 246.0715, found 246.0714.

2-(5-Bromo-2-methylthiophen-3-yl)-5-methylhex-3-yne-2,5-diol (65) Under an argon atmosphere, a 1.3M solution of *n*-butyllithium in hexanes (1.8 mL, 2.40 mmol) was added dropwise to a solution of 3-methyl-1-butyn-3-ol (204 mg, 2.42 mmol) in anhydrous ether (10 mL) at 0 ^oC. The reaction mixture was slowly warmed to room temperature, stirred for 2 h, and then added to a solution of **64** (597 mg, 2.43 mmol) in anhydrous ether at -78 ^oC. The resulting solution was stirred at -78 ^oC for 3 h and then warmed slowly to room temperature and stirred overnight, Aqueous NH_4Cl was added and the mixture was extracted with ether, dried ($MgSO_4$), and concentrated. The residue was purified by flash chromatography on silica gel (1:1 hexanes:EtOAc) to give **65** (398 mg, 55%) as an orange oil: ^1H NMR (400 MHz, $CDCl_3$) 6.99 (s,δ 1H), 4.30(s, 1H), 3.92(s, 1H), 2.47(s, 3H), 1.67(s, 3H), 1.48(s, 3H); ^{13}C NMR (100 MHz, $CDCl_3$) δ 141.4, 136.2, 130.1, 106.2, 88.7, 85.2, 67.0, 65.2, 31.7, 31.2, 14.5; MS (EI) m/z 301(M+, 5), 287(100), 271(69); HRMS (EI) calcd for $C_{12}H_{15}O_2SBr$: 301.9976, found 301.9972.

3-[1-(5-Bromo-2-methylthiophen-3-yl)ethylidene]-4-(propan-2-ylidene)dihydrofuran-2,5-dione (42) and 2-[1-(5-Bromo-2-methylthiophen-3-yl)ethylidene]-3-(propan-2-ylidene)succinic acid (67) Under an atmosphere of carbon

monoxide (640-700 psi), a mixture of **65** (1.31 g, 4.30 mmol), I_2 (55 mg, 0.22 mmol), and $Pt(OAc)_2$ (52 mg, 0.23 mmol) in anhydrous benzene (10 mL) was heated to 90 ^oC in an autoclave for 18 h. The reaction mixture was then concentrated, and the residue purified by flash chromatography on silica gel (9:1 hexanes to EtOAc) to give **67** (277 mg, 18%) as a white solid and **42** (366 mg, 25%) as a brownish solid, which was further purified by recrystallization from EtOH to give a white solid.

Compound **42**: mp 130–131 ^oC; ^1H NMR (400 MHz, $CDCl_3$) δ 6.78 (s, 1H), 2.52 (s, 3H), 2.25 (s, 3H), 2.09 (s, 3H), 1.26 (s, 3H); ^{13}C NMR (100 MHz, $CDCl_3$) δ 163.6, 162.9, 156.4, 147.1, 140.4, 138.3, 130.0, 122.2, 120.5, 109.9, 25.9, 23.0, 22.9, 15.0; MS (EI) m/z 340(M+, 21), 261(89), 217(100); HRMS (EI) calcd for $C_{14}H_{13}O_3SBr$: 339.9769, found 339.9785.

Compound **67**: mp 121–122 ^oC; ^1H NMR (400 MHz, $CDCl_3$) δ 6.76 (s, 1H), 2.36 (s, 3H), 2.23 (s, 3H), 2.02 (s, 3H), 1.95 (s, 3H); ^{13}C NMR (100 MHz, $CDCl_3$) δ 163.2, 160.9, 155.2, 145.1, 142.3, 136.3, 129.3, 123.2, 121.3, 108.7, 27.3, 26.5, 22.7, 14.5; MS (ES) m/z 359([M+H]+, 100); HRMS (ES) calcd for $C_{14}H_{16}O_4SBr$: 358.9953, found 358.9943.

Compound **42** can be synthesized from the by-product **67** in the following way: a mixture of **67** (400 mg, 1.12 mmol) and acetic anhydride (10 mL) was heated to reflux for 5 days. The reaction mixture was then concentrated to a black oil, which was purified by flash

chromatography on silica gel (9:1 hexanes: EtOAc) to give **42** (198 mg, 52%) as a brownish solid, which was further purified by recrystallization from EtOH.

3-[1-(5-Bromo-2-methylthiophen-3-yl)ethylidene]-1-octyl-4-(propan-2-ylidene)pyrrolidine-2,5-dione (43a) To a solution of **42** (425 mg, 1.25 mmol) in anhydrous benzene (12 mL) was added a solution of octylamine (163 mg, 1.26 mmol) in anhydrous benzene (5 mL). After stirring for 1 h at room temperature, zinc chloride power (141 mg, 1.29 mmol, dried at 190 ^{o}C overnight) was added to the reaction mixture in one portion. The reaction mixture was then heated to reflux, and a solution of hexamethyldisilazane (303 mg, 1.88 mmol) in anhydrous benzene (5 mL) was added within 10 min. The reaction mixture was then heated to reflux for 4 hrs. After removal of the solvent, the crude product was purified by flash chromatography on silica gel (20:1 hexanes:EtOAc) to give **43a** (383 mg, 68 %) as a sticky orange solid: mp 110-111 ^{o}C; ^{1}H NMR (400 MHz, $CDCl_3$ 6.75) δ (s, 1H), 3.50 (t, *J*=7.2 Hz, 2H), 2.50 (s, 3H), 2.20 (s, 3H), 2.05 (s, 3H), 1.55-1.19 (m, 15H), 0.79 (t, *J*=6.1 Hz, 3 H); ^{13}C NMR (100 MHz, $CDCl_3$) δ 168.7, 168.3, 149.0, 141.5, 141.0, 137.3, 130.5, 125.7, 123.1, 109.0, 38.0, 31.9, 29.3, 28.2, 27.1, 25.7, 22.8, 22.1, 21.9, 14.8, 14.2; MS (EI) m/z 451(M+, 21), 372(93), 283(23), 217(100); HRMS (EI) calcd for $C_{22}H_{30}NO_2SBr$: 451.1181, found 451.1161.

3-{1-[5-(4-Methoxymethoxyphenyl)-2-methylthiophen-3-yl]ethylidene}-1-octyl-4-(propan-2-ylidene)pyrrolidine-2,5-dione (44a) Under an Ar atmosphere, a mixture of

$Pd(PPh_3)_4$ (88 mg, 0.076 mmol), Na_2CO_3 (389 mg, 3.67mmol), **69** (313 mg, 1.71 mmol) and **43a** (491 mg, 1.09 mmol) in water (12.5 mL), benzene (25 mL) and EtOH (15 mL) was stirred under reflux for 24 h. The reaction mixture was then poured into water and extracted with ether. The combined extracts were washed with brine, dried ($MgSO_4$) and concentrated. The residue was purified by flash chromatography on silica gel (20:1 hexanes/EtOAc) to give **44a** (464.95 mg, 83 %) as a purple solid: mp 128–129 ^oC; ^1H NMR (400 MHz, $CDCl_3$) 7.46 (d,δ *J*=8.8 Hz, 2H), 7.06 (d, *J*=8.6 Hz, 2H), 6.97(s, 1H), 5.21 (s, 2H), 3.61 (d, *J*=7.3 Hz, 2H), 3.51 (s, 3H), 2.67 (s, 3H), 2.29 (s, 3H), 2.22(s, 3H), 1.66-1.29 (m, 15H), 0.89 (t, *J*=6.8 Hz, 3 H); ^{13}C NMR (100 MHz, $CDCl_3$) δ 169.1, 168.6, 157.1, 149.1, 142.7, 141.9, 141.3, 134.8, 128.1, 126.9, 125.1, 123.3, 122.9, 116.9, 116.7, 94.6, 56.2, 38.0, 32.0, 29.4, 28.4, 27.2, 25.8, 22.8, 22.2, 22.1, 15.1, 14.3; MS (EI) m/z 509(M+, 95), 494(100); HRMS (EI) calcd for $C_{30}H_{39}NO_4S$: 509.2600, found 509.2604.

3-{1-[5-(4-Hydroxyphenyl)-2-methylthiophen-3-yl]ethylidene}-1-octyl-4-(propan-2-ylidene)pyrrolidine-2,5-dione (70) A mixture of **44a** (370 mg, 0.73 mmol), HCl (38%, 9 mL), IPA (25 mL) and THF (17 mL) was stirred for 12.5 h. The reaction mixture was then concentrated and the residue was purified by flash chromatography on silica gel (20:1 hexanes/EtOAc) to give **70** (312 mg, 92 %) as a sticky red solid: mp 77–78 ^oC; ^1H NMR (400 MHz, $CDCl_3$) 7.40 (d,δ *J*=8.3 Hz, 2H), 7.06 (d, *J*=8.6 Hz, 2H), 6.94(s, 1H), 6.90(d, *J*=8.6 Hz, 2H), 3.63 (t, *J*=7.3 Hz, 2H), 2.67 (s, 3H), 2.30 (s, 3H), 2.22 (s, 3H), 1.66-1.27 (m, 15H), 0.88 (t, *J*=6.7 Hz, 3 H); ^{13}C NMR (100 MHz, $CDCl_3$) δ 169.3, 168.7,

156.0, 149.3, 143.1, 141.8, 141.6, 134.5, 127.1, 126.7, 125.0, 123.3, 122.5, 116.1, 38.1, 32.1, 29.9, 29.6, 29.4, 28.4, 27.2, 25.8, 22.8, 22.2, 15.0, 14.3; MS (EI) m/z 465(M+, 64), 450(100), 295(76); HRMS (EI) calcd for $C_{28}H_{35}NO_3S$: 465.2338, found 465.2341.

3-[1-(5-Bromo-2-methylthiophen-3-yl)ethylidene]-1-butyl-4-(propan-2-ylidene)pyrrolidine-2,5-dione (43b) The procedure described for the synthesis of **43a** was repeated with **42** (81 mg, 1.12 mmol), butylamine (73.14 mg, 1.0 mmol), zinc chloride power (157 mg, 1.15 mmol), and hexamethyldisilazane (271 mg, 1.68 mmol) to give **43b** (287 mg, 66 %) as a sticky orange solid: mp 115-116^{o}C; ^{1}H NMR (400 MHz, $CDCl_3$ 6.75 (s, 1H), 3.51 (t,) δ *J*=7.2 Hz, 2H), 2.50 (s, 3H), 2.20 (s, 3H), 2.05 (s, 3H), 1.56-1.19 (m, 7H), 0.86 (t, *J*=7.5 Hz, 3 H); ^{13}C NMR (100 MHz, $CDCl_3$) δ 168.7, 168.3, 149.1, 141.4, 141.0, 137.2, 130.4, 125.6, 123.1, 108.9, 37.6, 30.3, 25.7, 22.1, 21.8, 20.3, 14.8, 13.8; MS (EI) m/z 395(M+, 8), 316(48), 280(16), 217(100); HRMS (EI) calcd for $C_{18}H_{22}NO_2SBr$: 395.0555, found 395.0551.

1-Butyl-3-{1-[5-(4-methoxymethoxyphenyl)-2-methylthiophen-3-yl]ethylidene}-4-(propan-2-ylidene)pyrrolidine-2,5-dione (44b) The procedure described for the synthesis of **44a** was repeated with $Pd(PPh_3)_4$ (40 mg, 0.035 mmol), Na_2CO_3 (182 mg, 1.72 mmol), 69 (140 mg, 0.77 mmol) and **43b** (198 mg, 0.50 mmol) in water (6 mL), benzene (11 mL) and EtOH (7 mL) to give **44b** (183 mg, 81 %) as a sticky orange solid: mp 132-133 ^{o}C; ^{1}H NMR (400 MHz, $CDCl_3$) δ 7.46 (d, *J*=8.3 Hz, 2H), 7.06 (d, *J*=8.3 Hz,

2H), 6.97(s, 1H), 5.21 (s, 2H), 3.63 (d, *J*=7.3 Hz, 2H), 3.51 (s, 3H), 2.67 (s, 3H), 2.29 (s, 3H), 2.22(s, 3H), 1.68-1.29 (m, 7H), 0.97 (t, *J*=7.3 Hz, 3 H); ^{13}C NMR (100 MHz, $CDCl_3$) δ 169.2, 168.6, 157.1, 149.1, 142.8, 141.9, 141.3, 134.9, 128.0, 126.9, 125.1, 123.3, 122.9, 116.9, 94.6, 56.3, 37.8, 30.5, 25.8, 22.2, 22.1, 20.5, 15.1, 13.9; MS (EI) m/z 453(M+, 74), 438(100), 339(80); HRMS (EI) calcd for $C_{26}H_{31}NO_4S$: 453.1974, found 453.1973.

6.2 Tilt angle measurements

6.2.1 Sample preparation

Liquid crystal mixtures were prepared by combining the appropriate amounts of dopant and liquid crystal host in a 0.5 mL Reacti-Vial as a mixing container. The mixtures were heated to the isotropic phase, and swirled with a small glass rod repeatedly to achieve a homogeneous mixture. Nylon-coated glass cells with a 1 μm spacing and an indium/tin oxide (ITO) electrode with an area of 0.1 cm^2 were filled with the liquid crystal mixtures by capillary action above the clearing point of the mixture. The cell was placed in a Linkam LTS 350 hot stage fitted with electrical contacts for the addressed area. These contacts were connected to a Displaytech APT III Automated Polarization Testbed. Each cell was heated to the isotropic phase under an AC triangular wave (100 Hz, 6 V/μm) and held until any bubbles in the addressed area disappeared. Good alignment was achieved by slow cooling (0.1 K/min) from the isotropic phase while applying a triangular AC field (3Hz, 4V/μm) across the film.

6.2.2 Tilt angle measurement

Tilt angles were measured in the SmC* phase by applying a DC field to the Nylon-coated 1 μm cell via the cell holder. The DC voltage was provided by the APTIII instrumentation through a menu command. The cell and cell holder assembly fitted in the Linkam LTS 350 hot stage were fixed on the rotating stage of the Nikon Eclipse E600 POL polarizing microscope. Tilt angle measurements were obtained by determining the angular position of the rotating stage that produced light extinction through the addressed area of the cell. By using this procedure, two angular position readings were recorded for each of the two orientations of the DC electric field, and the tilt angle was calculated as half the difference between the two readings.

6.3 Photoisomerization of fulgide 42 and fulgimide 43a, 44b in solution

The following procedure is representative: a 3.67 X 10^{-4} M solution of **42** in HPLC grade hexanes was placed into a sealed UV cell (0.1 cm path length), and irradiated at ambient temperature using a PTI A6000 450W Xe arc lamp (25A, 18V) fitted with a water filter. The lamp output was filtered to select the light in the range λ=365 nm ± 5nm. The photoisomerization process was monitored by UV-visible spectroscopy and HPLC analysis. UV-visible spectra were recorded at room temperature using a Varian Cary 3 spectrophotometer. HPLC analyses and separations were performed on a system consisting of a Waters 501 single piston pump, a Supelguard C18

LC-Si silica guard column (2 cm X 4.0 mm i.d.), a semi-preparative HPLC column (Xcm x Xmm i.d.) (I will find out the detail of the column after I go back to the lab), and a D-Star DWW-10 variable-wavelength UV detector. 49:1 hexanes: EtOAc or 24:1 hexanes:EtOAc mixtures were used as the eluant (1 mL/min).

6.4 Rubbed nylon-coated ITO glass cell fabrication

Cutting the Cells: ITO sheets were provided by Dr. Noel Clark at University of Colorado at Boulder. There are two types of cell patterns on the ITO plates, which are "T's" and "U's" (Scheme 6-1). The cells were cut from the ITO sheet on the opposite side of the ITO layer along the glass/ITO interface so as to have the ITO pattern on the edge.

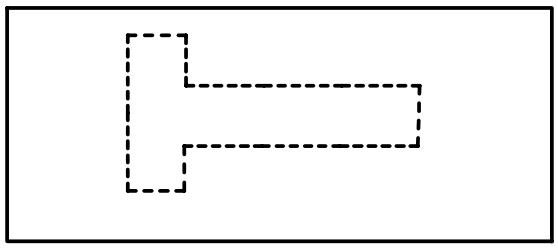

T

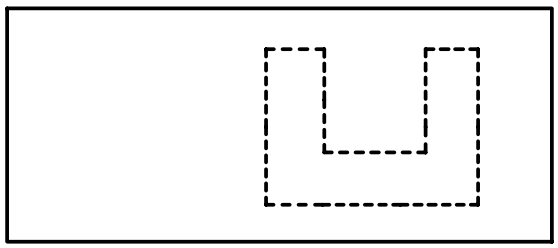

U

Scheme 6-1

Washing: The cell pieces were immersed in a clean beaker filled with a detergent mixture (0.2% Sparkleen in 18 Ω distilled H_2O). The cell pieces were sonicated for 10 minutes, the detergent was removed and the beaker rinsed with 18 Ω distilled water. Fresh distilled water was added and the cells were sonicated for an additional 10 minutes. This was repeated until all soap residues were gone.

Cleaning: 1) On a flat surface in a laminar flow fume hood, a cell plate was taken from the distilled water bath and was placed on a fresh piece of aluminum foil using clean tweezers. 2) The cell plate was dried with N_2 using a syringe as a way to concentrate the gas stream until no water can be seen on the cell plate. 3) A voltmeter was used to determine which side of the cell plate has ITO coating. Once the ITO side had been determined, the cell plate was placed with the ITO side up. 4) A piece of Kodak lens paper was cut in half using clean scissors, and then folded three times horizontally and once vertically (as to have a surface that has not been touched by fingers). 5) A couple of drops of methanol were added onto the lens paper and the cell plate was wiped. This procedure was repeated twice (three times in total, each time use a fresh piece of lens paper). A couple of drops of acetone were added onto a fresh piece of lens paper and the cell was wiped once. After this cleaning, the cell should be free of water, dust and oils. After cleaning, the cell plate was placed in a Petrie dish and covered to protect it from dust. "T's" and "U's" were segregated.

Coating: A solution of a Nylon material (Elvamide 8023) in methanol (1 mg Elvamide in 1 mL methanol) was prepared. A cell plate was placed in a spin coater, 3 drops of the solution was placed on the center of the glass, and the cell was spun for 30 seconds. After spin coating, the cell plate should be transparent, with no localized thickly coated areas.

Alignment: The cell plate was placed on a brushing apparatus. The "T's" were placed upside down and the "U's" thick side down. The brush was brushed towards the bracing plate and rotated for 170 times to get good alignment.

Assembly: A small amount of epoxy (1 : 0.83 weight of base: weight of hardener) was placed on a fresh piece of foil and a small amount of silica beads was stirred in. Using a capillary (360 μm in diameter), the glue was dotted in very small droplets along the sides of the "T" plate, with two dots on each side of the plate (not on the ITO pattern). Then, the "U" plate was placed on top of the "T" plate such that the ITO pattern is accessible on both sides (so the plates should be offset by a few mm). This should be done in one fluid motion as to not rub the plates against each other because it will ruin the alignment. The plates were clamped together, and the glue allowed to cure overnight at room temperature then in the oven (110^{o}C) for another night. Cell thicknesses were determined by the capacitance of an empty cell using a Displaytech APT-III polarization testbed (Displaytech Inc., Longmont, CO).

6.5 References

(1) Vlahakis, Z. J.; Maly, E. K.; Lemieux, P. R.; *J. Mater. Chem.* **2001**, 11, 2459.

(2) McCubbin, A. J.; Tong, X.; Zhao, Y.; Snieckus, V.; Lemieux, P. R.; *Chem. Mater.* **2005**, 17, 2574.

(3) Aoki, Y.; Nohira, H.; *Chem. Lett.* **1993**, 1, 113.

(4) Sahlen, F.; Trollsas, M.; Hult A.; Gedde, W. U.; *Chem. Mater.* **1996**, 8, 382.

(5) Schnurpfeil, G.; Harder, A.; Schroder, H.; Wohrle, D.; Hartwig, A.; Hennemann, O.; *Macromol. Chem. Phys.* **2001**, 202, 180.

(6) Lecommandoux, S.; Noirez, L.; Mauzac, M.; Hardouin, F.; *Journal de Physique II* **1994**, 4, 2249.

(7) Kawai, H. S.; Gilat, L. S.; Ponsinet, R.; Lehn, M. J.; *Chem. Eur. J.* **1995**, 1, 285.

(8) Thomas, J. C.; Wolak, A. M.; Birge, R. R.; Lees, J. W.; *J. Org. Chem.* **2001**, 66, 1914.

(9) Luo, Q.; Sheng, S.; Cheng, S.; Tian, H.; *Australian Journal of Chemistry* **2005**, 58, 321.

(10) Kobatake, S.; Kuma, S.; Irie, M.; *J. Phys. Org. Chem.* **2007**, 20, 960.

(11) Kato, N.; Miyaura, N.; *Tetrahedron* **1996**, 52, 13347.

(12) Choshi, T.; Yamada, S.; Sugino, E.; Kuwada, T.; Hibino, S.; *J. Org. Chem.* **1995**, 60, 5899.

Appendix 1. ^{1}H NMR spectra of key compounds

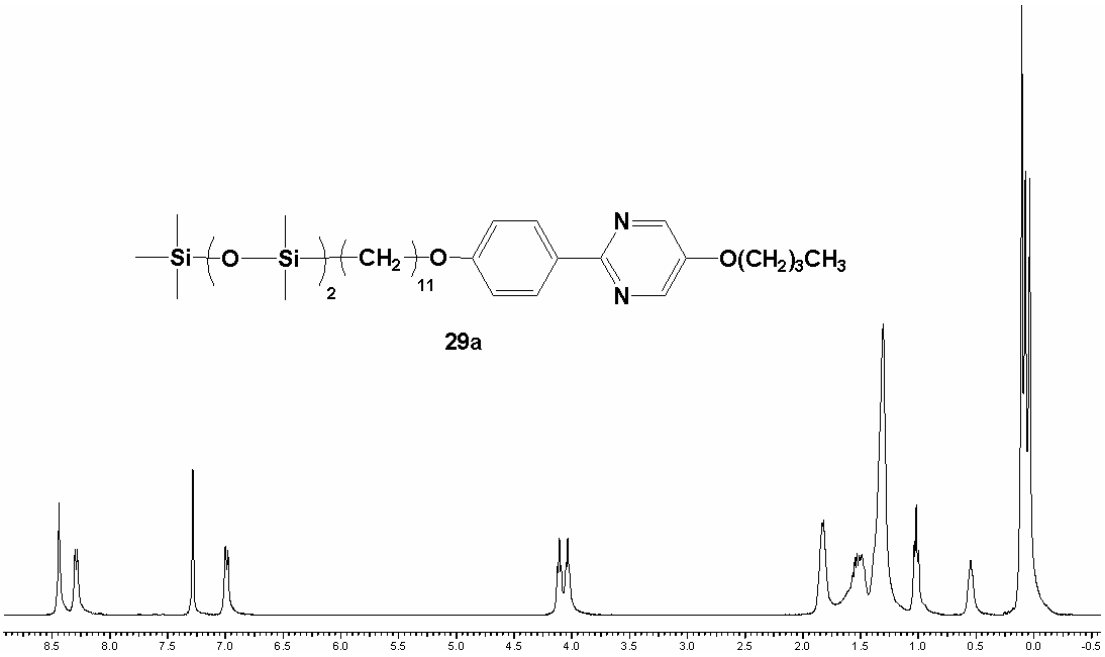

Figure A1-1. 400MHz ^{1}HNMR spectrum of **29a**.

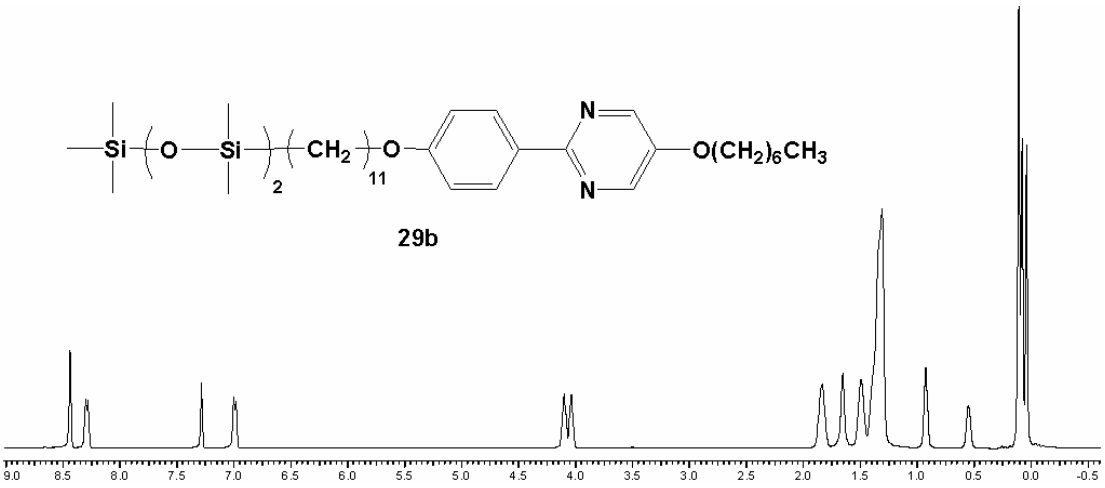

Figure A1-2. 400MHz ^{1}HNMR spectrum of **29b**.

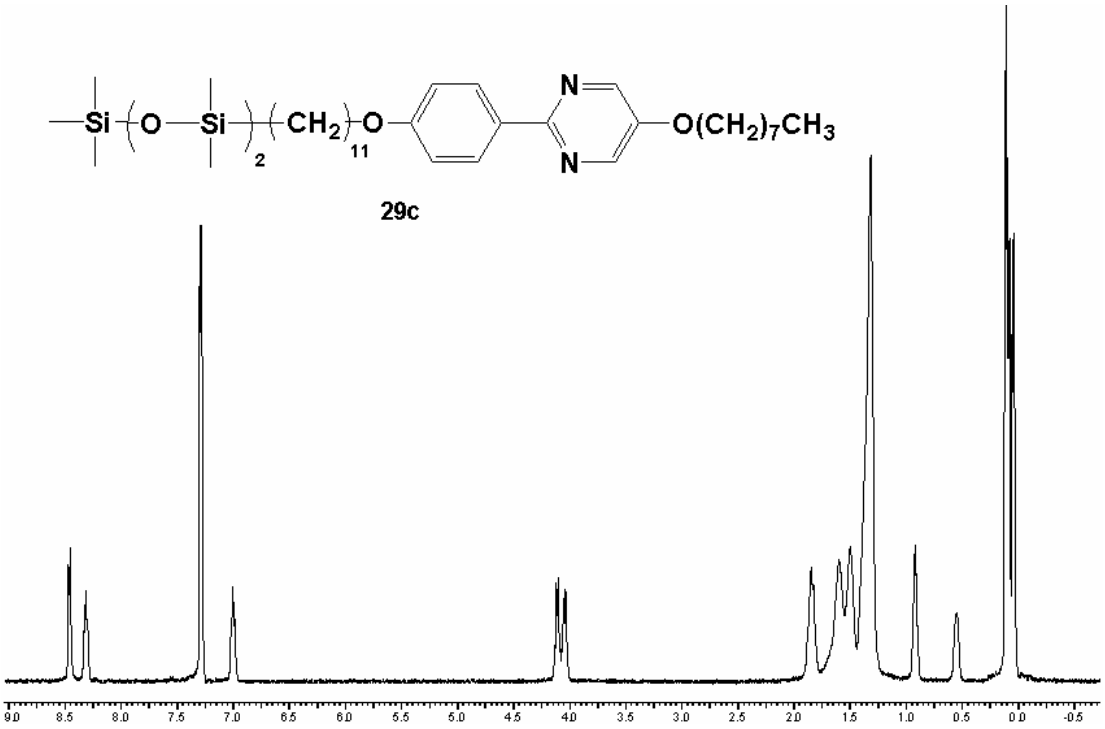

Figure A1-3. 400MHz ^{1}HNMR spectrum of **29c**.

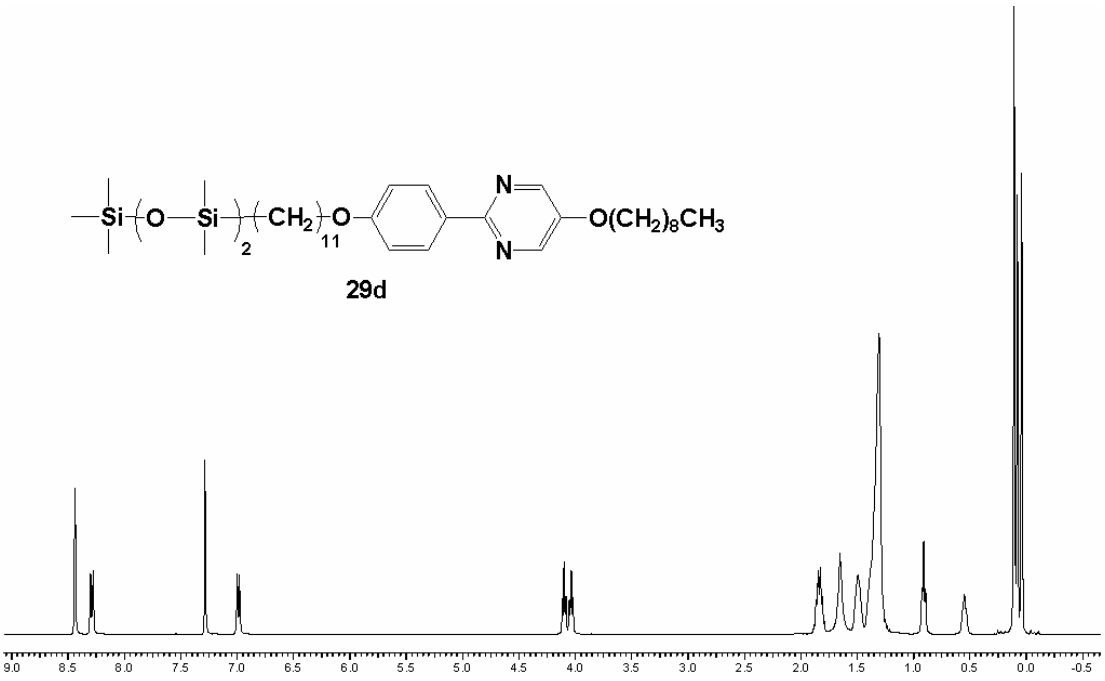

Figure A1-4. 400MHz ^{1}HNMR spectrum of **29d**.

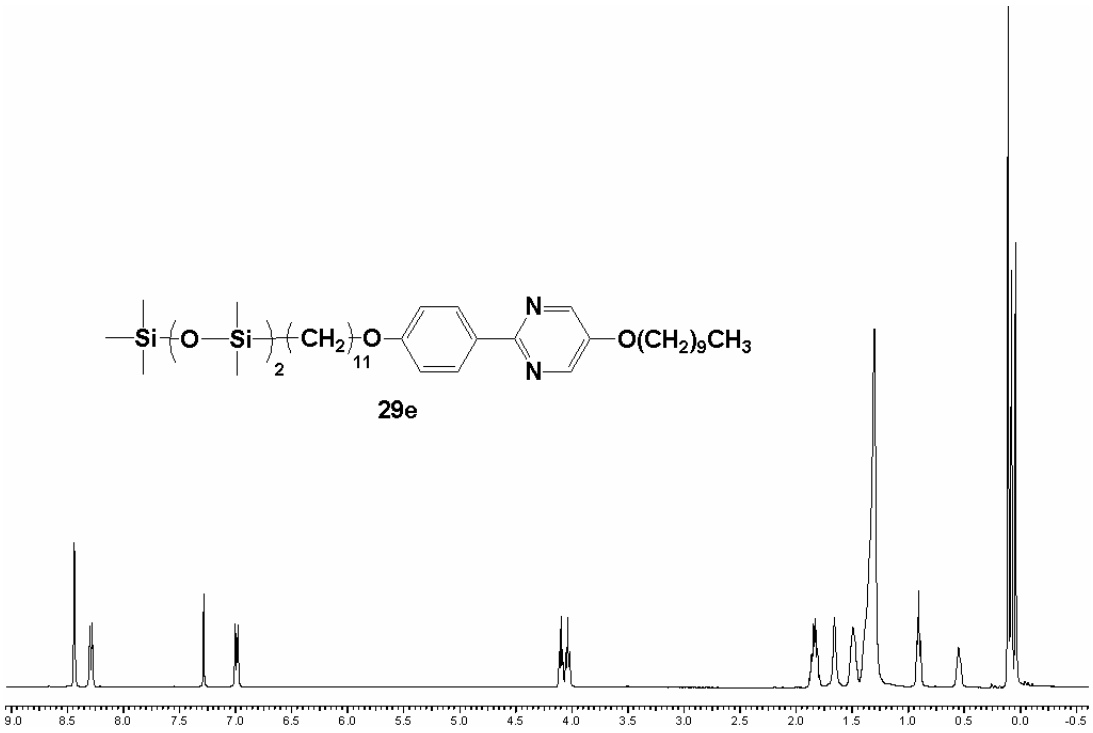

Figure A1-5. 400MHz ^{1}HNMR spectrum of **29e**.

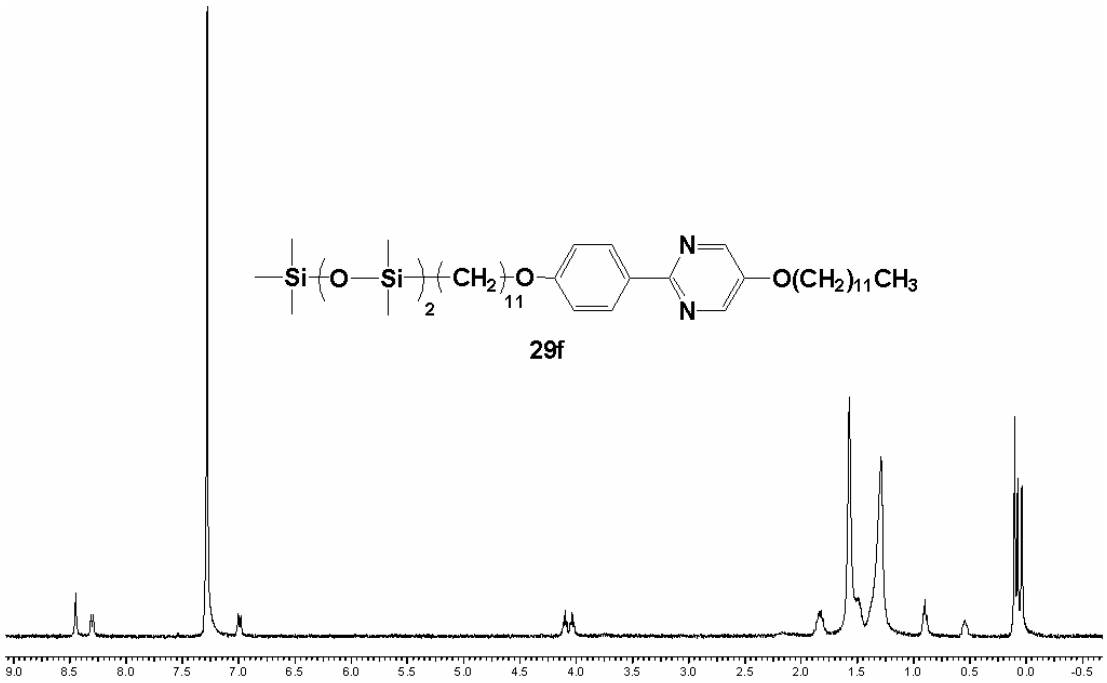

Figure A1-6. 400MHz ^{1}HNMR spectrum of **29f**.

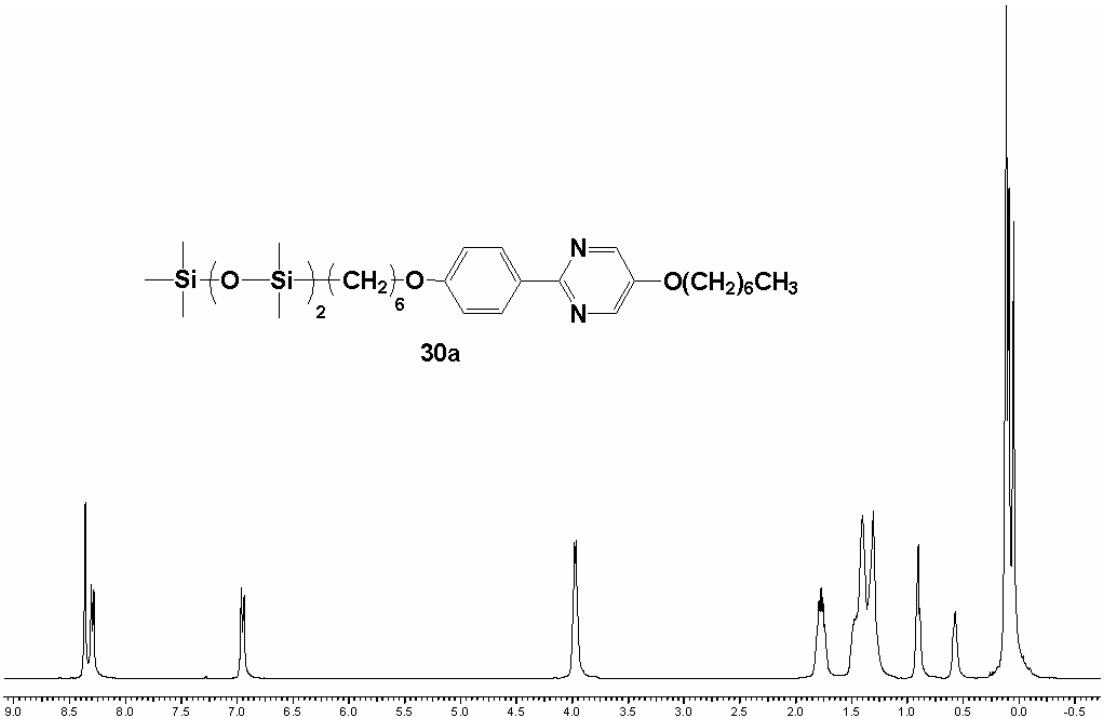

Figure A1-7. 400MHz ^{1}HNMR spectrum of **30a**.

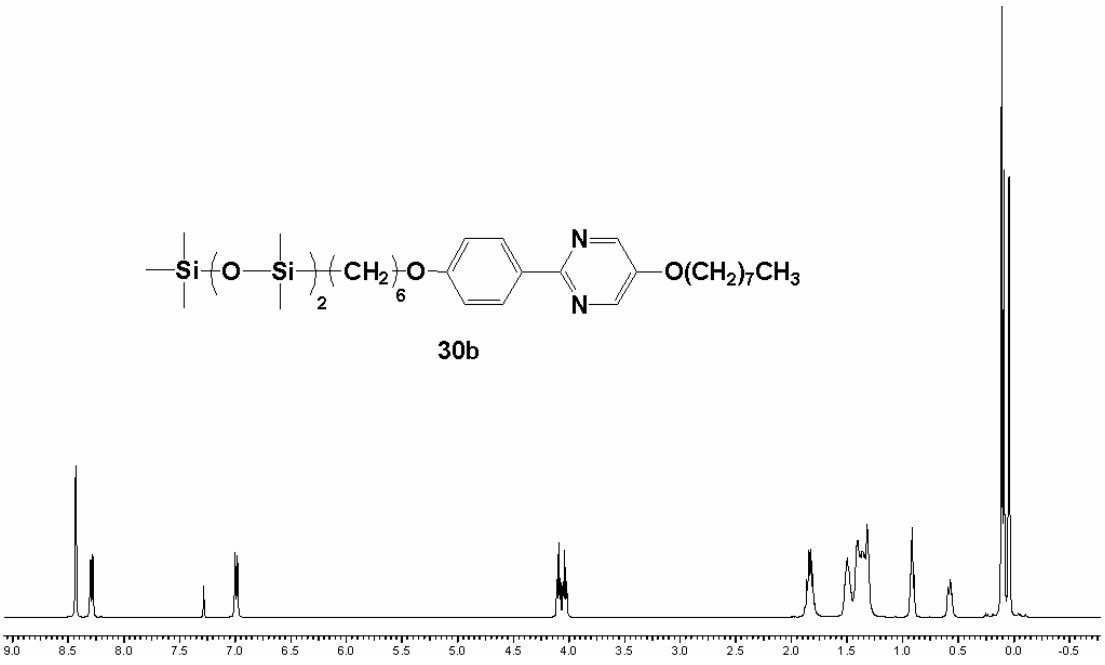

Figure A1-8. 400MHz ^{1}HNMR spectrum of **30b**.

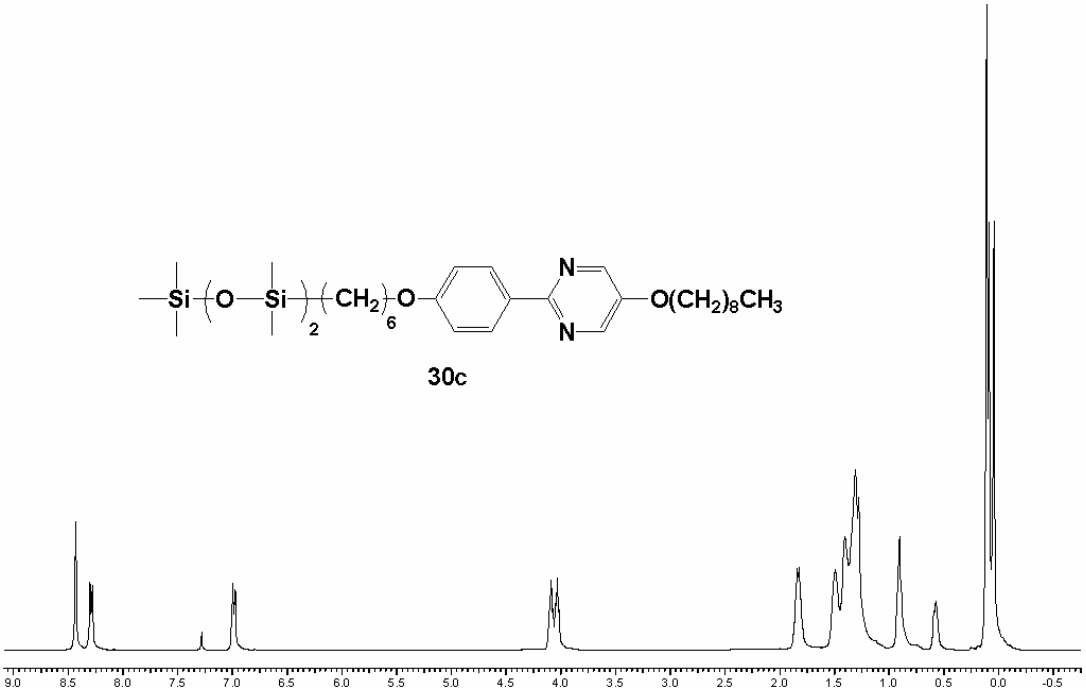

Figure A1-9. 400MHz ^{1}HNMR spectrum of **30c**.

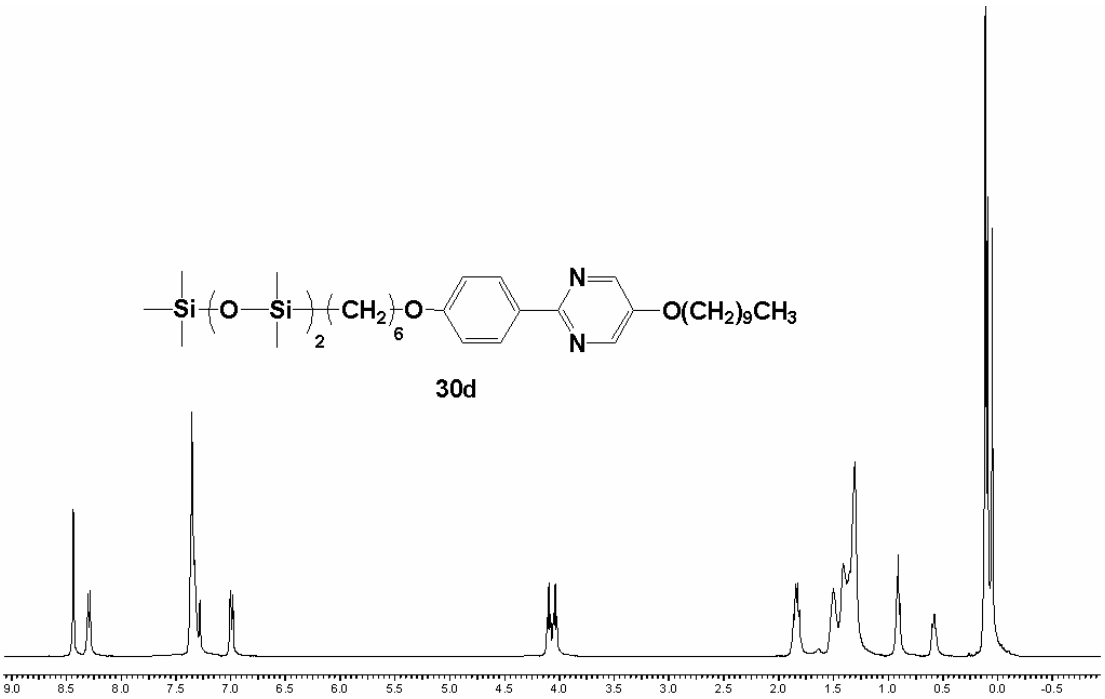

Figure A1-10. 400MHz ^{1}HNMR spectrum of **30d**.

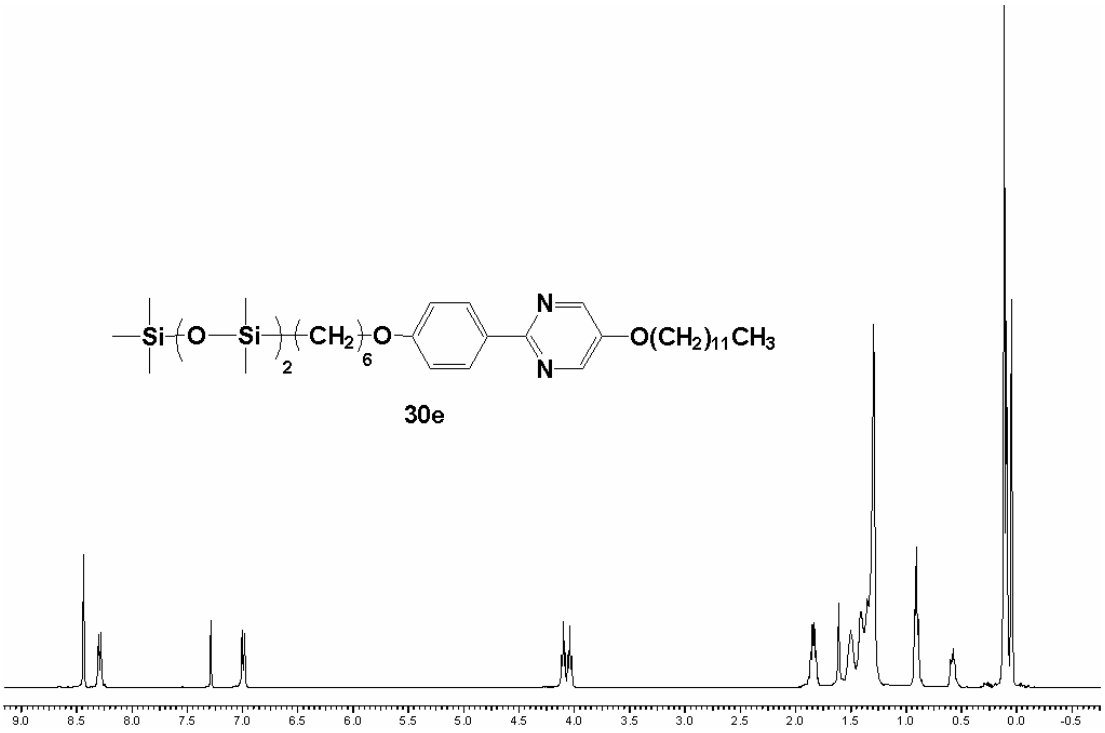

Figure A1-11. 400MHz ^{1}HNMR spectrum of **30e**.

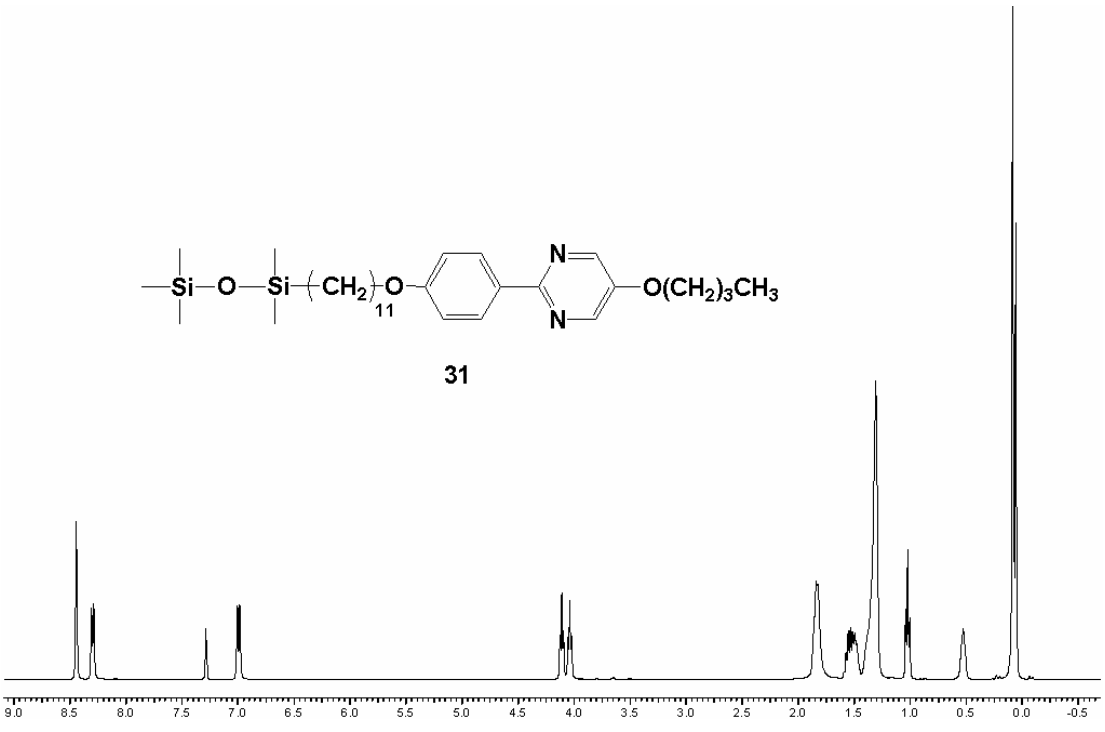

Figure A1-12. 400MHz ^{1}HNMR spectrum of **31**.

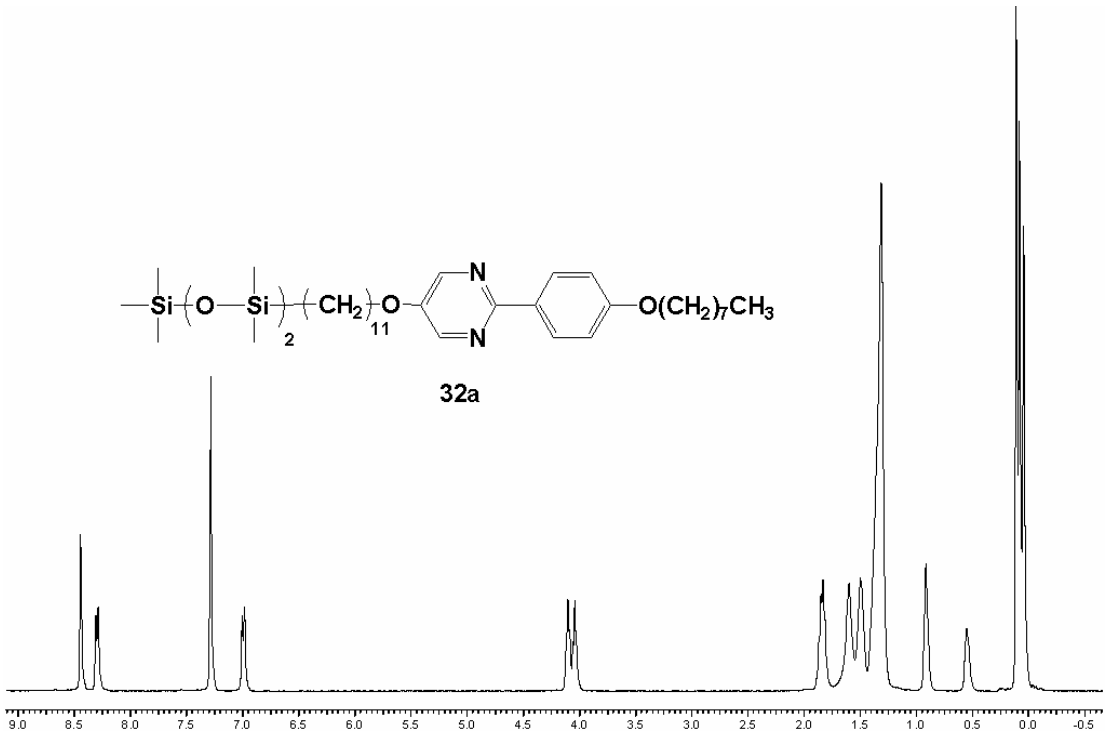

Figure A1-13. 400MHz ^{1}HNMR spectrum of **32a**.

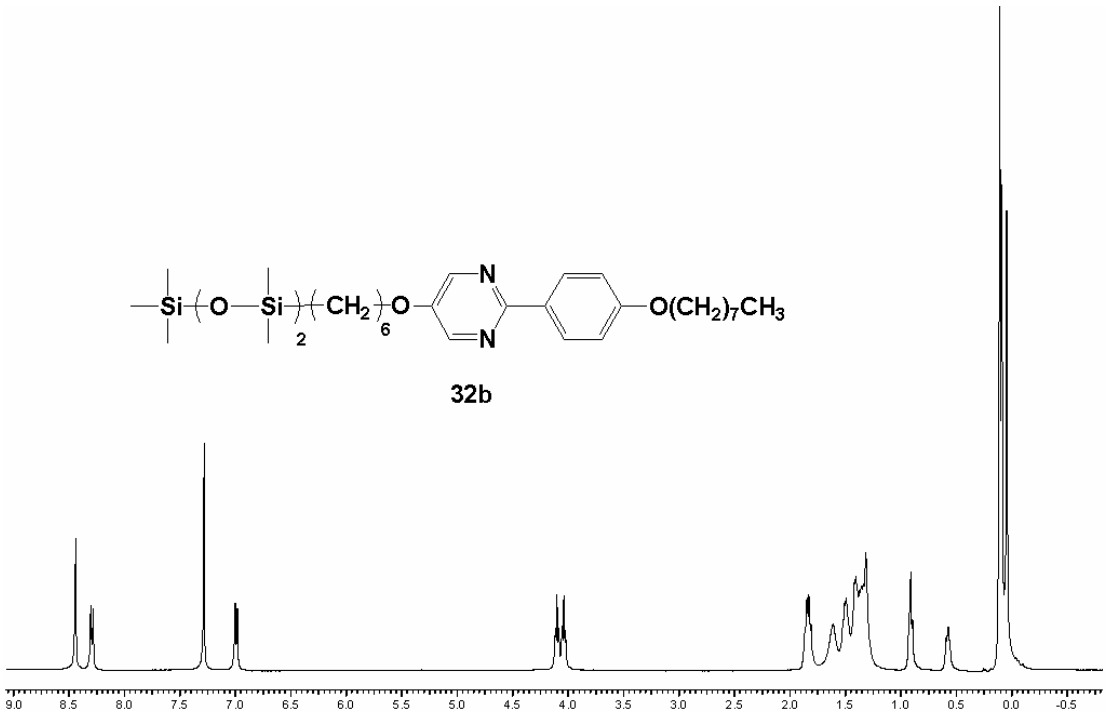

Figure A1-14. 400MHz ^{1}HNMR spectrum of **32b**.

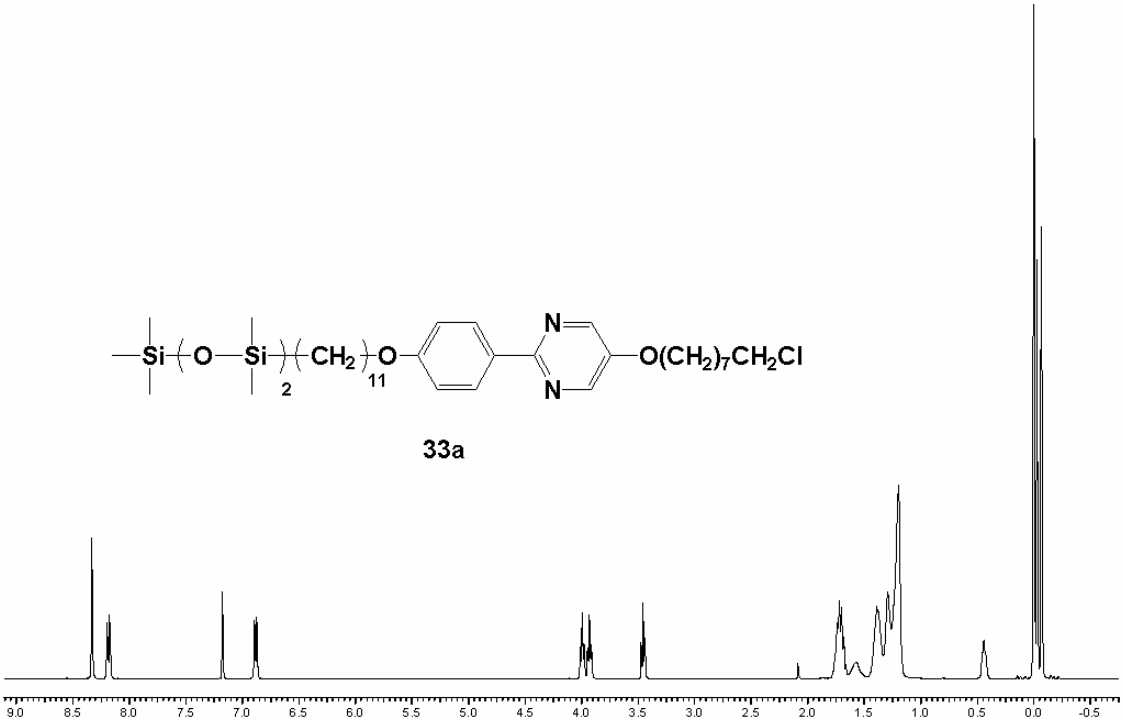

Figure A1-15. 400MHz ^{1}HNMR spectrum of **33a**.

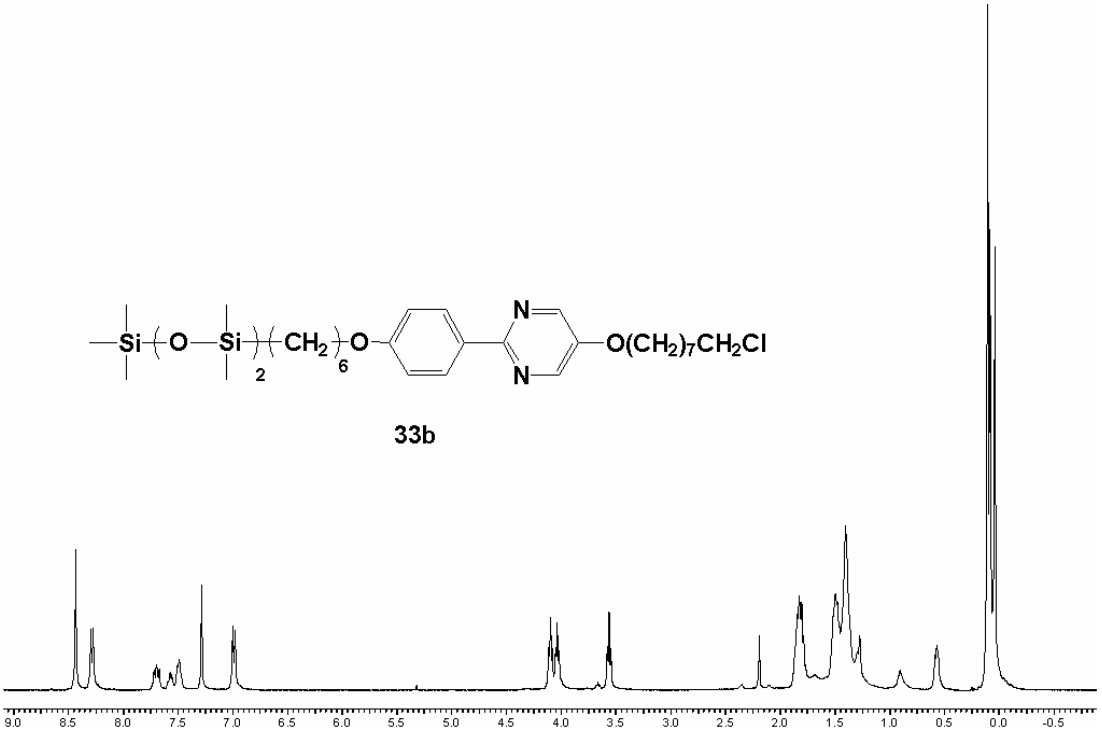

Figure A1-16. 400MHz ^{1}HNMR spectrum of **33b**.

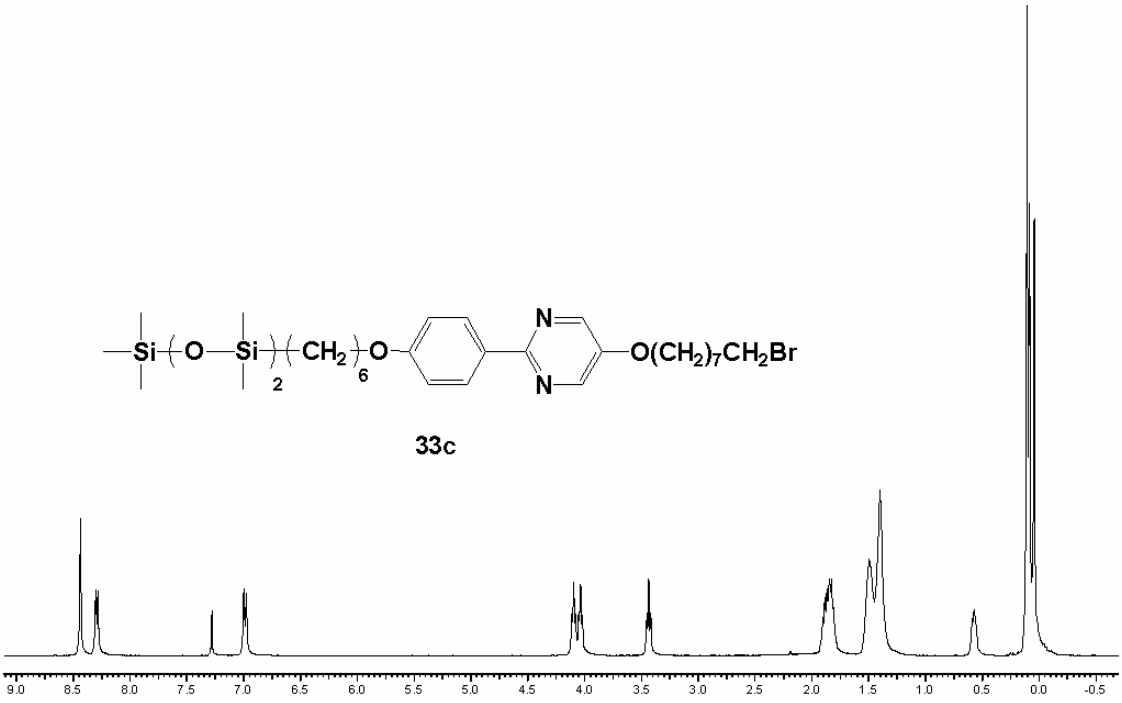

Figure A1-17. 400MHz ^{1}HNMR spectrum of **33c**.

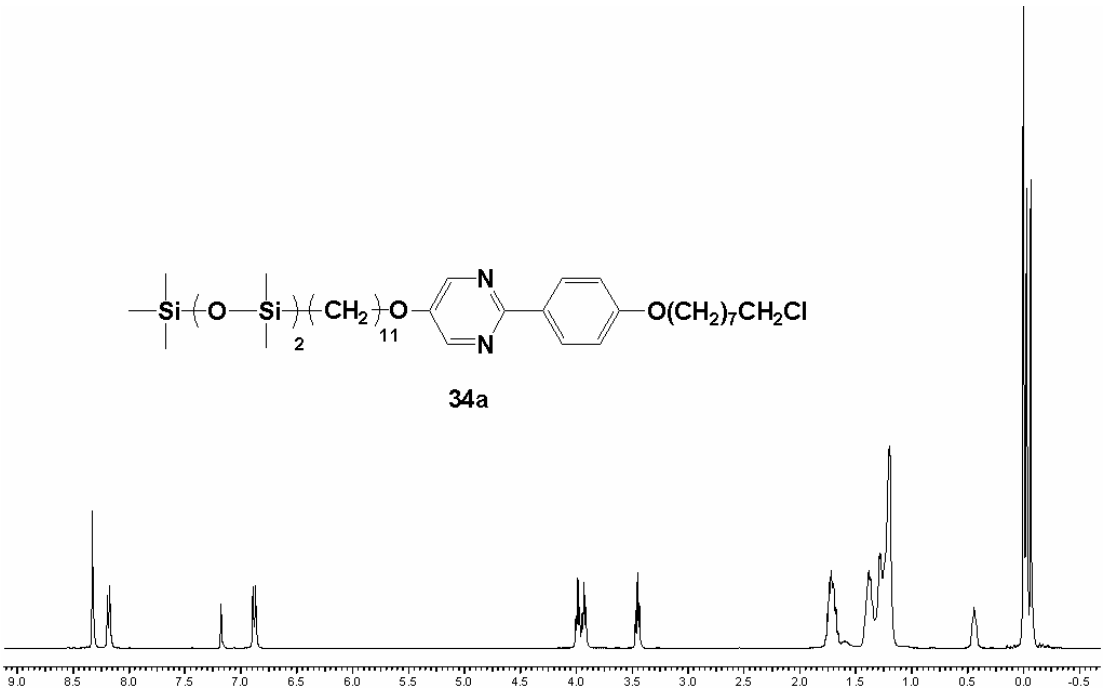

Figure A1-18. 400MHz ^{1}HNMR spectrum of **34a**.

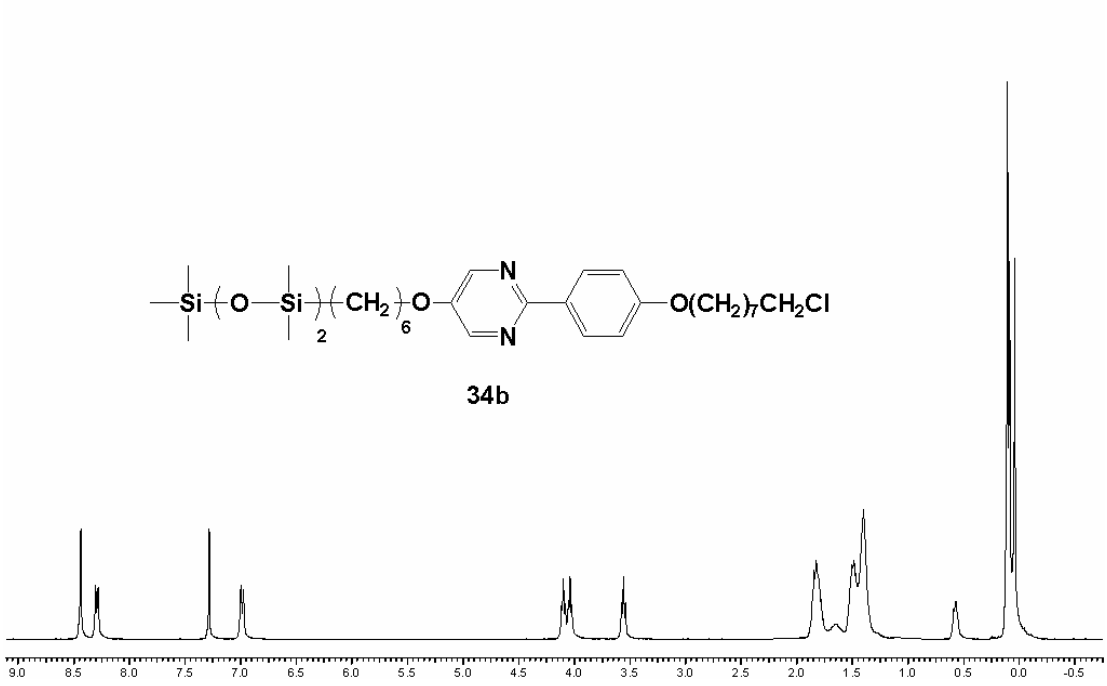

Figure A1-19. 400MHz ^{1}HNMR spectrum of **34b**.

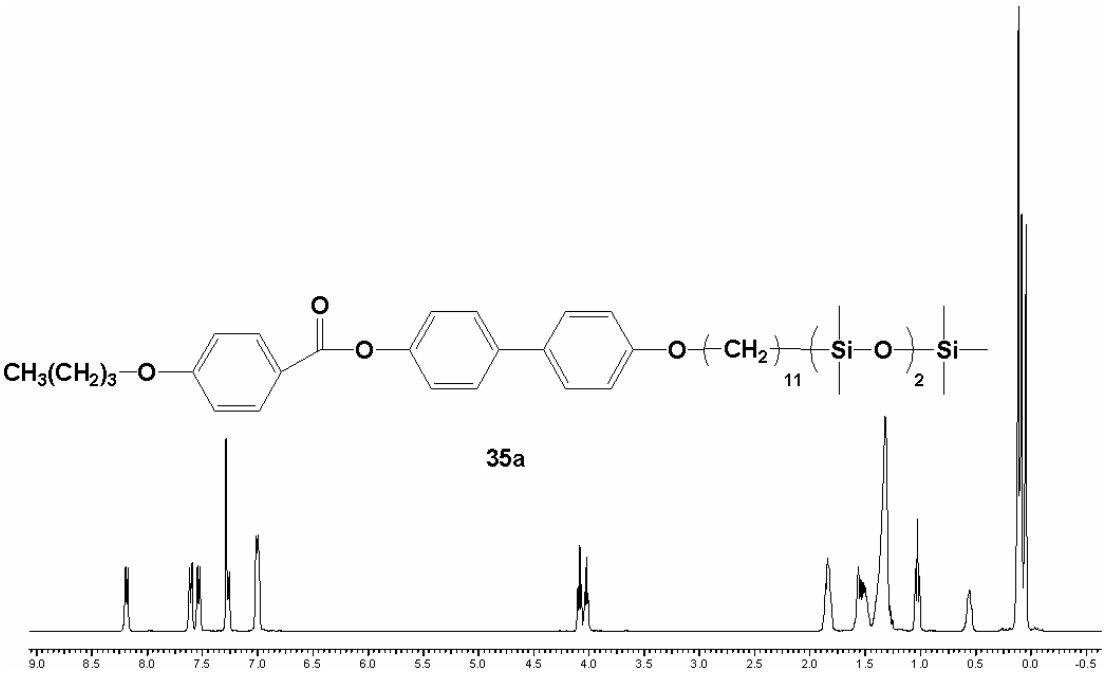

Figure A1-20. 400MHz ^{1}HNMR spectrum of **35a**.

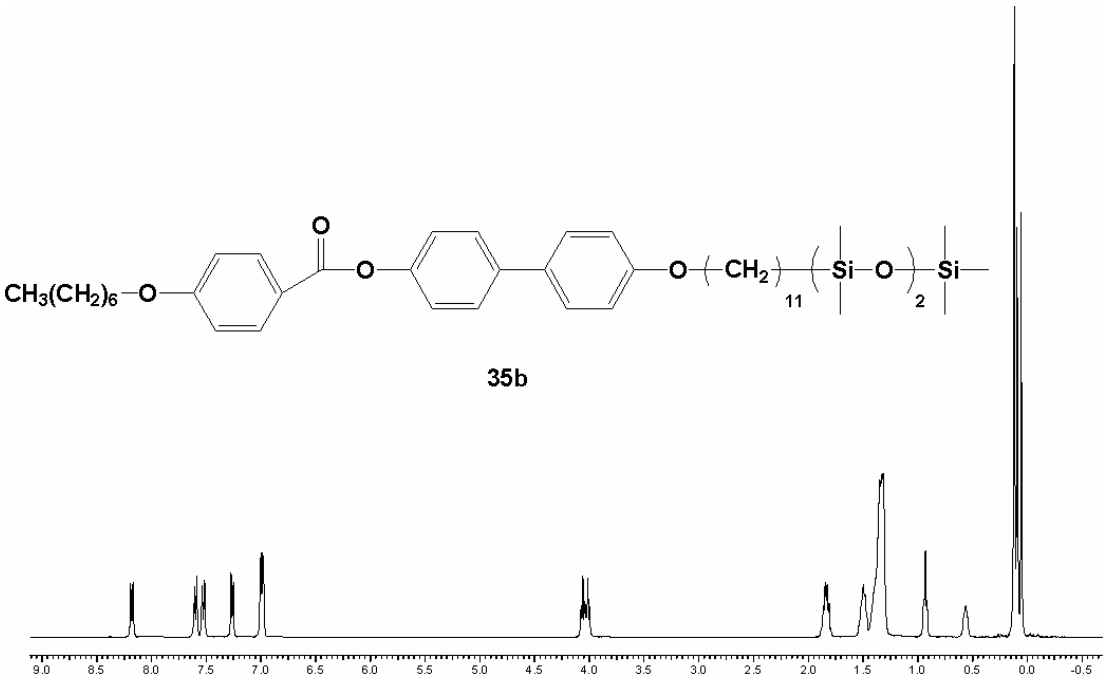

Figure A1-21. 400MHz ^{1}HNMR spectrum of **35b**.

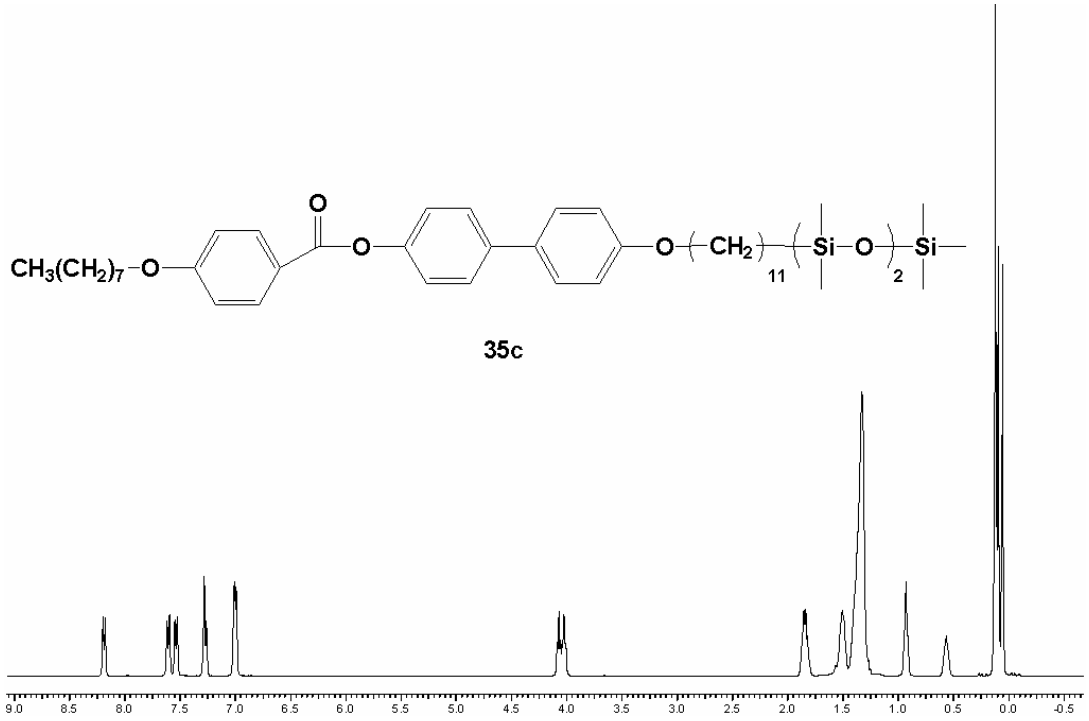

Figure A1-22. 400MHz ^{1}HNMR spectrum of **35c**.

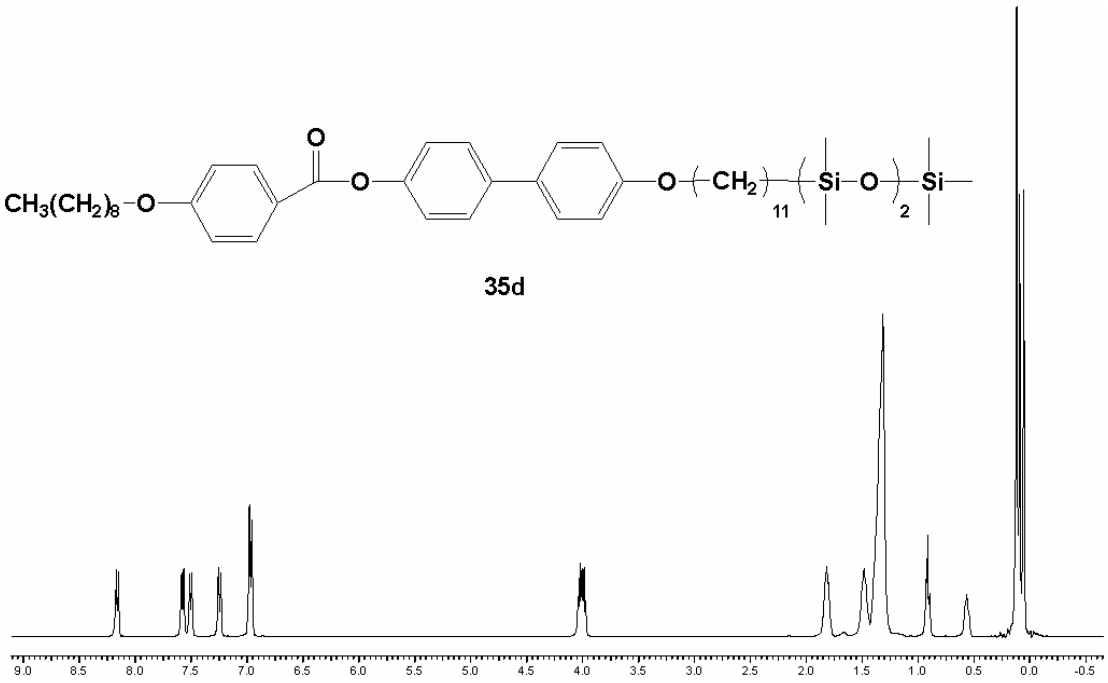

Figure A1-23. 400MHz ^{1}HNMR spectrum of **35d**.

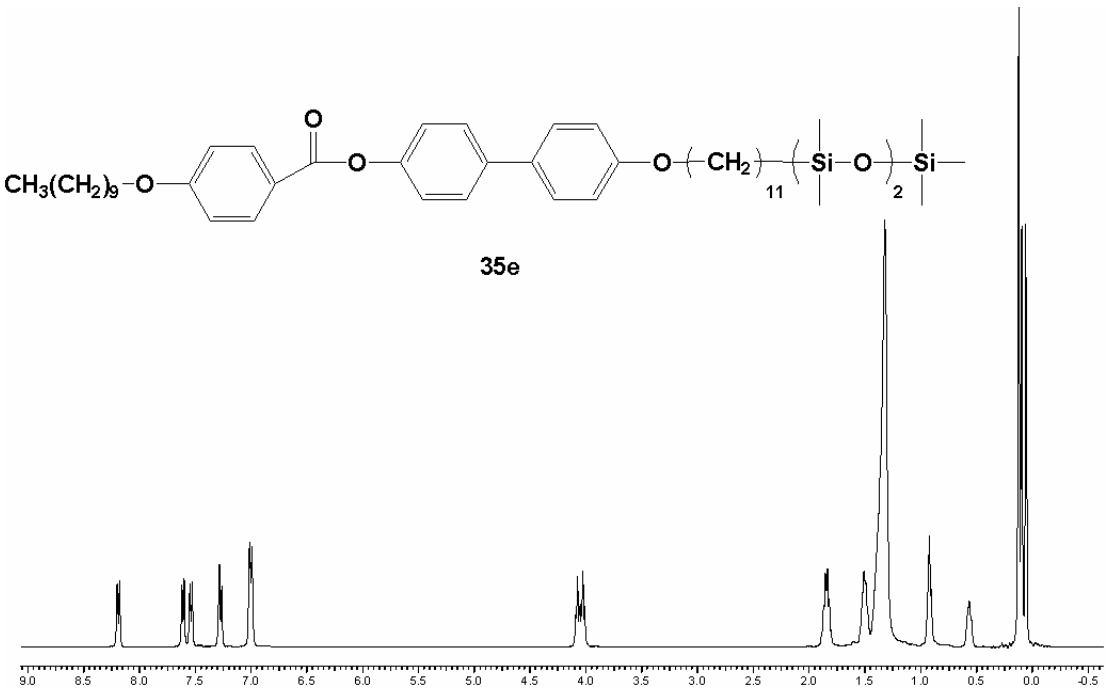

Figure A1-24. 400MHz ^{1}HNMR spectrum of **35e**.

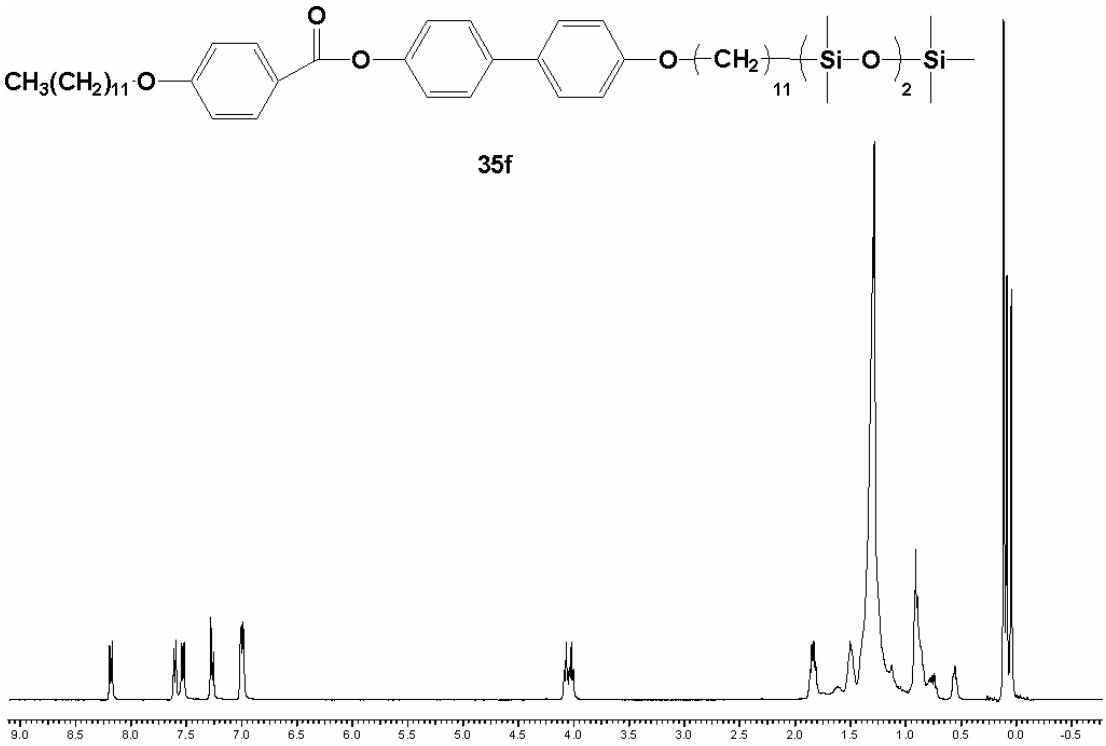

Figure A1-25. 400MHz ^{1}HNMR spectrum of **35f**.

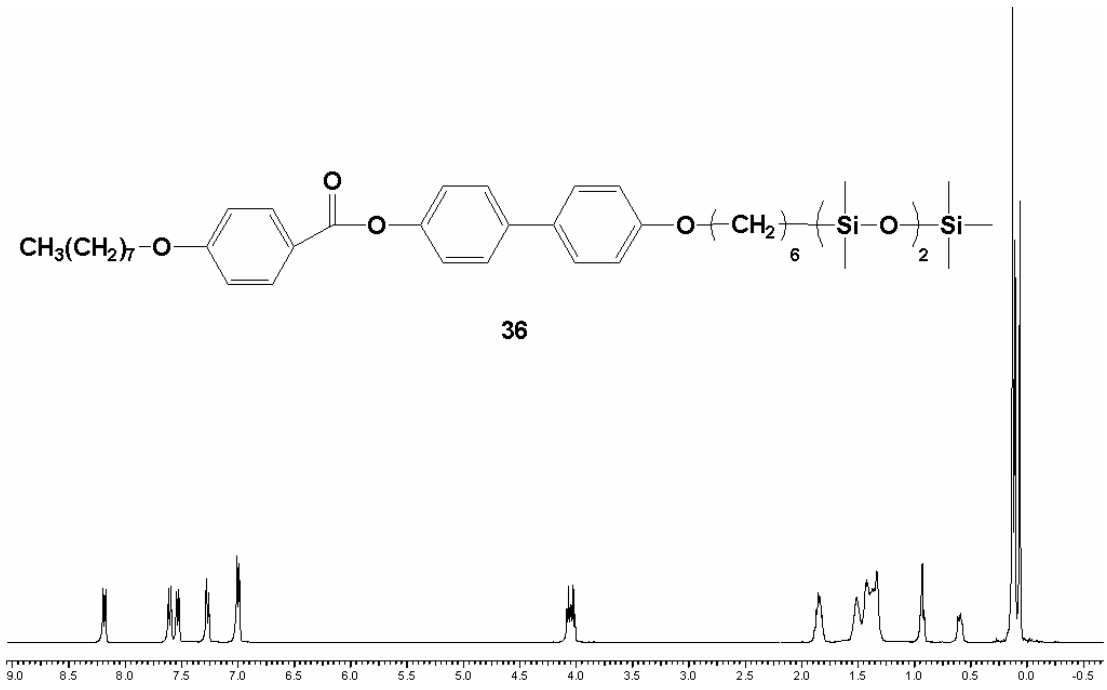

Figure A1-26. 400MHz ^{1}HNMR spectrum of **36**.

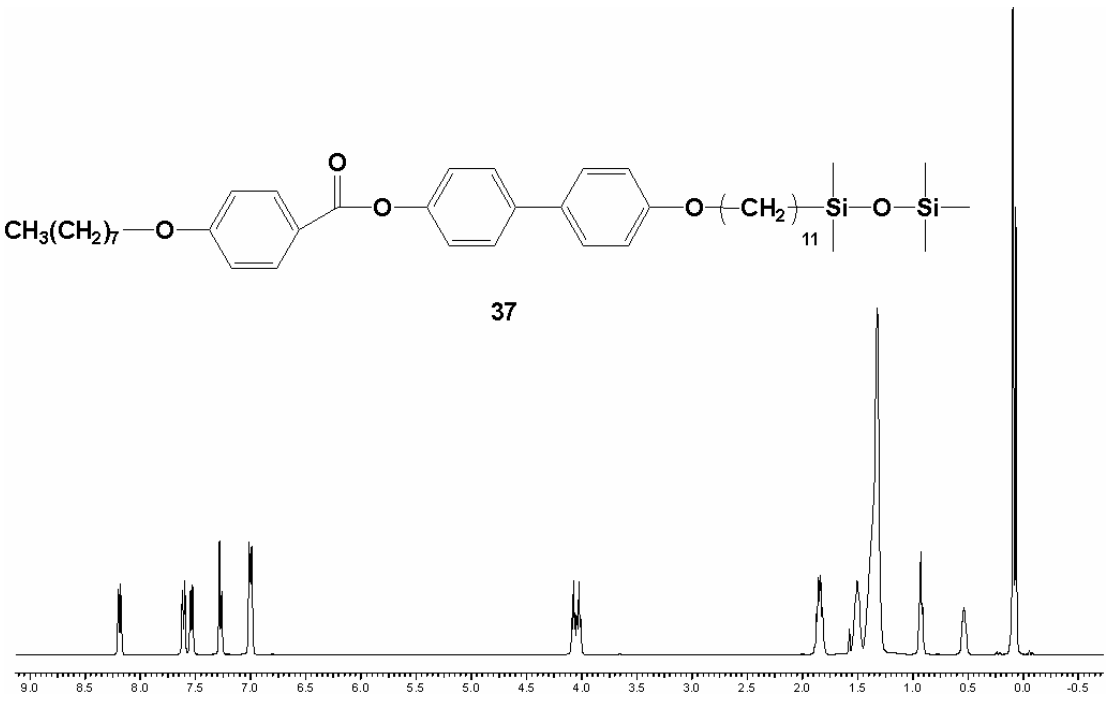

Figure A1-27. 400MHz ^{1}HNMR spectrum of **37**.

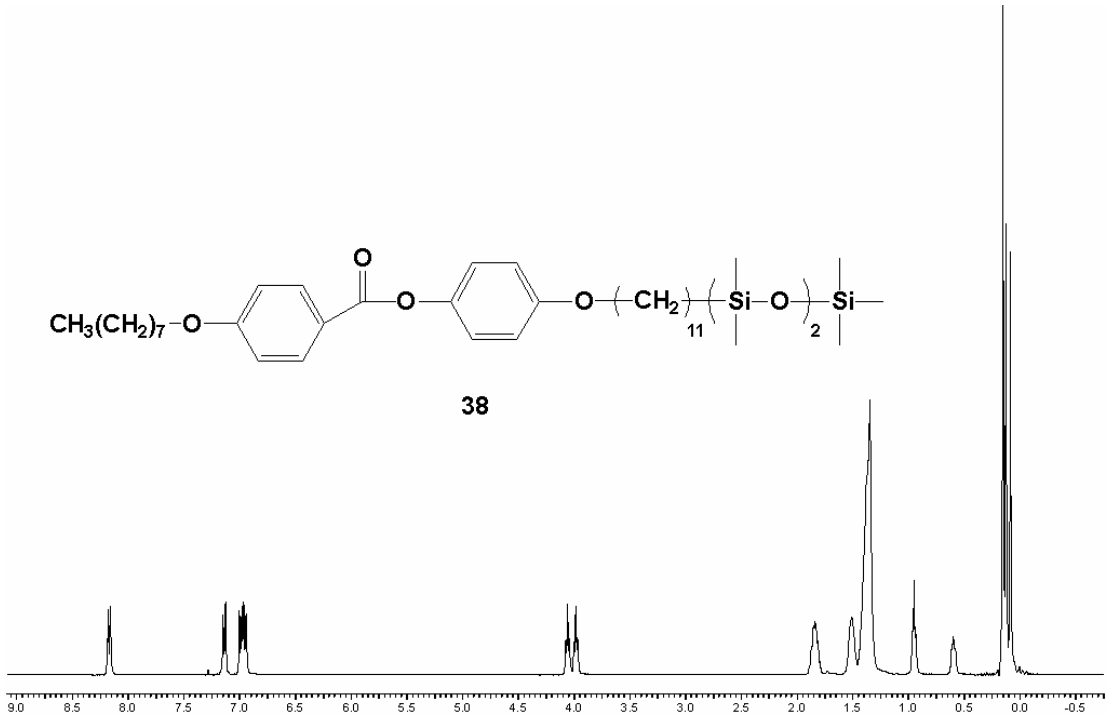

Figure A1-28. 400MHz ^{1}HNMR spectrum of **38**.

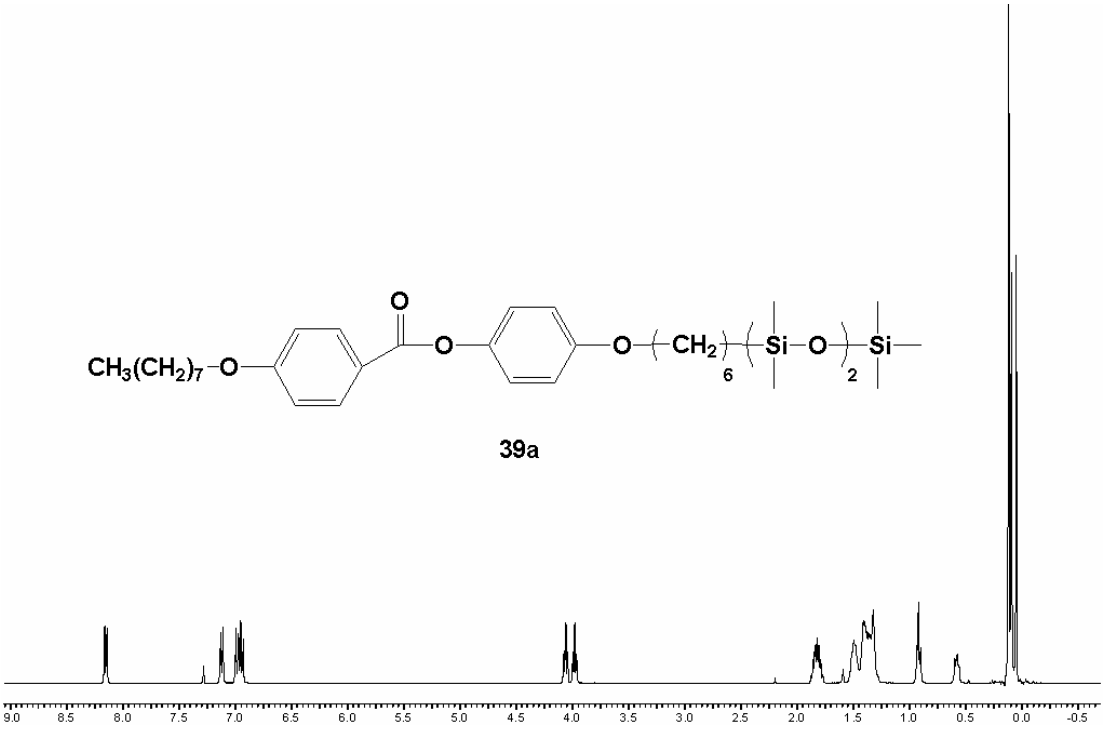

Figure A1-29. 400MHz ^{1}HNMR spectrum of **39a**.

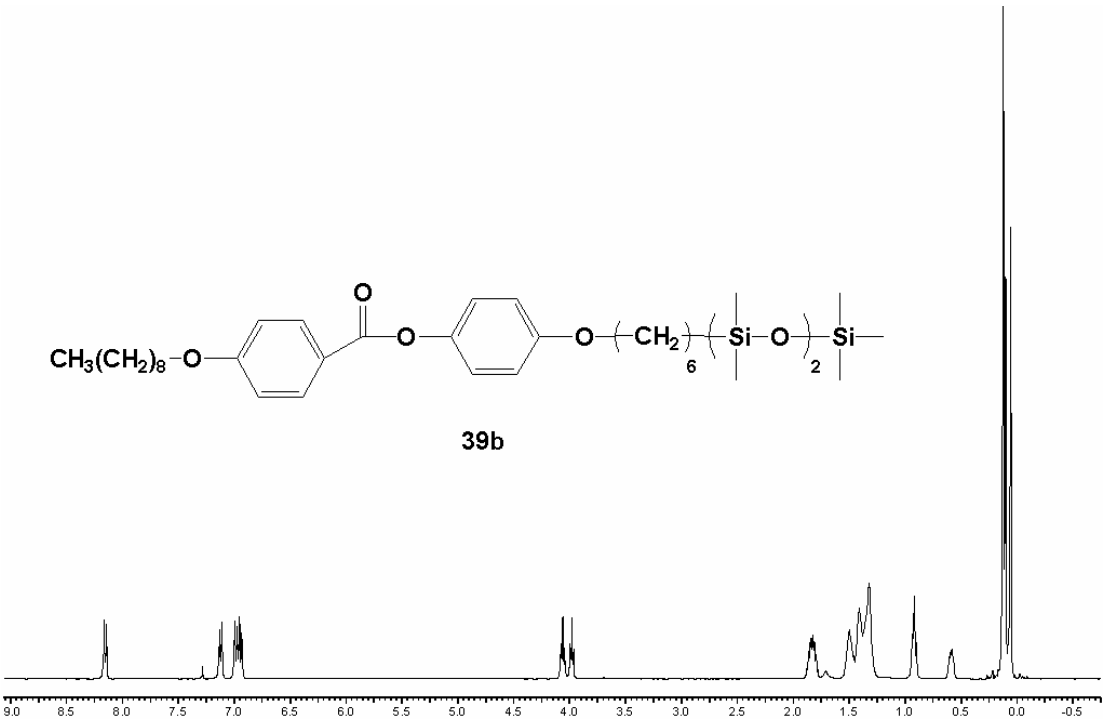

Figure A1-30. 400MHz ^{1}HNMR spectrum of **39b**.

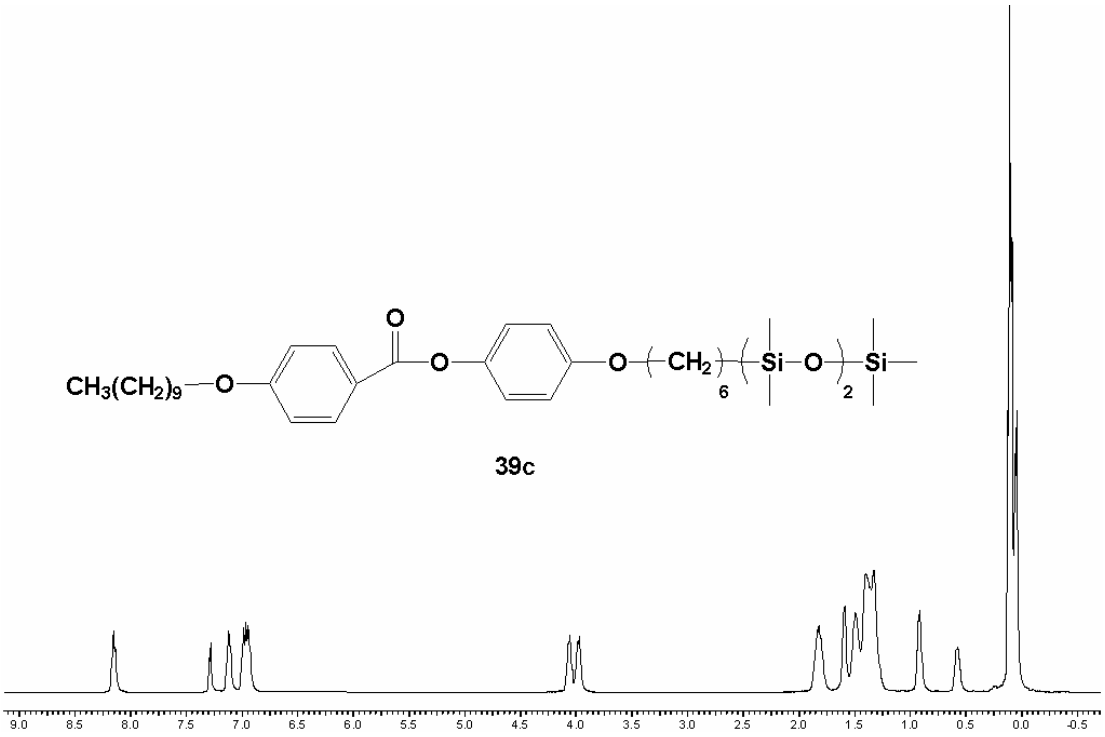

Figure A1-31. 400MHz ^{1}HNMR spectrum of **39c**.

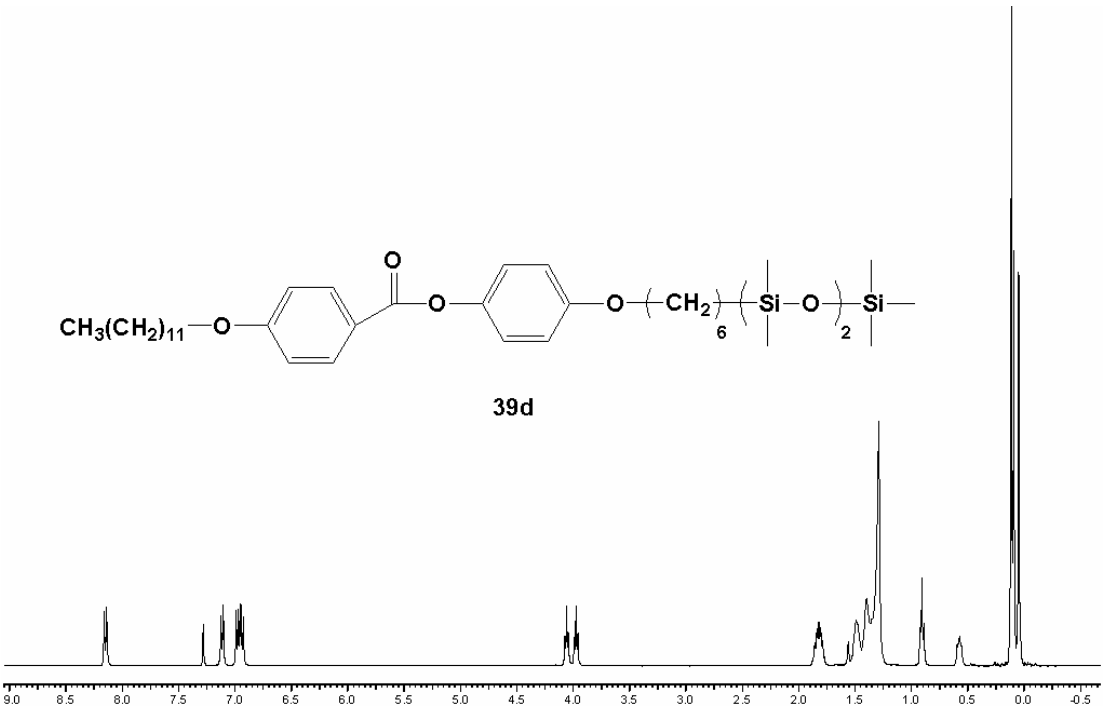

Figure A1-32. 400MHz ^{1}HNMR spectrum of **39d**.

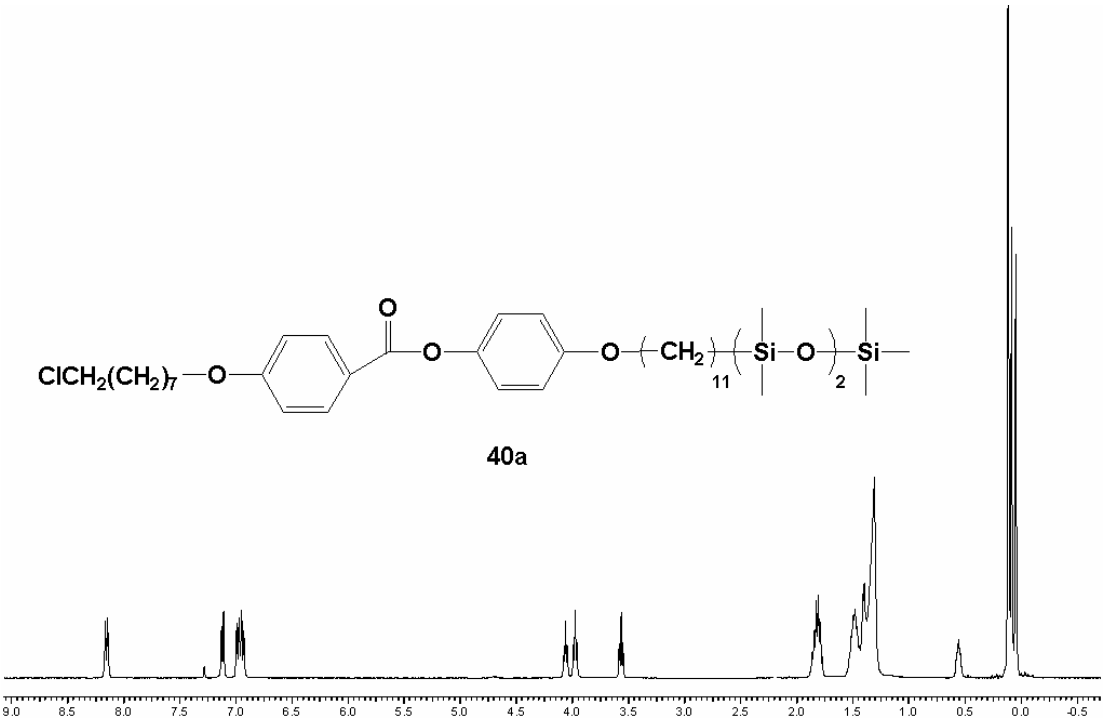

Figure A1-33. 400MHz ^{1}HNMR spectrum of **40a**.

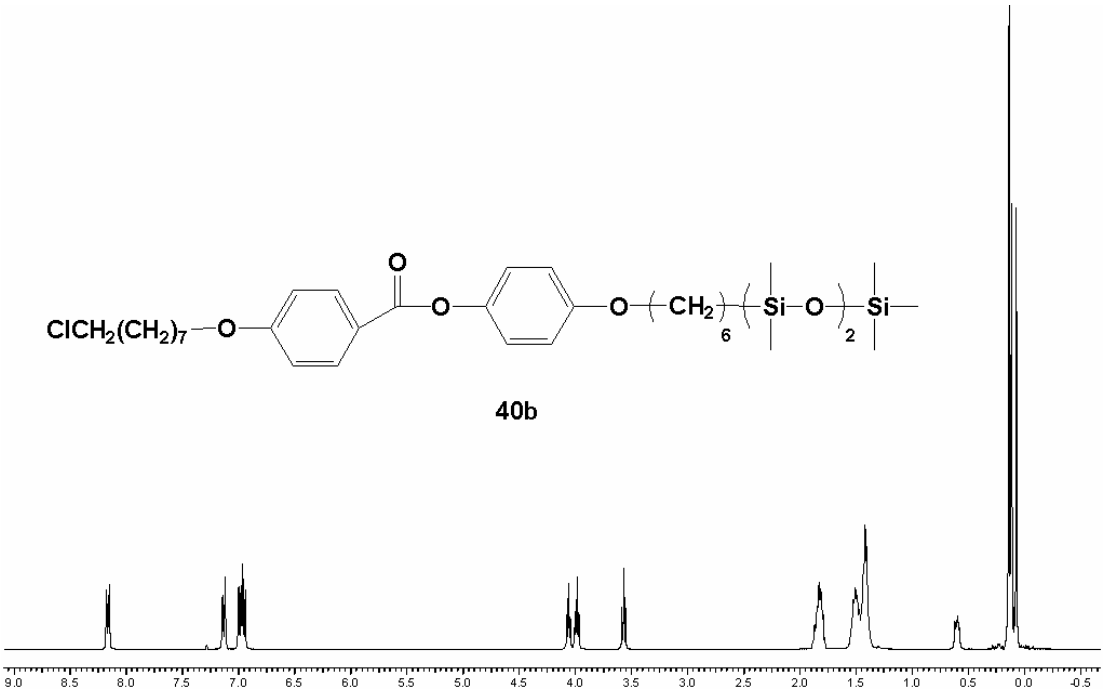

Figure A1-34. 400MHz ^{1}HNMR spectrum of **40b**.

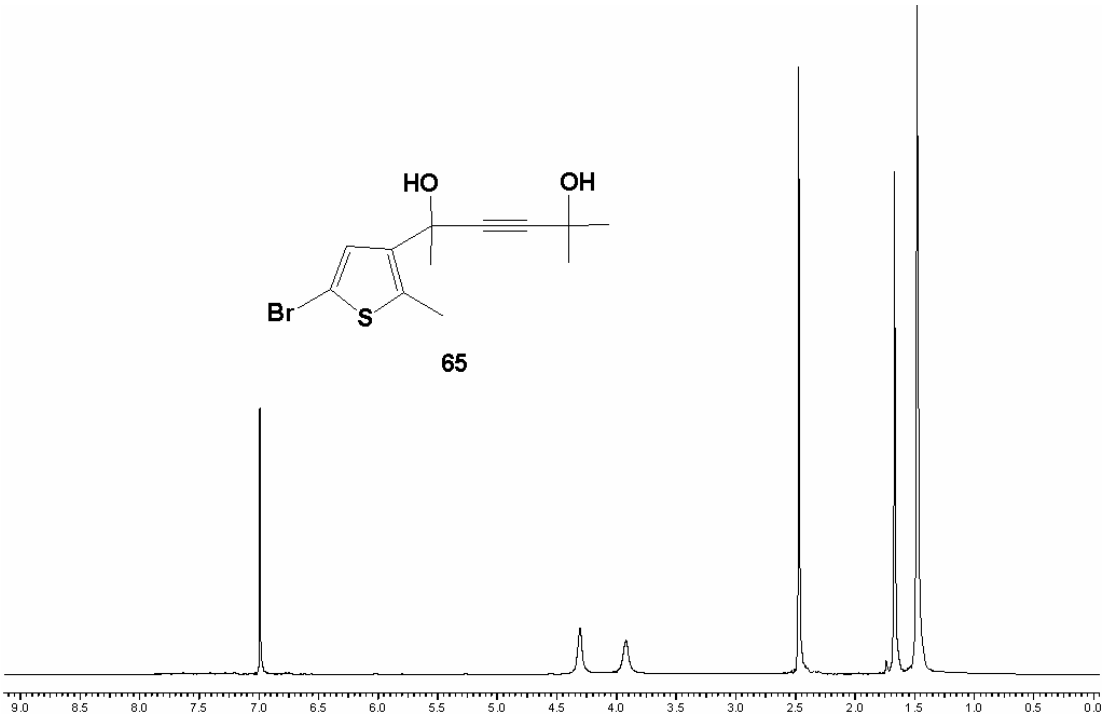

Figure A1-35. 400MHz ^{1}HNMR spectrum of **65**.

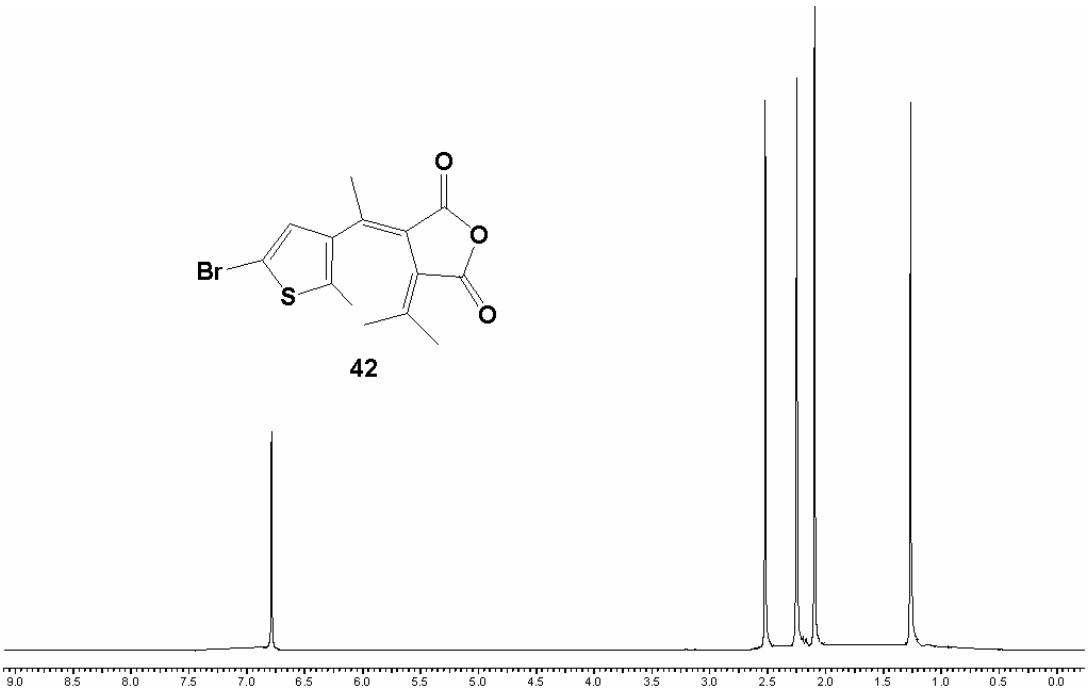

Figure A1-36. 400MHz ^{1}HNMR spectrum of **42**.

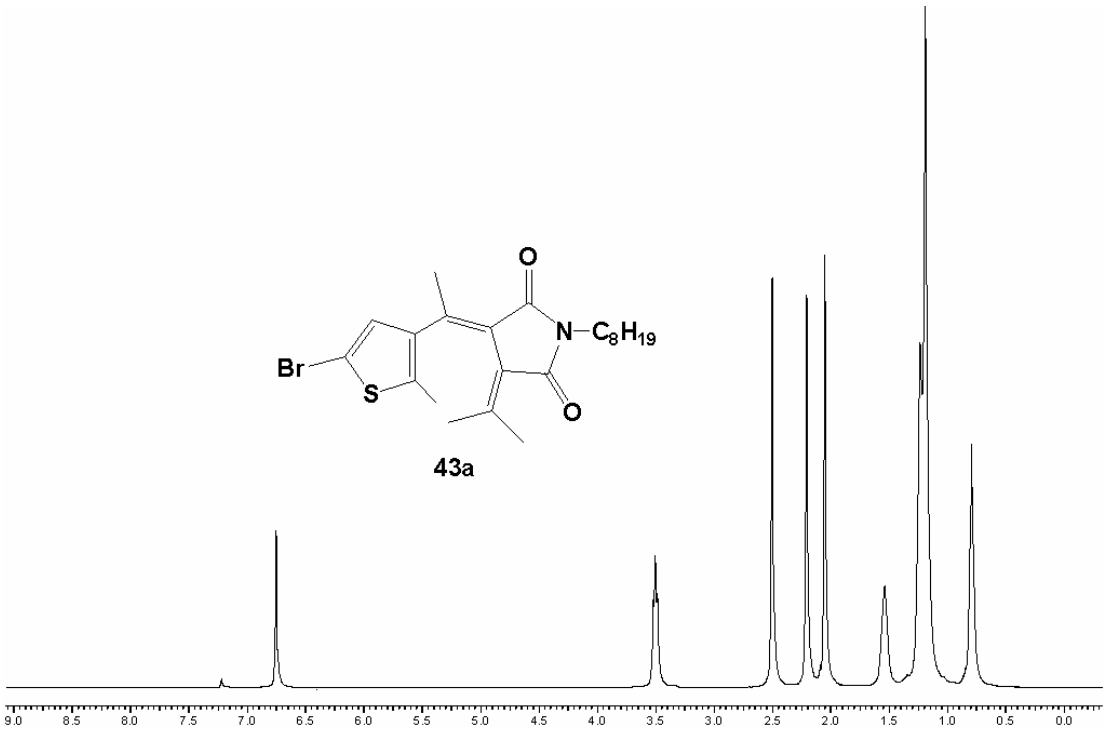

Figure A1-37. 400MHz ^{1}HNMR spectrum of **43a**.

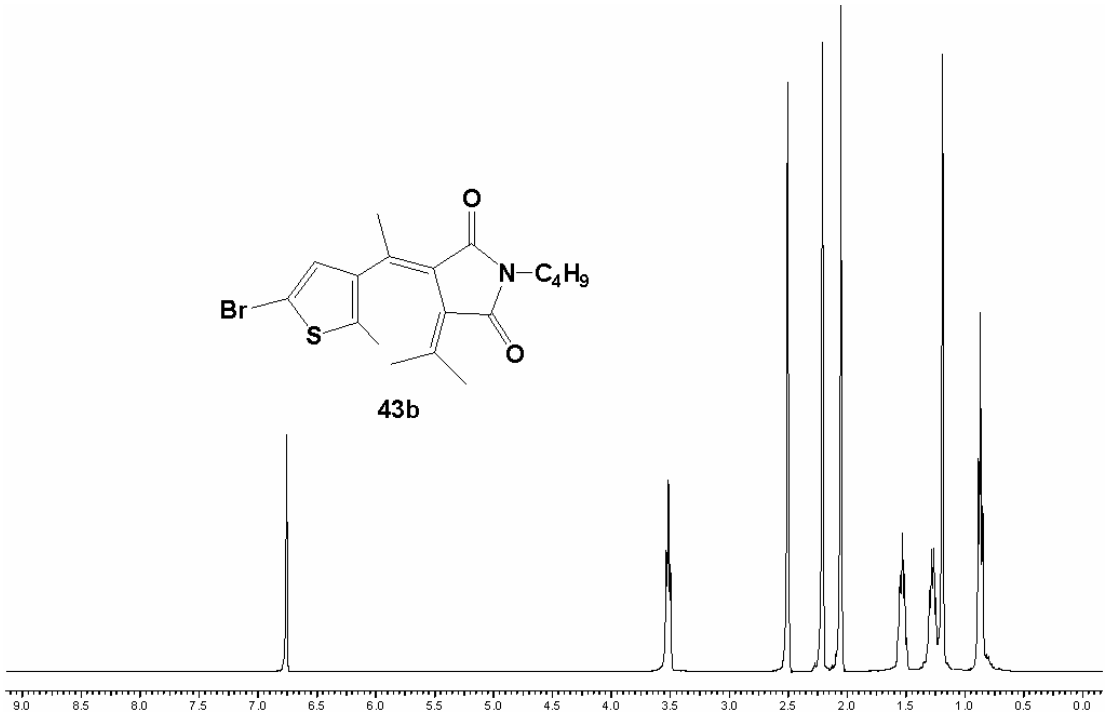

Figure A1-38. 400MHz ^{1}HNMR spectrum of **43b**.

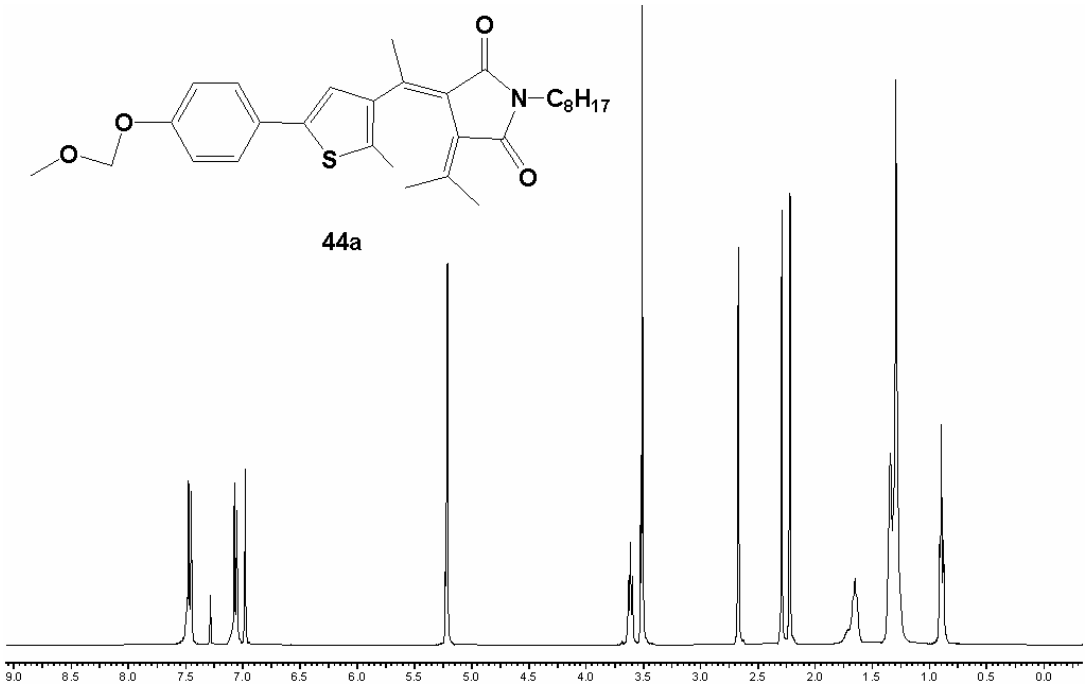

Figure A1-39. 400MHz ^{1}HNMR spectrum of **44a**.

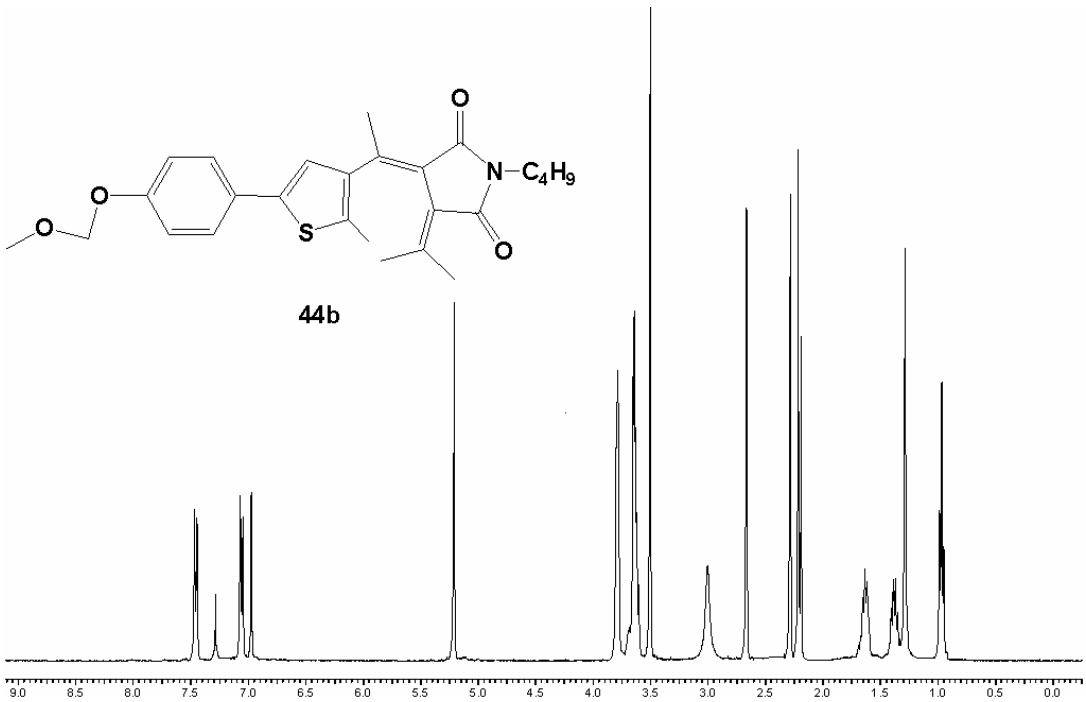

Figure A1-40. 400MHz ^{1}HNMR spectrum of **44b**.

Appendix 2. DSC profiles of liquid crystals

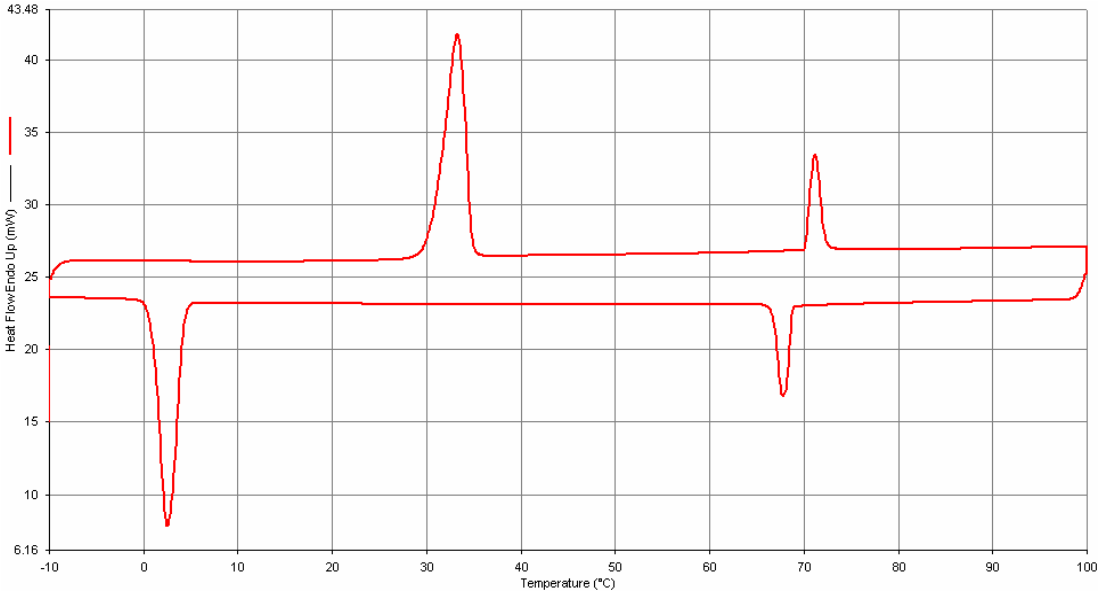

Figure A2-1. DSC profile for compound **29a** taken at a scan rate of 5K/min.

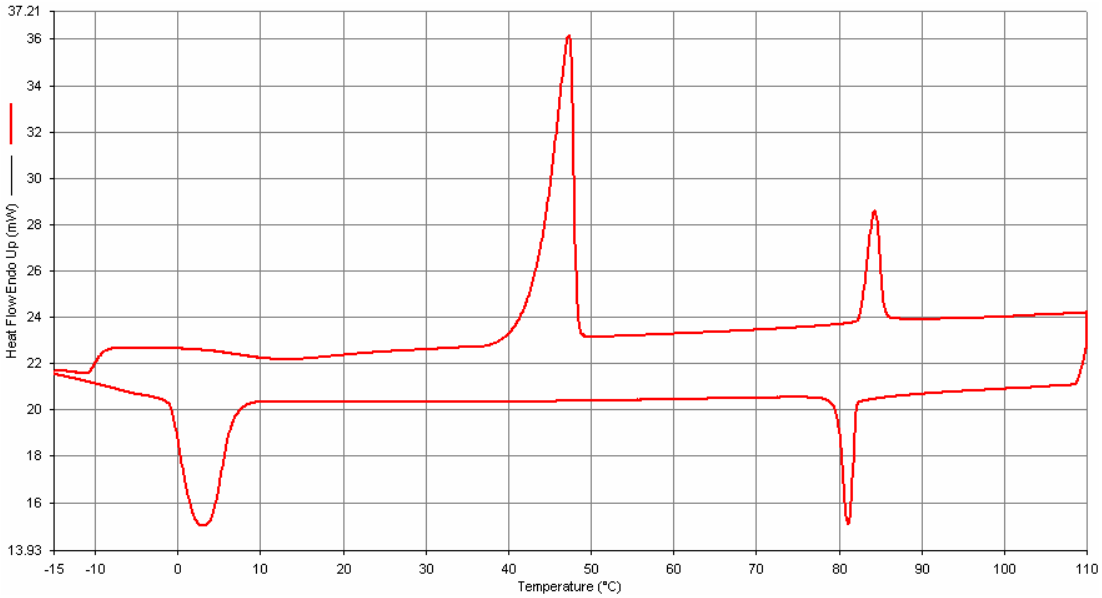

Figure A2-2. DSC profile for compound **29b** taken at a scan rate of 5K/min.

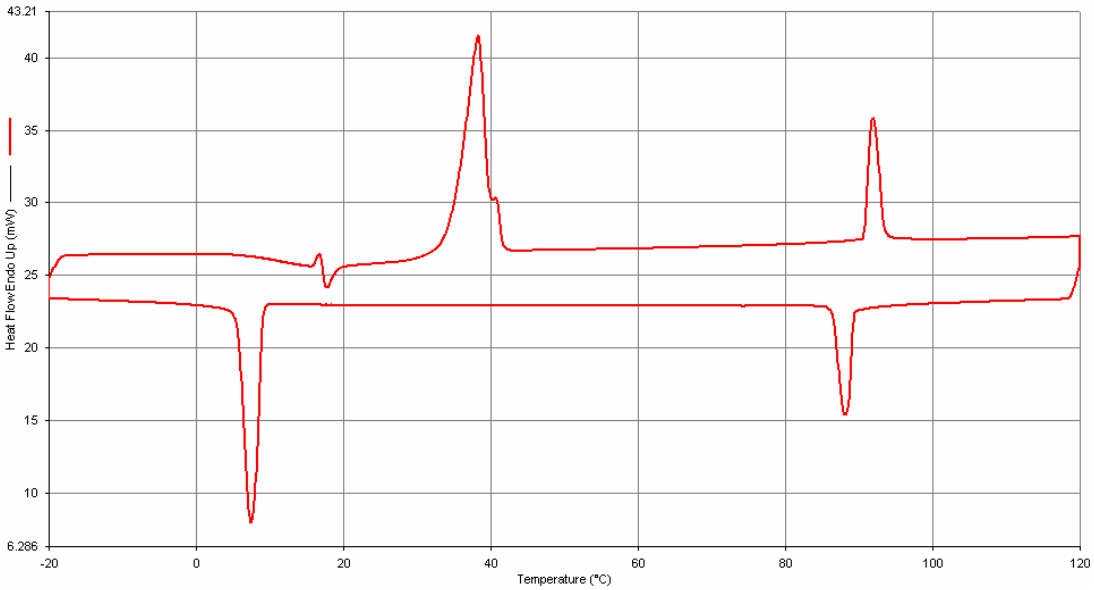

Figure A2-3. DSC profile for compound **29c** taken at a scan rate of 5K/min.

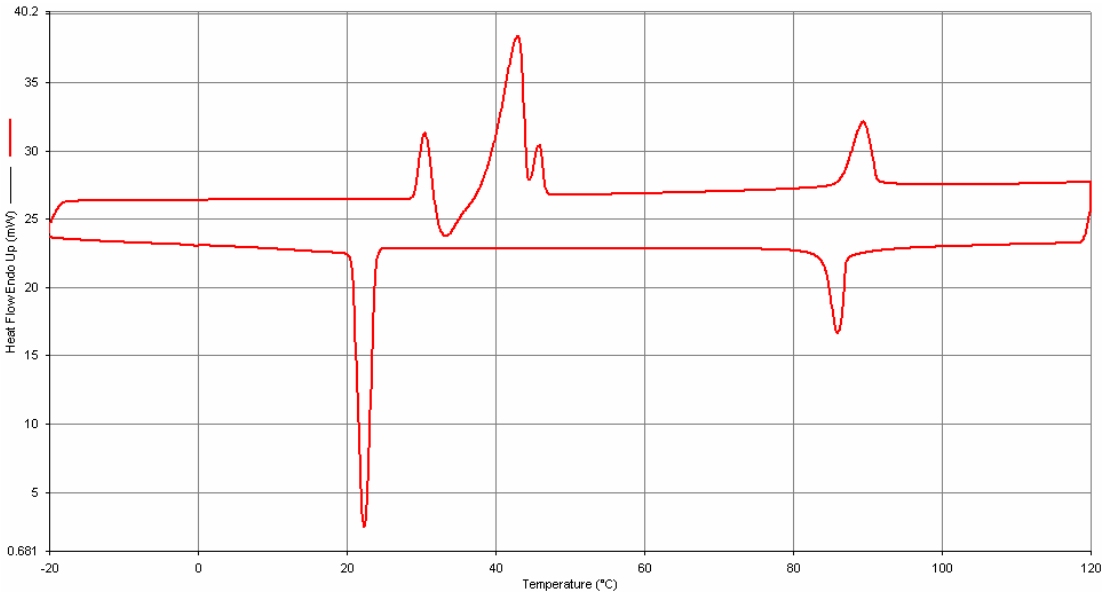

Figure A2-4. DSC profile for compound **29d** taken at a scan rate of 5K/min.

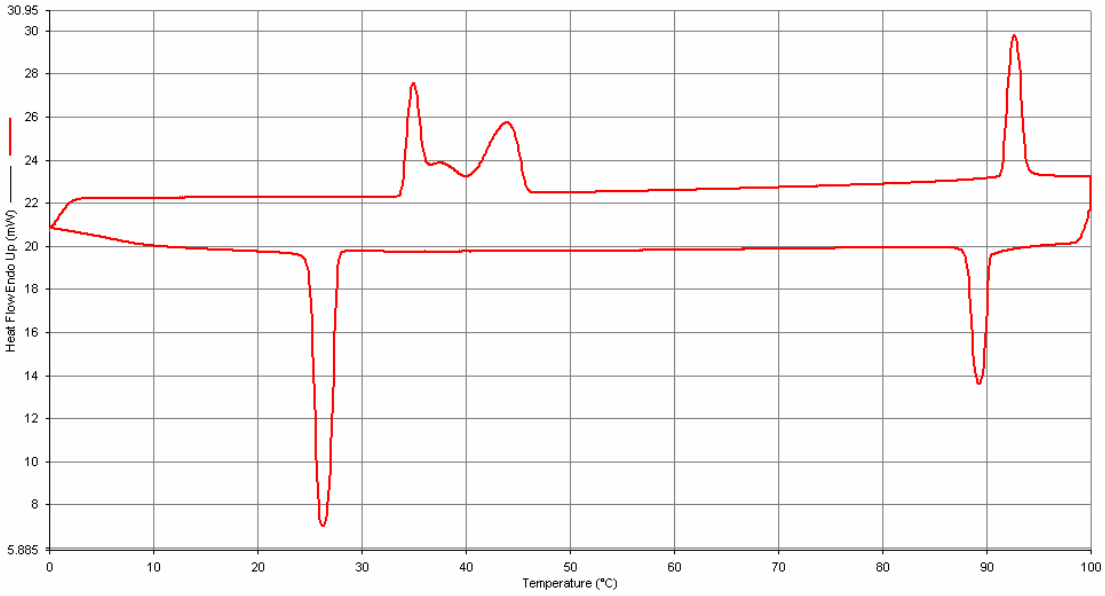

Figure A2-5. DSC profile for compound **29e** taken at a scan rate of 5K/min.

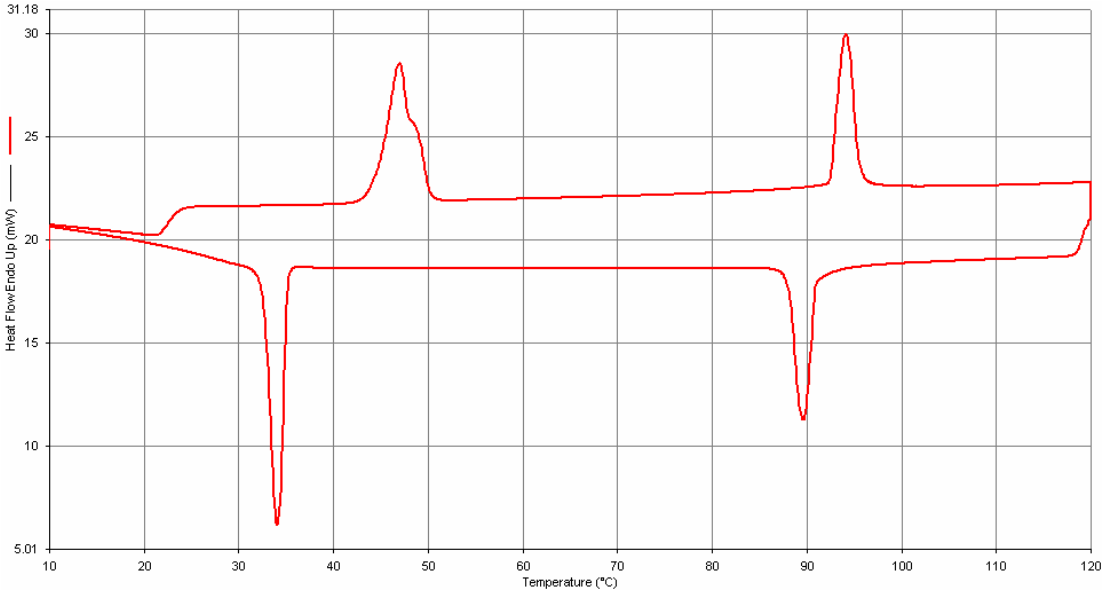

Figure A2-6. DSC profile for compound **29f** taken at a scan rate of 5K/min.

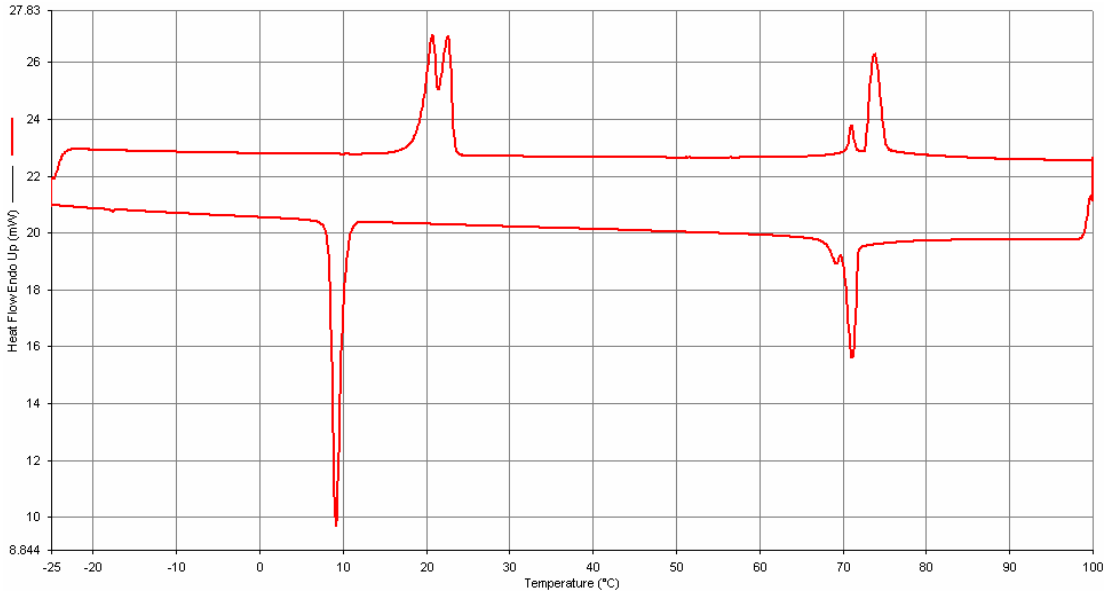

Figure A2-7. DSC profile for compound **30a** taken at a scan rate of 5K/min.

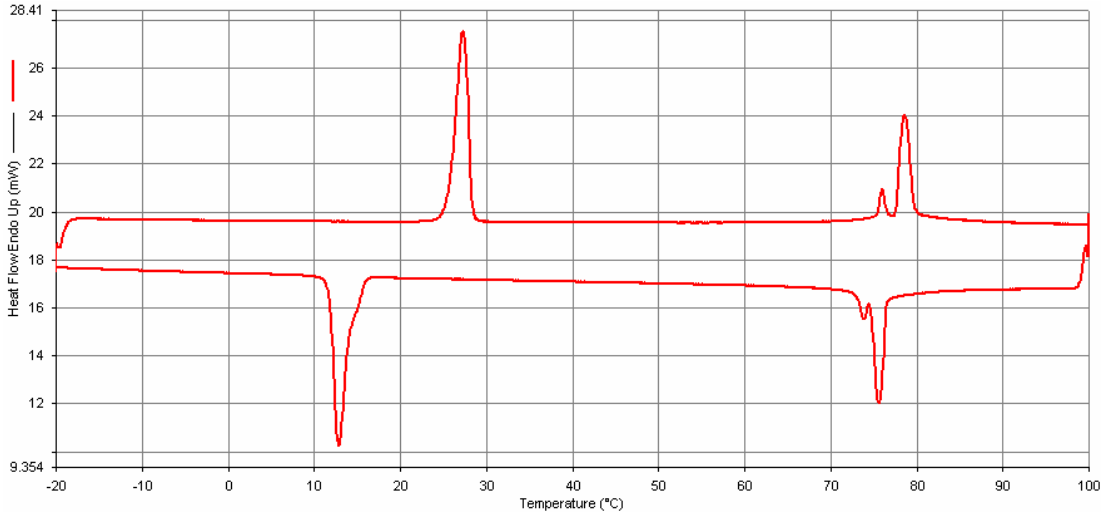

Figure A2-8. DSC profile for compound **30b** taken at a scan rate of 5K/min.

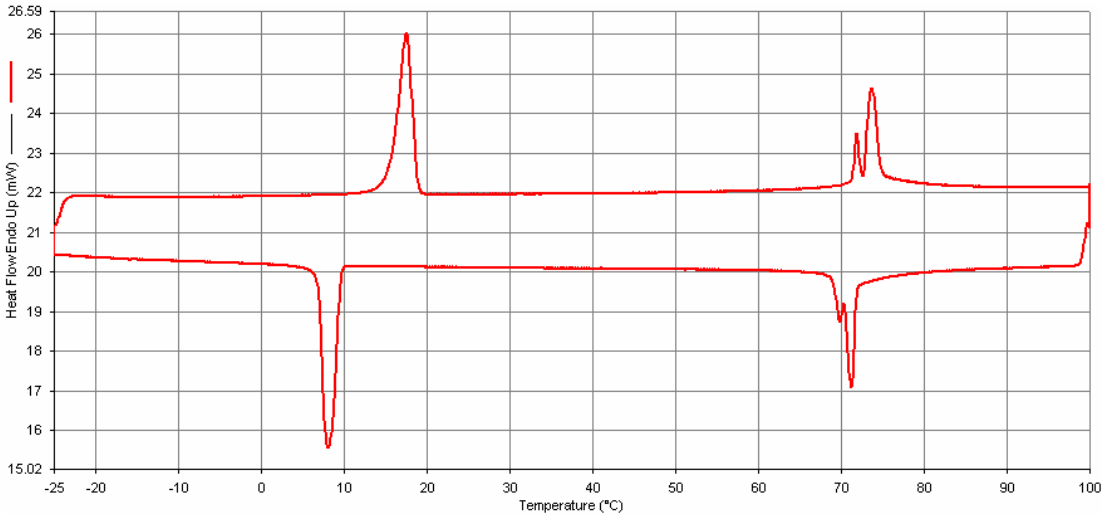

Figure A2-9. DSC profile for compound **30c** taken at a scan rate of 5K/min.

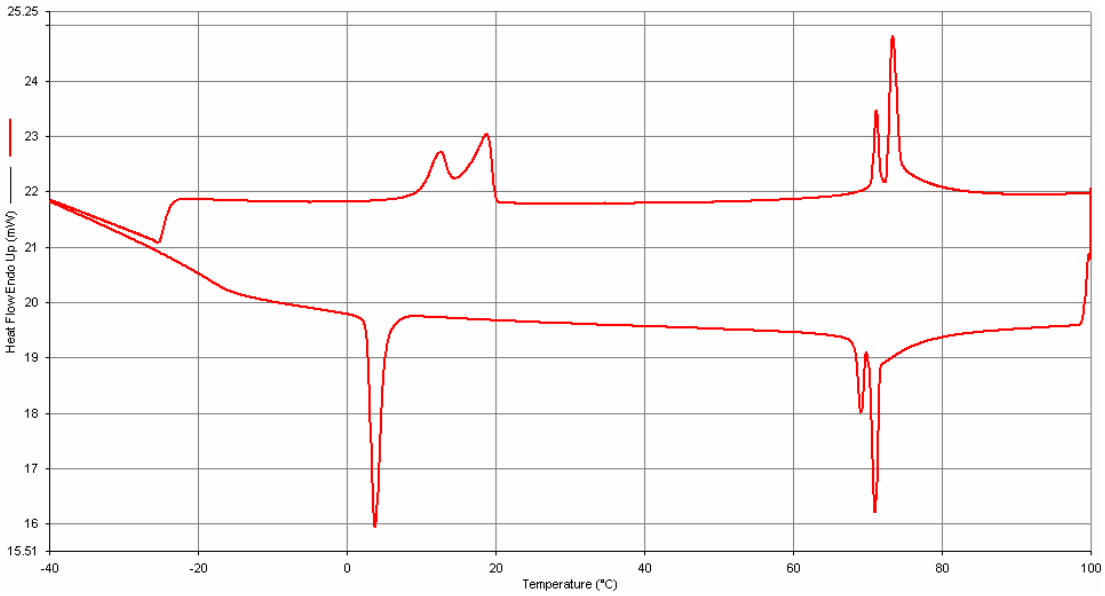

Figure A2-10. DSC profile for compound **30d** taken at a scan rate of 5K/min.

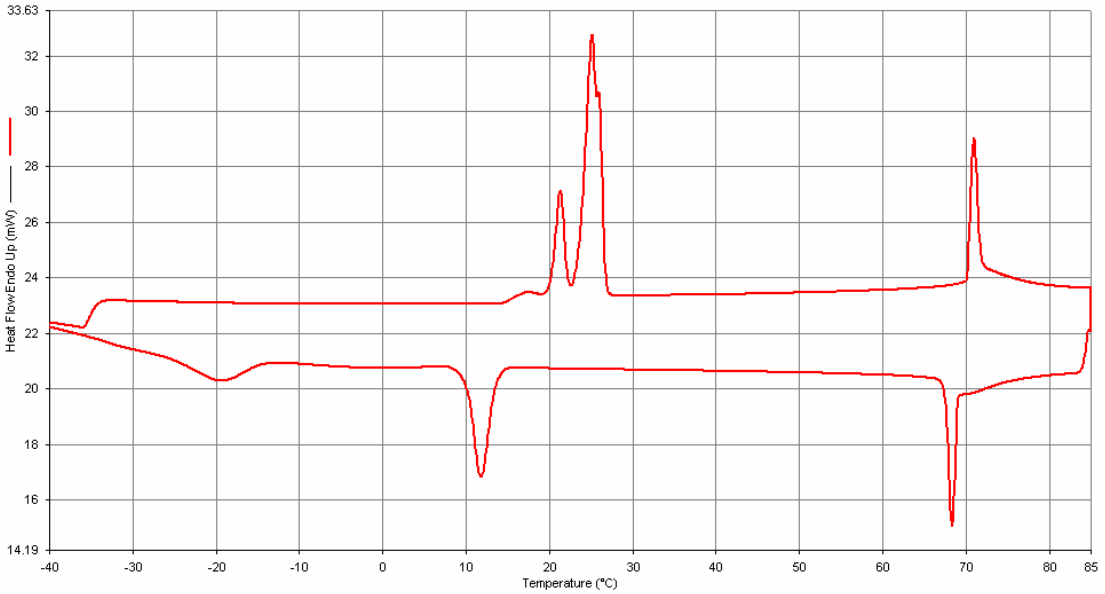

Figure A2-11. DSC profile for compound **30e** taken at a scan rate of 5K/min.

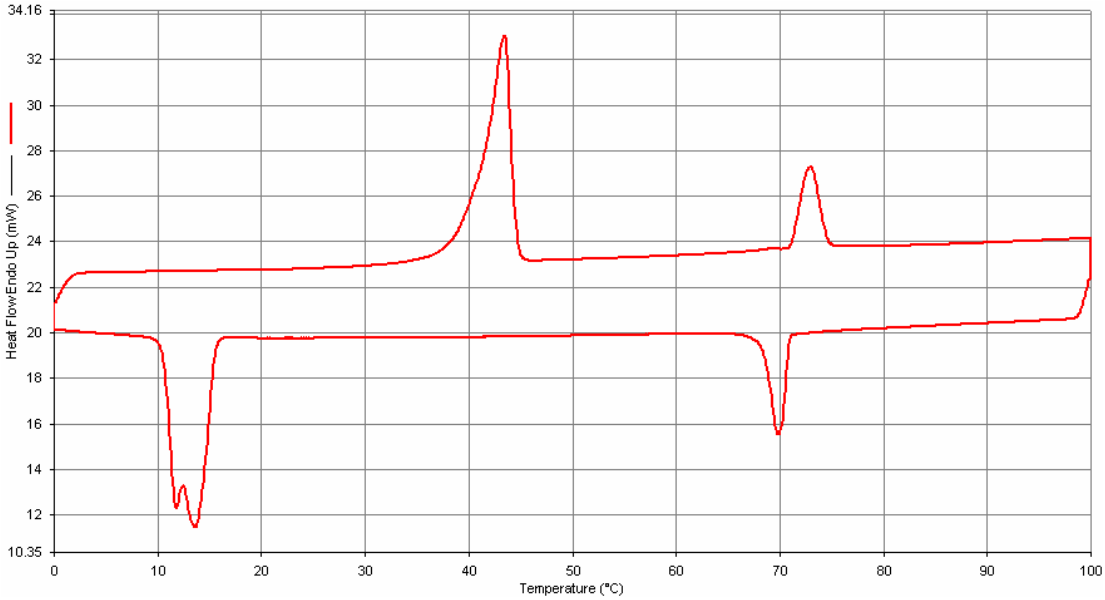

Figure A2-12. DSC profile for compound **31** taken at a scan rate of 5K/min.

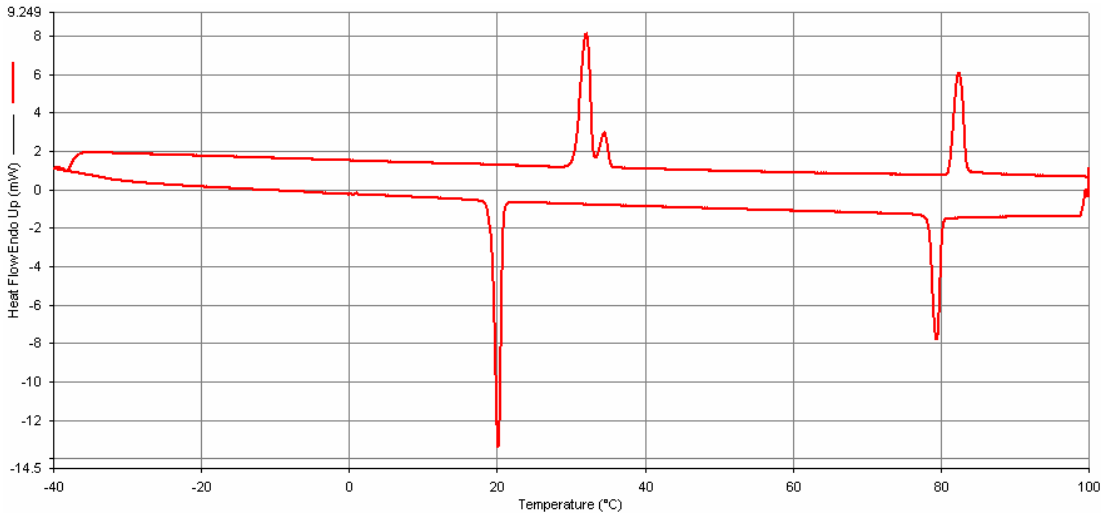

Figure A2-13. DSC profile for compound **32a** taken at a scan rate of 5K/min.

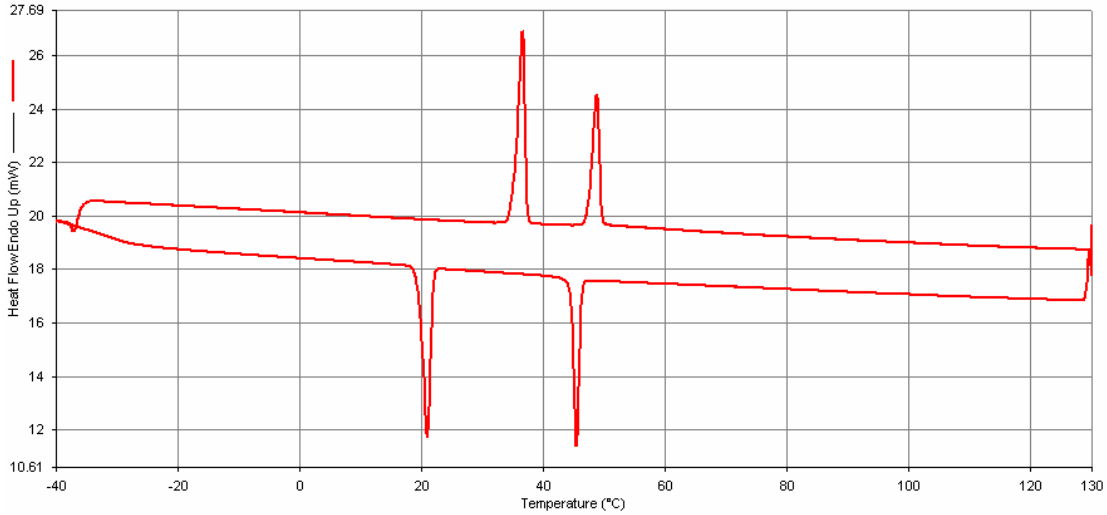

Figure A2-13. DSC profile for compound **32b** taken at a scan rate of 5K/min.

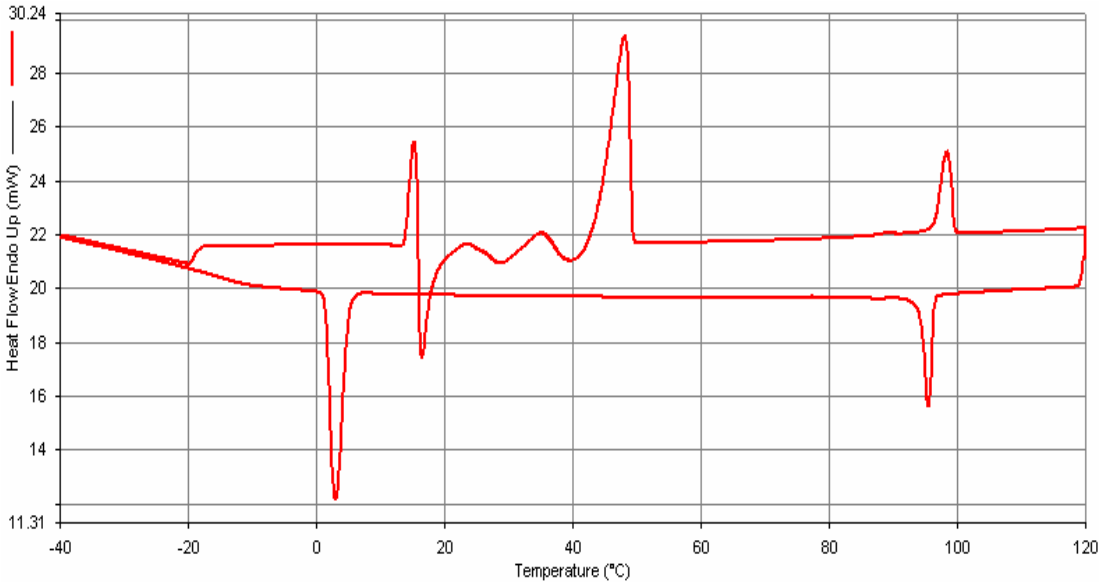

Figure A2-14. DSC profile for compound **33a** taken at a scan rate of 5K/min.

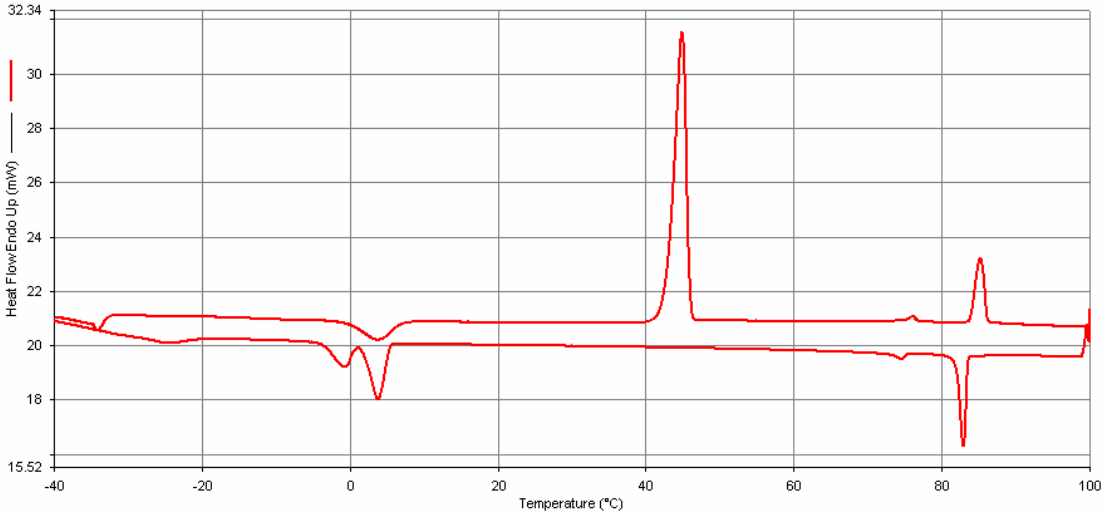

Figure A2-15. DSC profile for compound **33b** taken at a scan rate of 5K/min.

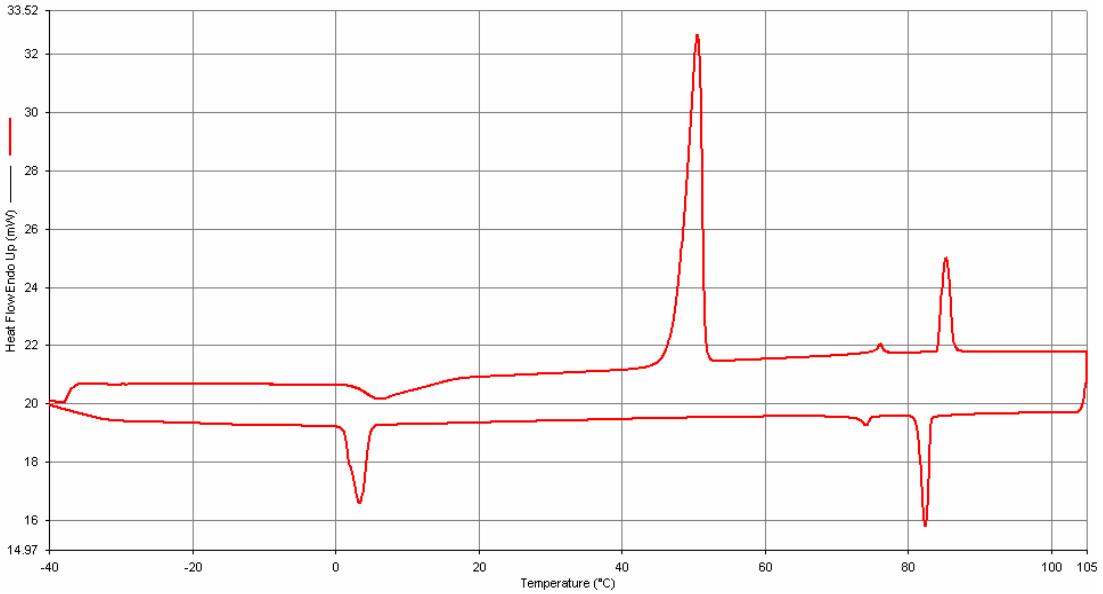

Figure A2-16. DSC profile for compound **33c** taken at a scan rate of 5K/min.

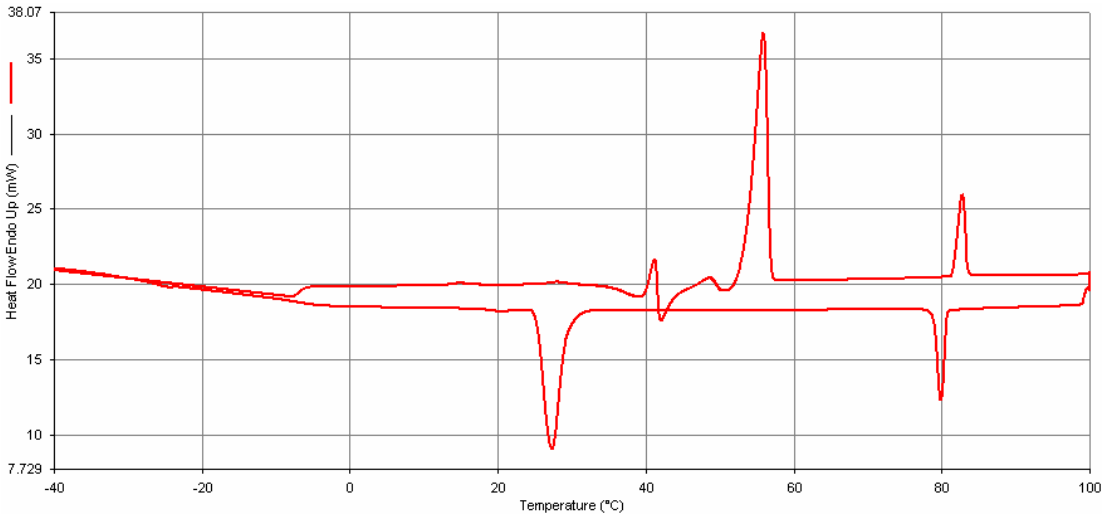

Figure A2-17. DSC profile for compound **34a** taken at a scan rate of 5K/min.

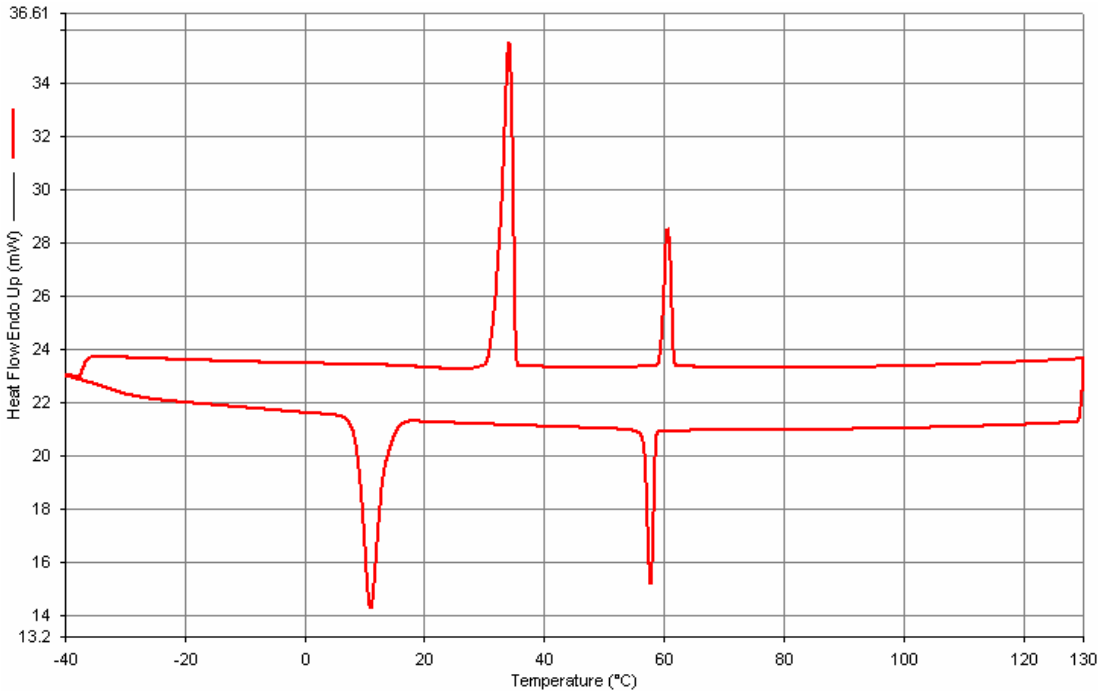

Figure A2-18. DSC profile for compound **34b** taken at a scan rate of 5K/min.

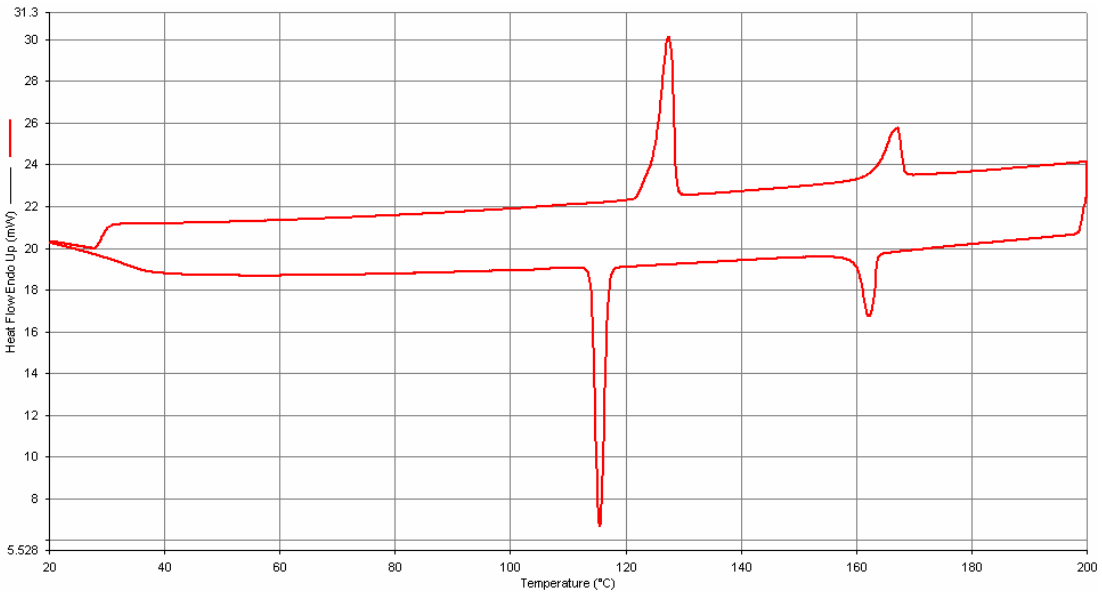

Figure A2-19. DSC profile for compound **35a** taken at a scan rate of 5K/min.

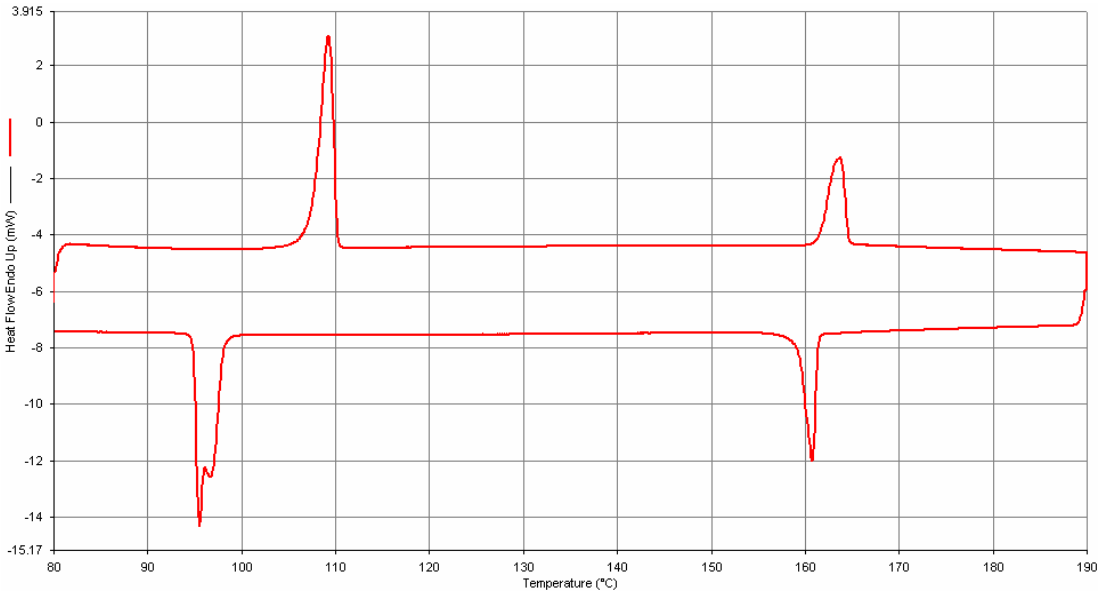

Figure A2-20. DSC profile for compound **35b** taken at a scan rate of 5K/min.

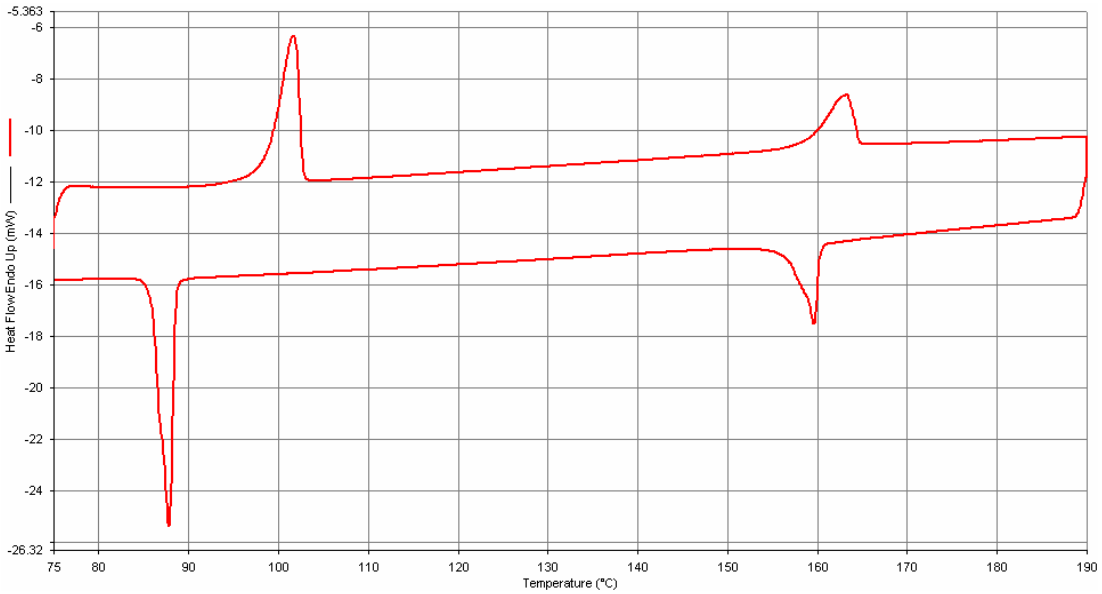

Figure A2-21. DSC profile for compound **35c** taken at a scan rate of 5K/min.

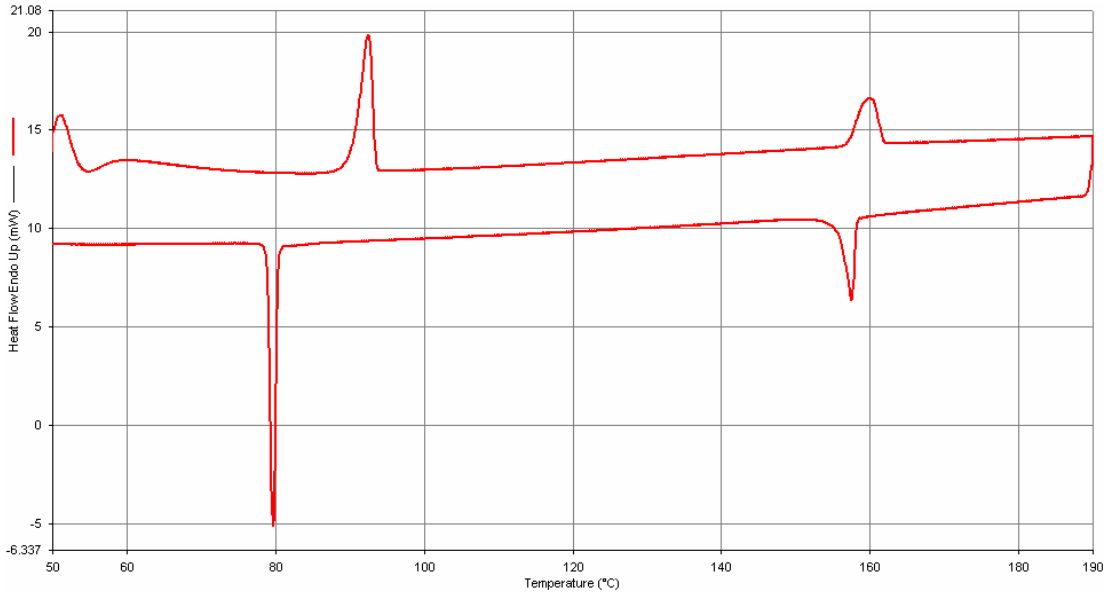

Figure A2-22. DSC profile for compound **35d** taken at a scan rate of 5K/min.

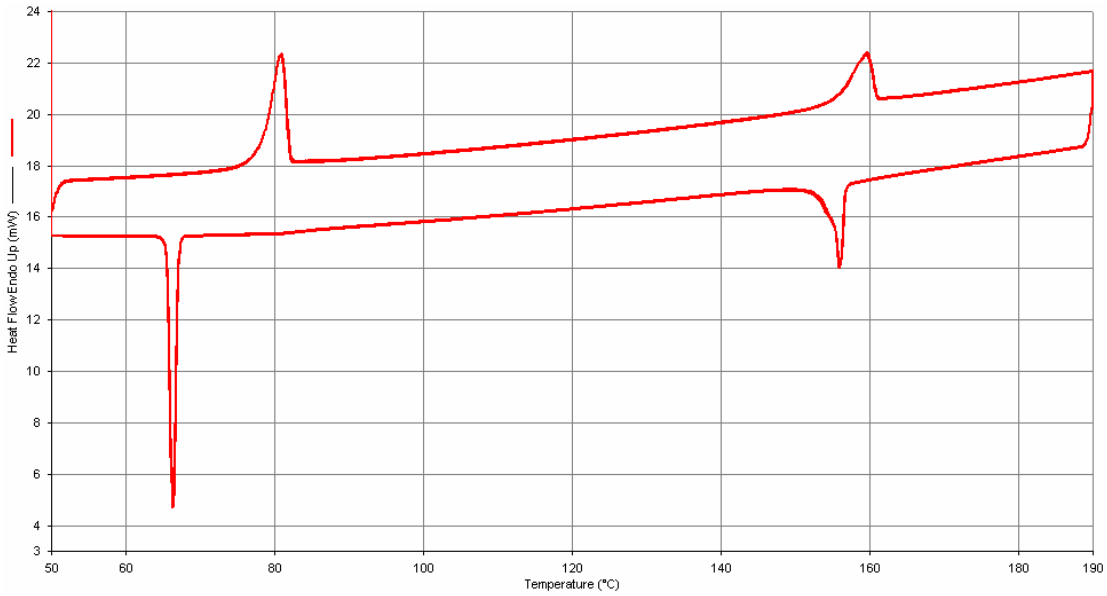

Figure A2-23. DSC profile for compound **35e** taken at a scan rate of 5K/min.

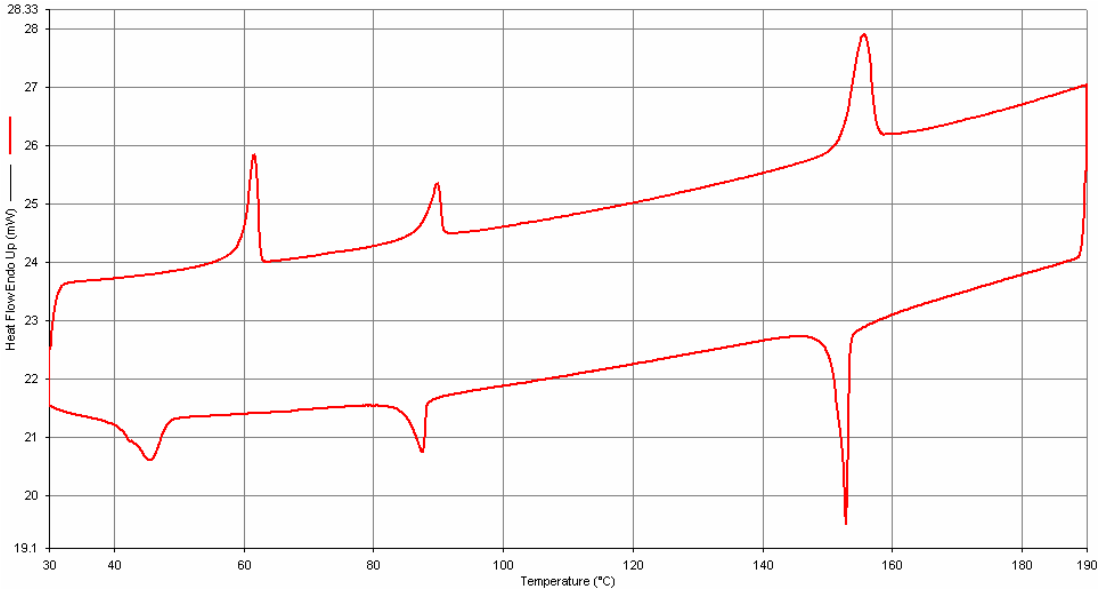

Figure A2-24. DSC profile for compound **35f** taken at a scan rate of 5K/min.

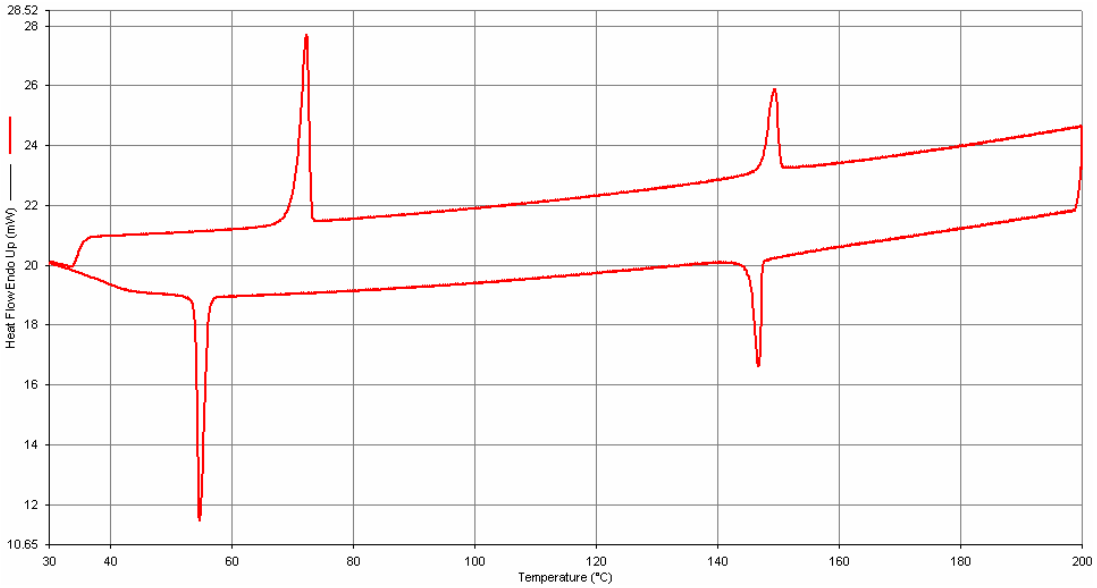

Figure A2-25. DSC profile for compound **36** taken at a scan rate of 5K/min.

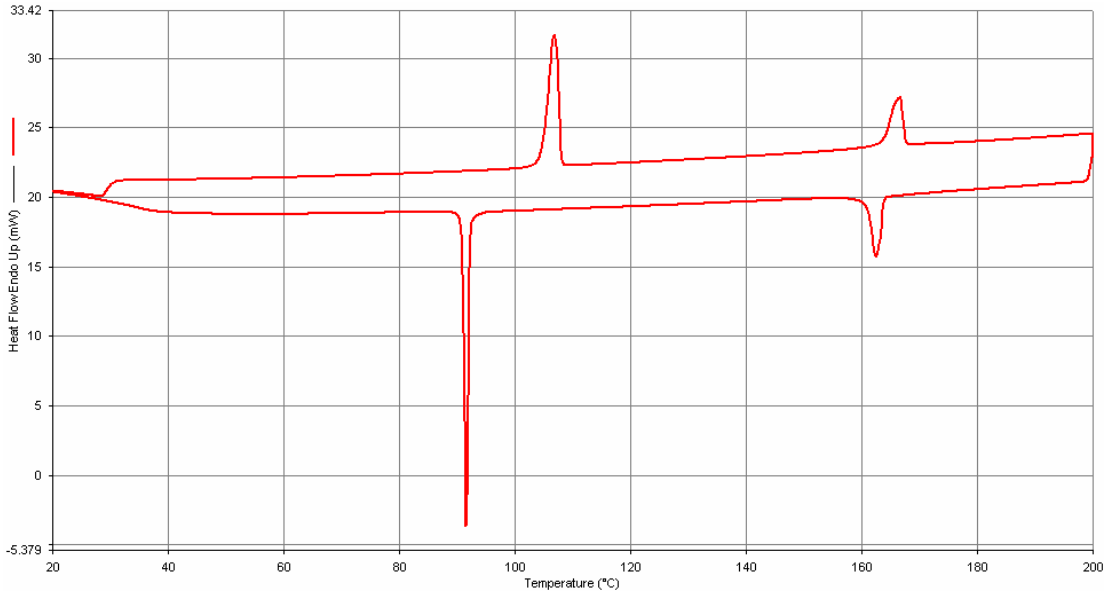

Figure A2-26. DSC profile for compound **37** taken at a scan rate of 5K/min.

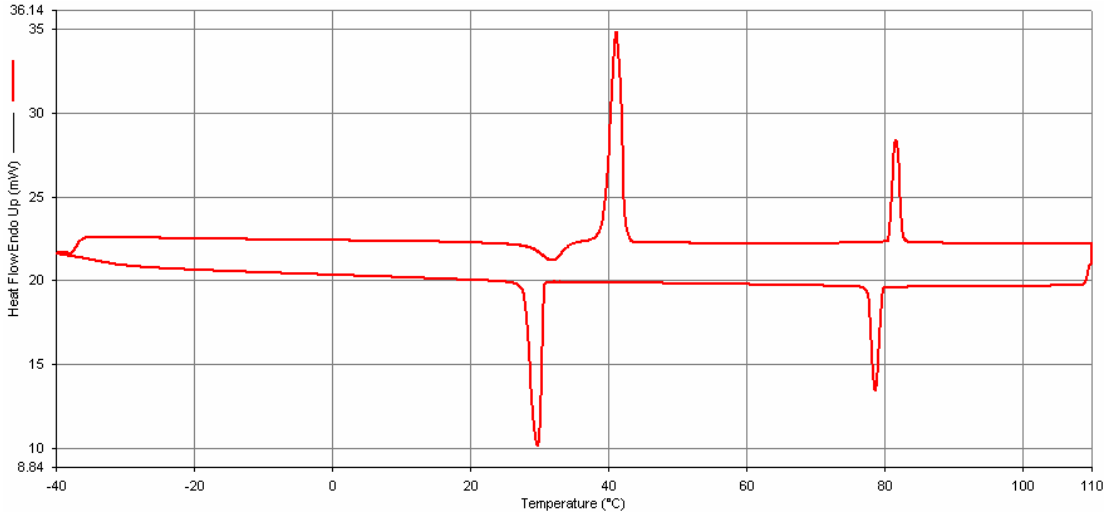

Figure A2-27. DSC profile for compound **38** taken at a scan rate of 5K/min.

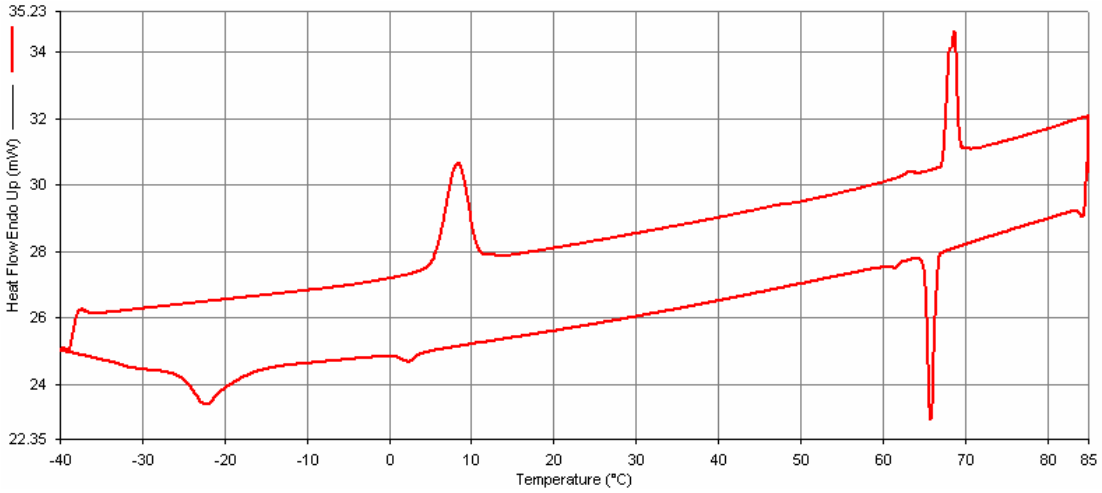

Figure A2-28. DSC profile for compound **39a** taken at a scan rate of 5K/min.

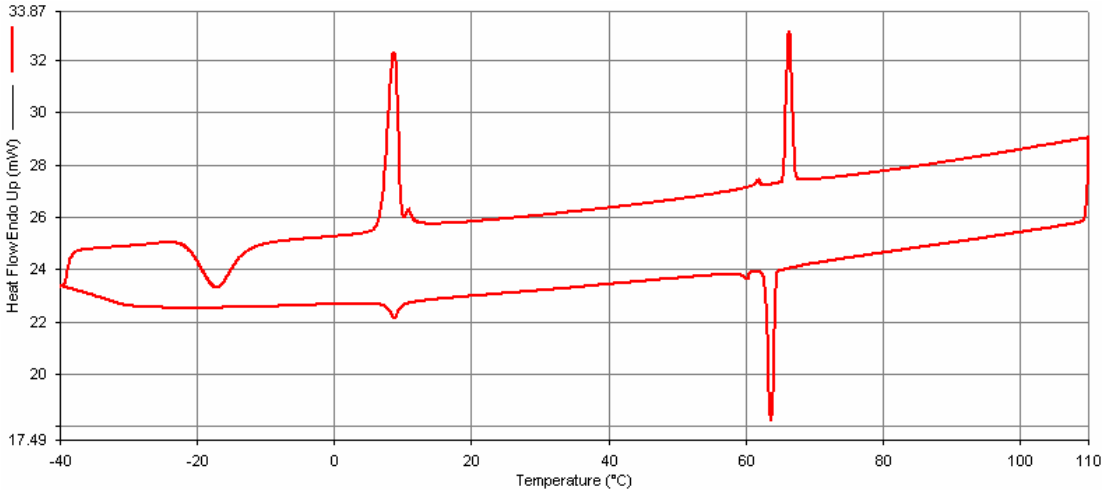

Figure A2-29. DSC profile for compound **39b** taken at a scan rate of 5K/min.

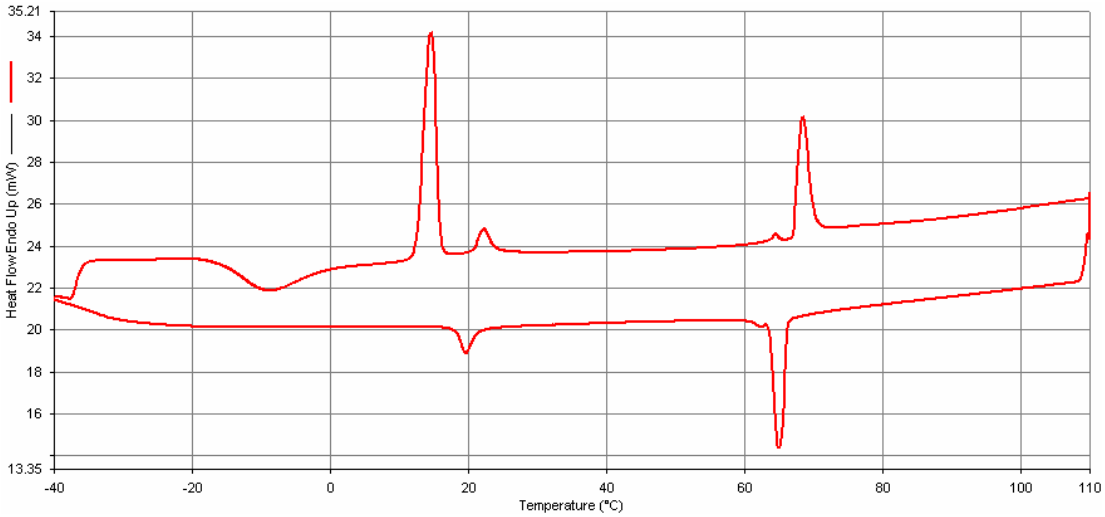

Figure A2-30. DSC profile for compound **39c** taken at a scan rate of 5K/min.

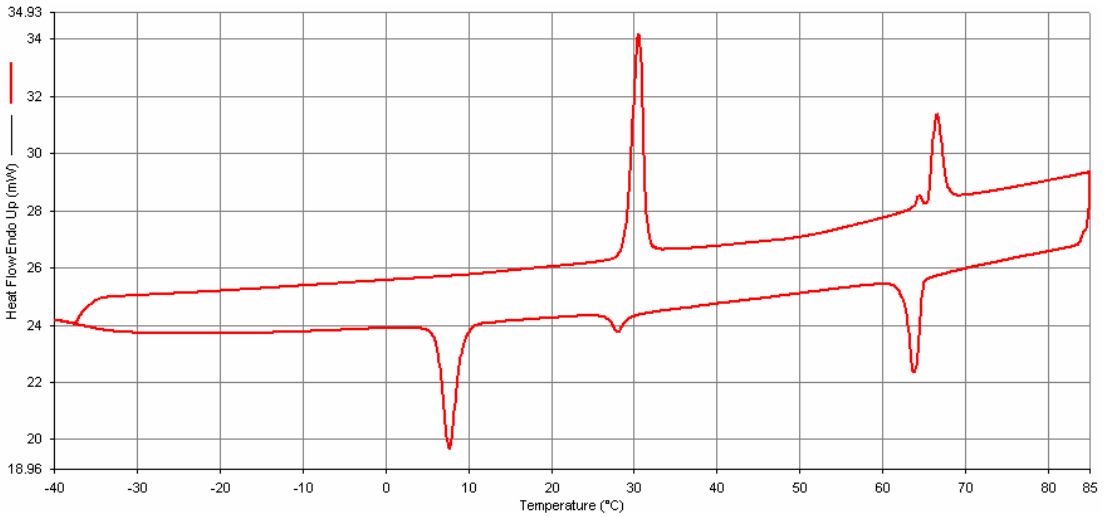

Figure A2-31. DSC profile for compound **39d** taken at a scan rate of 5K/min.

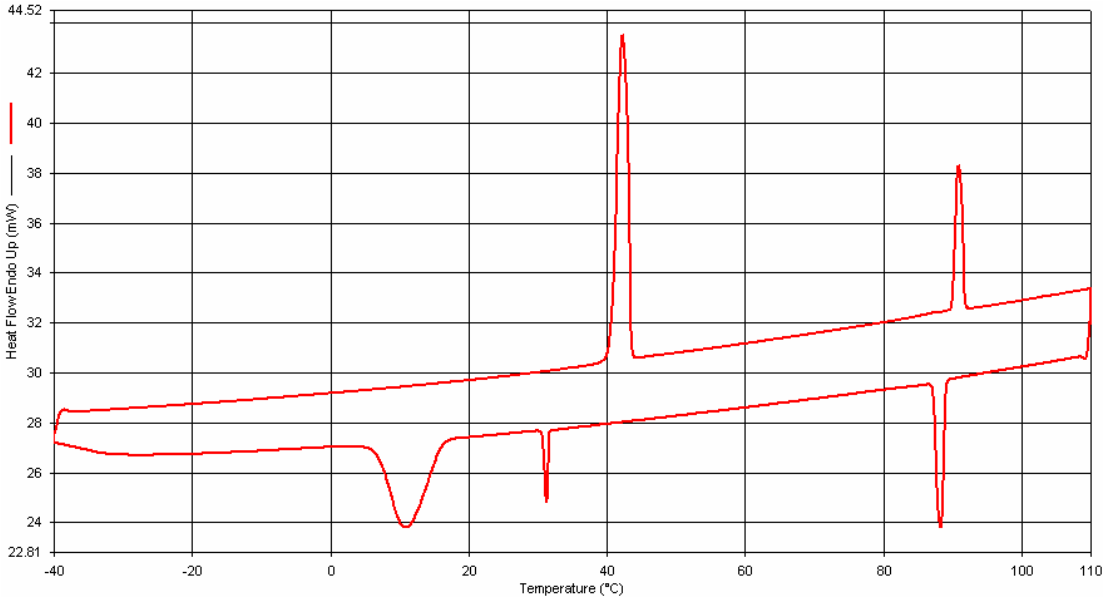

Figure A2-32. DSC profile for compound **40a** taken at a scan rate of 5K/min.

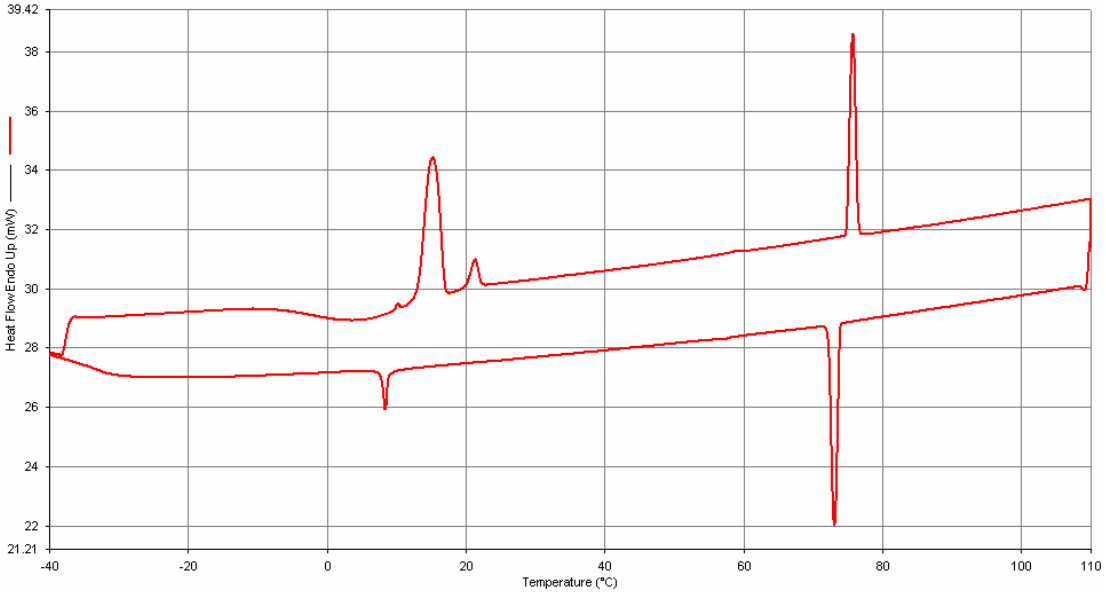

Figure A2-33. DSC profile for compound **40b** taken at a scan rate of 5K/min.

Appendix 3. Textures of liquid crystals by polarized microscopy

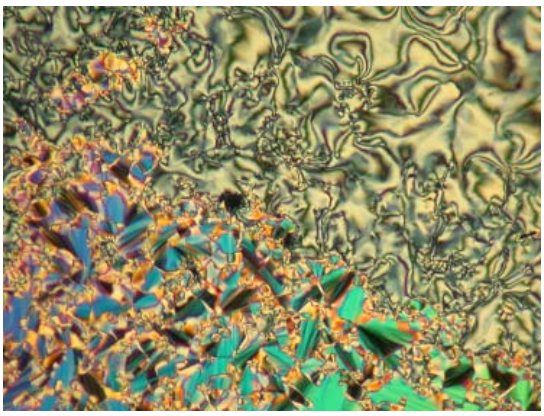

Figure A3-1. Textures of compound **29a** observed by polarized microscopy on cooling: in the SmC phase at 52^{o}C. (100X Magnification)

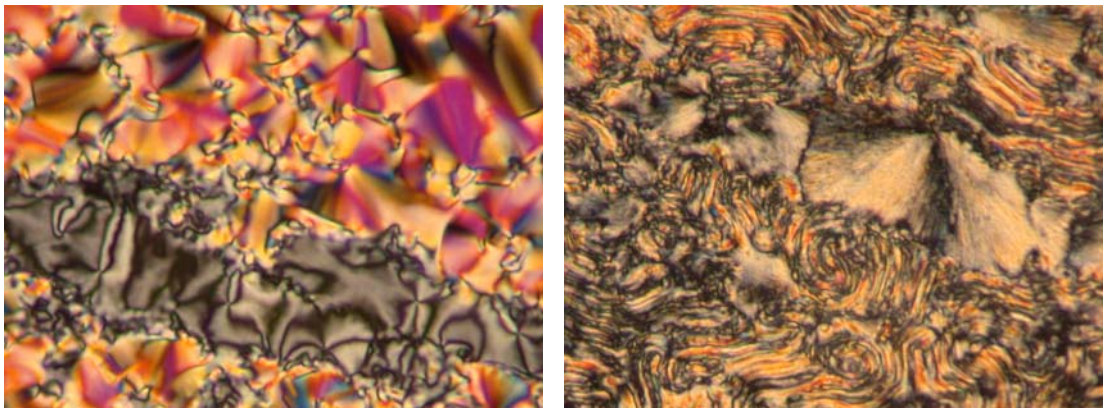

(a) (b)

Figure A3-2. Textures of compound **29b** observed by polarized microscopy on cooling: (a) SmC phase at 50^{o}C, and (b) Cr phase at -10^{o}C. (100X Magnification)

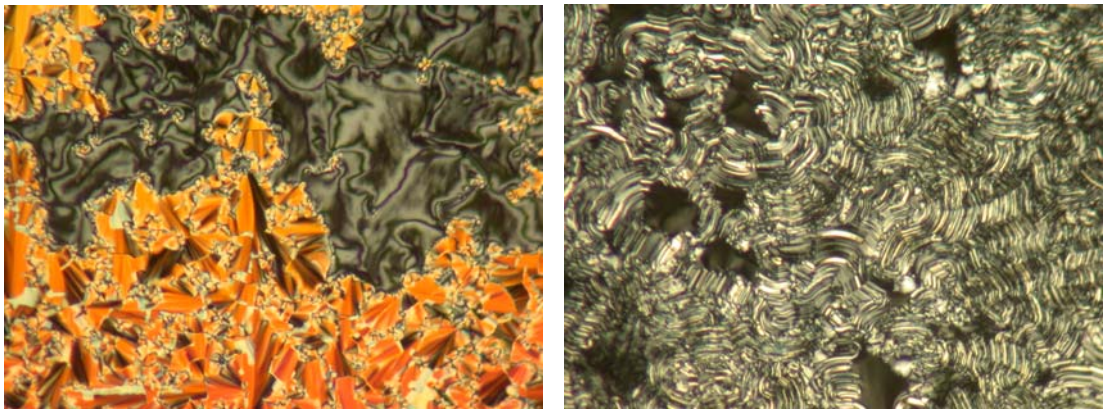

(a) (b)

Figure A3-3. Textures of compound **29c** observed by polarized microscopy on cooling: (a) SmC phase at 85°C, and (b) Cr phase at 3°C. (100X Magnification)

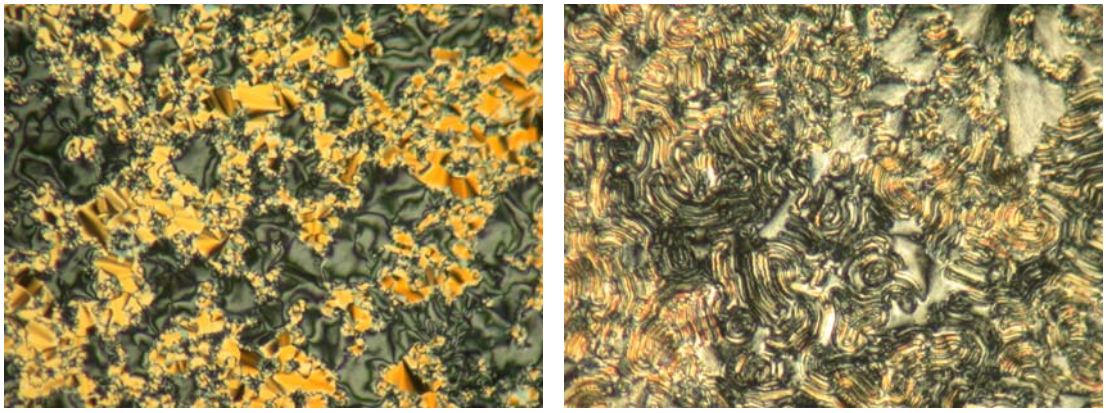

(a) (b)

Figure A3-4. Textures of compound **29d** observed by polarized microscopy on cooling: (a) SmC phase at 56°C, and (b) Cr phase at 8°C. (100X Magnification)

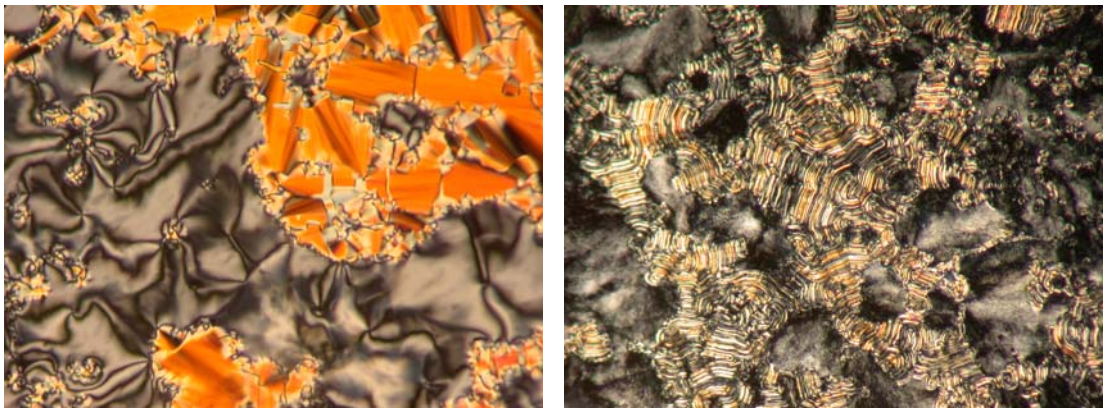

(a) (b)

Figure A3-5. Textures of compound **29e** observed by polarized microscopy on cooling: (a) SmC phase at 82°C, and (b) Cr phase at 15°C. (100X Magnification)

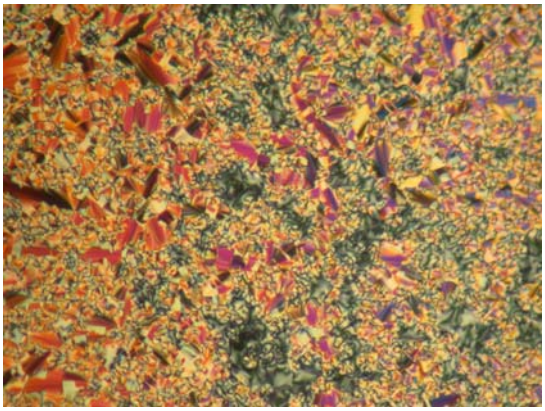

Figure A3-6. Textures of compound **29f** observed by polarized microscopy on cooling: SmC phase at 83°C. (100X Magnification)

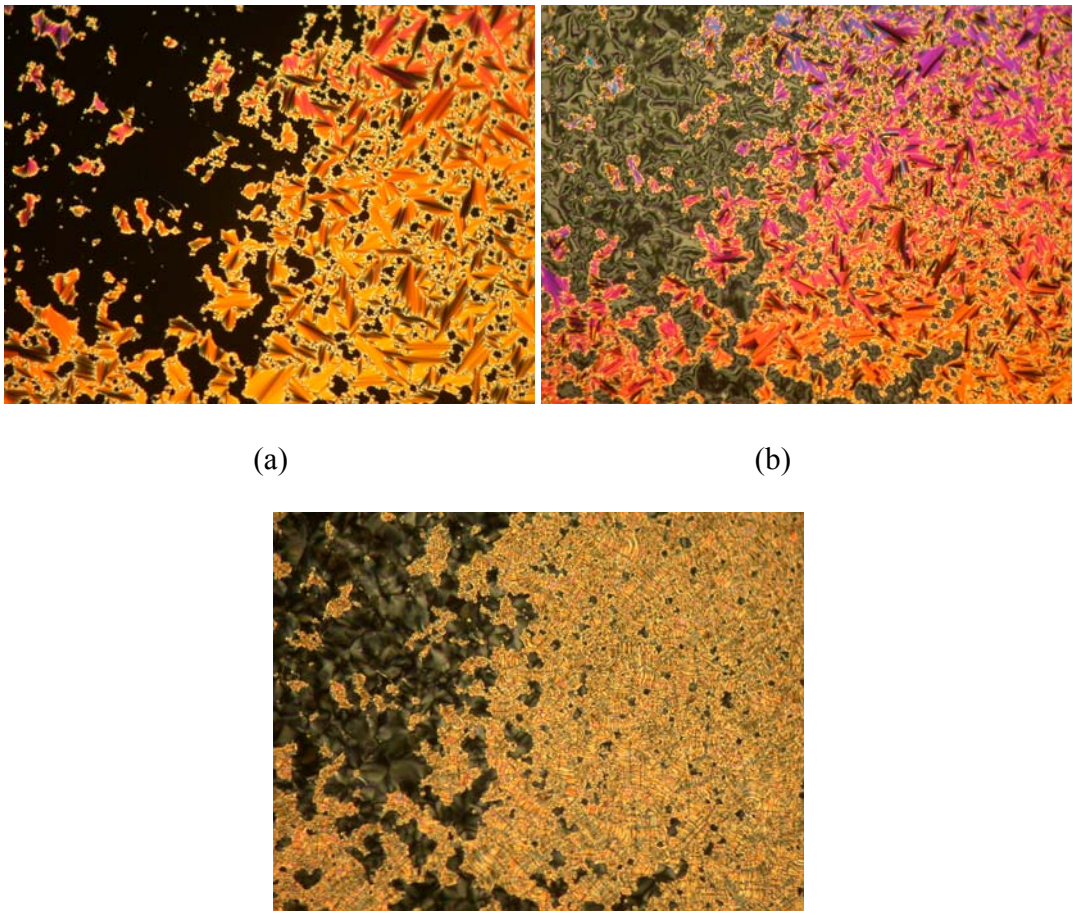

Figure A3-7. Textures of compound **30a** observed by polarized microscopy on cooling: (a) SmA phase at 70°C, (b) SmC phase at 59°C, and (c) Cr phase at -1°C. (100X Magnification)

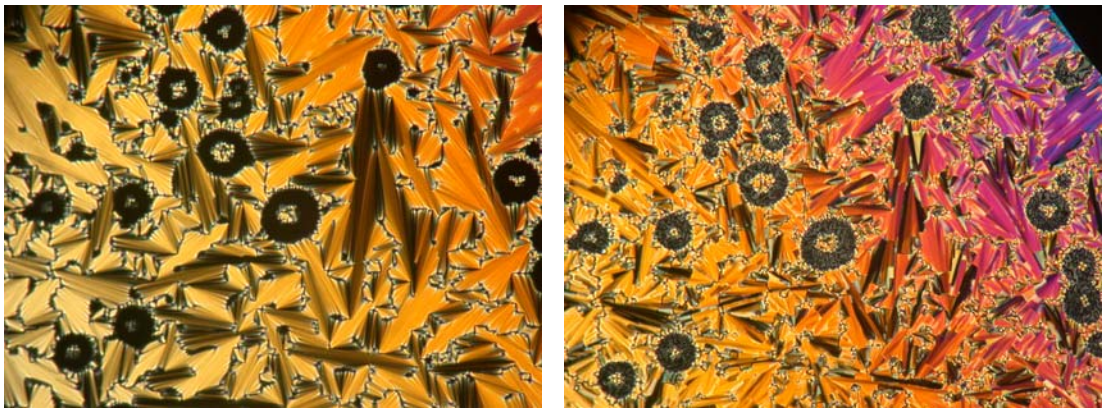

(a) (b)

Figure A3-8. Textures of compound **30b** observed by polarized microscopy on cooling: (a) SmA phase at 73°C, and (b) SmC phase at 72°C. (100X Magnification)

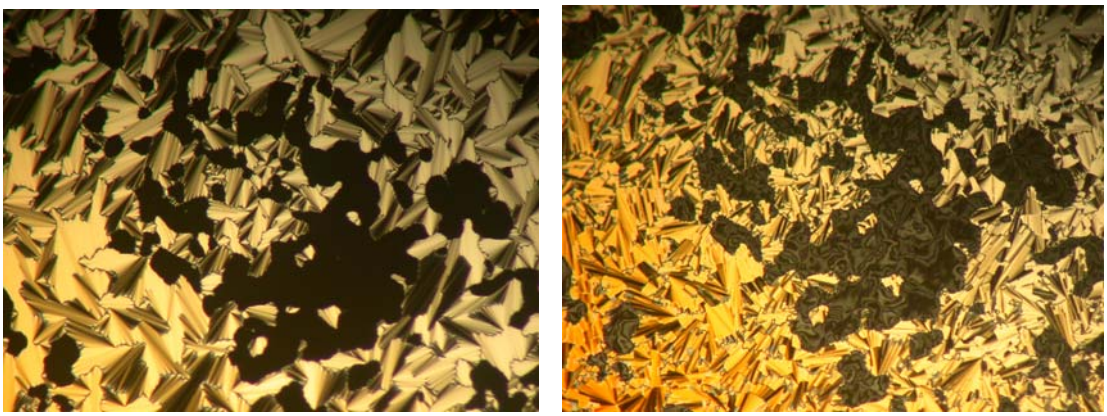

(a) (b)

Figure A3-9. Textures of compound **30c** observed by polarized microscopy on cooling:: (a) in the SmA phase at 70°C, and (b) in the SmC phase at 50°C. (100X Magnification)

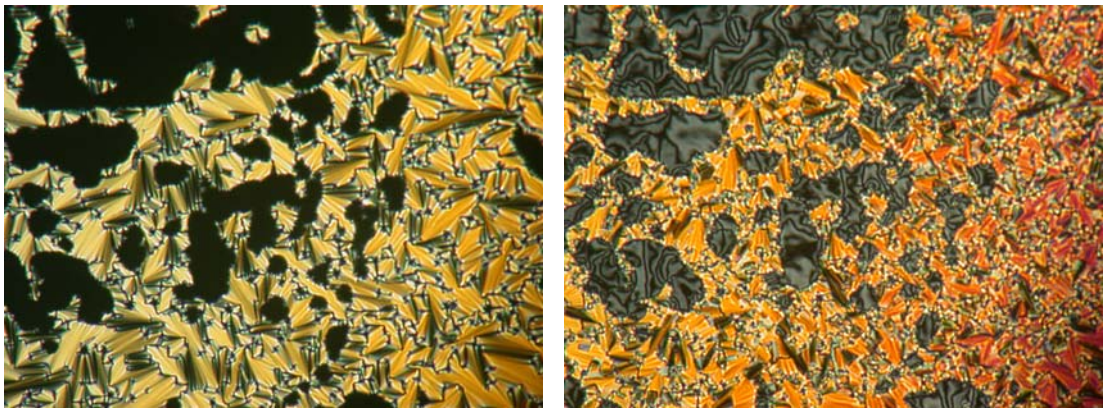

(a) (b)

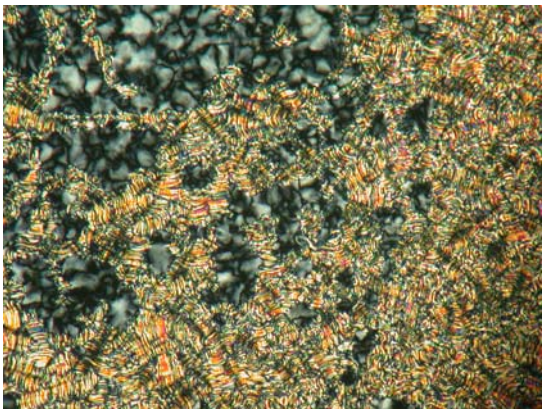

(c)

Figure A3-10. Textures of compound **30d** observed by polarized microscopy on cooling: (a) in the SmA phase at 70°C, (b) in the SmC phase at 58°C, (c) in the Cr phase at -16°C. (100X Magnification)

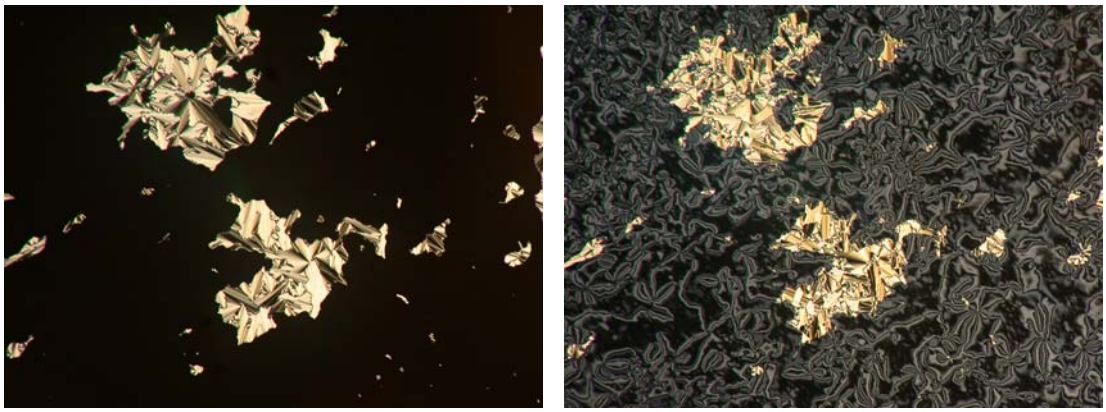

(a) (b)

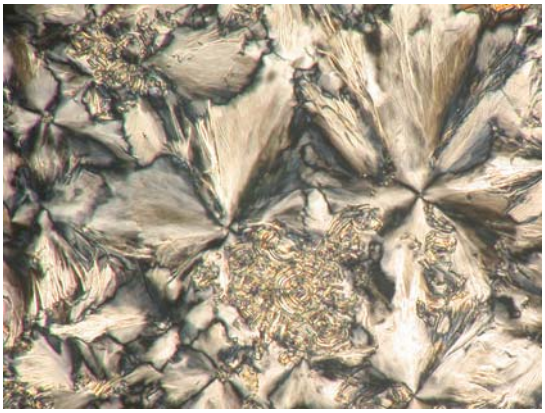

(c)

Figure A3-11. Textures of compound **30e** observed by polarized microscopy on cooling:e: (a) in the SmA phase at 68^{o}C, (b) in the SmC phase at 63^{o}C, (c) in the Cr phase at -2^{o}C. (100X Magnification)

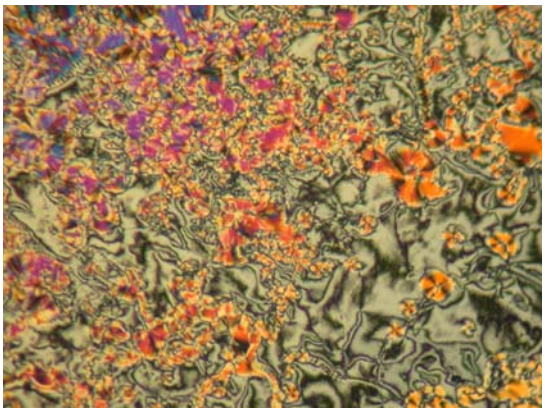

Figure A3-12. Textures of compound **31** observed by polarized microscopy on cooling: in the SmC phase at 62^{o}C. (100X Magnification)

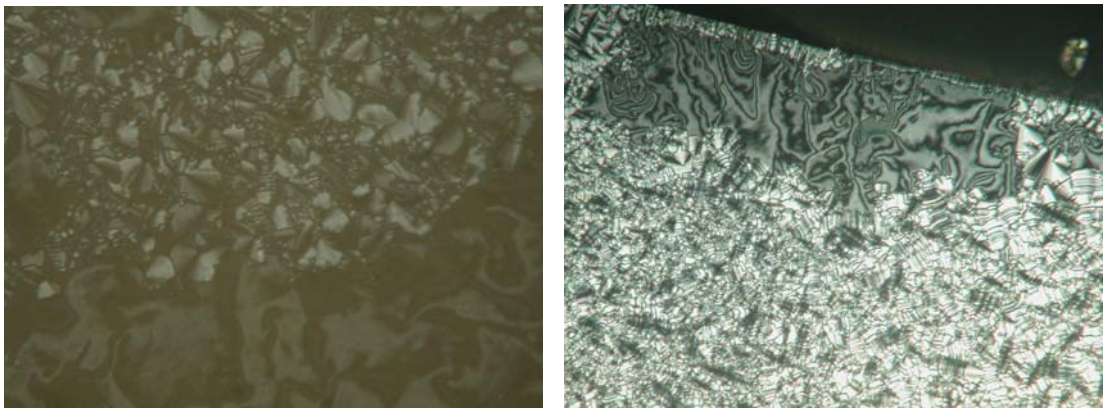

(a) (b)

Figure A3-13. Textures of compound **32a** observed by polarized microscopy on cooling: (a) SmC phase at 78^{o}C, and (b) Cr phase at 13^{o}C. (100X Magnification)

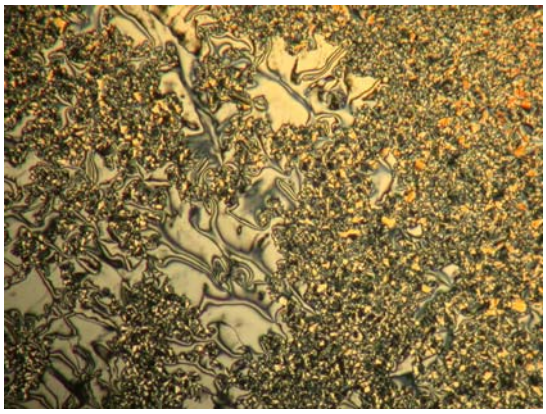

(a)

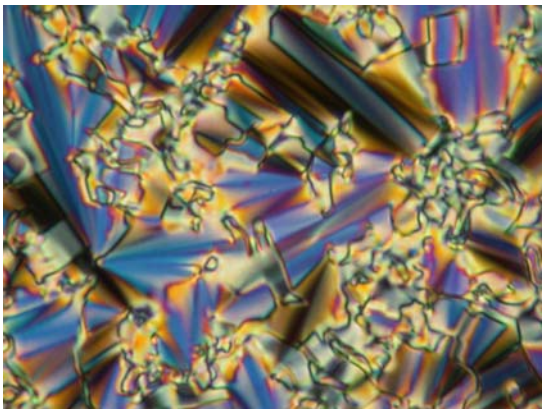

(b)

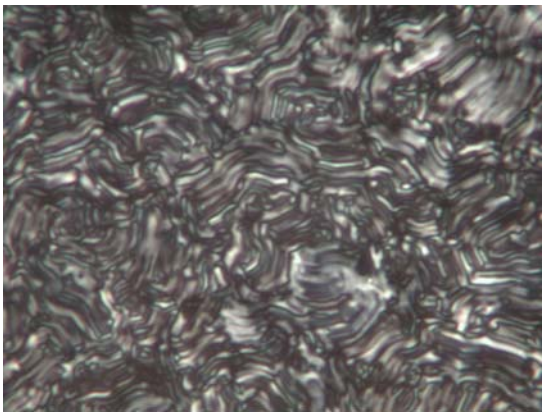

(c)

Figure A3-14. Textures of compound **32b** observed by polarized microscopy on cooling: (a) SmC phase at 44^{o}C, (b) SmC phase at 44^{o}C, and (c) Cr phase at -39^{o}C. (100X Magnification)

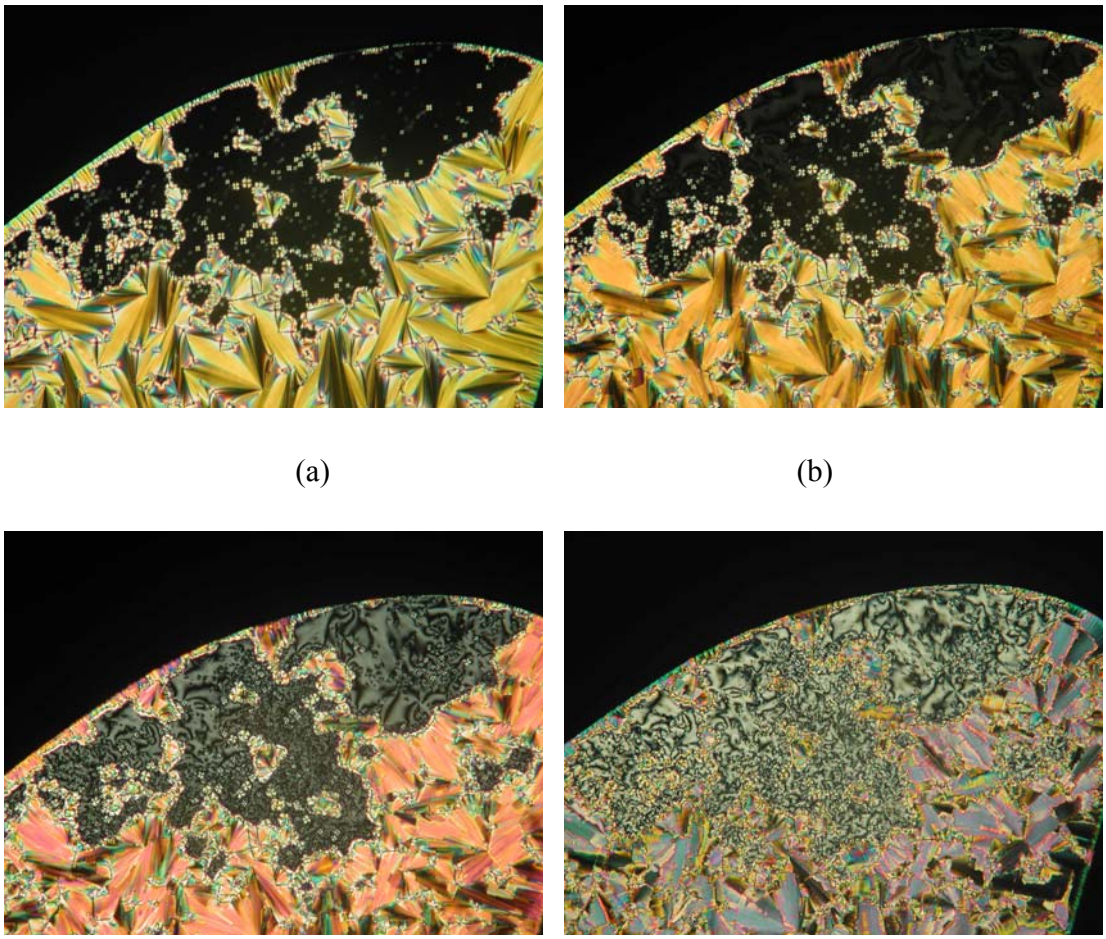

(a) (b)

(c) (d)

Figure A3-15. Textures of compound **33a** observed by polarized microscopy on cooling: (a) in the SmA phase at 91°C, (b) just below the SmA–SmC phase transition at 86°C, (c) in the SmC phase at 82°C, and (d) in the Cr phase at 24°C. (100X Magnification)

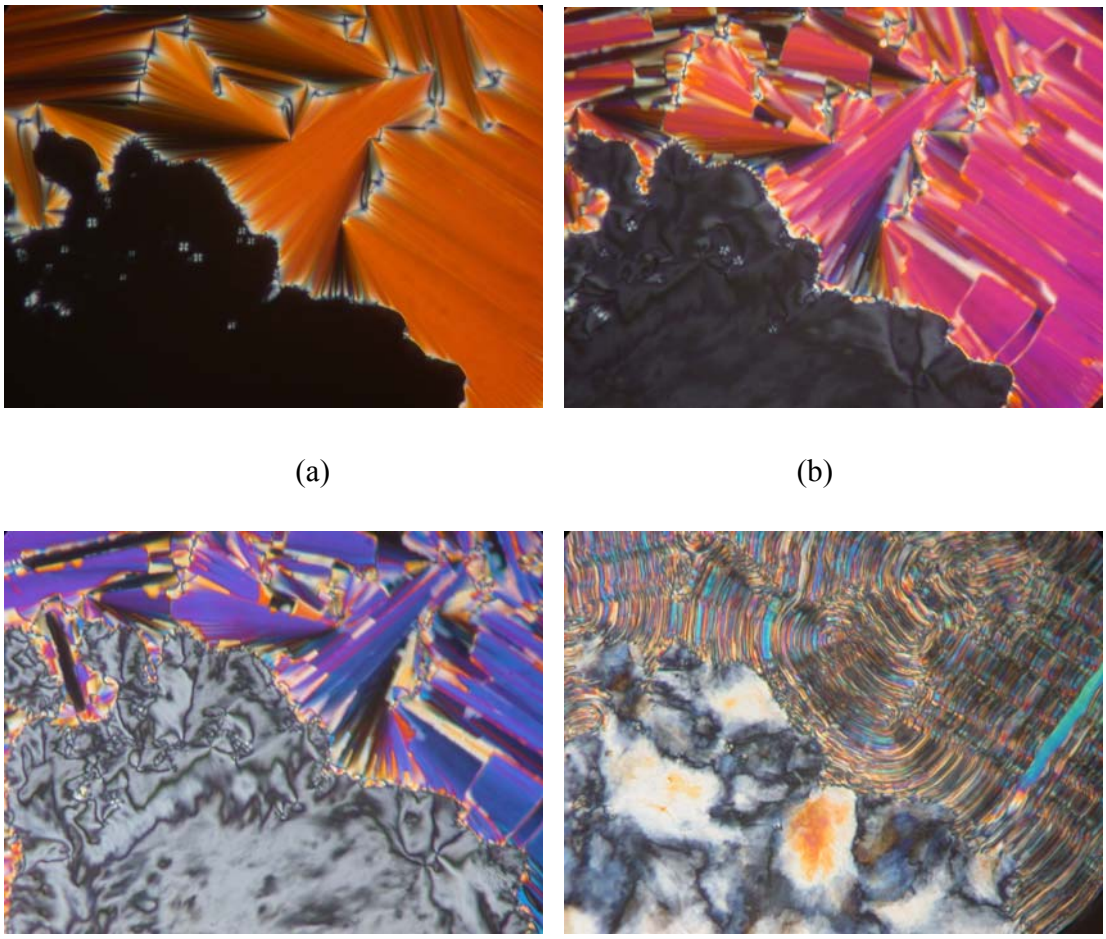

(a) (b)

(c) (d)

Figure A3-16. Textures of compound **33b** observed by polarized microscopy on cooling: (a) in the SmA phase at 82°C, (b) just below the SmA–SmC phase transition at 73°C, (c) in the SmC phase at 62 °C, and (d) in the Cr phase at -2 °C. (100X Magnification)

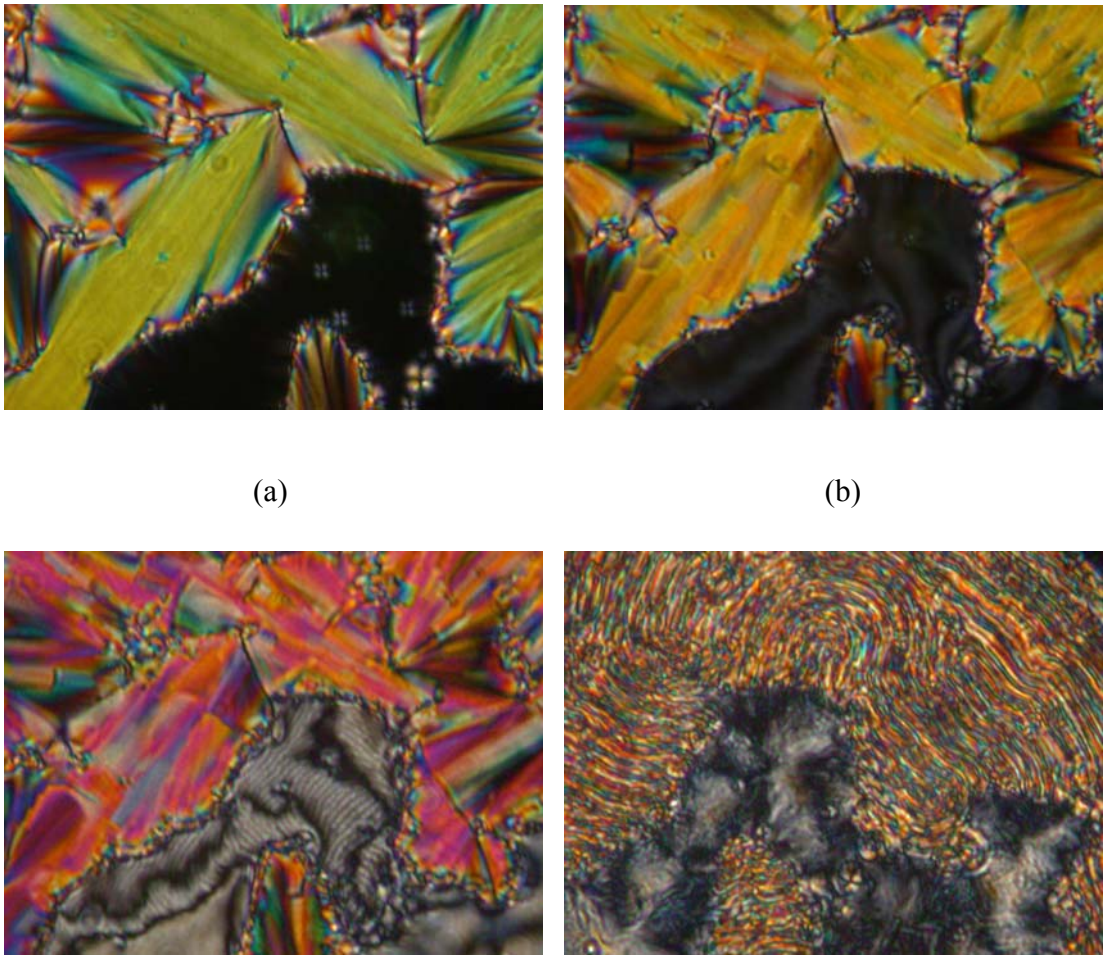

(a) (b)

(c) (d)

Figure A3-17. Textures of compound **33c** observed by polarized microscopy on cooling: (a) in the SmA phase at 85°C, (b) just below the SmA–SmC phase transition at 76°C, (c) in the SmC phase at 66 °C, and (d) in the Cr phase at -1 °C. (100X Magnification)

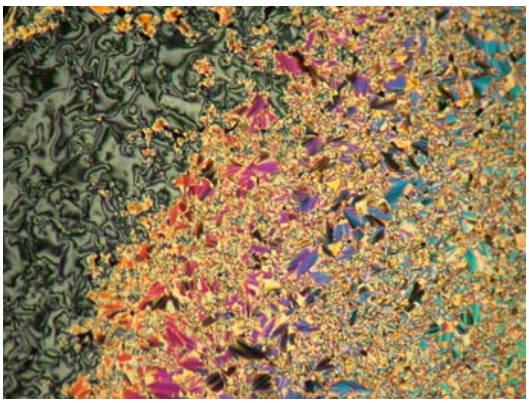

Figure A3-18. Textures of compound **34a** observed by polarized microscopy on cooling: in the SmC phase at 76^{o}C. (100X Magnification)

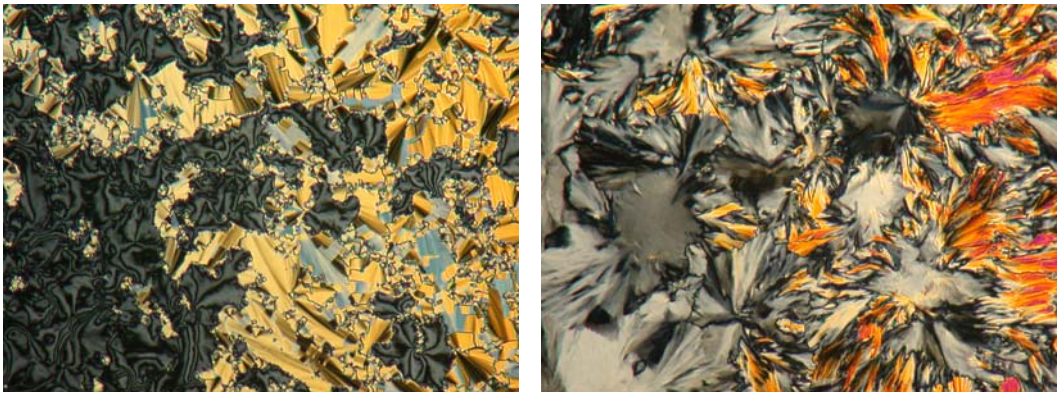

(a) (b)

Figure A3-19. Textures of compound **34b** observed by polarized microscopy on cooling: (a) in the SmC phase at 49^{o}C, and (b) in the Cr phase at 7 ^{o}C. (100X Magnification)

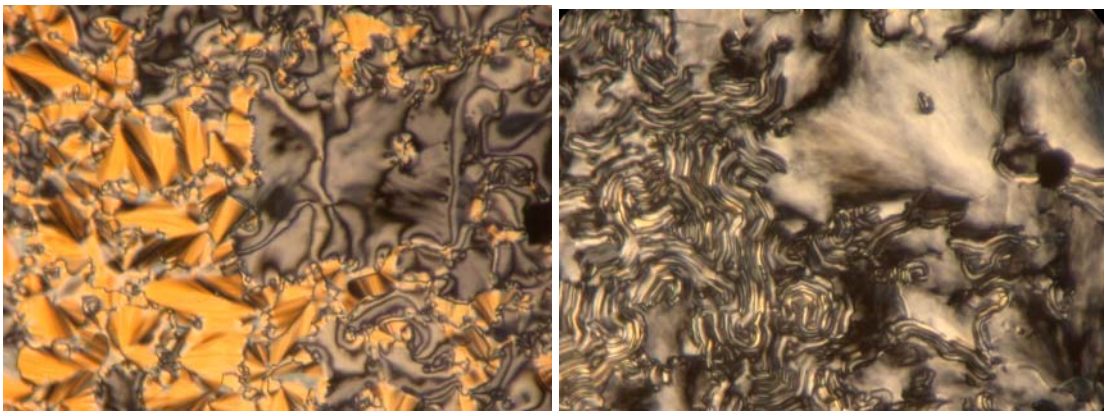

(a) (b)

Figure A3-20. Textures of compound **35a** observed by polarized microscopy on cooling: (a) SmC phase at 140 ^{o}C, and (b) Cr phase at 82 ^{o}C. (100X Magnification)

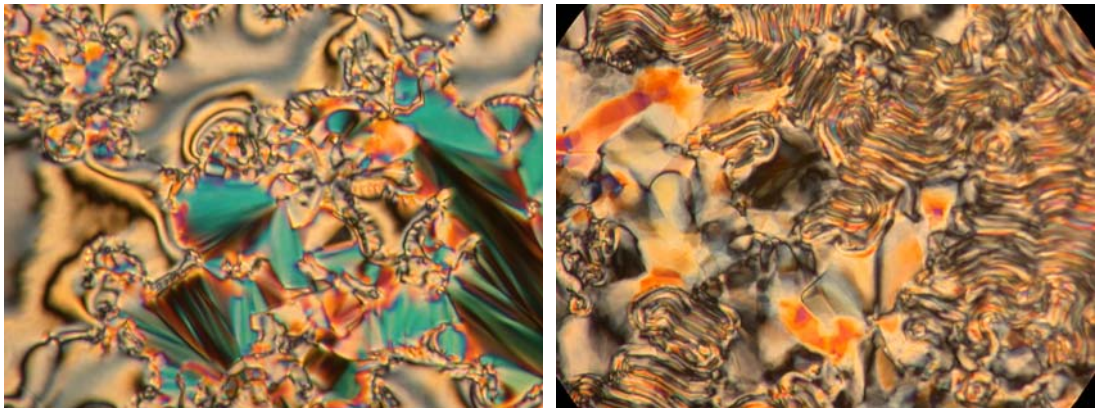

(a) (b)

Figure A3-21. Textures of compound **35b** observed by polarized microscopy on cooling: (a) SmC phase at 155 ^{o}C, and (b) Cr phase at 84 ^{o}C. (100X Magnification)

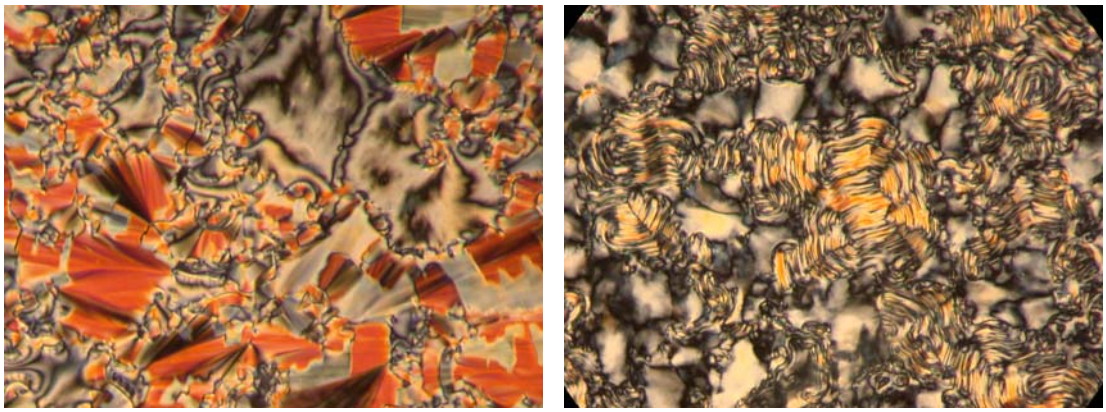

(a) (b)

Figure A3-22. Textures of compound **35c** observed by polarized microscopy on cooling: (a) SmC phase at 152 ^{o}C, and (b) Cr phase at 77 ^{o}C. (100X Magnification)

Figure A3-23. Textures of compound **35d** observed by polarized microscopy on cooling: SmC phase at 150 ^{o}C. (100X Magnification)

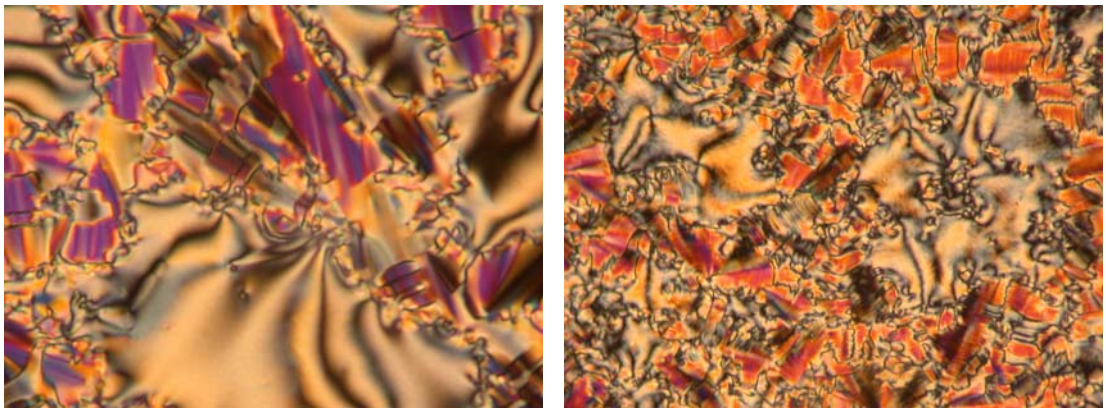

(a) (b)

Figure A3-24. Textures of compound **35e** observed by polarized microscopy on cooling: (a) SmC phase at 151°C, and (b) Cr phase at 55°C. (100X Magnification)

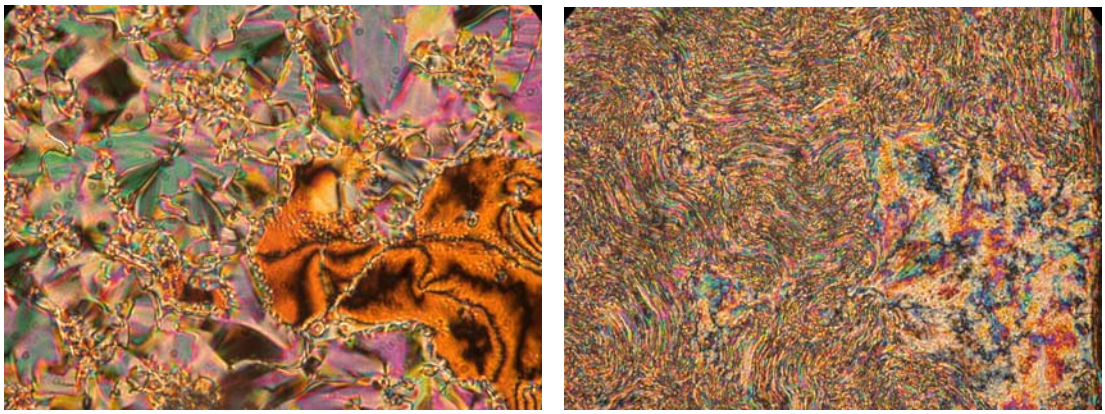

(a) (b)

Figure A3-25. Textures of compound **36** observed by polarized microscopy on cooling: (a) SmC phase at 141°C, and (b) Cr phase at 41°C. (100X Magnification)

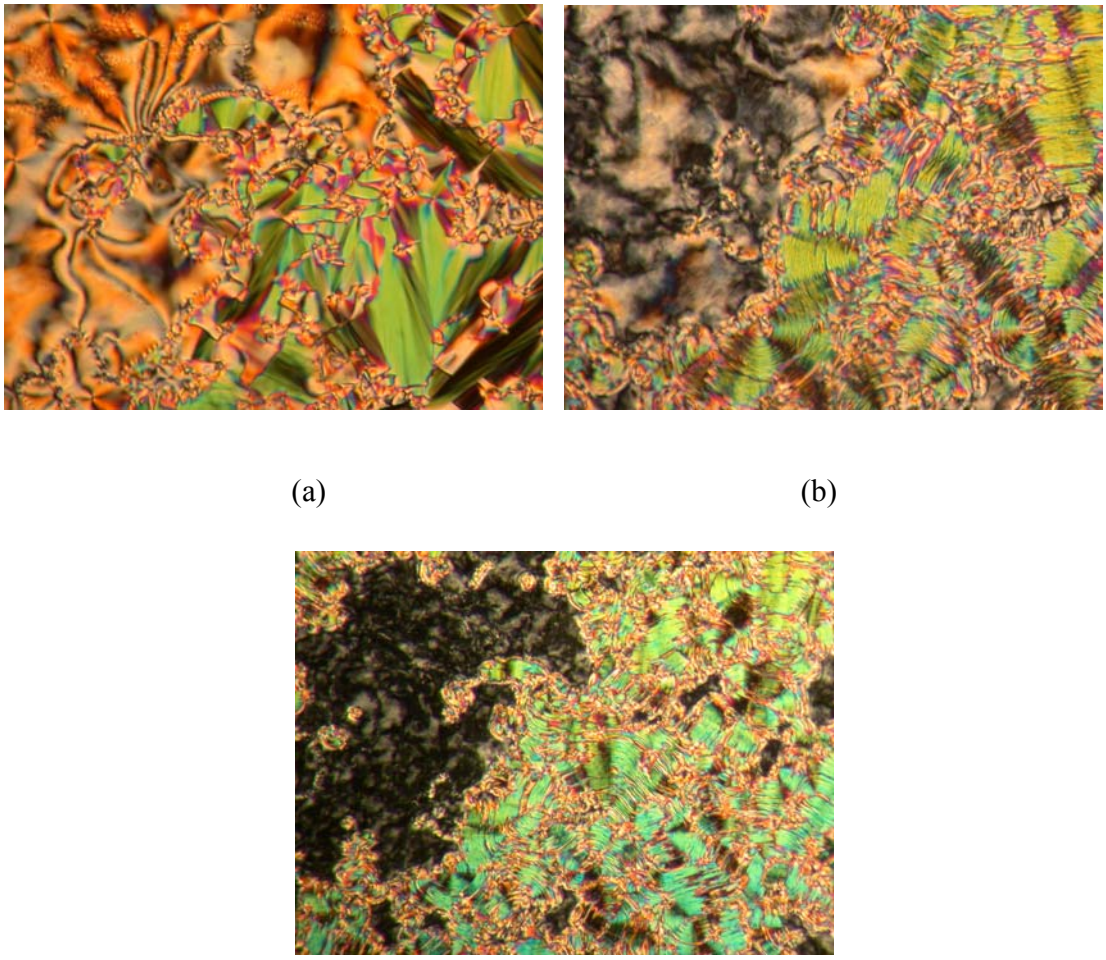

(a) (b)

(c)

Figure A3-26. Textures of compound **35f** observed by polarized microscopy on cooling: (a) SmC phase at 135 ^{o}C, (b) X phase at 75 ^{o}C, and (c) Cr phase at 45 ^{o}C. (100X Magnification)

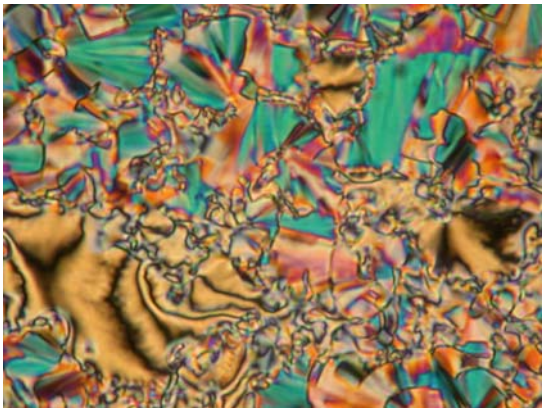

Figure A3-27. Textures of compound **37** observed by polarized microscopy on cooling: SmC phase at 153^{o}C. (100X Magnification)

Figure A3-28. Textures of compound **38** observed by polarized microscopy on cooling: SmC phase at 58 ^{o}C. (100X Magnification)

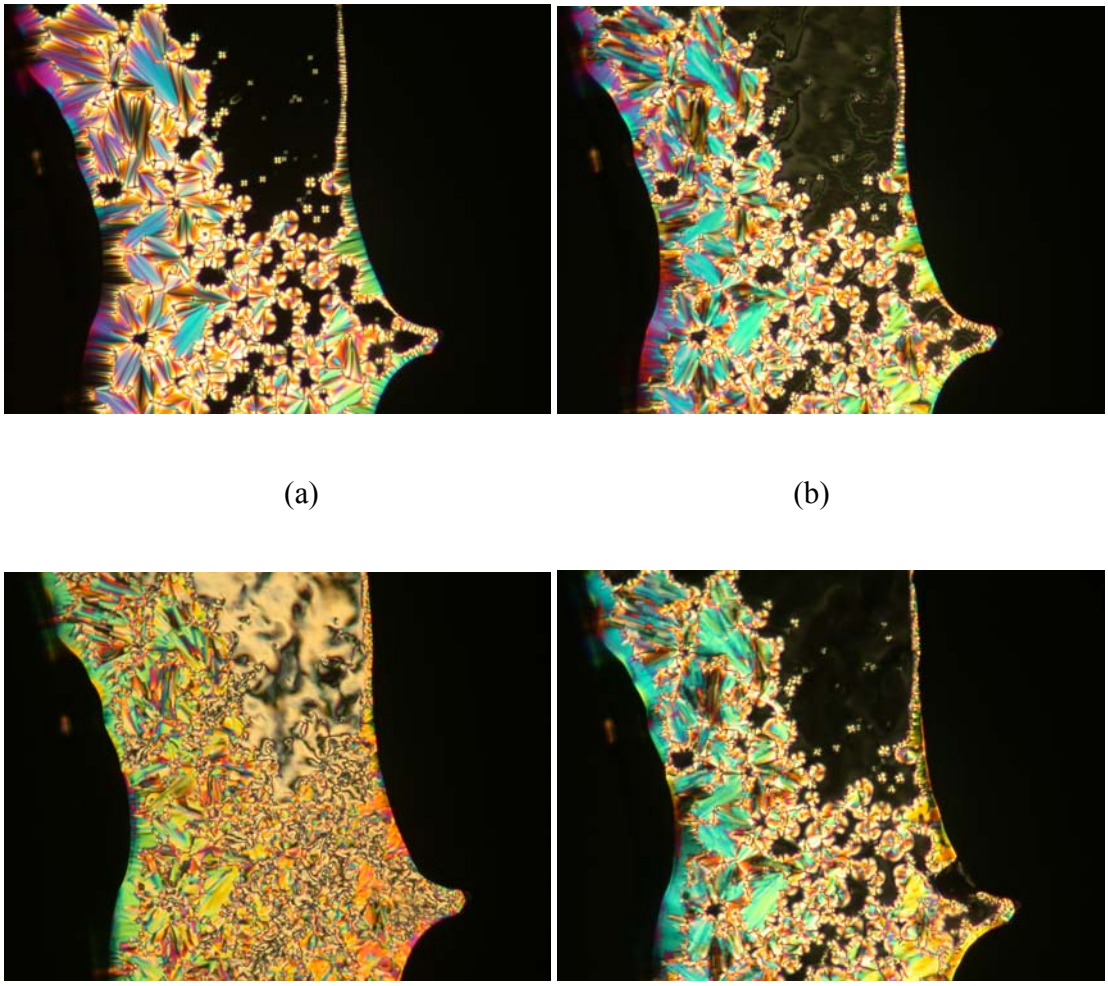

(a) (b)

(c) (d)

Figure A3-29. Textures of compound **39a** observed by polarized microscopy on cooling: (a) SmA phase at 59^{o}C, (b) SmC phase at 57^{o}C, (c) SmI phase at -3^{o}C, and (d) Cr phase at -26^{o}C. (100X Magnification)

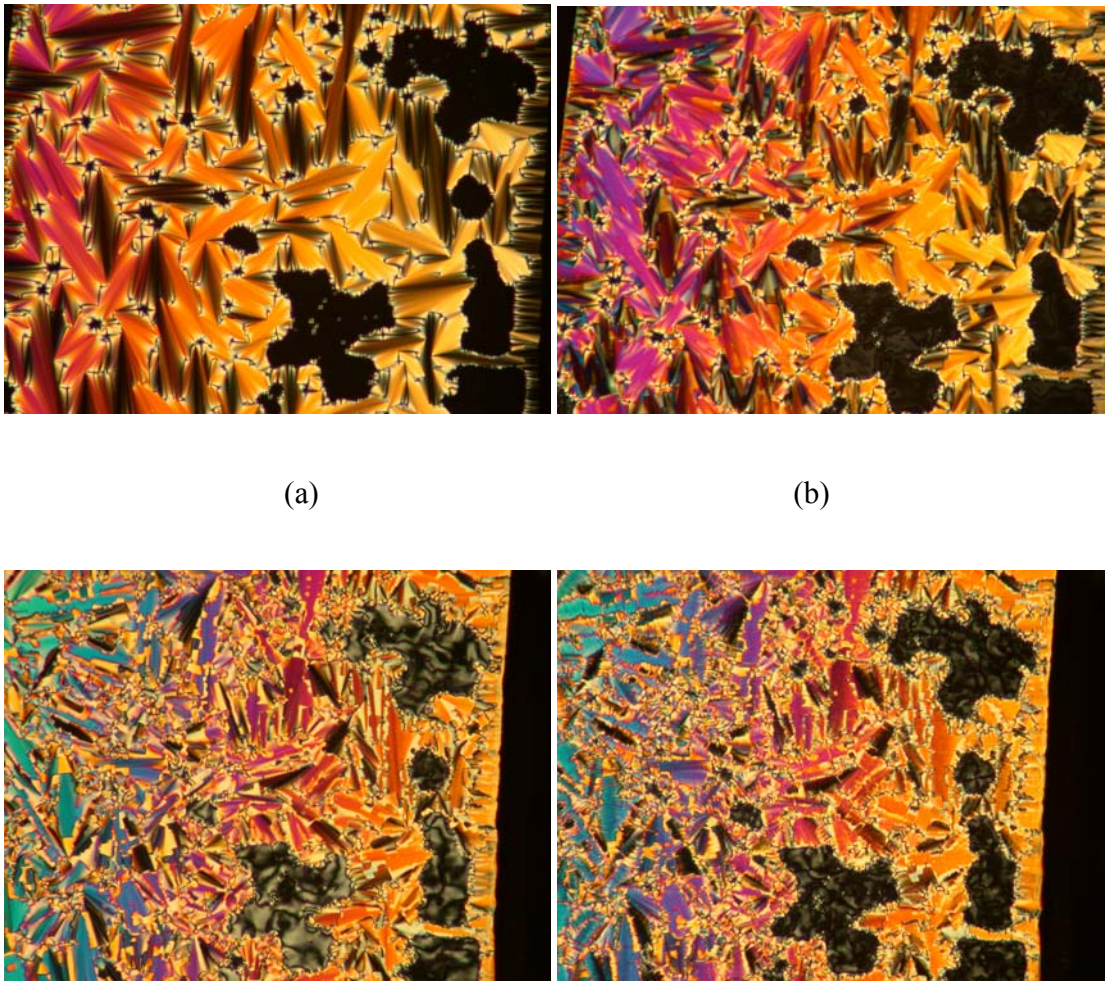

(a) (b)

(c) (d)

Figure A3-30. Textures of compound **39b** observed by polarized microscopy on cooling: (a) SmA phase at 60°C, (b) SmC phase at 57°C, (c) SmI phase at 5°C, and (d) Cr phase at -14°C. (100X Magnification)

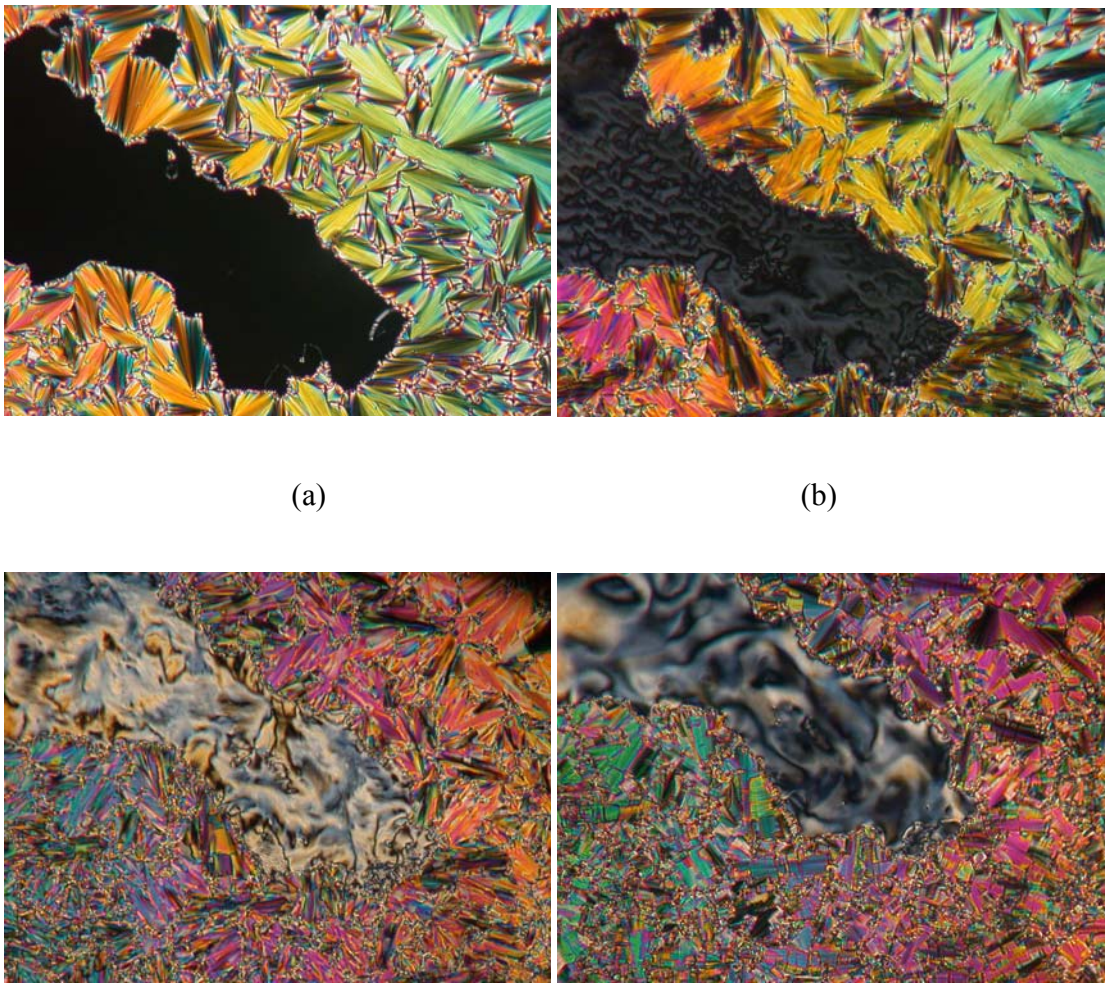

(a) (b)

(c) (d)

Figure A3-31. Textures of compound **39c** observed by polarized microscopy on cooling: (a) SmA phase at 65^{o}C, (b) SmC phase at 62^{o}C, (c) SmI phase at 12^{o}C, and (d) Cr phase at -8^{o}C. (100X Magnification)

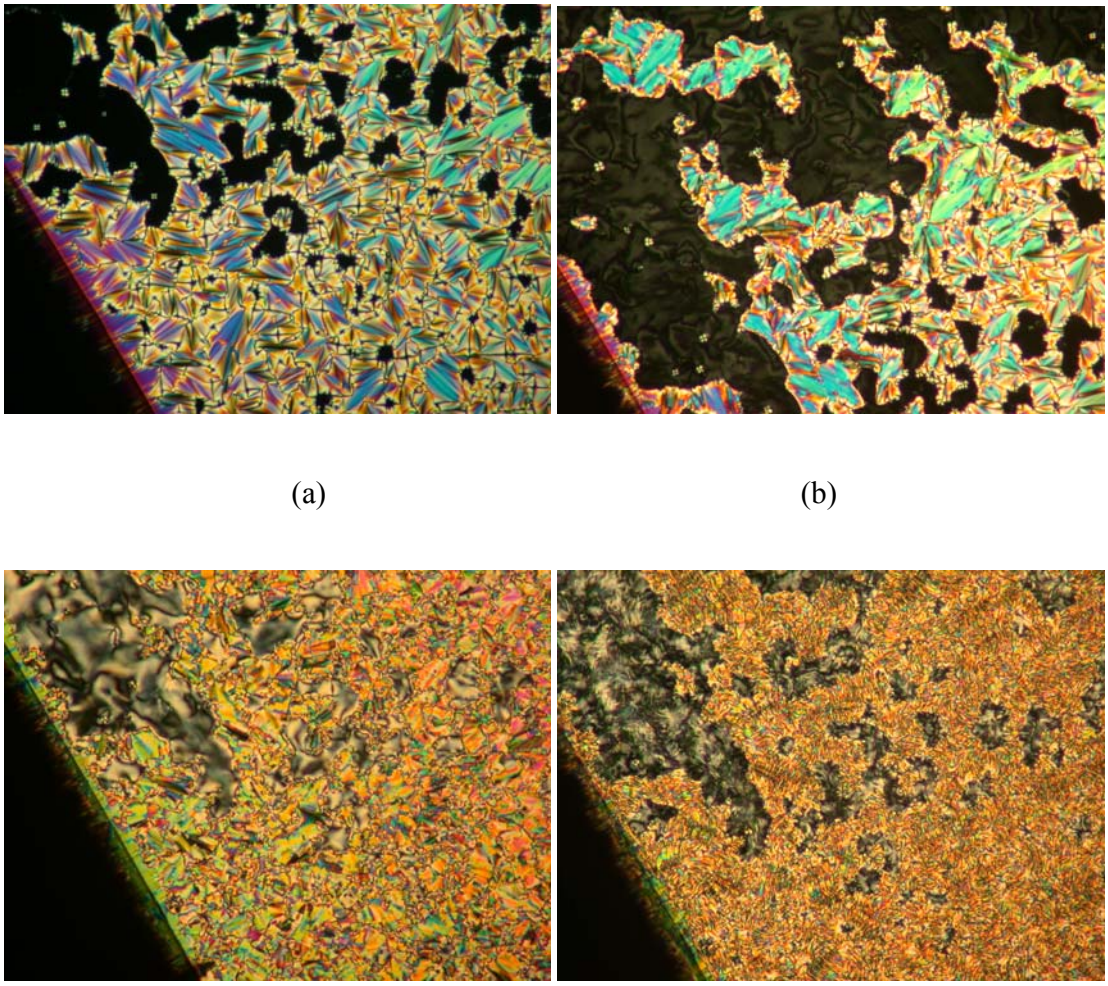

(a) (b)

(c) (d)

Figure A3-32. Textures of compound **39d** observed by polarized microscopy on cooling: (a) SmA phase at 59^{o}C, (b) SmC phase at 58^{o}C, (c) SmI phase at 22^{o}C, and (d) Cr phase at 3^{o}C. (100X Magnification)

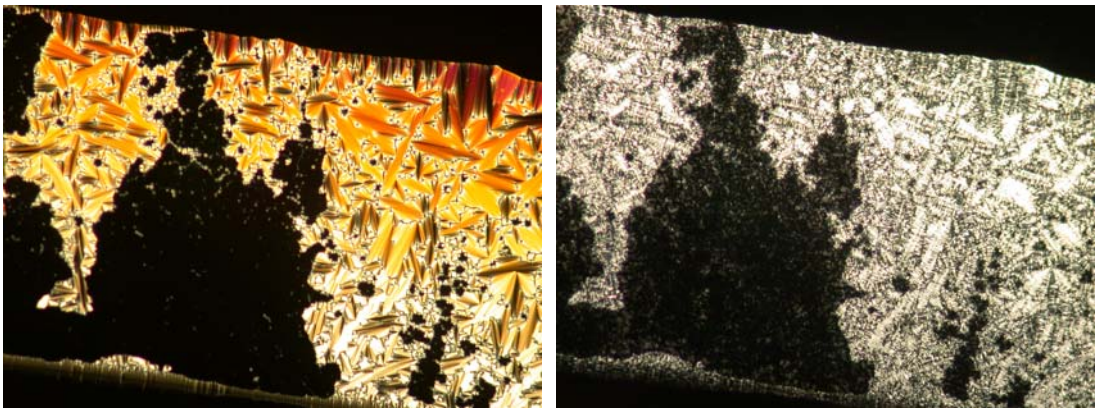

(a) (b)

Figure A3-33. Textures of compound **40a** observed by polarized microscopy on cooling: (a) SmA phase at 85 ^{o}C, and (b) Cr phase at 11 ^{o}C. (100X Magnification)

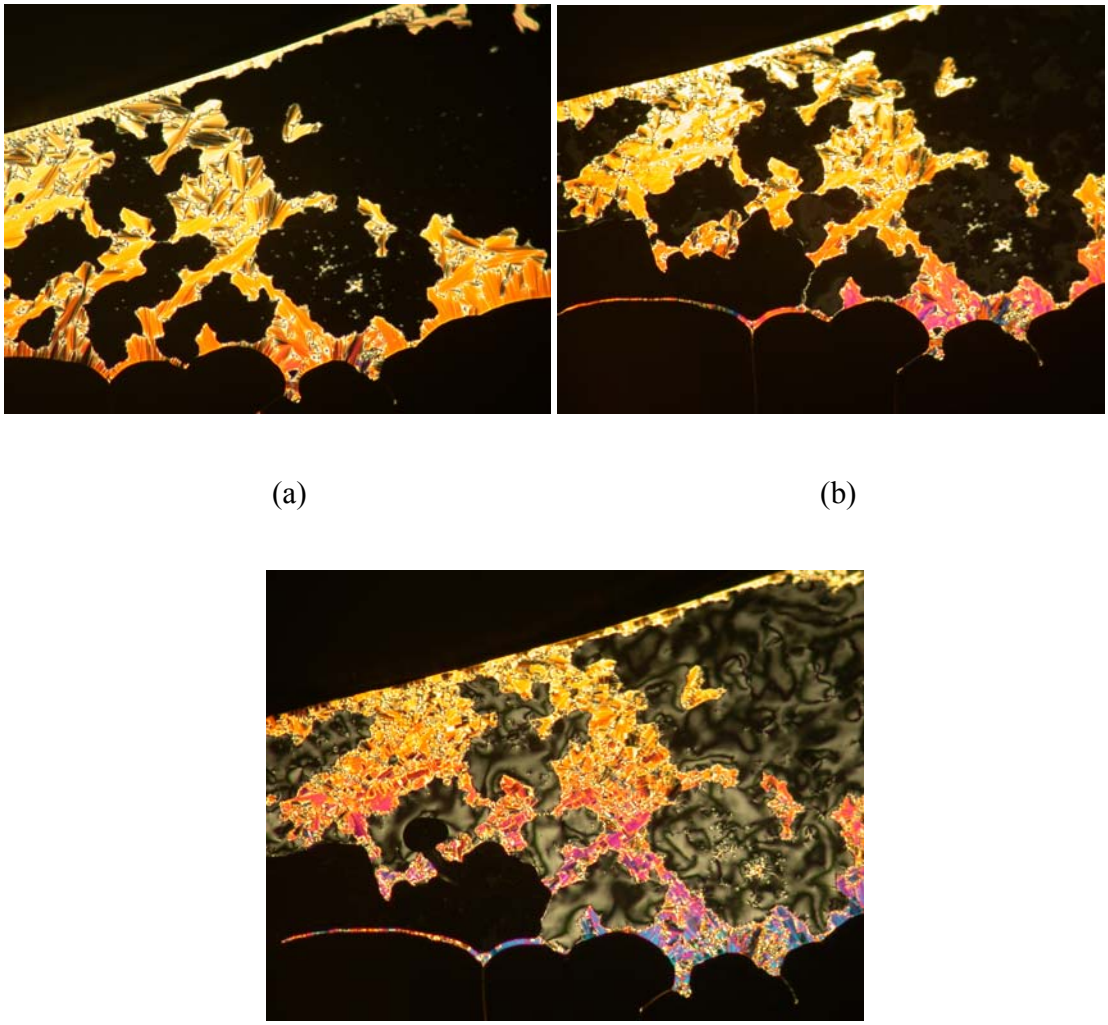

(a) (b)

(c)

Figure A3-34. Textures of compound **40b** observed by polarized microscopy on cooling: (a) SmA phase at 61°C, and (b) SmC phase at 54°C, (c) SmI phase at 3°C. (100X Magnification)